South San Francisco Bay Long Wave Modeling Report

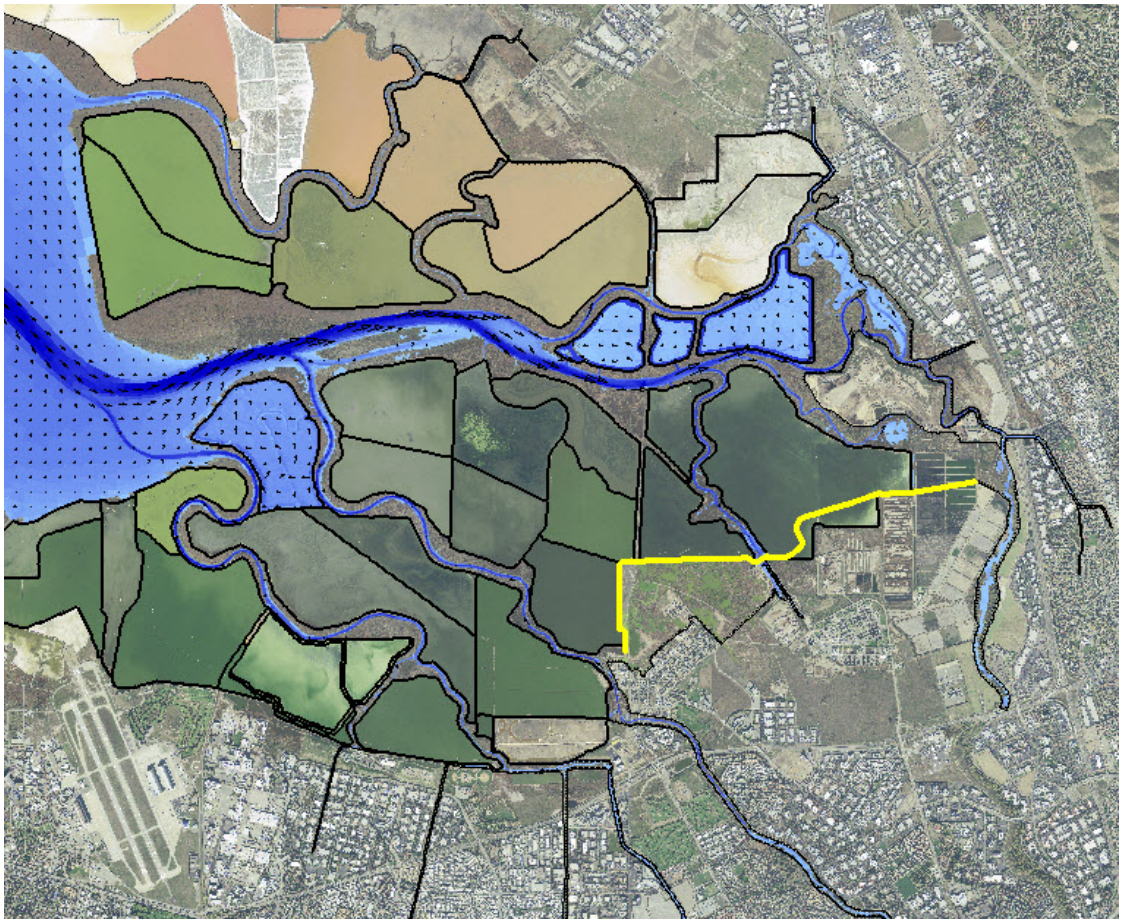

Prepared For:

U.S. Army Corps of Engineers
San Francisco District

Prepared By:

Michael L. MacWilliams, Ph.D., Nina E. Kilham, Ph.D., Aaron J. Bever, Ph.D.

DELTA MODELING ASSOCIATES

[This page intentionally left blank.]

Executive Summary

The South San Francisco Bay Shoreline Study (SSFBSS) is being conducted by the USACE San Francisco District (SPN) and is co-sponsored by the Santa Clara Valley Water District (SCVWD) and California Coastal Conservancy (CCC). The SSFBSS has the dual functions of providing shoreline protection and restoring salt ponds in Far South San Francisco Bay.

The UnTRIM San Francisco Bay-Delta model was refined to include a high resolution model grid and the most recent available high resolution bathymetric data in the project area. The model was calibrated using observed water level data during periods with the most extensive spatial availability of water level observations in the project area in 2005 and 2011. The model was validated using peak water level data from five separate storm periods between 1983 and 2006. These simulation periods include ten of the 47 highest observed water levels during storm events based on a ranking of the maximum verified tide data value at the San Francisco NOAA tide station (9414290), including all of the top five ranked events. The resulting model was applied to predict peak water levels in the project area under with project conditions.

The calibrated and validated model was applied to a set of six preliminary alternatives to predict peak water levels in the project area for a single flood event. The six preliminary alternatives were developed by combining the two most likely Flood Risk Management (FRM) levee alignments, with a suite of ecosystem restoration (ER) options based on feedback from the Project Delivery Team (PDT) and the project sponsors. The results from these preliminary alternative simulations were used in the selection of the two alternatives to be used for detailed analysis of flood risks with project conditions.

Based on this suite of preliminary alternatives, two FRM alternatives were evaluated under year 0 (2017) conditions. The two alternatives were the designated as the Locally Preferred Alignment (LPA) and a tentative National Economic Development (NED) alignment. A set of synthesized events that cover the ranges of all the controlling parameters, such as tide, residual surge, wind speed, and wind direction and levee failures was developed for year 0 conditions. Predicted peak water levels for each year 0 event were provided in lookup tables to allow for the interpretation of the responses of all the synthesized events randomly selected by the Monte Carlo Simulation (MCS) process during statistical analysis.

The Locally Preferred Alignment (LPA) was combined with an Ecosystem Restoration (ER) scenario to develop project conditions for year 50 (2067), with 0.649 m (2.13 ft) of sea level rise (SLR). The year 50 project bathymetry was developed through a combination of historical analysis of bathymetric change in the project area, an analysis of predicted deposition in the project area through numerical simulation, and prediction of the potential for channel scour following the opening of the salt ponds to tidal action. The year 50 simulations incorporate both the expected accretion within the project ponds, as well as estimated channel evolution in the vicinity of the project area. The year 50 production simulations were also performed for a set of synthesized events that cover the ranges of all the controlling parameters, such as tide, residual surge, wind speed, and wind direction. Predicted peak water levels for each year 50 event were provided in lookup tables to allow for the interpretation of the responses of all the

synthesized events randomly selected by the Monte Carlo Simulation (MCS) process during statistical analysis. The results of MCS will be used to establish flood stage frequency and overtopping flow for mapping.

Abbreviations

3D	Three-Dimensional
BAW	Bundesanstalt für Wasserbau (German Federal Waterways Engineering and Research Institute)
BDM	Bay-Delta Model
CCC	California Coastal Conservancy
CFS	Cubic Feet per Second
DEM	Digital Elevation Model
ER	Ecosystem Restoration
FRM	Flood Risk Management
GLS	Generic Length Scale
GPS	Global Positioning System
JALBTCX	Joint Airborne LiDAR Bathymetry Technical Center of Expertise
LiDAR	Light Detection And Ranging
LPA	Locally Preferred Alignment
LPP	Locally Preferred Plan
MCS	Monte Carlo Simulation
MHHW	Mean Higher High Water
MHW	Mean High Water
MLLW	Mean Lower Low Water
MLW	Mean Low Water
MTL	Mean Tide Level
NAD83	North American Datum of 1983
NAVD88	North American Vertical Datum of 1988
NED	National Economic Development
NOAA	National Oceanic & Atmospheric Administration
PDT	Project Delivery Team
RTK	Real Time Kinematic
R&U	Risk & Uncertainty
SCVWD	Santa Clara Valley Water District
SFPORTS	San Francisco Physical Oceanographic Real-Time System
SSFBSS	South San Francisco Bay Shoreline Study
SSC	Suspended Sediment Concentration
TRIM	Tidal, Residual, Intertidal & Mudflat Model
UnTRIM	Unstructured Tidal, Residual, Intertidal & Mudflat Model
USACE	United States Army Corps of Engineers
USGS	United States Geological Survey
UTM	Universal Transverse Mercator

Table of Contents

1. Introduction 1

2. South San Francisco Bay Shoreline Study—Long Wave Modeling Approach 2

2.1 Project Site 2

2.2 Project Objectives 3

2.3 Modeling Approach 3

3. UnTRIM Bay-Delta Model Description 4

3.1 Governing Equations 4

3.2 Turbulence Model 6

3.3 Previous Applications 6

3.4 UnTRIM Bay-Delta Model 6

3.5 South San Francisco Bay Model Grid and Bathymetry Refinements 8

3.6 Model Boundary Conditions 10

3.7 Model Uncertainty 11

4. South San Francisco Bay Model Calibration and Verification 14

4.1 Model Calibration and Validation Approach 14

4.2 Simulation Periods for Model Calibration 19

4.3 Results of Model Calibration 22

4.3.1 Model Calibration for 2011 Simulation period 22

4.3.2 Model Calibration for 2005 Simulation period 27

4.4 Simulation Periods for Model Validation 34

4.5 Results of Model Validation 40

4.5.1 Model Verification for January 1983 Storm 40

4.5.2 Model Verification for December 1983 Storm 43

4.5.3 Model Verification for November and December 1997 Storms 45

4.5.4 Model Verification for February 1998 Storm 49

4.5.5 Model Verification for December 2006 Storm 53

4.6 Assessment of Model Accuracy for All Simulated Storm Peaks 56

4.7 Evaluation of Storm Surge Propagation and Effect of Wind 59

4.7.1 Simulation of December 1983 using Astronomical Tides 60

4.7.2 Evaluation of Storm Surge Propagation during December 1983 Storm 64

4.7.3 Evaluation of Effect of Wind during December 1983 Storm 66

4.7.4 Evaluation of Effect of Wind during January 1983 Storm 71

5. Screening of Preliminary Alternatives 76

5.1 Description of Preliminary Alternatives 76

5.2 Evaluation Approach for Preliminary Alternatives 83

5.2.1 Model Boundary Conditions 83

5.2.2 Ponds A9 through A15 83

5.2.3 Ponds A16 and A17 83

5.2.4 Pond A18 84

5.2.5 Artesian Slough Tide Gate 84
5.2.6 New Chicago Marsh Tide Gate 84
5.2.7 Evaluation Locations 85

5.3 Results of Preliminary Alternative Evaluation 86
5.3.1 Effect of FRM Alignment 87
5.3.2 Effect of Sedimentation Rate 87
5.3.3 Effect of Upland Fill 87

6. Year 0 Model Production Simulations and Analysis 89

6.1 Boundary Conditions for Year 0 Model Production Simulations 89
6.1.1 Tidal Boundary Conditions for Year 0 Production Simulations 89
6.1.2 River Inflows for Year 0 Production Simulations 95
6.1.3 Wind Boundary Conditions for Year 0 Production Simulations 97

6.2 Description of Year 0 Flood Risk Management Alternatives 99
6.2.1 LPA and NED FRM Alignments 99
6.2.2 Ponds A9 through A15 99
6.2.3 Ponds A16 and A17 100
6.2.4 Pond A18 100
6.2.5 New Chicago Marsh 100
6.2.6 Artesian Slough Tide Gate 101
6.2.7 Evaluation Locations 101
6.2.8 Outer Levee Failure Conditions 102

6.3 Year 0 Model Production Simulation Results 103
6.3.1 Peak Water levels for Year 0 Production Simulations without Wind 103
6.3.2 Effect of Wind on Peak Water levels for Year 0 Production Simulations 103
6.3.3 Peak Water levels for Year 0 Production Simulations with Levee Failures 105

7. Development of Year 50 Project Conditions 120

7.1 Evaluation of Bathymetric Evolution Following Island Pond Breaches 120
7.1.1 Bathymetric Data Sources 121
7.1.2 Coyote Creek Cross-Sections 122
7.1.3 Evaluation of Bathymetric Change by Geomorphic Zone 127
7.1.4 Masking 127
7.1.5 Results 129

7.2 Evaluation of Deposition Patterns in Mudflat and Marsh Areas 138
7.2.1 UnTRIM – SediMorph model coupling 138
7.2.2 Far South San Francisco Bay Hydrodynamic and Sediment Simulation 139
7.2.3 Results of Sediment Deposition Simulations 140

7.3 Evaluation of the Potential for Channel Scour Following Pond Restoration 146

7.4 Development of Projected Bathymetry in the Project Area for Year 50 151

8. Year 50 Model Production Simulations and Analysis 156

8.1 Boundary Conditions for Year 50 Model Production 156
8.1.1 Tidal Boundary Conditions for Year 50 Production Simulations 156
8.1.2 River Inflows for Year 50 Production Simulations 156
8.1.3 Wind Boundary Conditions for Year 50 Production Simulations 157

8.2 Description of Year 50 Flood Risk Management Alternatives 157
8.2.1 LPA FRM Alignments 157
8.2.2 Ponds A9 through A15 157

8.2.3 Ponds A16 and A17 157
8.2.4 Pond A18 158
8.2.5 New Chicago Marsh 158
8.2.6 Artesian Slough Tide Gate 158
8.2.7 Evaluation Locations 158
8.2.8 Outer Levee Failure Conditions 159

8.3 Year 50 Model Production Simulation Results 159
8.3.1 Peak Water levels for Year 50 Production Simulations without Wind 159
8.3.2 Effect of Wind on Peak Water levels for Year 50 Production Simulations 160

9. Summary and Conclusions 165

Acknowledgments 167

References 168

1. Introduction

This report documents the three-dimensional hydrodynamic modeling study conducted for the long wave modeling component of the South San Francisco Bay Shoreline Study. This report is divided into nine major sections:

- **Section 1. Introduction.** This section provides a summary of the scope and organization of the report.
- **Section 2. South San Francisco Bay Shoreline Study—Long Wave Modeling Approach.** This section provides a brief overview of the project study area, project approach, and project objectives.
- **Section 3. UnTRIM Bay-Delta Model Description.** This section provides a brief description of the UnTRIM hydrodynamic model and the UnTRIM Bay-Delta model, as well as a description of the data sources used to develop the model bathymetry and boundary conditions for the South San Francisco Bay long wave modeling study.
- **Section 4. South San Francisco Bay Model Calibration and Verification.** This section presents the model calibration based on reproduction of water levels for baseline conditions and verification of predicted water levels when compared to observations for a series of storm events.
- **Section 5. Screening of Preliminary Alternatives.** This section describes the scenarios and model results used for a set of preliminary project alternatives.
- **Section 6. Year 0 Model Production Simulations and Analysis.** This section presents the results of the model production simulations for year 0 conditions.
- **Section 7. Development of Year 50 Project Conditions.** This section describes the approach and analysis used to develop bathymetric conditions for the project in year 50.
- **Section 8. Year 50 Model Production Simulations and Analysis.** This section presents the results of the model production simulations for year 50 conditions.
- **Section 9. Summary and Conclusions.** This section presents a summary of the work conducted in this study and the conclusions drawn from this work.

2. South San Francisco Bay Shoreline Study—Long Wave Modeling Approach

The South San Francisco Bay Shoreline Study (SSFBSS) is being conducted by the USACE San Francisco District (SPN). The SSFBSS has the dual functions of providing shoreline protection and restoring salt ponds. The goal of the modeling component of the SSFBSS is to provide hydrodynamic conditions with respect to a variety of synthesized events, allowing a Monte Carlo Simulation (MCS) of responses leading to guidelines for developing appropriate shoreline protection and restoration alternatives. San Francisco District and the co-sponsors, Santa Clara Valley Water District (SCVWD) and California Coastal Conservancy (CCC), have completed a F3 feasibility study under without project conditions (Letter and Sturm, 2010). The long wave modeling results presented in this document are part of the F4 feasibility study, which evaluates with project conditions.

2.1 Project Site

The South San Francisco Bay Shoreline Study project site is located south of the Dumbarton Bridge at the far southern end of San Francisco Bay (Figure 2.1-1). For the F4 study, the specific study area is bounded by Coyote Creek and Alviso Slough. This area encompasses Ponds A9 through A18, which were previously used for salt production by Cargill, Inc. Ponds A9 through A17 are now owned by US Fish and Wildlife Service (USFWS) as part of the Don Edwards San Francisco Bay National Wildlife Refuge, while Pond A18 is now owned by the City of San Jose.

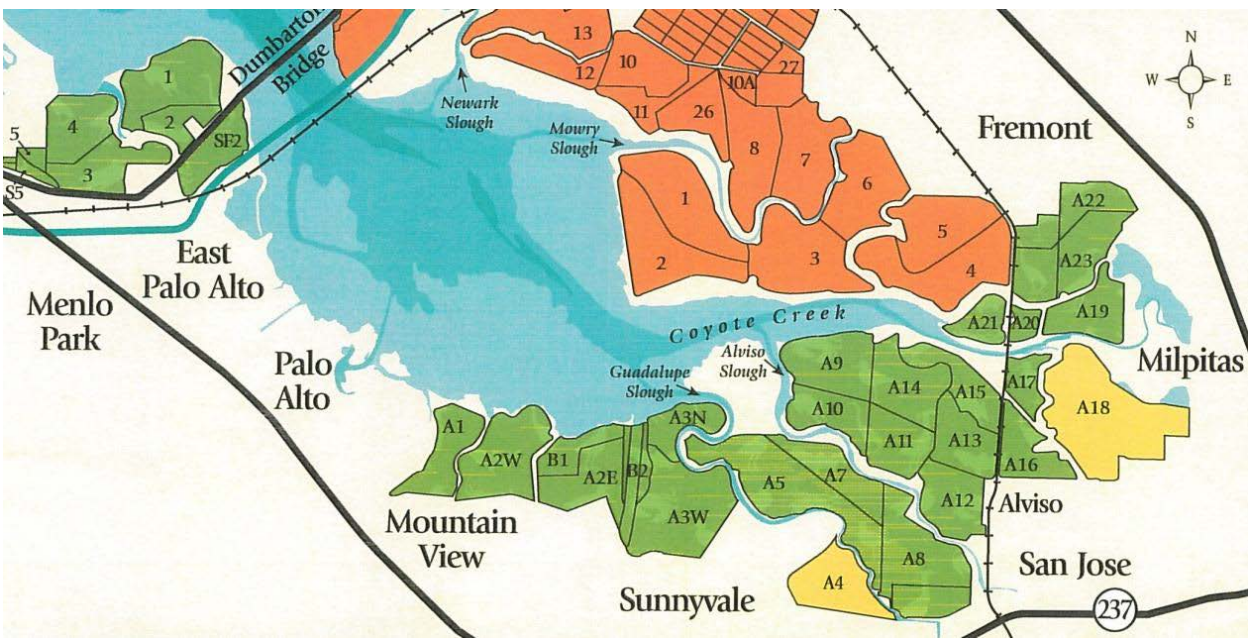

Figure 2.1-1. South San Francisco Bay Shoreline Study project site (from Noble Consultants, 2012).

2.2 Project Objectives

The primary objective of the long wave modeling component of the SSFBSS is to provide predictions of water levels for a set of synthesized events that cover the ranges of all the controlling parameters, such as tide, residual surge, wind speed, and wind direction under with project conditions for both year 0 and year 50 conditions. The model simulation results will be summarized in lookup tables. These lookup tables will allow the interpretation of the responses of all the synthesized events randomly selected by the Monte Carlo Simulation (MCS) process during statistical analysis phase of the SSFBSS project. The results of MCS will be used to establish flood stage frequency and overtopping flow for flood mapping.

2.3 Modeling Approach

The UnTRIM Bay-Delta Model (MacWilliams et al., 2007; MacWilliams and Gross, 2007; MacWilliams et al., 2008; MacWilliams et al., 2009) is being applied to evaluate water levels in the project area under with project conditions. The UnTRIM Bay-Delta model extends from the Pacific Ocean through all of San Francisco Bay and the entire Sacramento-San Joaquin Delta. A high-resolution model grid of the project site was developed using the most recent available bathymetry. This high resolution grid of the project area was merged into the existing model grid of the San Francisco Bay-Delta. The resulting model provides significant advantages for the SSFBSS application. The model takes advantage of the grid flexibility allowed in an unstructured mesh by gradually varying grid cell sizes, beginning with large grid cells in the Pacific Ocean and gradually transitioning to finer grid resolution in the smaller sloughs and tidal channels in the project area. This approach offers significant advantages both in terms of numerical efficiency and accuracy, and allows for local grid refinement for detailed analysis of local hydrodynamics in the region of the study site, while still incorporating the overall hydrodynamics of San Francisco Bay and the Sacramento-San Joaquin Delta into a single model.

The UnTRIM model of the San Francisco Bay-Delta (Section 3) was calibrated using water level data collected in the vicinity of the project study site in 2005 and 2011 (Section 4), and then validated through simulation of five storm events, which include ten of the forty-seven storm events with the highest peak water levels recorded at Fort Point, including all of the five highest ranked events between 1901 and 2005 (Cheng and Wu, 2008). The calibrated and validated model was applied to a set of six preliminary alternatives (Section 5) which were developed by combining the two most likely Flood Risk Management (FRM) levee alignments, with a suite of ecosystem restoration (ER) options. The model was then applied to evaluate the two final project alternative plans for year 0 (2017) conditions (Section 6). Year 50 project bathymetry was developed through a combination of historical analysis of bathymetric change in the project area, an analysis of predicted deposition in the project area through numerical simulation, and prediction of the potential for channel scour following the opening of pond groups to tidal action (Section 7). The model was then applied to evaluate the two final project alternative plans for year 50 (2067) conditions (Section 8), with 0.649 m (2.13 ft) of sea level rise (SLR).

3. UnTRIM Bay-Delta Model Description

The hydrodynamic model used in this technical study is the three-dimensional hydrodynamic model UnTRIM (Casulli and Zanolli, 2002). A complete description of the governing equations, numerical discretization, and numerical properties of UnTRIM are described in Casulli and Zanolli (2002, 2005), Casulli (1999), and Casulli and Walters (2000).

The UnTRIM model solves the three-dimensional Navier-Stokes equations (3.1-3.3) on an unstructured grid in the horizontal plane. The boundaries between vertical layers are at fixed elevations, and cell heights can be varied vertically to provide increased resolution near the surface or other vertical locations. Volume conservation is satisfied by a volume integration of the incompressible continuity equation (3.4), and the free-surface is calculated by integrating the continuity equation over the depth (3.5), and using a kinematic condition at the free-surface as described in Casulli (1990). The numerical method allows full wetting and drying of cells in the vertical and horizontal directions. The governing equations are discretized using a finite difference – finite volume algorithm. Discretization of the governing equations and model boundary conditions are presented in detail by Casulli and Zanolli (2002) and is not reproduced here. All details and numerical properties of this state-of-the-art three-dimensional model are well-documented in peer reviewed literature (Casulli and Zanolli, 2002; 2005).

3.1 Governing Equations

Three-dimensional simulations were made using the three-dimensional non-hydrostatic hydrodynamic model for free-surface flows on unstructured grids, UnTRIM, described in Casulli and Zanolli (2002). The UnTRIM model solves the full three-dimensional momentum equations for an incompressible fluid under a free-surface on a rotational reference frame (earth surface) given by

$$\frac{\partial u}{\partial t}+u\frac{\partial u}{\partial x}+v\frac{\partial u}{\partial y}+w\frac{\partial u}{\partial z}-fv=-\frac{\partial p}{\partial x}+\nu^h\left(\frac{\partial^2 u}{\partial x^2}+\frac{\partial^2 u}{\partial y^2}\right)+\frac{\partial}{\partial z}\left(\nu^v\frac{\partial u}{\partial z}\right) \tag{3.1}$$

$$\frac{\partial v}{\partial t}+u\frac{\partial v}{\partial x}+v\frac{\partial v}{\partial y}+w\frac{\partial v}{\partial z}+fu=-\frac{\partial p}{\partial y}+\nu^h\left(\frac{\partial^2 v}{\partial x^2}+\frac{\partial^2 v}{\partial y^2}\right)+\frac{\partial}{\partial z}\left(\nu^v\frac{\partial v}{\partial z}\right) \tag{3.2}$$

$$\frac{\partial w}{\partial t}+u\frac{\partial w}{\partial x}+v\frac{\partial w}{\partial y}+w\frac{\partial w}{\partial z}=-\frac{\partial p}{\partial z}+\nu^h\left(\frac{\partial^2 w}{\partial x^2}+\frac{\partial^2 w}{\partial y^2}\right)+\frac{\partial}{\partial z}\left(\nu^v\frac{\partial w}{\partial z}\right)-\frac{\rho}{\rho_0}g \tag{3.3}$$

where $u(x,y,z,t)$ and $v(x,y,z,t)$ are the velocity components in the horizontal *x* - and *y* - directions, respectively; $w(x,y,z,t)$ is the velocity component in the vertical *z* - direction; *t* is the time; $\rho(x,y,z,t)$ is the density; $p(x,y,z,t)$ is the normalized pressure defined as the pressure divided by a constant reference density, ρ_0; f is the Coriolis parameter; g is the gravitational acceleration; and ν^h and ν^v are the coefficients of horizontal and vertical eddy viscosity, respectively (Casulli and Zanolli, 2002). Conservation of volume is expressed by the incompressibility condition

$$\frac{\partial u}{\partial x}+\frac{\partial v}{\partial y}+\frac{\partial w}{\partial z}=0. \tag{3.4}$$

The free-surface equation is obtained by integrating the continuity equation over depth and using a kinematic condition at the free-surface (Casulli and Cheng, 1992)

$$\frac{\partial \eta}{\partial t}+\frac{\partial}{\partial x}\left[\int_{-h}^{\eta} u dz\right]+\frac{\partial}{\partial y}\left[\int_{-h}^{\eta} v dz\right]=0, \tag{3.5}$$

where $h(x,y)$ is the prescribed bathymetry measured downward from the reference elevation and $\eta(x,y,t)$ is the free-surface elevation measured upward from the reference elevation. Thus, the total water depth is given by $H(x,y,t)=h(x,y)+\eta(x,y,t)$.

The boundary conditions at the free-surface are specified by the prescribed wind stresses as (Casulli and Zanolli, 2002)

$$\nu^{v}\frac{\partial u}{\partial z}=\tau_x^w, \qquad \nu^{v}\frac{\partial v}{\partial z}=\tau_y^w, \qquad \text{at } z=\eta \tag{3.6}$$

where τ_x^w and τ_y^w are the wind stress components in the *x* and *y* direction, respectively. Similarly, at the sediment-water interface the bottom friction is specified by

$$\nu^{v}\frac{\partial u}{\partial z}=\tau_x^b, \qquad \nu^{v}\frac{\partial v}{\partial z}=\tau_y^b, \qquad \text{at } z=-h \tag{3.7}$$

Where τ_x^b and τ_y^b are the bottom stress components in the *x* and *y* direction, respectively. A quadratic stress formula is applied at each boundary. At the free-surface the coefficient of drag is specified as a function of wind speed using the formulation of Large and Pond (1981). At the bottom boundary the coefficient of drag is estimated using a specified roughness coefficient (z_0).

The governing equation for salt transport (Casulli and Zanolli, 2002) is

$$\frac{\partial s}{\partial t}+\frac{\partial(us)}{\partial x}+\frac{\partial(vs)}{\partial y}+\frac{\partial(ws)}{\partial z}=\frac{\partial}{\partial x}\left(\varepsilon_h\frac{\partial s}{\partial x}\right)+\frac{\partial}{\partial y}\left(\varepsilon_h\frac{\partial s}{\partial y}\right)+\frac{\partial}{\partial z}\left(\varepsilon_v\frac{\partial s}{\partial z}\right) \tag{3.8}$$

where *s* is the salinity concentration; ε_h is the horizontal diffusion coefficient; and ε_v is the vertical diffusion coefficient. The estimation of eddy viscosity and eddy diffusivity is discussed below. The system is closed by an equation of state of the form $\rho=\rho(C)$ which relates the water density to the concentration of salinity using a linear equation of state.

The pressure in Equations 3.1 to 3.3 can be decomposed into the sum of its hydrostatic component and a nonhydrostatic component. The hydrostatic pressure component is

determined from Equation 3.3 by neglecting the convective and the viscous acceleration terms. Thus the pressure can be expresses as (Casulli and Zanolli, 2002)

$$p(x,y,z,t) = p_a(x,y,t) + g[\eta(x,y,t) - z] + g\int_z^{\eta} \frac{\rho - \rho_0}{\rho_0} d\zeta + q(x,y,z,t) \tag{3.9}$$

where $p_a(x,y,t)$ is the atmospheric pressure, the second and third terms on the right side of Equation 3.9 represents the barotropic and the baroclinic contributions to the hydrostatic pressure, and $q(x,y,z,t)$ denotes the nonhydrostatic pressure component. For the simulations made in this study, the hydrostatic approximation was made and $q = 0$ is assumed throughout.

3.2 Turbulence Model

The turbulence closure model used in the present study is a two-equation model comprised of a turbulent kinetic energy equation and a generic length-scale equation. The parameters of the generic length-scale (GLS) equation are chosen to yield the k-ε closure. The Kantha and Clayson (1994) quasi-equilibrium stability functions are used. All parameter values used in the k-ε closure are identical to those used by Warner et al. (2005a), except for the minimum eddy diffusivity and eddy viscosity values which were 5×10^{-6} m^2/s. The numerical method used to solve the equations of the turbulence closure is a semi-implicit method that results in tridiagonal positive-definite matrices in each water column and ensures that the turbulent variables remain positive (Deleersnijder et al., 1997).

3.3 Previous Applications

The TRIM3D model (Casulli and Cheng, 1992) and UnTRIM model have been applied previously to San Francisco Bay (Cheng and Casulli, 2002; MacWilliams and Cheng, 2007; MacWilliams and Gross, 2007; MacWilliams et al., 2007; MacWilliams et al., 2008; MacWilliams et al., 2009). The TRIM3D model (Casulli and Cattani 1994) which follows a similar numerical approach on structured horizontal grids has been widely applied in San Francisco Bay (e.g., Cheng et al. 1993; Cheng and Casulli, 1996; Gross et al., 1999; Gross et al., 2006), and a 2D version, TRIM2D, is used in San Francisco Bay Physical Oceanographic Real-Time System, SFPORTS (URL: http://sfports.wr.usgs.gov/sfports) (Cheng and Smith, 1998). Thus, the UnTRIM numerical approach has been well-tested in San Francisco Bay, and is very well suited to perform the types of analysis used in this study.

3.4 UnTRIM Bay-Delta Model

The UnTRIM San Francisco Bay-Delta model (UnTRIM Bay-Delta model) is a three-dimensional hydrodynamic model of San Francisco Bay and the Sacramento-San Joaquin Delta, which has been developed using the UnTRIM hydrodynamic model (MacWilliams et al., 2007; MacWilliams et al., 2008; MacWilliams et al., 2009). The UnTRIM Bay-Delta model extends from the Pacific Ocean through the entire Sacramento-San Joaquin Delta (Figure 3.4-1). The UnTRIM Bay-Delta model takes advantage of the grid flexibility allowed in an unstructured mesh by gradually varying grid cell sizes, beginning with large grid cells in the Pacific Ocean and

gradually transitioning to finer grid resolution in the smaller channels of the Sacramento-San Joaquin Delta (Figure 3.4-2). This approach offers significant advantages both in terms of numerical efficiency and accuracy, and allows for local grid refinement for detailed analysis of local hydrodynamics, while still incorporating the overall hydrodynamics of the larger estuary in a single model. The UnTRIM Bay-Delta model has been calibrated using water level, flow, and salinity data collected in San Francisco Bay and the Sacramento-San Joaquin Delta (MacWilliams et al., 2008; MacWilliams et al., 2009). Predicted water levels were compared to observed water levels at NOAA and DWR stations in San Francisco Bay, and DWR and USGS flow and stage monitoring stations in the Sacramento-San Joaquin Delta.

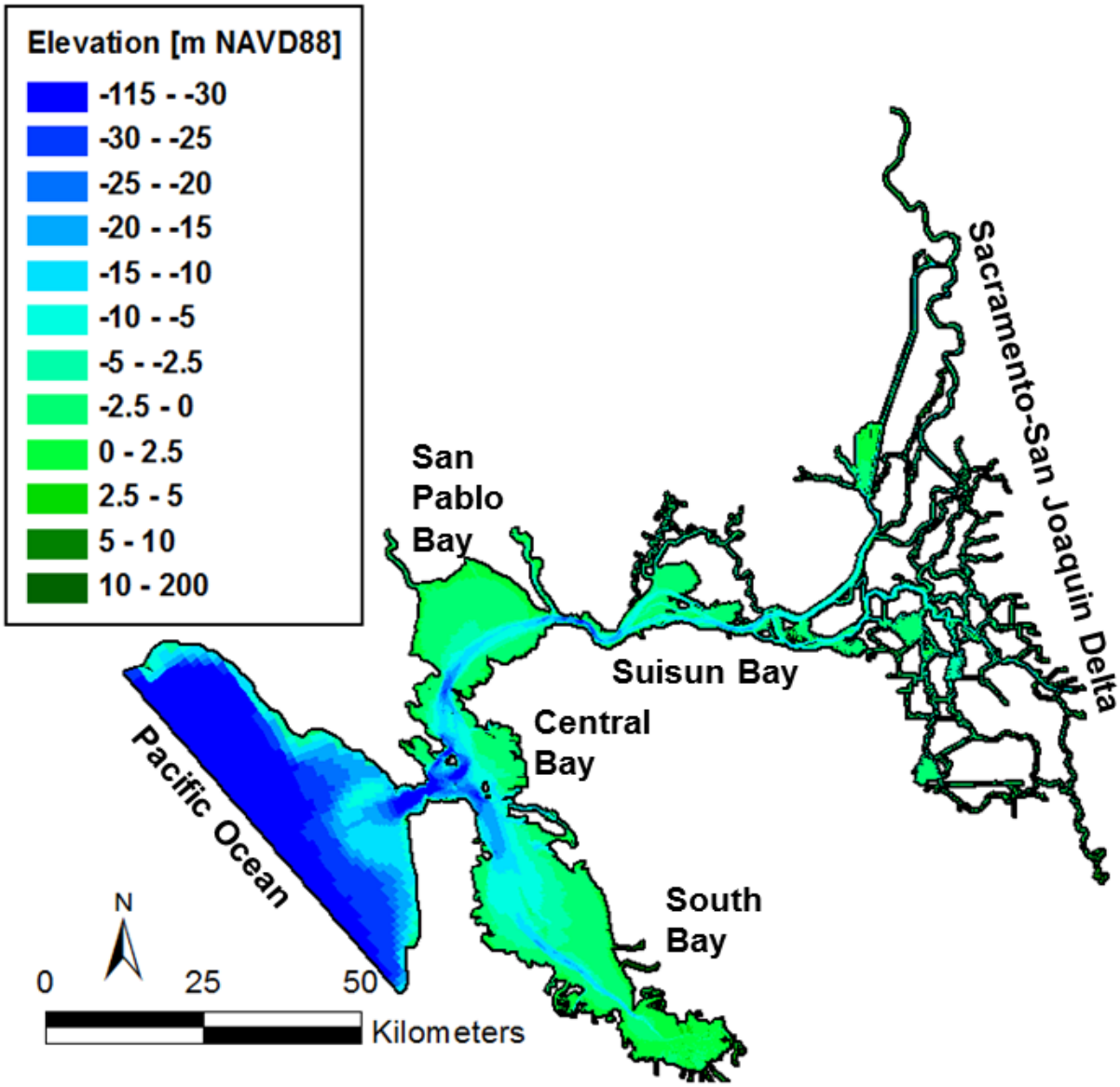

Figure 3.4-1. Model domain for the UnTRIM Bay-Delta model, showing the bed elevation in meters referenced to NAVD88.

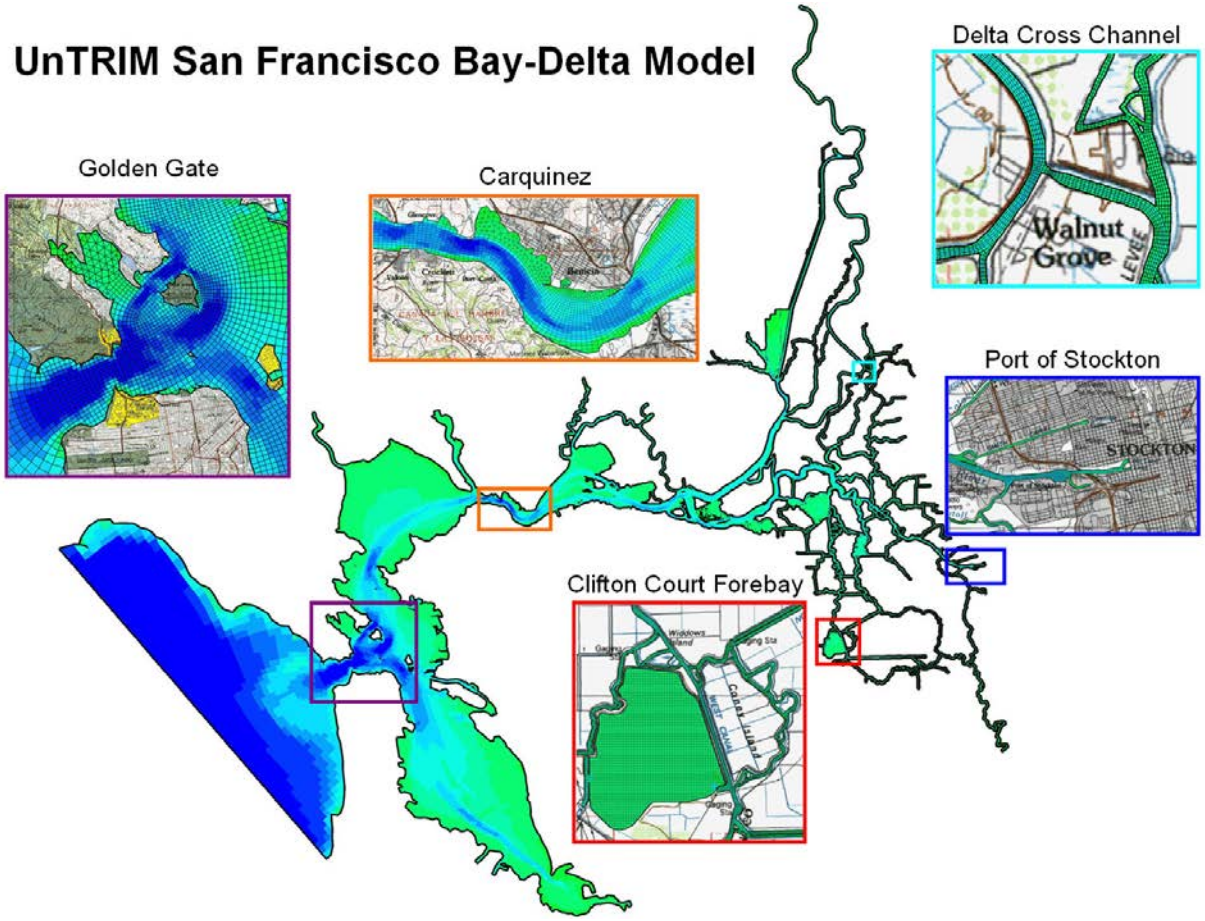

Figure 3.4-2. Model domain for the UnTRIM Bay-Delta model with insets showing the model grid in selected regions of the model domain.

3.5 South San Francisco Bay Model Grid and Bathymetry Refinements

The UnTRIM San Francisco Bay-Delta model was refined to include a high resolution model grid in the project area. The model grid was developed using the grid generator JANET (Lippert and Sellerhoff, 2007), and utilized quadrilateral cells aligned with the main channels in the project area. Pond and marsh areas were filled using triangular elements to allow for the grid to be exactly aligned to the levees surrounding each salt pond. The resulting model grid south of Dumbarton Bridge (Figure 3.5-1) includes a total of 134,895 horizontal grid cells. There are more horizontal grid cells South of Dumbarton Bridge in this mesh than were used in the entire grid of the San Francisco Bay-Delta by MacWilliams et al. (2009). The combined mesh which incorporates the high resolution Far South Bay model into the high resolution San Francisco Bay-Delta model consists of 269,962 horizontal grid cells and 1.8 million 3-D cells. This extremely high resolution mesh allows for resolution of detailed bathymetric features within the project area, including subtidal channels in the Alviso Island Ponds (Figure 3.5-2).

The UnTRIM San Francisco Bay-Delta model was also refined to include the most recent available high resolution bathymetric data in the project area. A high resolution DEM of the project area was developed by the USACE San Francisco District using the data sources shown in Figure 3.5-3. This DEM was applied to the high resolution mesh to provide the most accurate representation possible of the project area for this study.

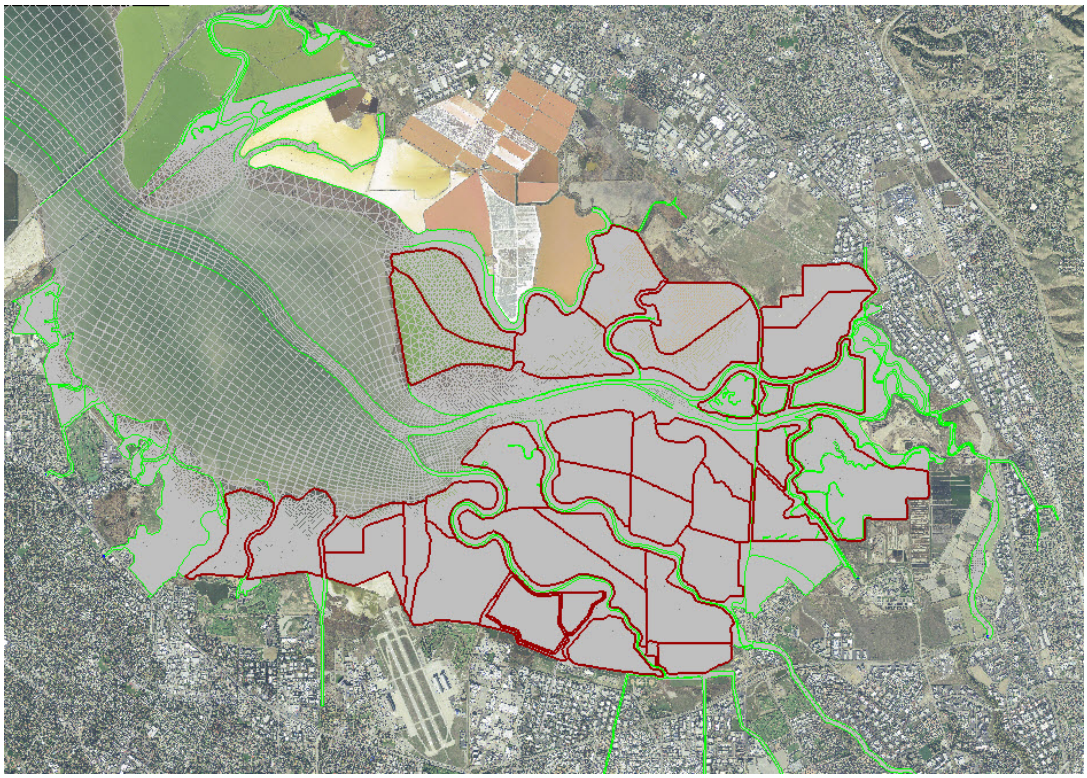

Figure 3.5-1 UnTRIM model grid for project area showing channel features (green) and levees (dark red) which are aligned with the model grid.

Figure 3.5-2 UnTRIM model grid in the vicinity of the Alviso Island ponds showing channel features (green) and levees (dark red) which are aligned with the model grid.

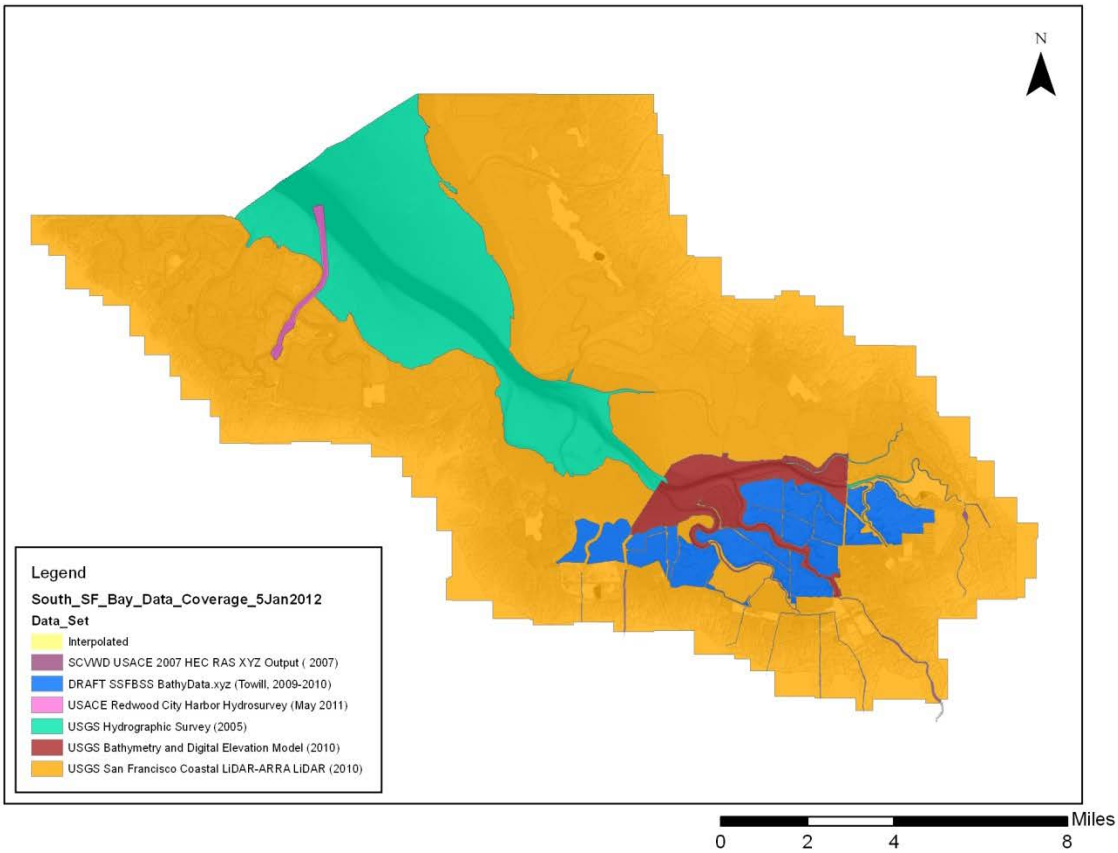

Figure 3.5-3 Data sets used in development of high resolution DEM of Far South San Francisco Bay (Source: USACE).

3.6 Model Boundary Conditions

A detailed description of all model boundary conditions applied in the UnTRIM Bay-Delta model is presented in MacWilliams et al. (2008) and MacWilliams et al. (2009). This section provides a brief overview of the model boundary conditions used in this study.

Observations of water surface elevation at the NOAA San Francisco (9414290) station were used as the tidal (ocean) boundary condition of the model domain. The San Francisco (9414290) station is the oldest tide station established in North America and is located in the Presidio near the southern end of the Golden Gate (see Figure 4.1-1). For simulation periods after January 1996, 6-minute observed water level data from San Francisco were filtered using a fourth order Butterworth filter with a cutoff frequency of 1/3 hours-1 to remove high frequency noise in the observed water levels. For periods prior to 1996, 6-minute water level data were not available, and hourly data from San Francisco were used instead. The observations were multiplied by an amplification factor to account for the difference in tidal range between observed San Francisco tides and tides along the model ocean boundary, and a phase lead of 49 minutes was applied to account for the phase difference between San Francisco and the model boundary, following the approach described in Gross et al. (2006). This approach has also been used by MacWilliams et al. (2008) and MacWilliams et al. (2009). The amplification factor and phase lag were updated during the model calibration; values were

selected to minimize the phase and amplitude difference between the observed and predicted water levels at San Francisco for the 2011 and 2005 calibration periods.

The river inflows to the model domain include both tributary inflows to the Delta, discharges from water pollution control plants, and other San Francisco Bay tributary inflows. At the landward boundaries of the Delta in the UnTRIM model, flow boundary conditions were applied to account for the primary freshwater inflows to San Francisco Bay from the Delta. Delta inflow values were obtained from daily averaged flows estimated at several locations in the Delta by the DAYFLOW program, made available by the California Department of Water Resources (CDWR, 1986). In addition to the Delta freshwater inflows, freshwater inflow from several rivers, creeks and water pollution control plants (WPCPs) are included in the simulations. The additional inflows considered in the simulations are Napa River, Sonoma Creek, Petaluma River, Novato River, San Lorenzo Creek, Alameda Creek, San Francisquito Creek, Matadero Creek, Saratoga Creek, Guadalupe River, Coyote Creek, and flows from the San Jose/Santa Clara WPCP.

Wind forcing was applied at the water surface as a wind stress. The wind drag coefficient is varied based on local wind speed according to the formulation of Large and Pond (1981). For simulations after 1990, observed hourly wind speed and direction from the Bay Area Air Quality Control District (BAAQCD) from five locations were used to account for spatial variability in wind velocities. Observed hourly wind data from San Carlos was used in South San Francisco Bay, observed hourly wind data collected at Point San Pablo was used in Central San Francisco Bay and San Pablo Bay, and observed hourly wind data at Pittsburg was used in Carquinez Strait and Suisun Bay. These stations were selected because they are considered to be the stations which provide measurements most representative of wind speeds over water, and because they provide a geographic distribution of wind speed and direction over the Bay. Observed hourly wind data at Rio Vista was used in the northern portion of the Delta, and observed hourly data at Bethel Island was used in the central and southern portions of the Delta. For the two 1983 simulation periods, wind observation data from the BAAQMD were not available. For this simulation period, observed wind speed and direction from San Francisco International Airport (NOAA, 1993) was used uniformly over the model domain.

3.7 Model Uncertainty

As discussed above, the TRIM and UnTRIM models have been widely used in San Francisco Bay, and numerous detailed model calibrations have been performed (e.g., Cheng et al., 1993; Gross and Schaaf & Wheeler, 2003; Gross et al., 2006; MacWilliams and Cheng, 2007; MacWilliams and Gross, 2007; MacWilliams et al., 2008; MacWilliams et al., 2009). Due to this extensive history of application, these models are the best established three-dimensional models of San Francisco Bay.

The equations governing fluid motion and salt transport, representing conservation of water volume, momentum and salt mass, are well established, but cannot be solved analytically for complex geometry and boundary conditions. Therefore numerical models are used to give approximate solutions to these governing equations. Many decisions are made in constructing and applying these numerical models. The governing equations are first chosen to represent

the appropriate physical processes in one, two or three-dimensions and at the appropriate time scale. Then these governing equations that describe fluid motion and salt transport in a continuum are discretized giving rise to a set of algebraic equations. The resulting discretized algebraic equations must be solved, often requiring the use of an iterative matrix solver. The discretization and matrix solution must be developed carefully to yield a numerical scheme that is consistent with the governing equations, stable and efficient. To apply the models, the bathymetric grid, boundary conditions, initial conditions and several model parameters must be specified. The accuracy of the model application depends on the appropriate choice of these inputs, including site-specific parameters, the numerical scheme for solving the governing equations, and the associated choice of time step and grid size.

The three-dimensional model applied in this project provides a more detailed description of fluid motion in San Francisco Bay than depth-averaged or one-dimensional models. The UnTRIM model, like almost all large scale hydrodynamic models, averages over the turbulent time scale to describe tidal time scale motions. The resulting three-dimensional hydrodynamic models represent turbulent mean motions as a result of small scale turbulent mixing of momentum and salt, parameterized by eddy viscosity and eddy diffusivity, respectively. These turbulent mixing coefficients are estimated from the tidal flow properties (velocity and density) by “turbulence closure” models embedded within the three-dimensional hydrodynamic models. Three-dimensional models estimate the variability in velocity and salinity in all three dimensions and through time-space over several tidal cycles, thereby providing a detailed description of the variations of hydrodynamics and salinity in both space and time. However, several sources of uncertainty are inherent in the application of these three-dimensional models:

- Spatial resolution/computational cost – the spatial discretization of the bathymetry of the model domain, and velocity and salinity distributions, is limited by the large computational expense associated with high-resolution models. The description of the Bay-Delta bathymetry is improved by the use of a flexible unstructured grid, with coarser grid resolution used in the bay portions of the grid and increasing grid resolution in the Delta and in the SSFBSS project area to optimize computational efficiency.
- Bathymetry data – limited spatial coverage and accuracy of bathymetry data can be a substantial source of uncertainty. Converting all data to a uniform vertical datum and horizontal datum can lead to some error. In particular, LiDAR data may have substantial errors in vertical datum and removing vegetation from the dataset can be difficult. Foxgrover et al. (2011a) report that the “bare earth” LiDAR data in Corte Madera Marsh were on average 0.23 m (0.75 ft) higher than elevations obtained by Real Time Kinematic (RTK) GPS measurements. In the present application, bathymetric data from multiple sources, including LiDAR measurements, were merged to develop the model bathymetry (Figure 3.5-3). The merging of these different data sets can also introduce some potential errors.
- Site-specific parameters – the UnTRIM model requires bottom friction coefficients to parameterize the resistance to flow at solid boundaries. These parameters are specified and adjusted in model calibration. The values used in the present application are similar to those applied in several recent applications (e.g., MacWilliams et al., 2007; MacWilliams et al., 2008; MacWilliams et al., 2009).

- Turbulence closure – the effect of turbulent motions on the tidal time scale motions is parameterized by a turbulence closure. While many turbulence closures are available (e.g., Warner et al., 2005a), this is an ongoing area of research and, particularly in stratified settings, the effect of turbulence on tidal flows and salinity is not easy to estimate accurately. Different turbulence closures may give significantly different results in stratified settings (e.g., Stacey, 1996).
- Numerical errors – a numerical method approximates the governing equations to some level of accuracy. The mathematical properties of the numerical method of the TRIM and UnTRIM models are well understood due to detailed mathematical analysis presented in several peer reviewed publications. While the stability and conservation properties of the method are ideal, a remaining source of error in the numerical method is some limited numerical diffusion of momentum, which may cause some damping of tidal propagation.
- Boundary conditions and initial conditions – The salinity in San Francisco Bay varies laterally (e.g., Huzzey et al., 1990) but this lateral variability cannot be described by existing observations. In addition, only limited observations are available to describe the vertical distribution of salinity. Therefore, lateral and vertical salinity distributions must be achieved by interpolation and extrapolation from the limited observations to obtain initial salinity fields. Inflows to the estuary are also quite uncertain in several regions due to un-gauged portions of watersheds and uncertainty in estimates of outflows and diversions in the Sacramento-San Joaquin Delta.

Though additional potential sources of uncertainty can be identified, the largest sources of uncertainty for hydrodynamic predictions are the accuracy and resolution of available bathymetry and the grid resolution used to represent this bathymetry in the model. This study makes use of the best available high resolution bathymetric data, and the finest computationally practical grid resolution throughout the SSFBSS project area. However, many of the available bathymetry data sets in other portions of the San Francisco Bay are fairly old and they required vertical and or horizontal coordinate transformations for the grid used in this project. In the SSFBSS project area, bare earth LiDAR data was used in many of the marsh and mudflat areas (Figure 3.5-3). The use of LiDAR data for bathymetry introduces significant uncertainty in the bathymetric representation, particularly for vegetated marshes. Foxgrover et al. (2011a) report that the “bare earth” LiDAR data in Corte Madera Marsh were on average 0.23 m (0.75 ft) higher than elevations obtained by RTK GPS measurements.

4. South San Francisco Bay Model Calibration and Verification

The model calibration and validation for the South San Francisco Bay Shoreline Study (SSFBSS) focuses on the prediction of water levels in South San Francisco Bay. The UnTRIM San Francisco Bay-Delta model was calibrated using observed water level data during periods with the most extensive concurrently available water level observations in the project area in 2005 and 2011. The model was then validated using peak water level data from five separate storm periods between 1983 and 2006. The model grid for the 2006 and 2011 simulations was adjusted to account for the breaching of the Alviso Island pond levees in March 2006, and the breaching of the Pond A6 in December 2010.

4.1 Model Calibration and Validation Approach

Water level observations are available for the model calibration and validation periods at between two and twelve NOAA observation stations (NOAA, 2012), as shown in Table 4.1-1. Observation data collected as part of the 2005 hydrographic survey of South San Francisco Bay (Foxgrover et al., 2007) were also available at two additional stations in Alviso slough and Artesian Slough. The periods in 2005 and 2011 have the most extensive spatial availability of water level observations, however neither of these periods contain a large storm event. The 2005 and 2011 periods were selected for model calibration (Section 4.2), and the model was validated for six storm periods (Section 4.3). The locations of the observation stations listed in Table 4.1-1 are shown on Figure 4.1-1 and Figure 4.1-2.

Table 4.1-1. Available observations for each model simulation period at tide stations maintained by NOAA in San Francisco Bay. Locations are shown in Figure 4-1.1.

LOCATION	NOAA Station	January 1983	December 1983	December 1997	February 1998	March 2005	December 2006	2011
San Francisco	9414290	x	x	x	x	x	x	x
San Mateo Bridge	9414458	x				x		
Dumbarton Bridge	9414509					x		x
Redwood City	9414523		x	x	x	x	x	x
Gold Street Bridge, Alviso Slough	9414551					x		
Coyote Creek	9414575		†			x		x
San Leandro Marina	9414688					x		
Alameda	9414750	x		x	x	x	x	x
Richmond	9414863			x	x	x		x
Port Chicago	9415144	x		x	x	x	x	x
Artesian Slough	none					x		
Coyote Creek Railroad Bridge	none					x		

† Maximum observed water level only.

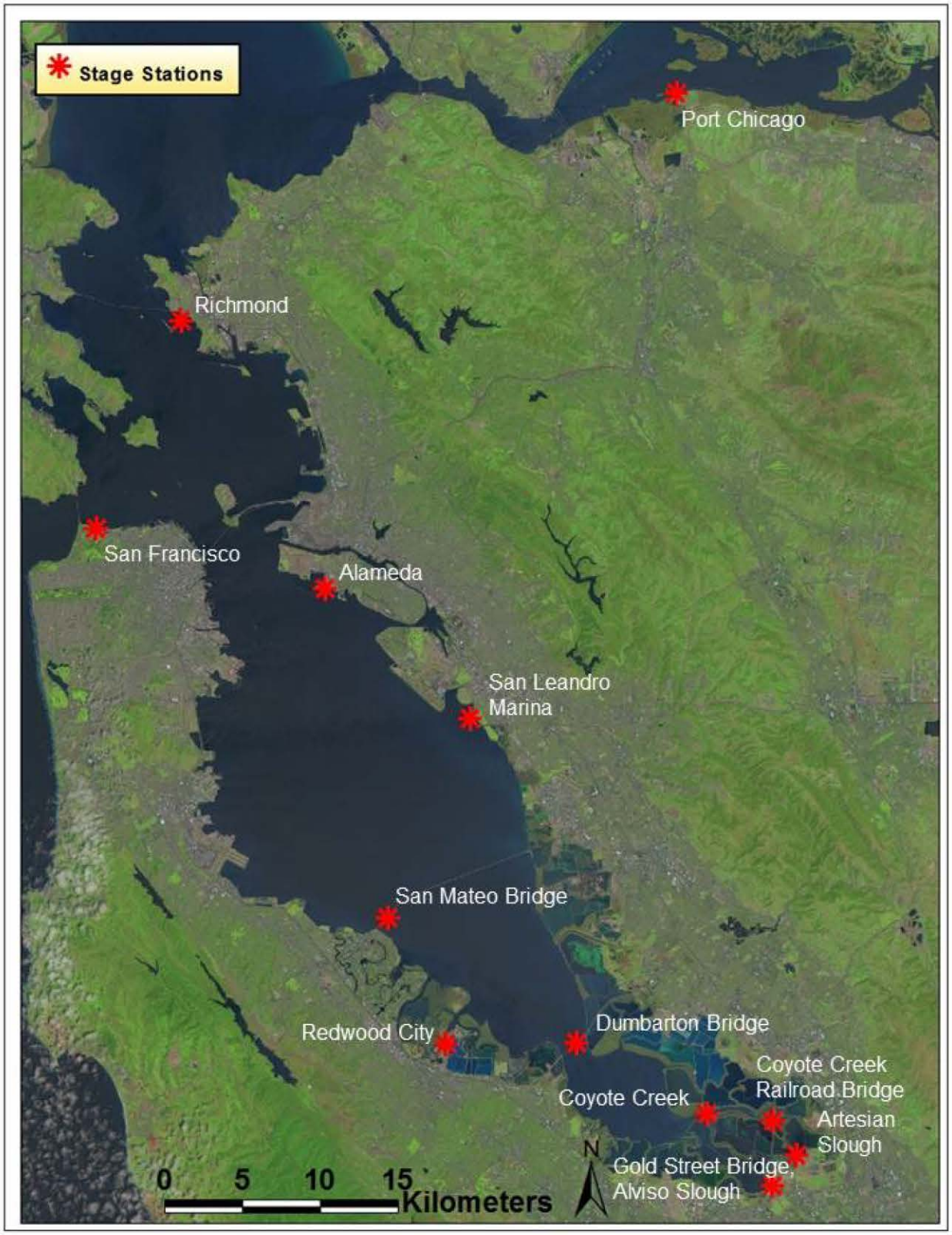

Figure 4.1-1 Water level stations around the San Francisco Bay used for model calibration.

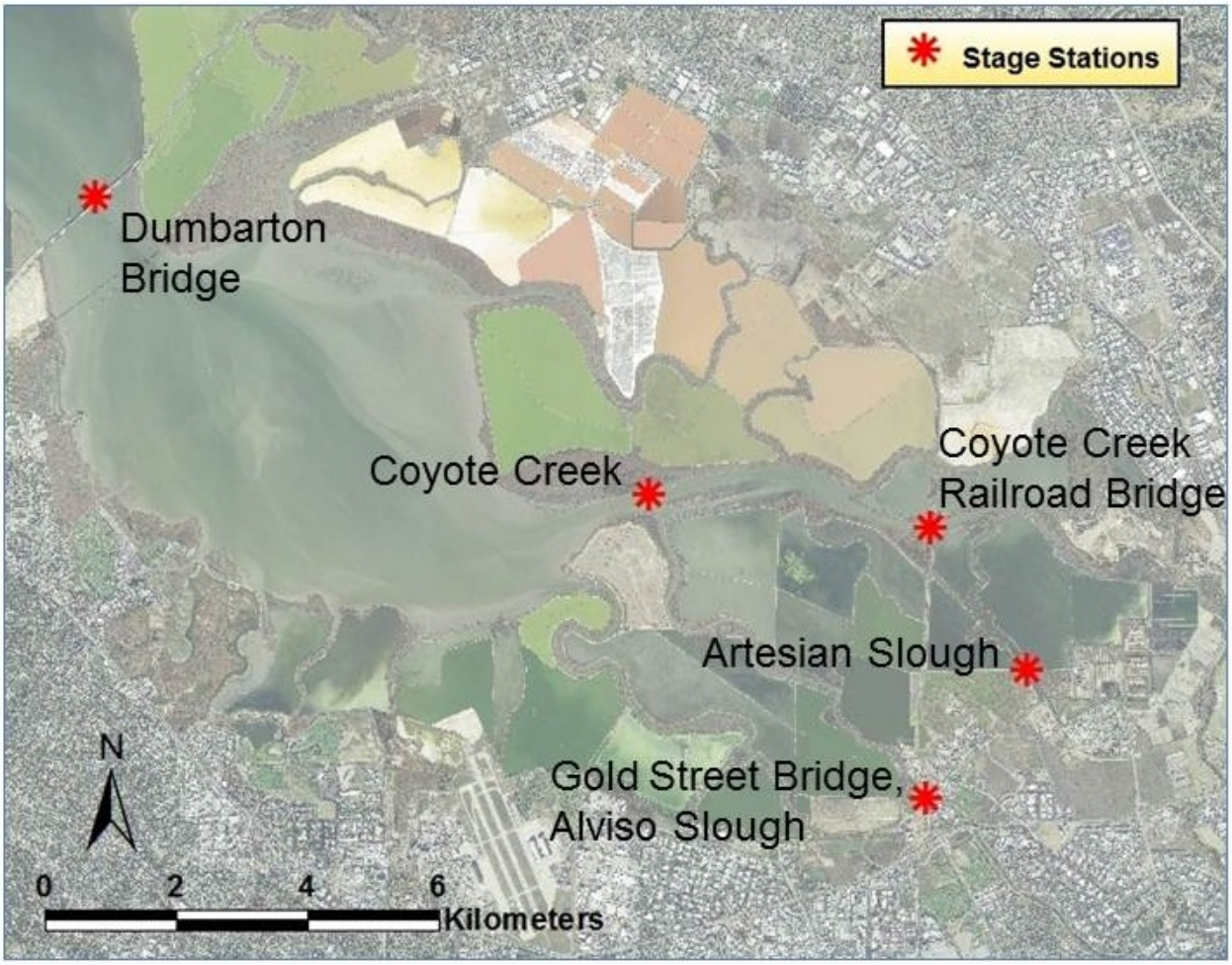

Figure 4.1-2 Locations of Far South San Francisco South Bay water level stations.

All water level observation data were converted to the North American Vertical Datum of 1988 (NAVD88). Table 4.1-2 shows the datum conversions used for each station where datum conversions were necessary for the comparisons made in this study. When available, reported datum conversions at the NOAA stations were used. Three historic NOS stations have not yet been updated to the NAVD88 geodetic datum as part of the National Geodetic Survey (NGS) Height Modernization efforts; these are referenced to the Mean Lower Low Water (MLLW) tidal datum for the 1983 to 2001 tidal epoch. For these three stations San Mateo Bridge (9414458), Dumbarton Bridge (9414509), and Redwood City (9414523)—the surveyed values of MLLW and NAVD88 provided by Foxgrover et al. (2007) were used to convert the NOAA data to the geodetic datum (NAVD88). As part of a 2005 Hydrographic Survey of the South San Francisco Bay, the USGS collected water level data at two NOAA stations—Alviso Slough at Gold Street Bridge (9414551) and the PG&E Tower in Coyote Creek (9414575)—as well as two additional locations in Artesian Slough and on the Coyote Creek Railroad Bridge (locations shown in Figure 4-1.2). Datum conversions to NAVD88 provided by Foxgrover et al. (2007) were also used for these stations. Observed water level data were collected by the USACE during 2011 at Dumbarton Bridge (9414509) and at Coyote Creek at Alviso (9414575). These data were provided by the USACE referenced to NAVD88.

Table 4.1-2. Datum Conversions.

Station Name	Station Number	MLLW to NAVD88 Offset		Station to NAVD88 Offset		Data Source
		(m)	(ft)	(m)	(ft)	
San Francisco	9414290	0.018	0.06	-1.804	-5.92	NOAA tides and currents
Alameda	9414750	-0.070	-0.23	-1.086	-3.56	NOAA tides and currents
Port Chicago	9415144	0.335	1.10	-0.880	-2.89	NOAA tides and currents
San Mateo Bridge	9414458	-0.228	-0.75	4.712	15.46	Foxgrover et al., 2007
Redwood City	9414523	-0.326	-1.07	2.376	7.80	Foxgrover et al., 2007
Dumbarton Bridge	9414509	-0.377	-1.24	4.055	13.30	Foxgrover et al., 2007
Coyote Creek	9414575	-0.457	-1.50	--	--	Foxgrover et al., 2007

The quality of fit between the water levels predicted by the model and observed stage time series data are assessed following a cross-correlation procedure similar to that used by RMA (2005). This approach has also been used by MacWilliams and Gross (2007), MacWilliams et al. (2008), and MacWilliams et al. (2009) and provides a thorough description of the differences between time series records through a quantitative measure of differences in terms of phase, mean, amplitude, and constant offsets. Statistical properties are derived to quantify the differences between model simulated (predicted) and observed time series data. Five types of statistics are presented in this report:

- Mean – Comparison of simple mean values of the predicted and observed time series.

- Phase Shift – The average shift in time between the predicted and observed time series.

- Amplitude Ratio – Comparison of the time series range, which ideally would equal to 1. This value is estimated after removing the phase shift between predicted and observed time series.

- Coefficient of Determination, R^2 – The correlation coefficient (R), is a measure of the correlation between the model simulated (subscript *model*) and observations (subscript *obs*) values,

$$R = \frac{\sum\left(X_{model} - \overline{X_{obs}}\right)\left(X_{obs} - \overline{X_{obs}}\right)}{\left[\sum\left(X_{model} - \overline{X_{model}}\right)^2 \sum\left(X_{obs} - \overline{X_{obs}}\right)^2\right]^{1/2}} \qquad (4\text{-}1)$$

where X is the variable being compared, and $\overline{X}$ is the time average of X over the simulated time period. The correlation coefficient measures the strength and the direction of a linear relationship between the model predictions and the observations. The value of the correlation coefficient, R, ranges from -1.0 (perfect negative correlation) to 1.0 (perfect positive correlation), with a value of 0.0 indicating no

correlation. A perfect correlation occurs when all of the data points lie exactly on a straight line. The coefficient of determination, R^2, is a measure of the goodness of fit, i.e., how well the linear regression represents the data and gives the proportion of the variance of the observations that is predictable from the model. For $R^2 = 0.90$, 90 percent of the total variation in the observations can be explained by the model. Note that R^2 is a measure of the scatter around a best-fit line, on the scatter plots.

• Skill – Willmott (1981) defined the predictive skill based on the quantitative agreement between observations (subscript *obs*) and model predictions (subscript *model*) as

$$Skill = 1 - \frac{\sum \left| X_{model} - X_{obs} \right|^2}{\sum \left(\left| X_{model} - \overline{X_{obs}} \right| + \left| X_{obs} - \overline{X_{obs}} \right| \right)^2} \qquad (4\text{-}2)$$

where *X* is the variable being compared, and $\overline{X}$ is the time average of X over the simulated time period. Perfect agreement between model results and observations yields a skill of 1.0 and complete disagreement results in a skill of 0.0. This measurement of model skill has been used in a range of estuarine modeling studies (e.g., Warner et al., 2005b).

For each stage time series comparison, three different plots are shown on each figure. The top plot shows the tidal time scale variations for a period of up to fifteen days. On the lower left, a tidally-averaged plot is shown for the full analysis period to evaluate spring-neap and longer time scale variability, as well as non-tidal forcing such as storm surge. Tidal averages are computed by filtering twice using a 24.75 hour running average filter. On the lower right, the scatter plot shows a comparison between the observed and predicted data over the analysis period. The scatter plot is produced by first running a cross-correlation between the observed data and model predictions to find the average phase lag over the entire record. The cross-correlation was performed following the procedure outlined by RMA (2005). The process entails repeatedly shifting the predicted time series record at one minute increments relative to the observed time series and computing the correlation coefficient at each time shift. The correlation has a maximum value when the shifted model time series best matches the observed time series. The time shift when the maximum correlation occurs represents the phase difference in minutes between the predicted and observed data, with positive values indicating that the predicted time series lags the observed time series. The linear regression is then performed between the time shifted model results and observed data record to yield the amplitude ratio, best-fit line, the coefficient of determination, and model skill. A summary of the resulting statistics are reported on each scatter plot include the following:

• Mean Obs – Average value of observed time series for the analysis period

• Mean Pred – Average value of predicted time series for the analysis period

• Lag – Phase difference in minutes between observed and model predicted time series; a positive value indicates that the predicted time series lags behind the observed time series.

• Y = slope*X + offset – Best linear fit, where Y is model predicted, X is observed values. The slope value is used as the amplitude ratio.

• R^2 – coefficient of determination calculated using Equation 4-1.

• Skill – The model skill score (Wilmott, 1981) calculated using Equation 4-2.

The observed and predicted means, phase lag, amplitude ratio, and R^2 value, and model skill are also summarized in tables for each simulation period in the following sections.

4.2 Simulation Periods for Model Calibration

During 2011, water level data was collected by the USACE at Dumbarton Bridge (9414509) and at Coyote Creek near Alviso Slough (9414575). During this data collection period, the highest observed water level at the San Francisco station (9414290) occurred on May 17, 2011. Figure 4.2-1 shows the astronomical tides[1] developed from tidal harmonic constituents, observed water levels, and the residual, which is defined as the difference between the observed and astronomical water levels, at the San Francisco station (9414290) for the 2011 calibration period. On May 17, the peak observed water level at the San Francisco station (9414290) was 2.307 m NAVD88, and the peak tidal residual was 0.298 m. The 2011 calibration period was selected to include this peak, and spans from May 10, 2011 through June 9, 2011 (Figure 4.2-1). The model grid for the 2011 simulation was adjusted to account for the breaching of the Alviso Island pond levees in March 2006, and the breaching of the Pond A6 in December 2010.

As part of a 2005 Hydrographic Survey of the South San Francisco Bay (Foxgrover et al., 2007), water level data was collected at four stations in South San Francisco Bay during March and April of 2005 (Table 4.2-1). The 2005 calibration period was selected to span the period of the 2005 hydrographic survey when water level observations were collected at these stations. Therefore the 2005 model calibration spans from March 7, 2005 through April 6, 2005. Figure 4.2-2 shows the astronomical tides developed from tidal harmonic constituents, observed water levels, and the residual, at the San Francisco station (9414290) for the 2005 calibration

[1] In the comparison between observed (measured) water levels and simulated water levels (predicted) using UnTRIM (e.g., Figure 4.3-1), the nomenclature used in this report refers to the measured water levels as "observed" and the modeled water levels as "predicted." At the standard measurement stations, NOAA reports observed water levels as either "'preliminary" or "verified" and also reports a "predicted" water level. In this context the NOAA "predicted" water levels refer to the astronomical tides predicted from tidal harmonic constituents. Using this approach the astronomical tide is represented as the average water level plus a sum of terms for each tidal constituent. To avoid confusion between the NOAA "predicted" water levels and the water levels predicted by the numerical simulation, the model predictions are always referred to in this report as "predicted" and the water levels predicted using the harmonically derived constants are referred to as "astronomical" tides.

period. During this period, the peak observed water level at San Francisco (9414290) occurred on March 8, with a peak observed water level of 1.91 m NAVD88, and the peak tidal residual during this period was 0.301 m.

Table 4.2-1 Water Level data collection stations and date ranges from 2005 hydrographic survey of South San Francisco Bay (Foxgrover et al., 2007).

Location	NOAA Station	Date Collection Dates	File Name (.tid)
Coyote Creek	9414575	03/07/05 to 03/19/05	Coycrkearlymarch05
		03/20/05 to 03/31/05	Coycrklatemarch05
		04/01/05 to 04/06/06	Coycrkapril05
Coyote Creek Railroad Bridge	none	03/21/05 to 03/31/05	Rrbmarch05
		04/01/05 to 04/05/05	Rrbapril05
Artesian Slough	none	03/21/05 to 03/23/05	Artesiansloughmar05
Gold Street Bridge, Alviso Slough	9414551	04/01/05 to 04/05/05	Alvisoapril05

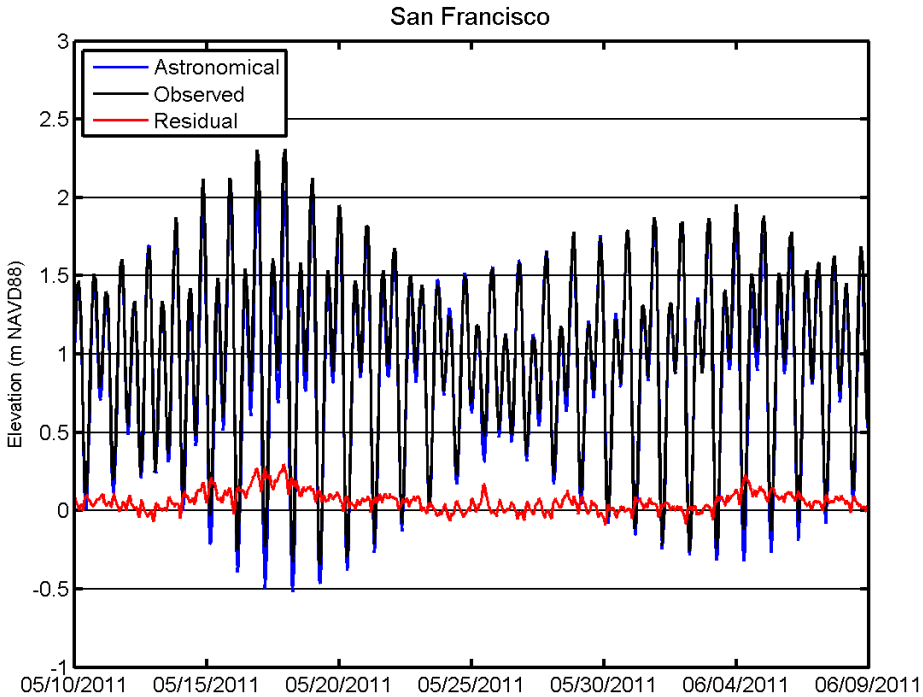

Figure 4.2-1 Astronomical tides, observed tides, and residual storm surge at San Francisco NOAA tide station (9414290) for the 2011 calibration period.

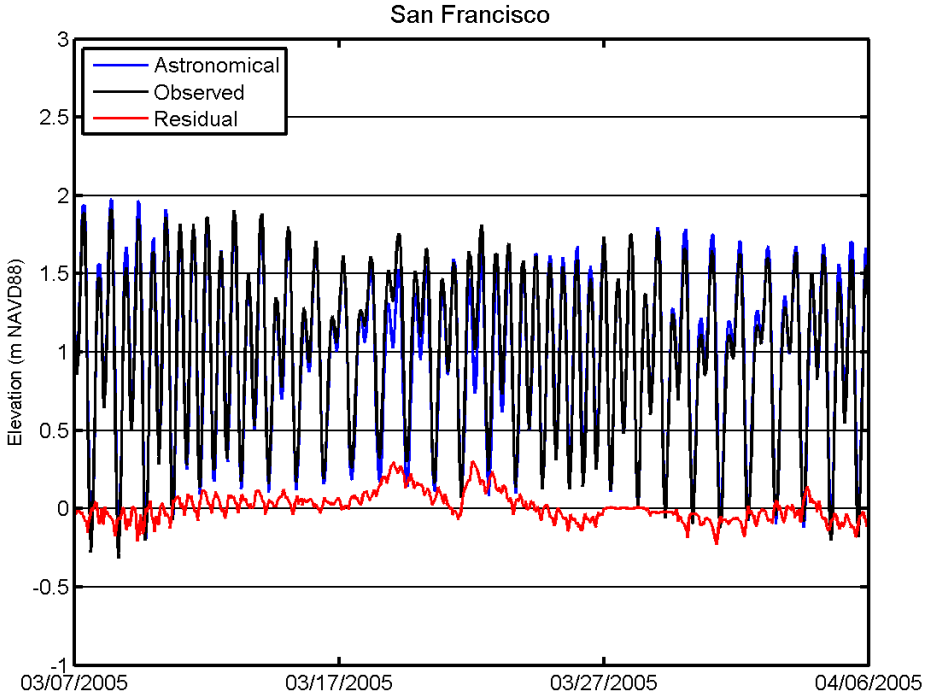

Figure 4.2-2 Astronomical tides, observed tides, and residual storm surge at San Francisco NOAA tide station (9414290) for the March 2005 calibration period.

4.3 Results of Model Calibration

This section presents the model calibration results for the 2011 and 2005 simulation periods. For each simulation period the model results were assessed using the cross-correlation procedure described in Section 4.1.

4.3.1 Model Calibration for 2011 Simulation period

During the 2011 simulation period, water level comparisons were made at seven stations in San Francisco Bay (Table 4.3-1). Water level comparisons were made at San Francisco (9414290) (Figure 4.3-1), Alameda (9414750) (Figure 4.3-2), Richmond (9414863) (Figure 4.3-3), Port Chicago (9415144) (Figure 4.3-4), Redwood City (9414523) (Figure 4.3-5), Dumbarton Bridge (9414509) (Figure 4.3-6), and Coyote Creek (9414575) (Figure 4.3-7). Predicted mean water levels are within 0.03 m of observed mean water levels at all seven stations during the simulation period. The values of the coefficient of determination between observed and predicted water levels are between 0.991 and 0.997, and the model skill values are between 0.996 and 0.999. The observed and predicted peak water level at each station is shown in Table 4.3-2. With the exception of Port Chicago, the predicted peak water levels during the 2011 simulation period are within 0.05 m (0.16 ft) of observed peak water levels at the remaining 6 stations. The predicted peak water level at Dumbarton Bridge during the 2011 simulation period is within 0.02 m (0.07 ft) of the observed peak water level, and the predicted peak water level at Coyote Creek during the 2011 simulation period is within 1 cm (0.04 ft) of the observed peak water level.

Table 4.3-1 Model calibration results and cross-correlation statistics for the 2011 simulation period.

Station Location	Mean Water Level			Amplitude Ratio	Lag (min)	Coefficient of Determination	Skill	Figure Number
	Observed (m)	Predicted (m)	Difference (m)					
San Francisco	0.96	0.96	0.00	1.02	-1	0.997	0.999	4.3-1
Alameda	0.97	1.01	0.04	1.02	15	0.997	0.998	4.3-2
Richmond	1.01	1.02	0.01	1.00	4	0.996	0.999	4.3-3
Port Chicago	1.19	1.22	0.03	0.96	9	0.991	0.996	4.3-4
Redwood City	1.03	1.02	-0.01	0.98	11	0.996	0.999	4.3-5
Dumbarton Br.	1.02	1.02	0.00	0.98	7	0.996	0.999	4.3-6
Coyote Creek	1.09	1.07	-0.02	0.97	6	0.995	0.998	4.3-7

Table 4.3-2 Model calibration results of peak water levels for the 2011 simulation period.

Station Location	Maximum Water Level (m NAVD88)			Maximum Water Level (ft NAVD88)		
	Observed (m)	Predicted (m)	Difference (m)	Observed (ft)	Predicted (ft)	Difference (ft)
San Francisco	2.31	2.29	-0.02	7.58	7.51	-0.07
Alameda	2.44	2.49	0.05	8.01	8.17	0.16
Richmond	2.37	2.37	0.00	7.78	7.78	0.00
Port Chicago	2.32	2.41	0.09	7.61	7.91	0.30
Redwood City	2.75	2.70	-0.05	9.02	8.86	-0.16
Dumbarton Br.	2.76	2.74	-0.02	9.06	8.99	-0.07
Coyote Creek	2.84	2.83	-0.01	9.32	9.28	-0.04

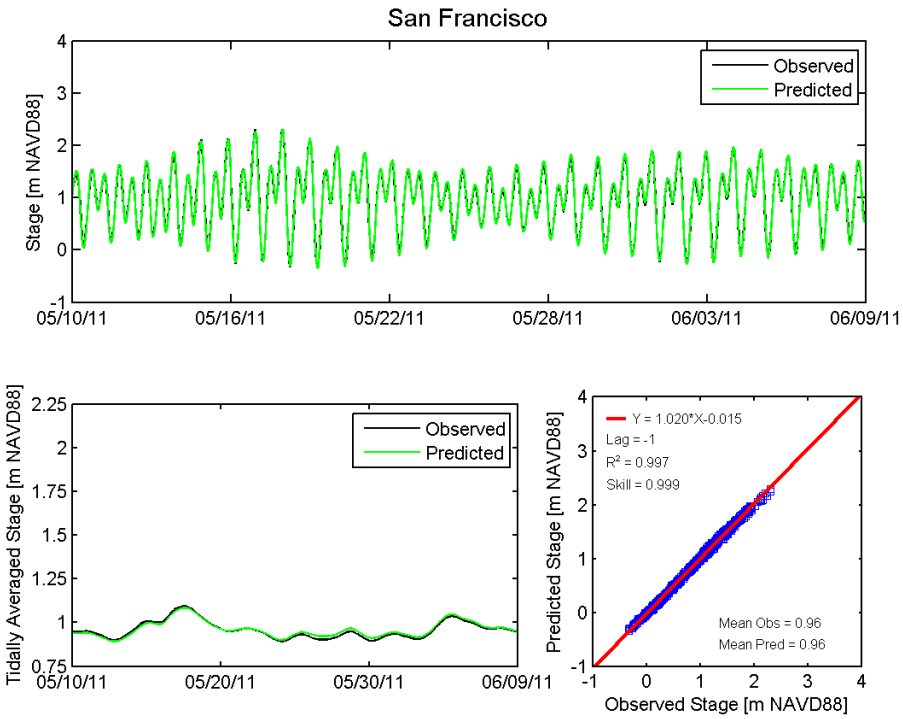

Figure 4.3-1 Observed and predicted stage at San Francisco NOAA tide station (9414290) during thirty days of the 2011 simulation period.

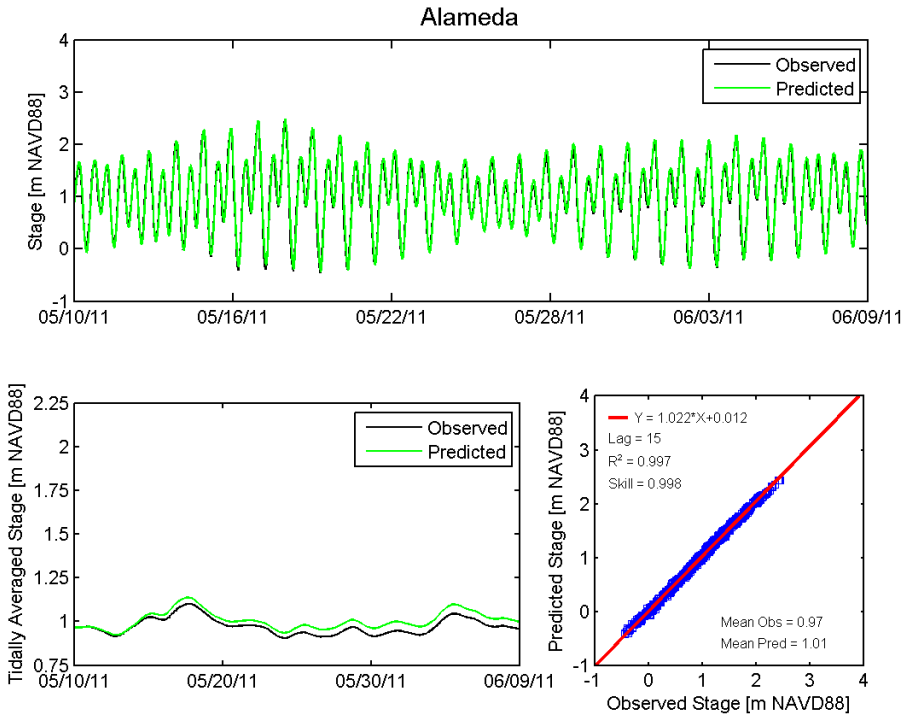

Figure 4.3-2 Observed and predicted stage at Alameda NOAA tide station (9414750) during thirty days of the 2011 simulation period.

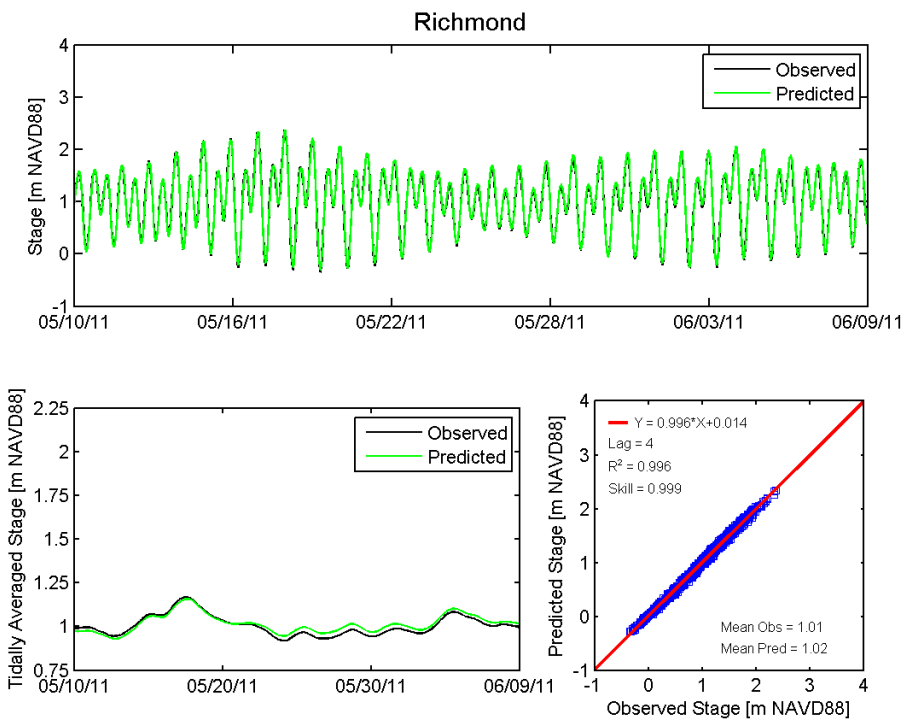

Figure 4.3-3 Observed and predicted stage at Richmond NOAA tide station (9414863) during thirty days of the 2011 simulation period.

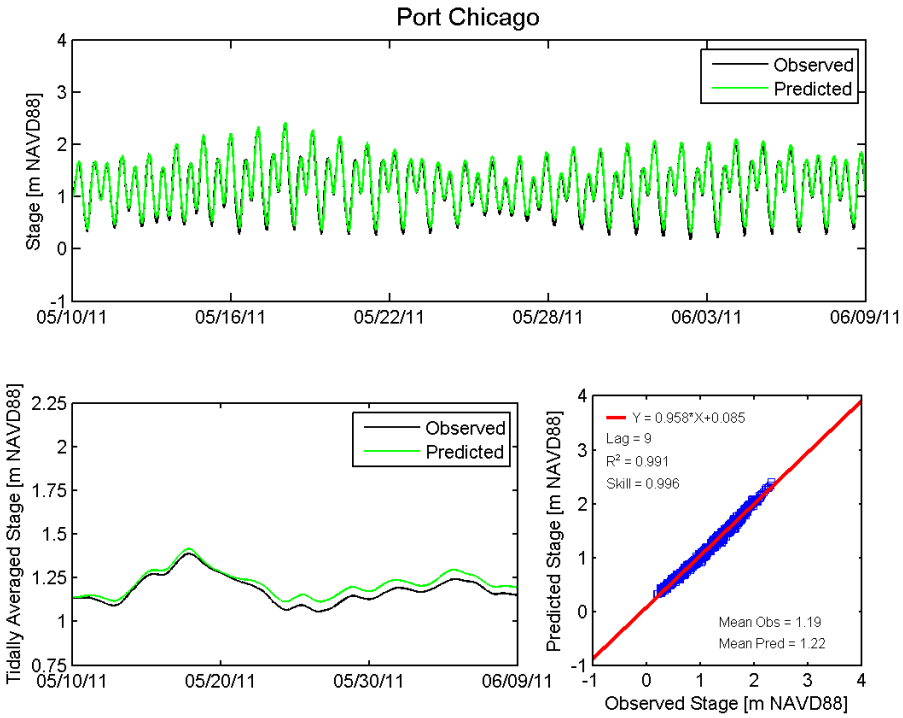

Figure 4.3-4 Observed and predicted stage at Port Chicago NOAA tide station (9415144) during thirty days of the 2011 simulation period.

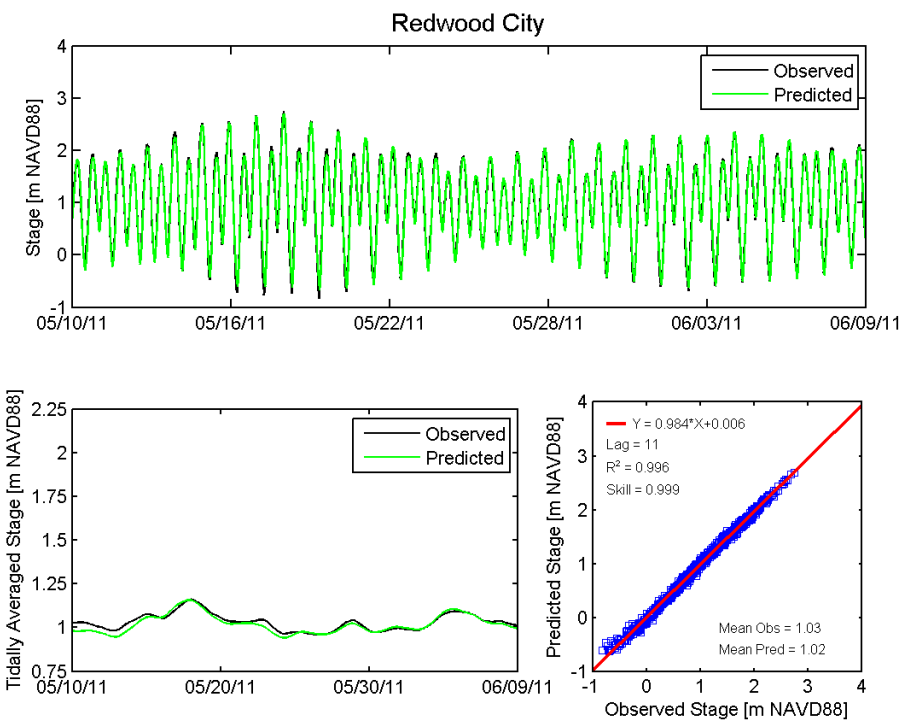

Figure 4.3-5 Observed and predicted stage at Redwood City NOAA tide station (9414523) during thirty days of the 2011 simulation period.

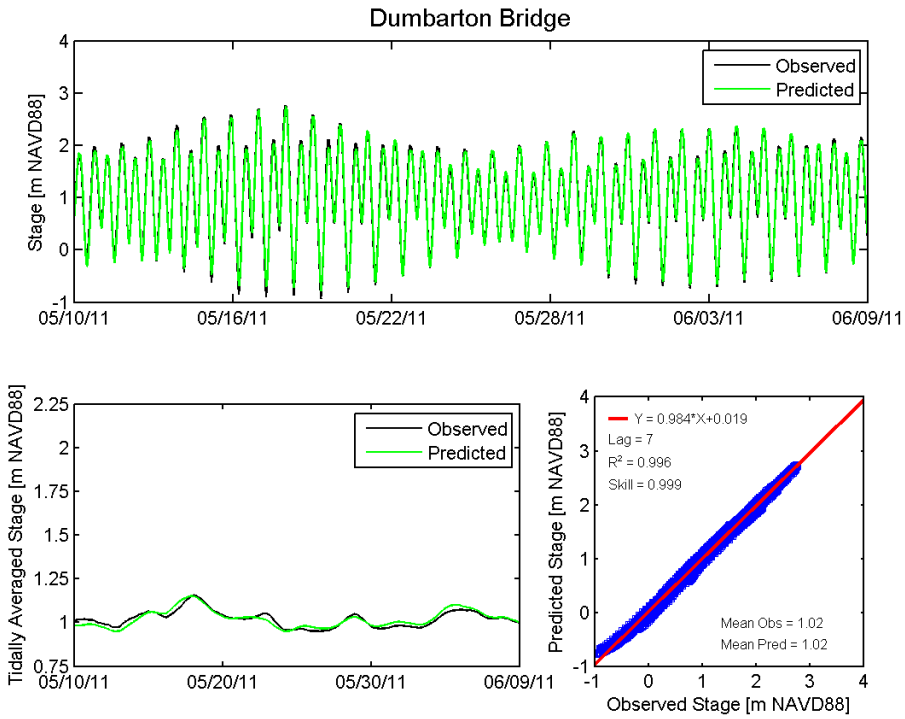

Figure 4.3-6 Observed and predicted stage at Dumbarton Bridge NOAA tide station (9414509) during thirty days of the 2011 simulation period.

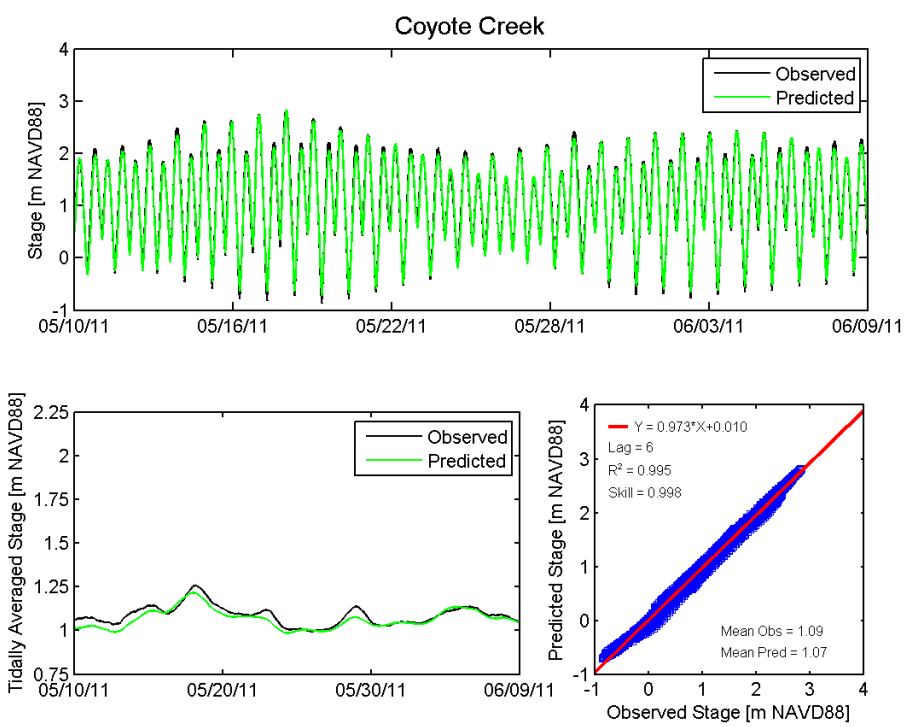

Figure 4.3-7 Observed and predicted stage at the Coyote Creek NOAA tide station (9414575) during thirty days of the 2011 simulation period.

4.3.2 Model Calibration for 2005 Simulation period

During the 2005 simulation period, water level comparisons were made at eleven stations in San Francisco Bay. Water level comparisons were made at San Francisco (9414290) (Figure 4.3-8), Alameda (9414750) (Figure 4.3-9), Richmond (9414863) (Figure 4.3-10), Port Chicago (9415144) (Figure 4.3-11), San Mateo Bridge (9414458) (Figure 4.3-12), Redwood City (9414523) (Figure 4.3-13), Dumbarton Bridge (9414509) (Figure 4.3-14), and Coyote Creek (9414575) (Figure 4.3-15). The resulting cross-correlation statistics for these 8 comparisons are summarized in Table 4.3-3. Predicted mean water levels are within 0.04 m of observed mean water levels at all seven stations during the simulation period. The values of the coefficient of determination between observed and predicted water levels are between 0.989 and 0.996, and the model skill values are between 0.996 and 0.999. At the remaining three stations, water level observations did not cover the full tidal range which prevented a detailed statistical analysis. However observed and predicted water level comparisons were made at Alviso Slough at Gold Street Bridge (9414551) (Figure 4.3-16), Artesian Slough (No station number) (Figure 4.3-17), and the Coyote Creek Railroad Bridge (No station number) (Figure 4.3-18) to evaluate the accuracy of prediction of peak water levels at these stations for the periods when peak water level data were available. The observed and predicted peak water levels at all eleven stations for which water level observation data were available during the 2005 simulation period are shown in Table 4.3-4. During the 2005 simulation period, peak water levels were under predicted at all South Bay stations by between 0.02 m (0.06 ft) and 0.11 m (0.36 ft).

The differences between observed and predicted peak water levels for the 2005 simulation period are somewhat larger than for the 2011 simulation period (Section 4.3.1). The maximum difference between the peak observed and peak predicted peak water level during the 2005 simulation period was 0.11 m (0.36 ft) at Coyote Creek, compared to a maximum difference of 0.01 m (0.04 ft) between the predicted and observed in peak water level at this same station in 2011. Some of the larger differences between observed and predicted water levels in the project area for the 2005 simulation can be attributed to uncertainty in the vertical datum of the water level and bathymetric data measurements collected in Lower Coyote Creek. For the 2005 bathymetric survey, temporary subordinate tide stations established at the San Leandro Marina (9414688), the west side of the San Mateo Bridge (9414458), and the east side of the Dumbarton Bridge (9414509). Foxgrover et al. (2007) report that the datum recovery was 0.1 ft (3 cm) or less at these three stations, which is within the expected generalized accuracy limits of +/-0.13 ft (4 cm) for a one-month long data series on the West Coast (Swanson, 1974). However, because the tide gauges on Alviso Slough and Artesian Slough were not installed low enough to capture a substantial number of lower low water observations at existing NOS stations and due to the failure of the acoustic gauge at Coyote Creek, precise datum conversions from MLLW to NAVD88 could not be computed for the regions of lower Coyote Creek (Foxgrover el at., 2007). The vertical datum conversion between MLLW and NAVD88 in the vicinity of the Coyote Creek (9414575) is reported to a precision of 0.1 ft, however similar conversions computed for 6 zones in the region of lower Coyote Creek, due to the loss of a substantial number of lower low water observations at existing NOS stations in the area (Foxgrover et al., 2007). Thus the uncertainty with the water level measurements and datum

conversions during 2005 period are greater than the largest difference between observed and predicted water levels during the 2011 simulation.

Table 4.3-3 Model calibration results and cross-correlation statistics for the 2005 simulation period.

Station Location	Mean Water Level			Amplitude Ratio	Lag (min)	Coefficient of Determination	Skill	Figure Number
	Observed (m)	Predicted (m)	Difference (m)					
San Francisco	0.96	0.97	0.01	1.02	-1	0.996	0.999	4.3-8
Alameda	0.99	1.01	0.02	1.02	14	0.995	0.998	4.3-9
Richmond	1.02	1.02	0.00	0.99	3	0.993	0.998	4.3-10
Port Chicago	1.17	1.20	0.03	0.96	8	0.990	0.997	4.3-11
San Mateo Br.	1.07	1.03	-0.04	1.00	6	0.996	0.998	4.3-12
Redwood City	1.05	1.03	-0.02	0.99	10	0.995	0.999	4.3-13
Dumbarton Br.	1.05	1.03	-0.02	1.00	7	0.995	0.999	4.3-.14
Coyote Creek	1.01	1.05	0.04	0.98	9	0.989	0.996	4.3-15

Table 4.3-4 Model calibration results of peak water levels for the 2005 simulation period.

Station Location	Maximum Water Level (m NAVD88)			Maximum Water Level (ft NAVD88)		
	Observed (m)	Predicted (m)	Difference (m)	Observed (ft)	Predicted (ft)	Difference (ft)
San Francisco	1.91	1.92	0.01	6.27	6.30	0.03
Alameda	2.12	2.11	-0.01	6.96	6.92	-0.04
Richmond	2.03	1.99	-0.04	6.66	6.53	-0.13
Port Chicago	2.06	2.03	-0.03	6.76	6.66	-0.10
San Mateo Bridge	2.34	2.27	-0.07	7.68	7.45	-0.23
Redwood City	2.39	2.34	-0.05	7.84	7.68	-0.16
Dumbarton Br.	2.42	2.36	-0.06	7.94	7.74	-0.20
Coyote Creek	2.53	2.42	-0.11	8.30	7.94	-0.36
Gold Street Br., Alviso Slough	2.22	2.20	-0.02	7.28	7.22	-0.06
Artesian Slough	2.41	2.34	-0.07	7.91	7.68	-0.23
Coyote Creek Railroad Bridge	2.23	2.20	-0.03	7.32	7.22	-0.10

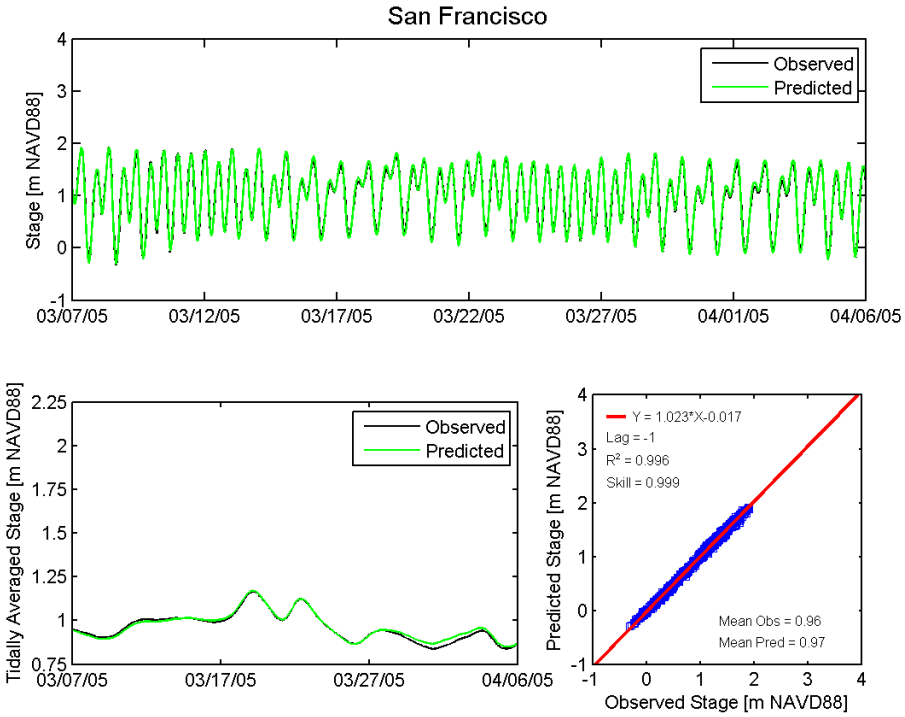

Figure 4.3-8 Observed and predicted stage at San Francisco NOAA tide station (9414290) during the 2005 simulation period.

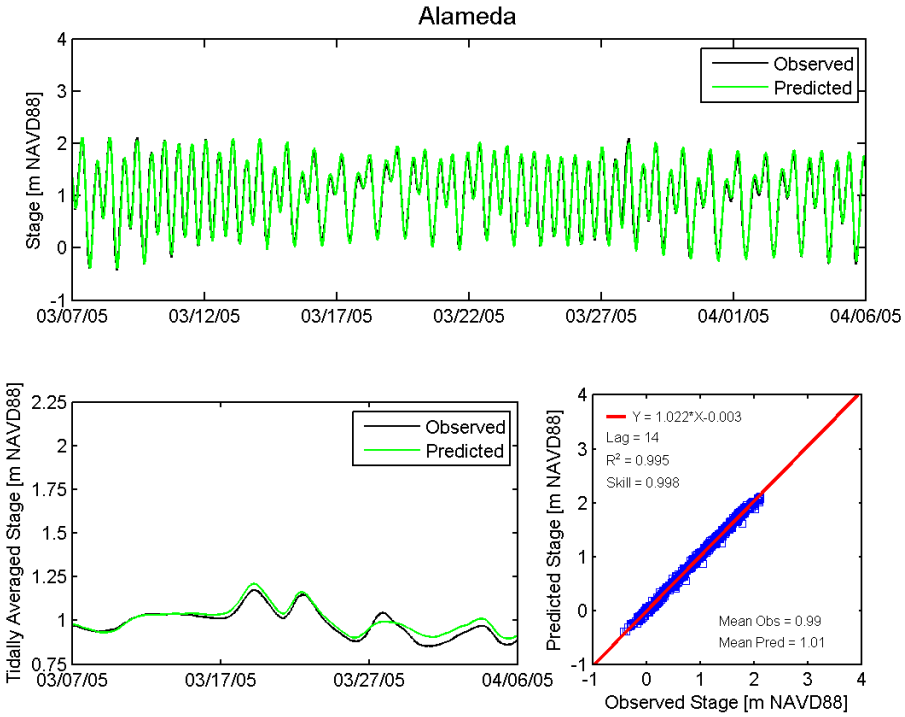

Figure 4.3-9 Observed and predicted stage at Alameda NOAA tide station (9414750) during the 2005 simulation period.

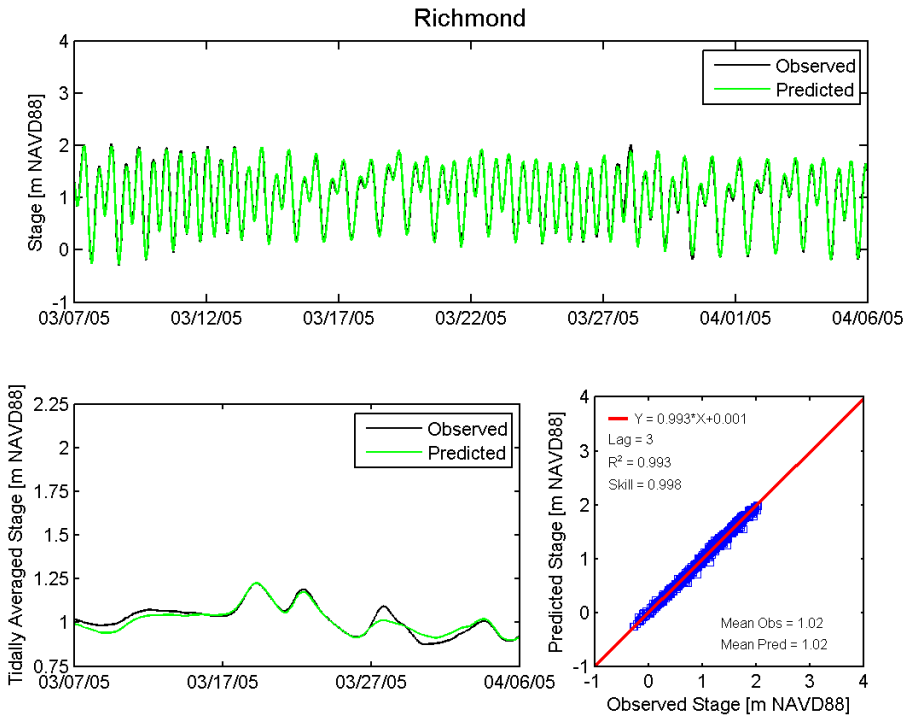

Figure 4.3-10 Observed and predicted stage at Richmond NOAA tide station (9414863) during the 2005 simulation period.

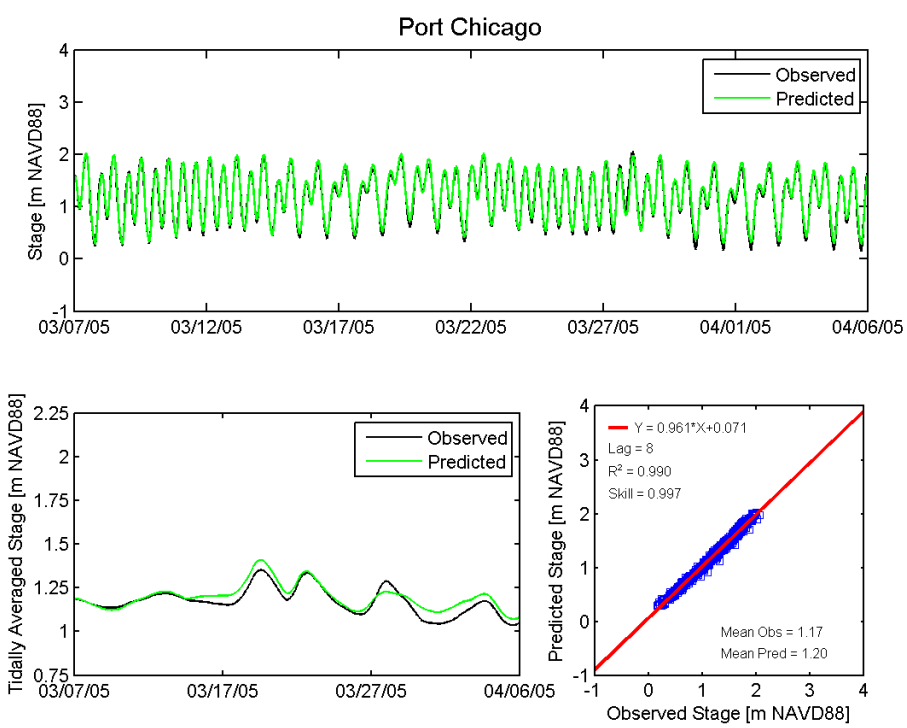

Figure 4.3-11 Observed and predicted stage at Port Chicago NOAA tide station (9415144) during the 2005 simulation period.

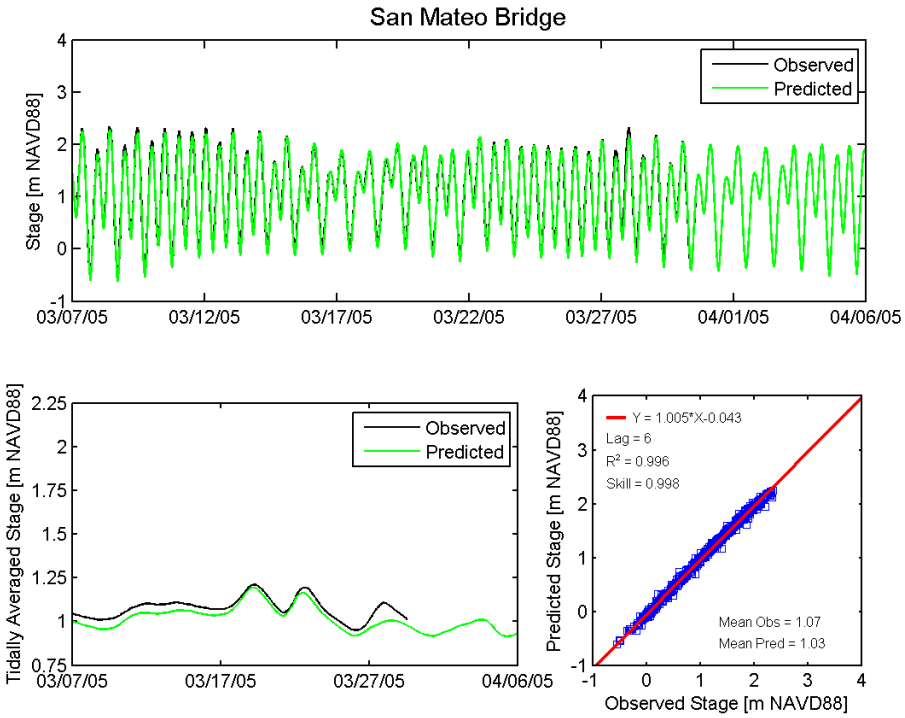

Figure 4.3-12 Observed and predicted stage at San Mateo Bridge NOAA tide station (9414458), and during the 2005 simulation period.

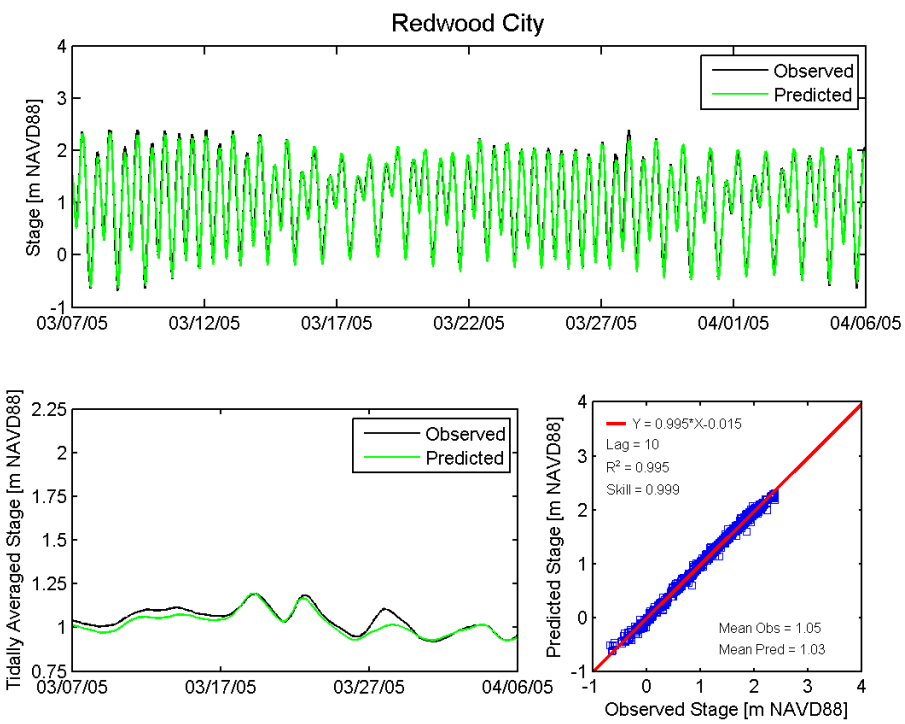

Figure 4.3-13 Observed and predicted stage at Redwood City NOAA tide station (9414523) during the 2005 simulation period.

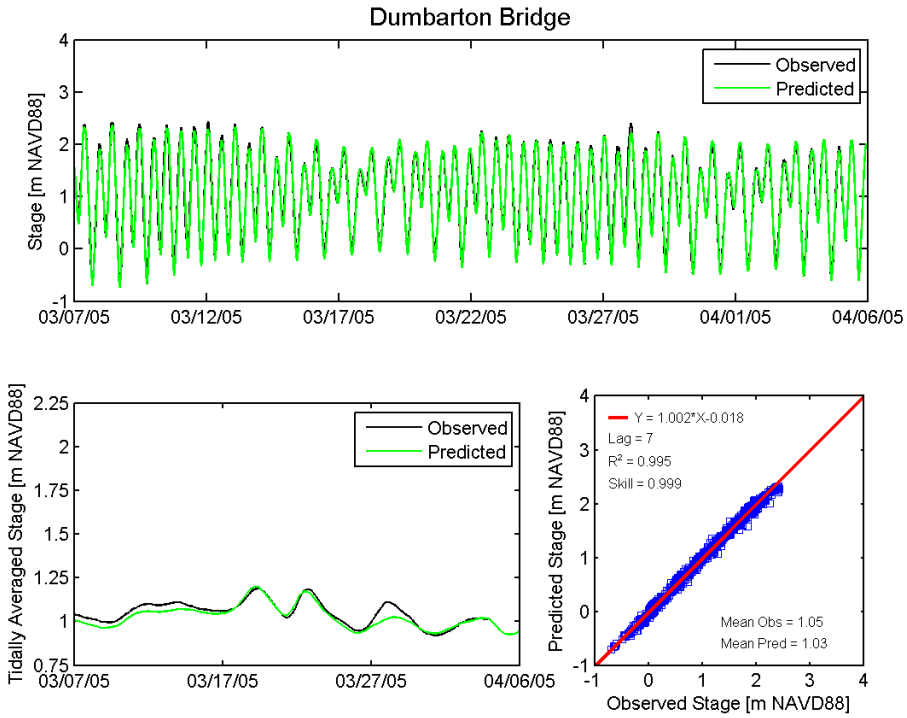

Figure 4.3-14 Observed and predicted stage at Dumbarton Bridge NOAA tide station (9414509) during the 2005 simulation period.

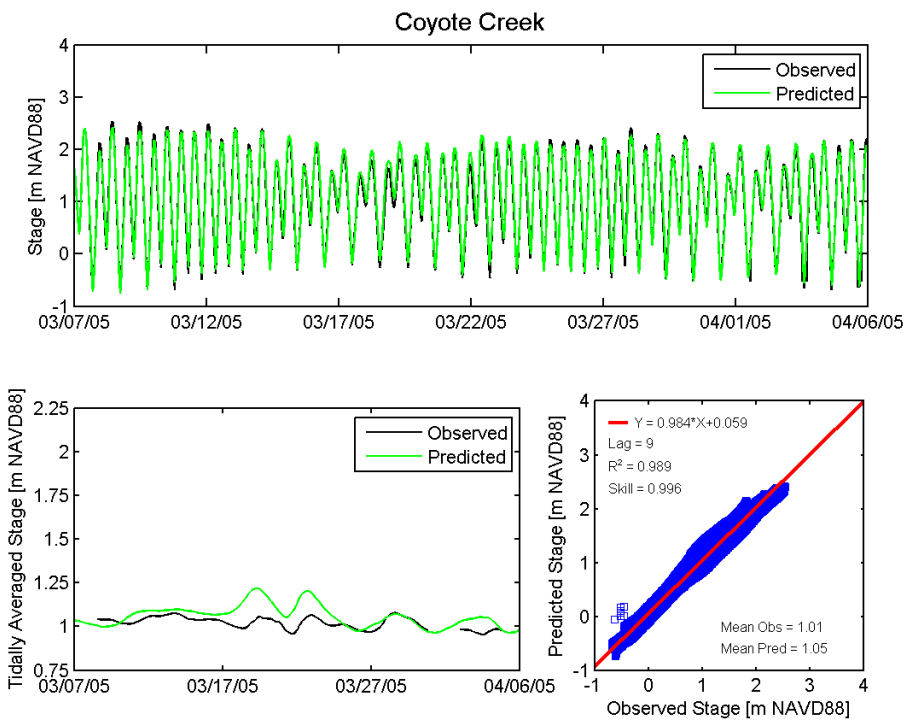

Figure 4.3-15 Observed and predicted stage at Coyote Creek NOAA tide station (9414575) during the 2005 simulation period.

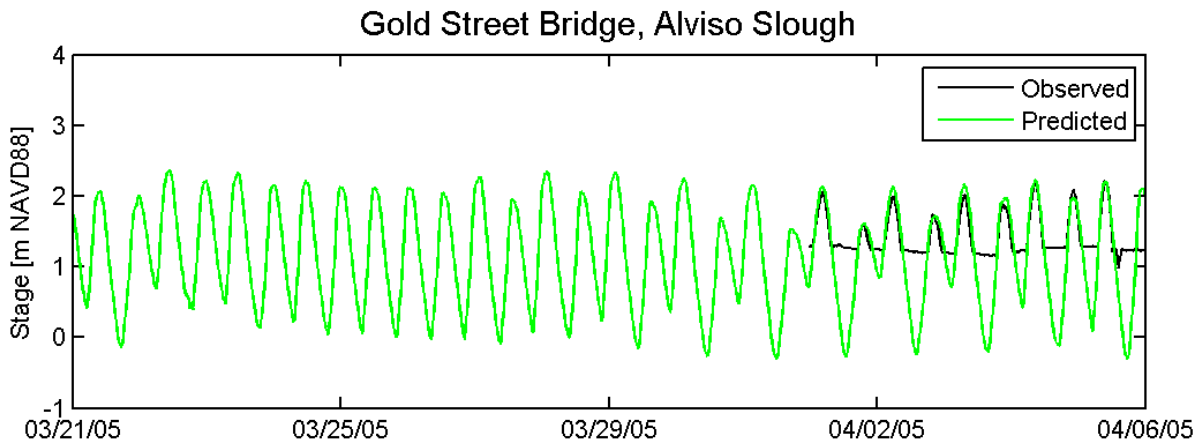

Figure 4.3-16 Observed and predicted stage at Gold Street Bridge, Alviso Slough NOAA tide station (9414551) during sixteen days of the 2005 simulation period.

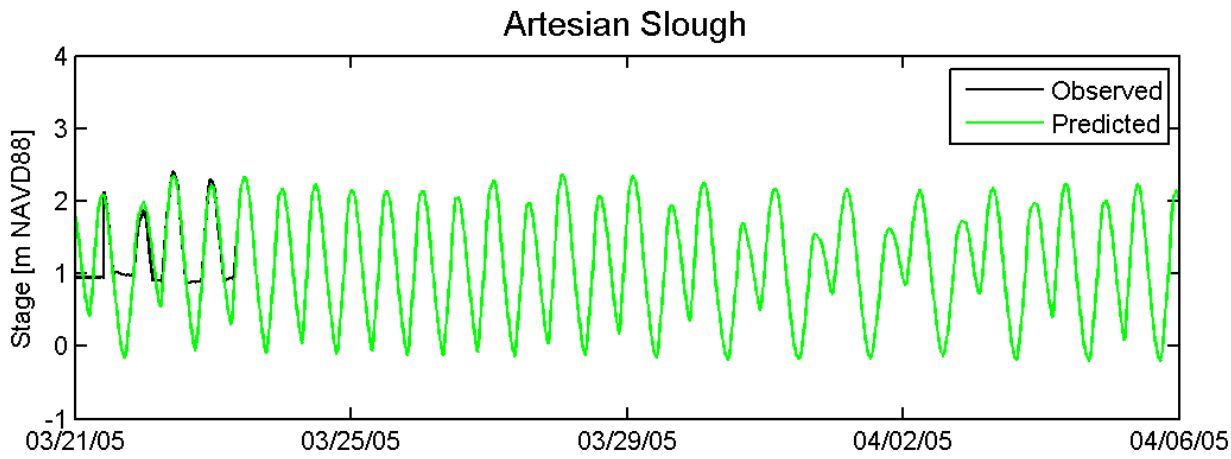

Figure 4.3-17 Observed and predicted stage at Artesian Slough during sixteen days of the 2005 simulation period.

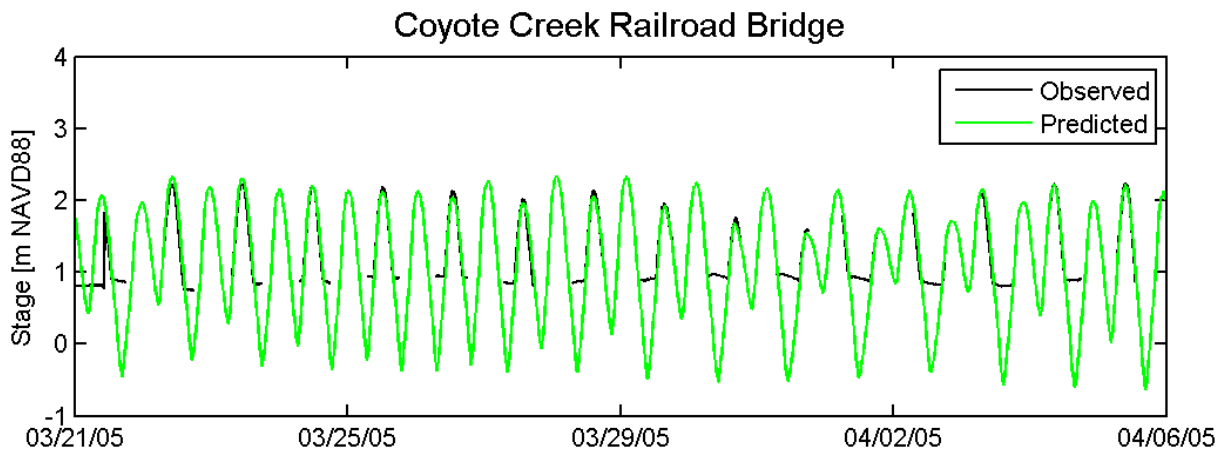

Figure 4.3-18 Observed and predicted stage at the Railroad Bridge over Coyote Creek during sixteen days of the 2005 simulation period.

4.4 Simulation Periods for Model Validation

The UnTRIM San Francisco Bay-Delta model was validated using peak water level data from five separate storm periods between 1983 and 2006. The five simulation periods were selected to capture the largest storm events occurring in South San Francisco Bay since 1901. Cheng and Wu (2008) ranked the maximum verified tide data values recorded at the San Francisco tide station (9414290). Four storms were selected based upon a ranking of the maximum observed water level corrected for sea level rise at San Francisco for January 1983, December 1983, December 1997, and February 1998. The two 1983 storm events produced the largest and second largest observed water levels at San Francisco tide station (9414290), and the February 1998 storm produced the third largest. Collectively these four storms include ten of the 47 ranked events listed in Table 4.4-1, including all of the top five events. A fifth storm during December 2006, with a maximum observed tide of about 2.0 m was also modeled. This event was selected for consistency with the events simulated by Letter and Strum (2010). The model grid for the 2006 simulation was adjusted to account for the breaching of the Alviso Island pond levees which occurred in March 2006.

Table 4.4-1 is modified from Table 2-2 in Cheng and Wu (2008), the memorandum of coastal analysis produced by the USACE for the South San Francisco Bay Shoreline Study. This table was generated from a conditional sampling of significant events recorded between 1901 and 2005. Residual heights were calculated as the difference between verified (observed) and astronomical tide data, after the observation data were corrected for long-term sea level rise, using 2005 as a reference year (Cheng and Wu, 2008). From the 105 year time series corrected for long-term sea level rise, selected tide data occurring at adjacent times were grouped together and 11-day tide time series of predicted and residual tide data were plotted across these groupings, producing 37 time series graphs (Plates 2-6 to 2-15 in Cheng and Wu, 2008). From examination of these 37 graphs, 47 high residual events (pulses along the residual time series) were identified, and 3-day time series were plotted across them. Maximum verified, predicted, and residual values were collected within each of these 47 3-day time series (Table 4.4-1). A significant event was characterized as the combination of high astronomical tides exceeding 1.37 m referenced to MLLW (4.5 feet MLLW) and large residual heights greater than 0.46 m (1.5 feet). This approach was designed such that multiple events could be selected from a given year, and multiple events could also occur within subsequent 3-day periods such that the 47 high residual events shown on Table 4.4-1 occur within the 37 11-day periods. The identical ranking of 47 storm events developed by Cheng and Wu (2008) was also used by Letter and Sturm (2010).

Figure 4.4-1 through Figure 4.4-5 show the astronomical tides developed from tidal harmonic constituents, observed water levels, and the tidal residual for each of the five model validation storm events simulation periods at the San Francisco station (9414290). As seen in these five figures, the predicted peak observed water level (black line) does not always occur at the same time as the peak residual water level (red line) during each event. This allows the decoupling of tide and surge for use in the Monte Carlo analysis. Table 4.4-2 provides the start and end dates for each simulation period, lists the ranked events which occur within each simulation period, and lists the maximum observed, astronomical, and residual tide during each simulation period.

The observed water levels in Table 4.4-1 include a correction for long-term sea level rise, while the observed water levels in Table 4.4-2 are not corrected for sea level rise. The differences between reported peaks in Table 4.4-1 and Table 4.4-2 result from the application of the long-term sea level rise correction to the peaks listed in Table 4.4-1.

Table 4.4-1 Forty-seven selected events from 1901 to 2005 ranked by the maximum verified tide data value recorded at San Francisco (9414290). Events were selected to meet the conditions described in Cheng and Wu (2008).

Beginning of Time Series	End of Time Series	Maximum Astronomical Tide Data Value in Time Series (m NAVD88)	Maximum Verified Tide Data Value in Time Series, Adjusted for Sea Level Rise (m NAVD88)	Maximum Residual Tide Data Value in Time Series, Adjusted for Sea Level Rise (m NAVD88)	Rank of the Maximum Verified Tide Data Value, Adjusted for Sea Level Rise
1/26/1983	1/29/1983	2.20	2.75	0.86	1
12/2/1983	12/5/1983	2.03	2.72	0.71	2
2/4/1998	2/7/1998	1.91	2.60	0.75	3
2/6/1998	2/9/1998	1.94	2.60	0.85	4
1/28/1983	1/31/1983	2.20	2.58	0.55	5
1/15/1973	1/18/1973	2.15	2.55	0.55	6
1/17/1973	1/20/1973	2.15	2.49	0.65	7
12/23/1940	12/26/1940	2.06	2.48	0.61	8
2/10/1941	2/13/1941	1.98	2.48	0.61	9
11/29/1982	12/2/1982	2.11	2.47	0.67	10
1/28/1915	1/31/1915	1.96	2.46	0.59	11
2/2/1998	2/5/1998	1.88	2.45	0.96	12
11/30/1952	12/3/1952	2.03	2.42	0.49	13
3/1/1983	3/4/1983	1.81	2.40	0.84	14
12/25/1921	12/28/1921	2.02	2.38	0.68	15
1/22/1983	1/25/1983	1.91	2.36	0.56	16
11/25/1997	11/28/1997	1.81	2.34	0.61	17
1/12/1969	1/15/1969	2.01	2.32	0.48	18
12/5/1987	12/8/1987	1.93	2.30	0.49	19
2/23/1917	2/26/1917	1.92	2.29	0.55	20
2/18/1993	2/21/1993	1.83	2.29	0.56	21
3/3/1978	3/6/1978	1.89	2.28	0.53	22
2/7/1915	2/10/1915	1.94	2.27	0.77	23
12/14/2002	12/17/2002	1.82	2.26	0.66	24
2/15/1959	2/18/1959	1.66	2.25	0.66	25
2/1/1915	2/4/1915	1.90	2.24	0.74	26
12/16/1940	12/19/1940	1.87	2.24	0.56	27
1/8/1995	1/11/1995	1.75	2.21	0.52	28

Table 4.4-1 continued.					
11/17/1982	11/20/1982	1.80	2.20	0.55	29
2/28/1941	3/3/1941	1.66	2.17	0.85	30
3/11/1906	3/14/1906	1.86	2.17	0.62	31
12/5/1997	12/8/1997	1.70	2.16	0.50	32
3/9/1904	3/12/1904	1.67	2.14	0.71	33
11/10/1983	11/13/1983	1.54	2.12	0.63	34
3/12/1905	3/15/1905	1.61	2.11	0.72	35
12/24/1983	12/27/1983	1.76	2.11	0.50	36
1/17/1916	1/20/1916	1.89	2.09	0.60	37
1/30/1926	2/2/1926	1.80	2.07	0.50	38
1/17/1983	1/20/1983	1.70	2.05	0.49	39
3/3/1941	3/6/1941	1.62	2.05	0.72	40
3/9/1995	3/12/1995	1.57	2.05	0.76	41
12/10/1906	12/13/1906	1.94	2.05	0.64	42
2/23/1969	2/26/1969	1.69	2.05	0.53	43
12/21/1982	12/24/1982	1.58	2.03	0.72	44
12/11/1995	12/14/1995	1.58	1.96	0.66	45
3/23/1907	3/26/1907	1.59	1.92	0.59	46
2/2/1926	2/5/1926	1.63	1.92	0.52	47

Table 4.4-2 Simulated storm events.

Simulation	Start Date	End Date	Ranked Events	Maximum Astronomical Tide (m)	Maximum Observed Tide (m)	Maximum Residual Storm Surge (m)	Date of Peak Observed Tide
January 1983	1/17/1983	1/31/1983	1,5,16, 39	2.198	2.707	0.803	1/27/1983
December 1983	11/26/1983	12/8/1983	2	2.026	2.674	0.648	12/3/1983
December 1997	11/26/1997	12/8/1997	17,32	1.899	2.321	0.575	11/26/1997
February 1998	1/28/1998	2/13/1998	3,4,12	2.069	2.587	0.934	2/6/1998
March 2005	3/7/2005	4/6/2005	none	1.973	1.91	0.301	3/8/2005
December 2006	12/20/2006	12/30/2006	none	1.984	1.996	0.265	12/21/2006
2011	5/10/2011	6/9/2011	none	2.07	2.307	0.298	5/17/2011

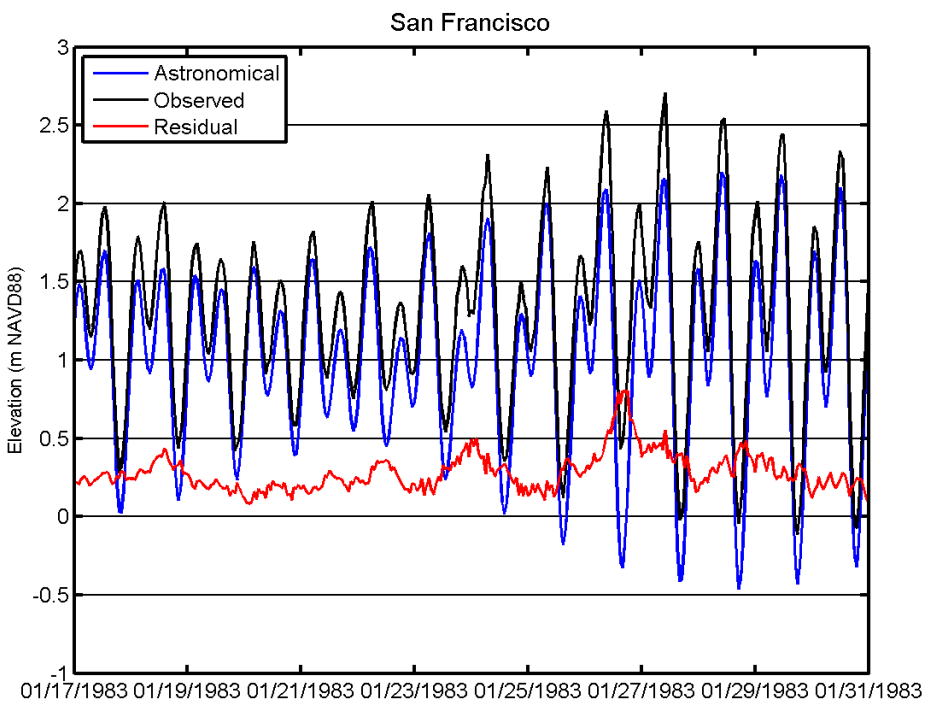

Figure 4.4-1 Astronomical tides, observed tides, and residual storm surge at San Francisco NOAA tide station (9414290) for the January 1983 simulation period.

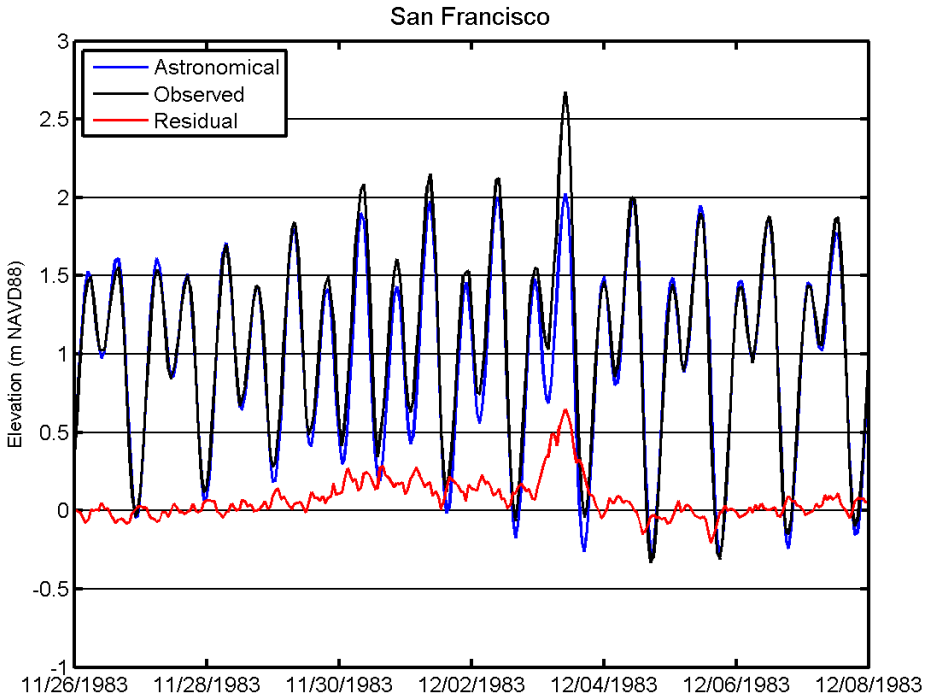

Figure 4.4-2 Astronomical tides, observed tides, and residual storm surge at San Francisco NOAA tide station (9414290) for the December 1983 simulation period.

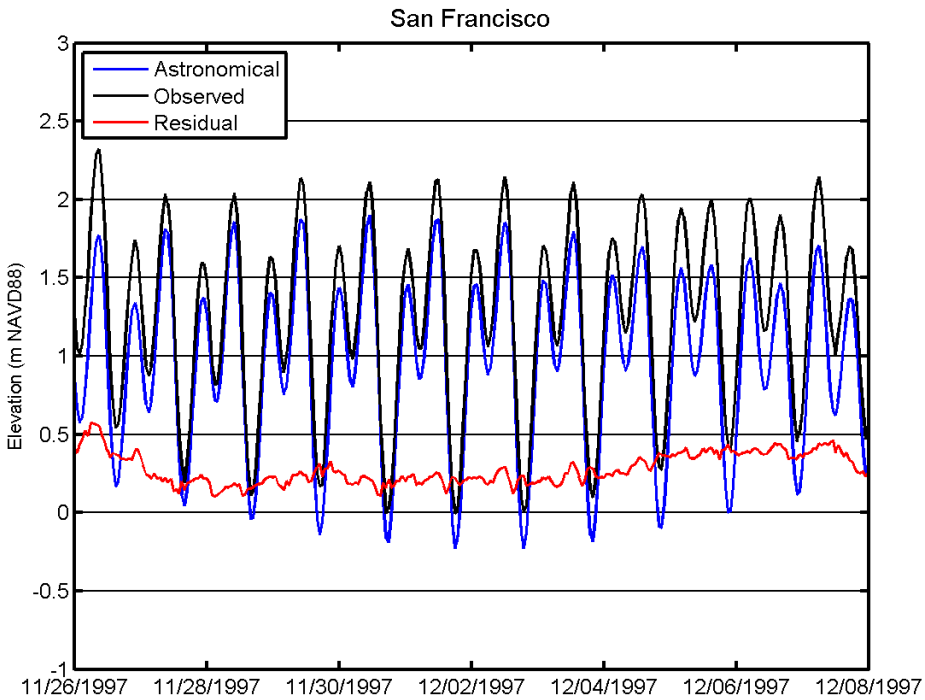

Figure 4.4-3 Astronomical tides, observed tides, and residual storm surge at levels at San Francisco NOAA tide station (9414290) for the December 1997 simulation period.

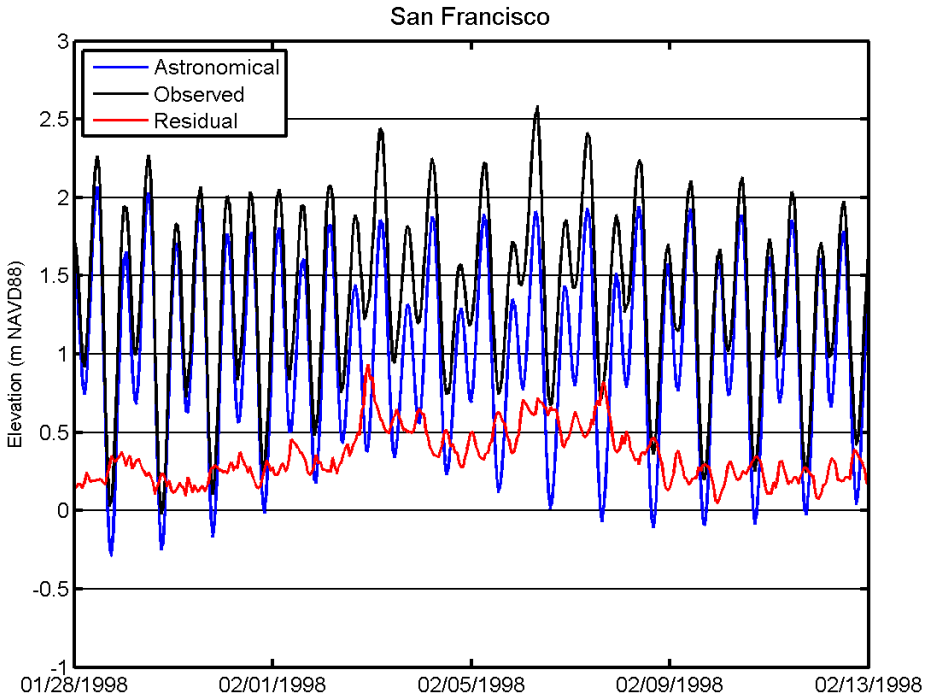

Figure 4.4-4 Astronomical tides, observed tides, and residual storm surge at San Francisco NOAA tide station (9414290) for the February 1998 simulation period.

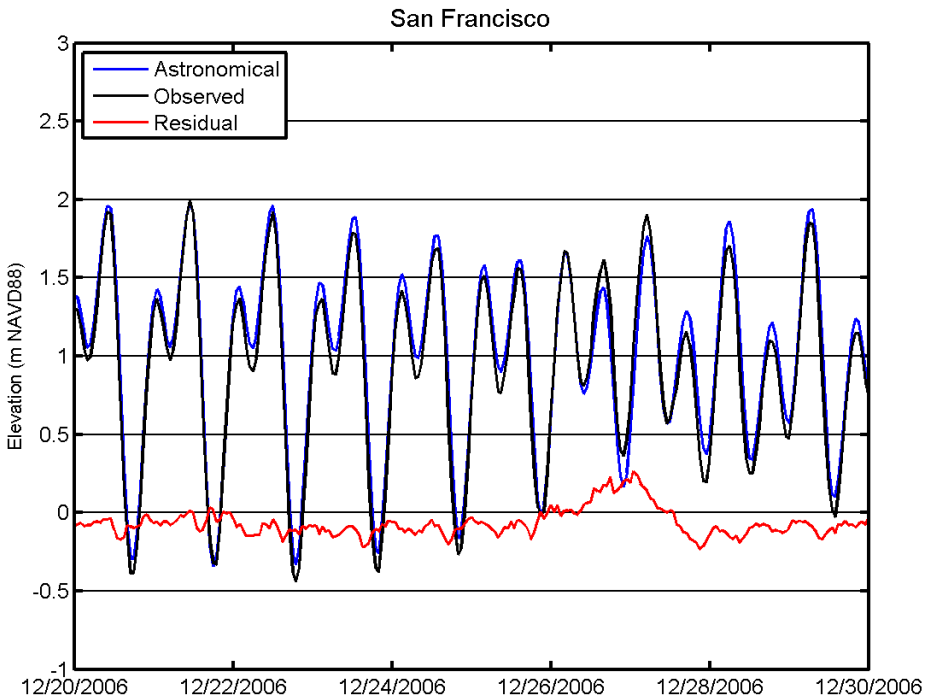

Figure 4.4-5 Astronomical tides, observed tides, and residual storm surge at San Francisco NOAA tide station (9414290) for the December 2006 simulation period.

4.5 Results of Model Validation

This section presents the model validation results for simulations of five storm events. For each simulation period, observed and predicted water levels were compared at all stations in San Francisco Bay where water level observation data were available using the cross-correlation procedure described in Section 4.1.

4.5.1 Model Verification for January 1983 Storm

The January 1983 simulation period spans from January 17, 1983 to January 31, 1983. This simulation period contains four of the 47 ranked events listed in Table 4.4-1. The peak observed water level at San Francisco (9414290) during this period occurred on January 27, 1983. Water level comparisons were made at San Francisco (9414290) (Figure 4.5-1), Alameda (9414750) (Figure 4.5-2), Port Chicago (9415144) (Figure 4.5-3), and San Mateo Bridge (9414458) (Figure 4.5-4). Water level observations were not available at any stations further south of San Mateo Bridge in San Francisco Bay during January 1983 (Table 4.1-1). The results of the cross-correlation analysis are summarized in Table 4.5-1. With the exception of Port Chicago (9415144), the predicted mean water levels during the January 1983 simulation period are within 0.03 m of observed peak water levels. The larger difference in mean water level at Port Chicago (9415144) may be indicative of a vertical datum difference at that station. The values of the coefficient of determination between observed and predicted water levels are between 0.985 and 0.995, and the model skill values are between 0.987 and 0.998. Section 4.6 provides discussion of peak water levels at San Francisco (9414290) (Table 4.6-1) and San Mateo Bridge (9414458) (Table 4.6-2) for each of the four ranked events during this simulation period.

Table 4.5-1 Model verification results for the January 1983 storm.

Station Location	Mean Water Level			Amplitude Ratio	Lag (min)	Coefficient of Determination	Skill	Figure Number
	Observed (m)	Predicted (m)	Difference (m)					
San Francisco	1.29	1.30	0.01	1.00	0	0.995	0.998	4.5-1
Alameda	1.31	1.34	0.03	1.02	17	0.994	0.998	4.5-2
Port Chicago	1.51	1.60	0.09	1.00	3	0.985	0.987	4.5-3
San Mateo Br.	1.34	1.35	0.01	0.99	2	0.994	0.998	4.5-4

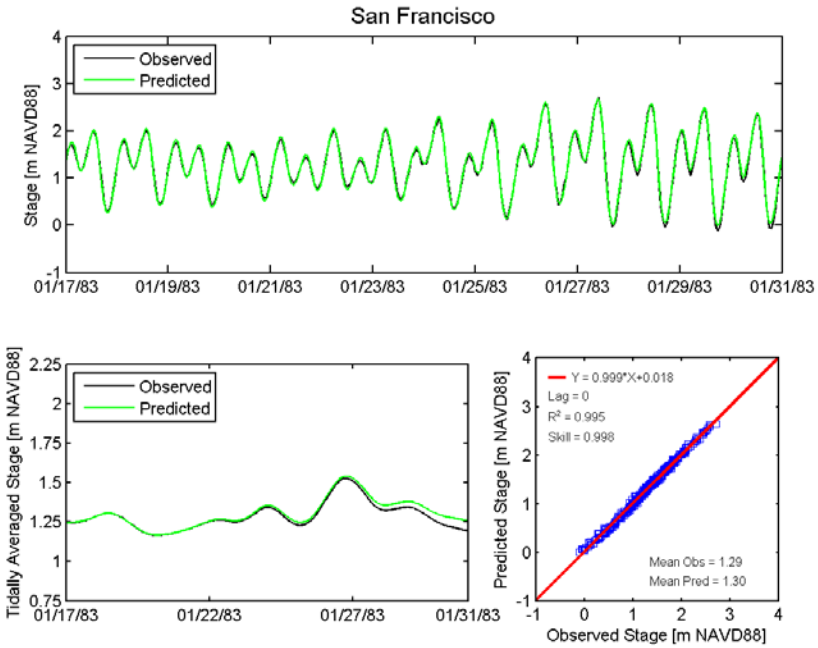

Figure 4.5-1 Observed and predicted stage at San Francisco NOAA tide station (9414290) during the January 1983 simulation.

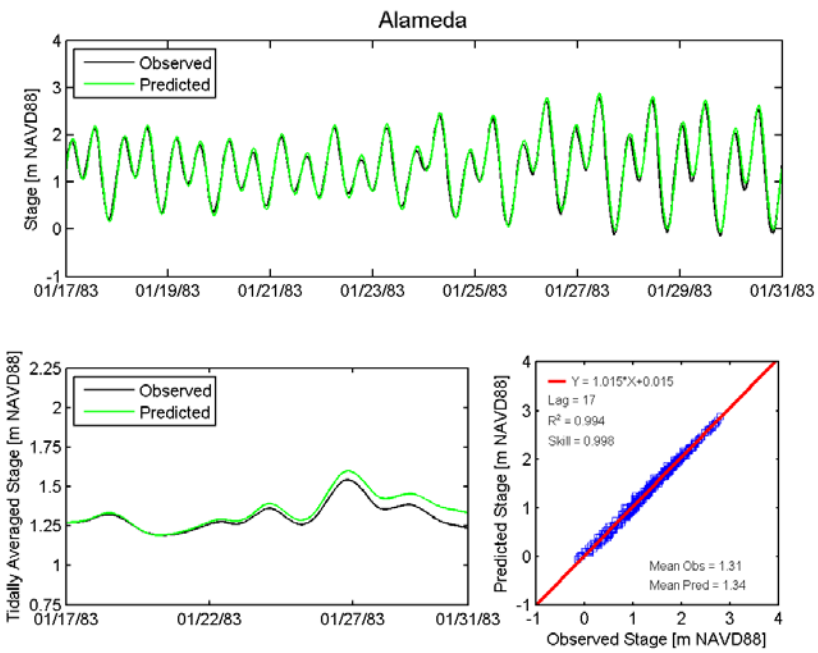

Figure 4.5-2 Observed and predicted stage at Alameda NOAA tide station (9414750) during the January 1983 simulation.

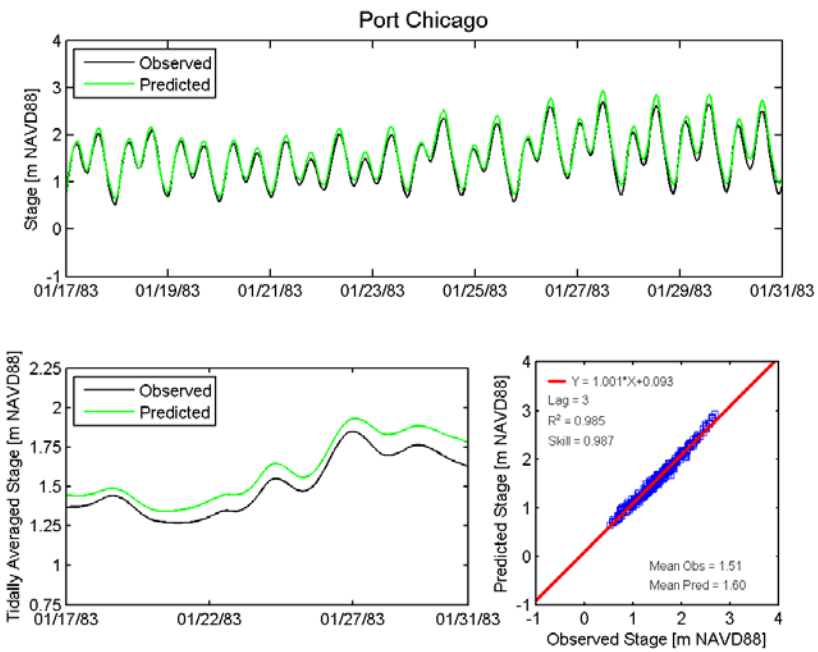

Figure 4.5-3 Observed and predicted stage at Port Chicago NOAA tide station (9415144) during the January 1983 simulation period.

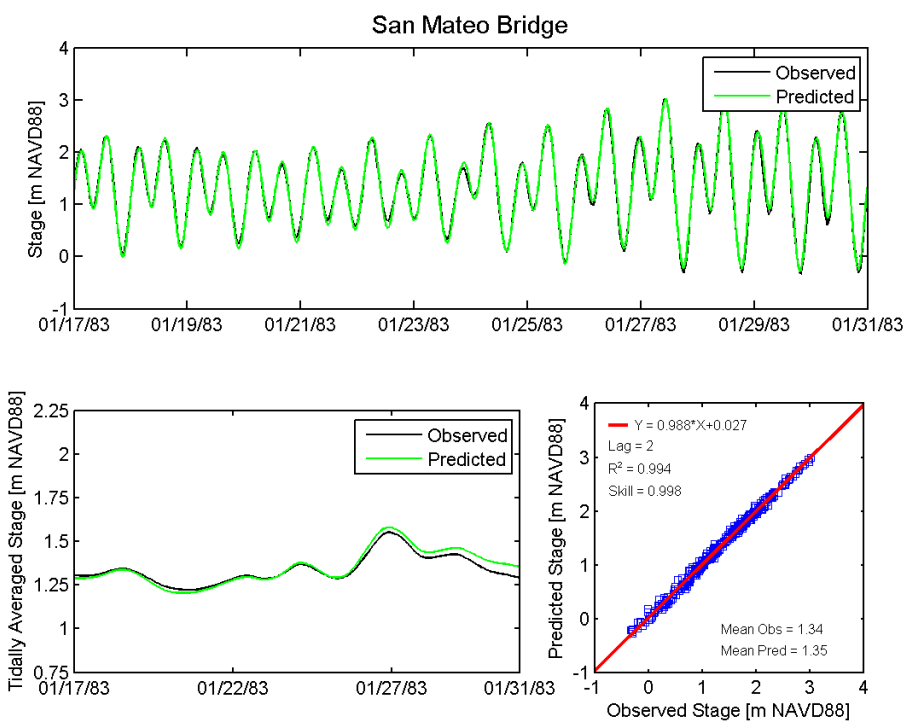

Figure 4.5-4 Observed and predicted stage at San Mateo Bridge NOAA tide station (9414458) during the January 1983 simulation period.

4.5.2 Model Verification for December 1983 Storm

The December 1983 simulation period spans from November 26, 1983 to December 8, 1983. This simulation period contains one of the 47 ranked events listed in Table 4.4-1. The peak observed water level at San Francisco (9414290) during this period occurred on December 3, 1983. Water level comparisons were made at San Francisco (9414290) (Figure 4.5-5) and Redwood City (9414523) (Figure 4.5-6). Maximum water level data at Coyote Creek (9414575) was also available for this storm event since the maximum recorded water level at Coyote Creek occurred on December 3, 1983. However, hourly water level data at Coyote Creek were not available from NOAA for this period. The results of the cross-correlation analysis at San Francisco and Redwood City are summarized in Table 4.5-2. The predicted mean water levels during the December 1983 simulation period are within 0.03 m of observed mean water levels at both stations. The values of the coefficient of determination between observed and predicted water levels are between 0.996 and 0.997, and the model skill is 0.999 at both stations. Section 4.6 provides discussion of peak water levels at San Francisco (9414290) (Table 4.6-1), Redwood City (9414575) (Table 4.6-2), and Coyote Creek (9414575) (Table 4.6-2) for the single ranked event during this simulation period.

Table 4.5-2 Model verification results for the December 1983 storm.

Station Location	Mean Water Level			Amplitude Ratio	Lag (min)	Coefficient of Determination	Skill	Figure Number
	Observed (m)	Predicted (m)	Difference (m)					
San Francisco	1.04	1.05	0.01	1.00	0	0.997	0.999	4.5-5
Redwood City	1.09	1.12	0.03	0.99	7	0.996	0.999	4.5-6

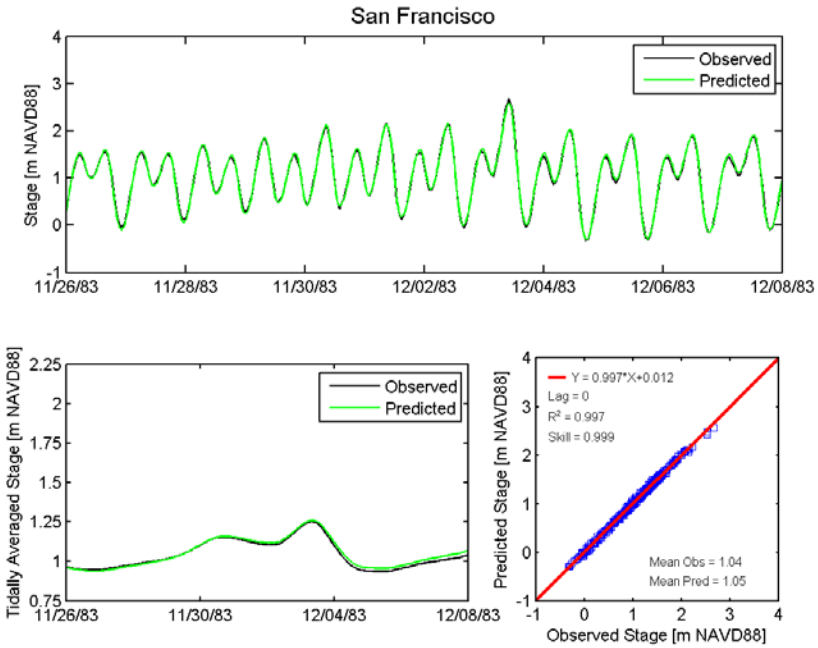

Figure 4.5-5 Observed and predicted stage at San Francisco NOAA tide station (9414290) during the December 1983 simulation period.

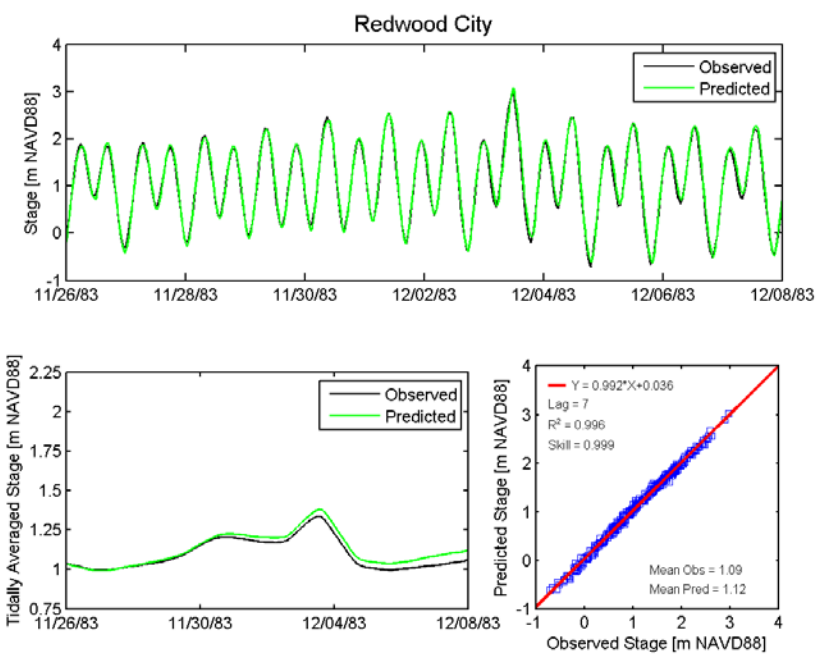

Figure 4.5-6 Observed and predicted stage at at Redwood City NOAA tide station (9414523) during the December 1983 simulation period.

4.5.3 Model Verification for November and December 1997 Storms

The November and December 1997 simulation period spans from November 26, 1997 to December 8, 1997. This simulation period contains two of the 47 ranked events listed in Table 4.4-1. The peak observed water level at San Francisco (9414290) during this period occurred on November 26, 1997. Water level comparisons were made at San Francisco (9414290) (Figure 4.5-7), Alameda (9414750) (Figure 4.5-8), Richmond (9414863) (Figure 4.5-9), Port Chicago (9415144) (Figure 4.5-10), and Redwood City (9414523) (Figure 4.5-11). The results of the cross-correlation analysis at each station are summarized in Table 4.5-3. With the exception of Port Chicago, the predicted mean water levels during the December 1997 simulation period are within 0.02 m of observed mean water levels at all stations. The values of the coefficient of determination between observed and predicted water levels are between 0.994 and 0.999, and the model skill values are between 0.994 and 0.999. Section 4.6 provides discussion of peak water levels at San Francisco (9414290) (Table 4.6-1) and Redwood City (9414523) (Table 4.6-2) for the two ranked events during this simulation period.

Table 4.5-3 Model verification results for the November and December 1997 storms.

Station Location	Mean Water Level			Amplitude Ratio	Lag (min)	Coefficient of Determination	Skill	Figure Number
	Observed (m)	Predicted (m)	Difference (m)					
San Francisco	1.24	1.22	-0.02	1.02	1	0.998	0.999	4.5-7
Alameda	1.25	1.26	0.01	1.03	15	0.999	0.999	4.5-8
Richmond	1.26	1.26	0.00	1.01	5	0.998	0.999	4.5-9
Port Chicago	1.34	1.40	0.06	1.01	7	0.994	0.994	4.5-10
Redwood City	1.26	1.28	0.02	1.01	10	0.998	0.999	4.5-11

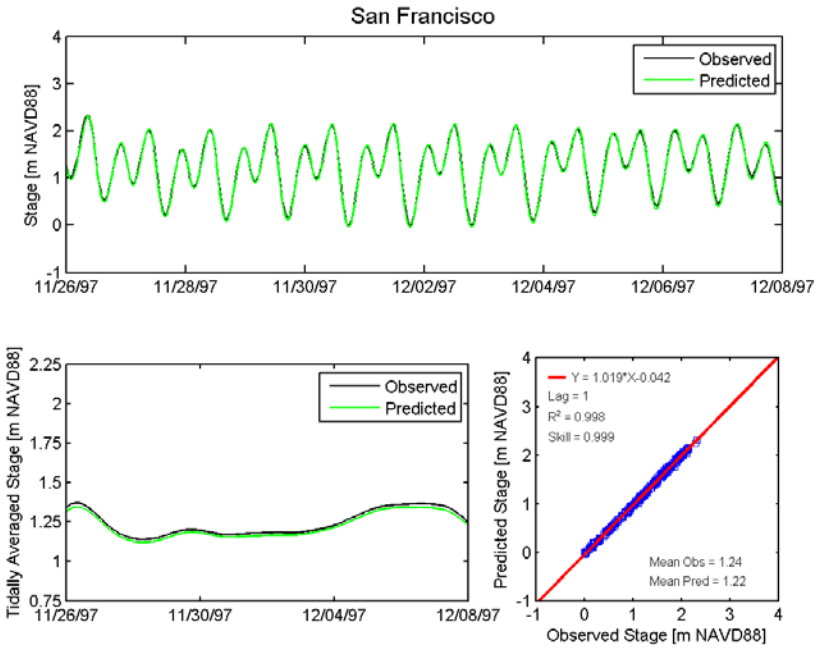

Figure 4.5-7 Observed and predicted stage at San Francisco NOAA tide station (9414290) during the November and December 1997 Storm simulation period.

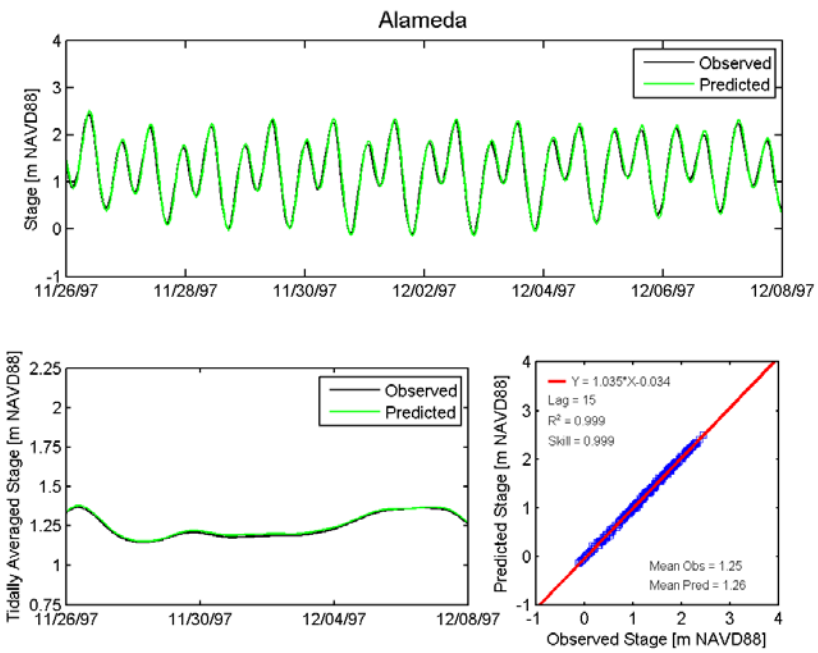

Figure 4.5-8 Observed and predicted stage Alameda NOAA tide station (9414750) during the November and December 1997 Storm simulation period.

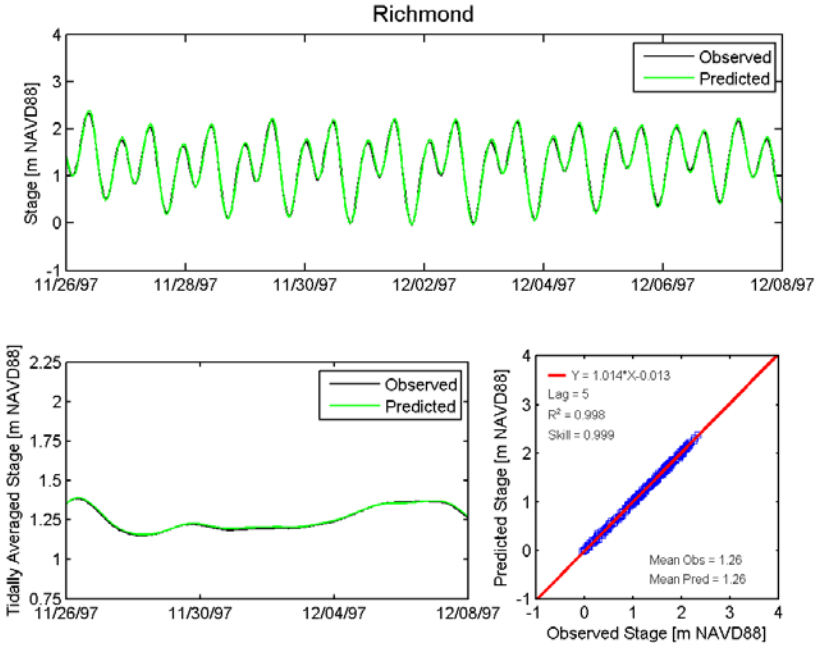

Figure 4.5-9 Observed and predicted stage at Richmond NOAA tide station (9414863) during the November and December 1997 simulation period.

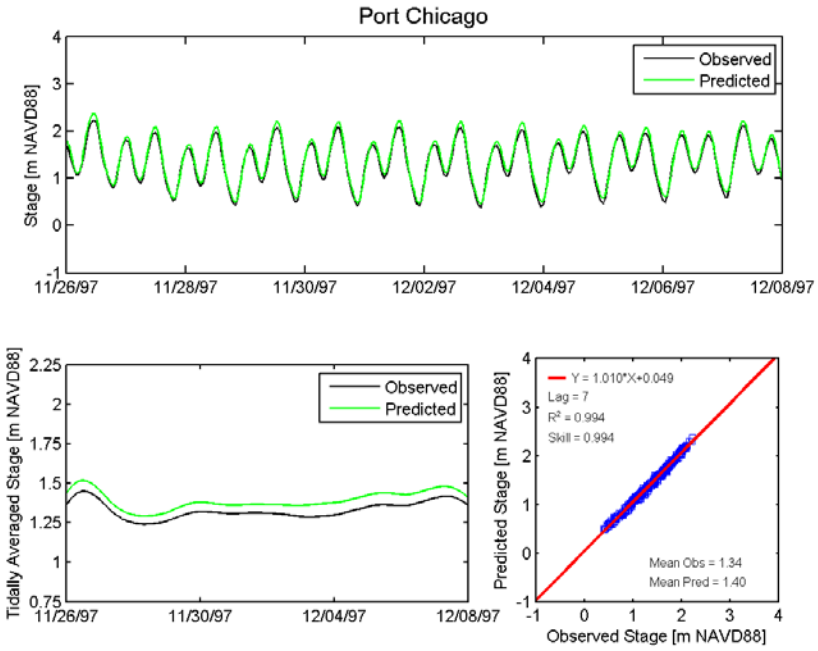

Figure 4.5-10 Observed and predicted stage at Port Chicago NOAA tide station (9415144) during the November and December 1997 simulation period.

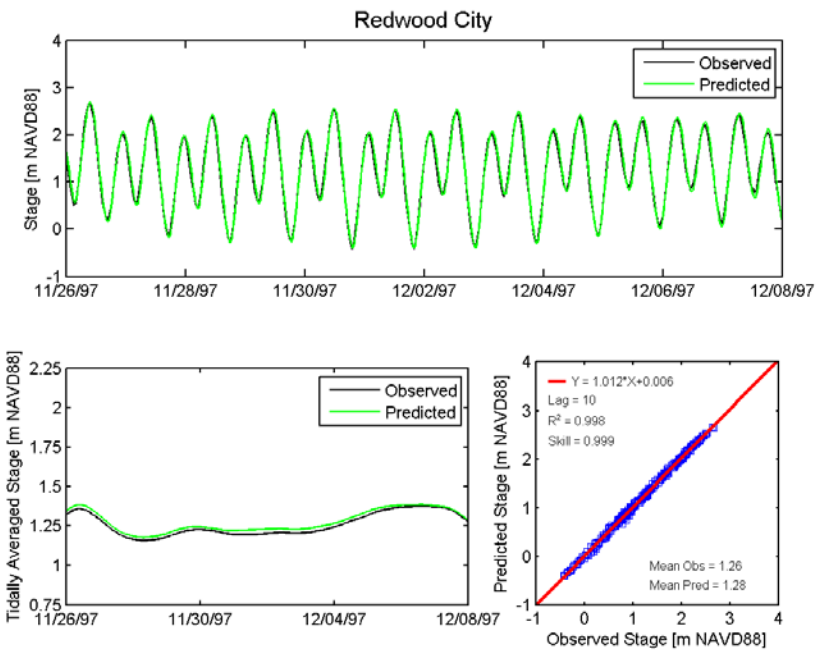

Figure 4.5-11 Observed and predicted stage at Redwood City NOAA tide station (9414523) during the November and December 1997 simulation period.

4.5.4 Model Verification for February 1998 Storm

The February 1998 simulation period spans from January 28, 1998 to February 13, 1998. This simulation period contains three of the 47 ranked events listed in Table 4.4-1. The peak observed water level at San Francisco (9414290) during this period occurred on February 6, 1998. Water level comparisons were made at San Francisco (9414290) (Figure 4.5-12), Alameda (9414750) (Figure 4.5-13), Richmond (9414863) (Figure 4.5-14), Port Chicago (9415144) (Figure 4.5-15), and Redwood City (9414523) (Figure 4.5-16). The results of the cross-correlation analysis at each station are summarized in Table 4.5-4. With the exception of Port Chicago (4415144), the predicted mean water levels during the December 1997 simulation period are within 0.03 m of observed mean water levels at all stations. The values of the coefficient of determination between observed and predicted water levels are between 0.987 and 0.995, and the model skill values are between 0.992 and 0.999. Section 4.6 provides discussion of peak water levels at San Francisco (9414290) (Table 4.6-1) and Redwood City (9414523) (Table 4.6-2) for the three ranked events during this simulation period.

Table 4.5-4 Model verification results for the February 1998 storm.

Station Location	Mean Water Level			Amplitude Ratio	Lag (min)	Coefficient of Determination	Skill	Figure Number
	Observed (m)	Predicted (m)	Difference (m)					
San Francisco	1.35	1.35	0.00	1.00	-2	0.994	0.999	4.5-12
Alameda	1.37	1.40	0.03	1.01	13	0.995	0.998	4.5-13
Richmond	1.40	1.43	0.03	0.98	2	0.991	0.997	4.5-14
Port Chicago	1.66	1.73	0.07	0.98	7	0.987	0.992	4.5-15
Redwood City	1.37	1.40	0.03	0.98	15	0.992	0.998	4.5-16

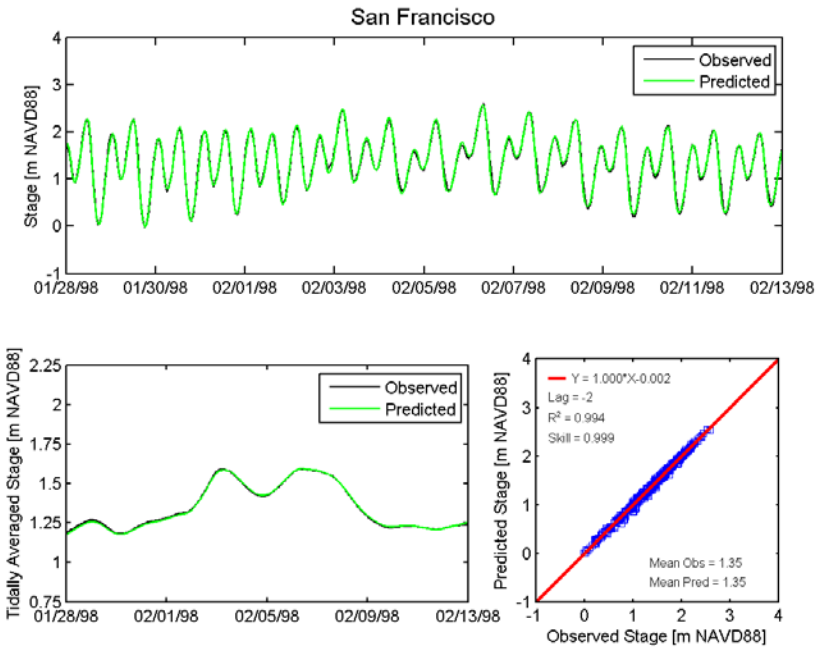

Figure 4.5-12 Observed and predicted stage at San Francisco NOAA tide station (9414290) during the February 1998 Storm simulation period.

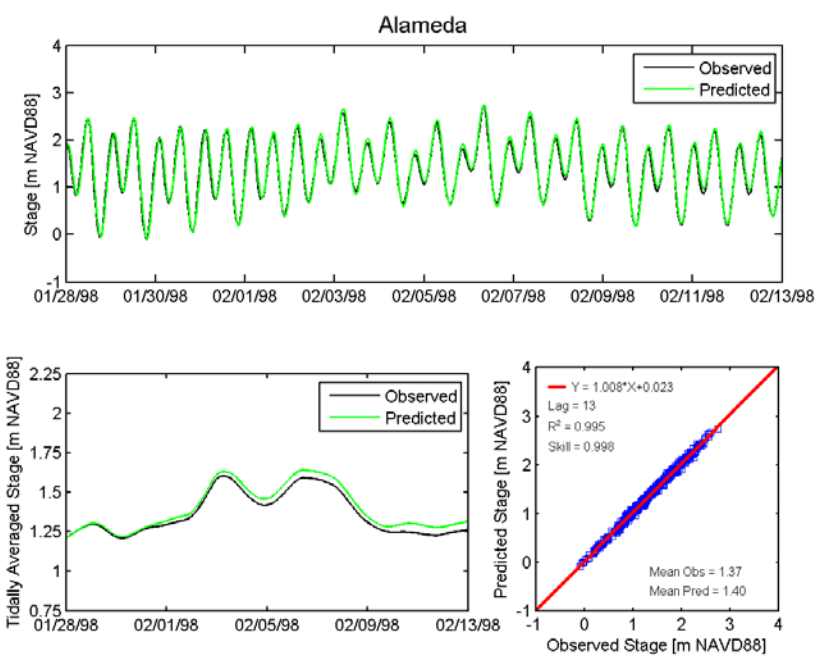

Figure 4.5-13 Observed and predicted stage at Alameda NOAA tide station (9414750) during the February 1998 Storm simulation period.

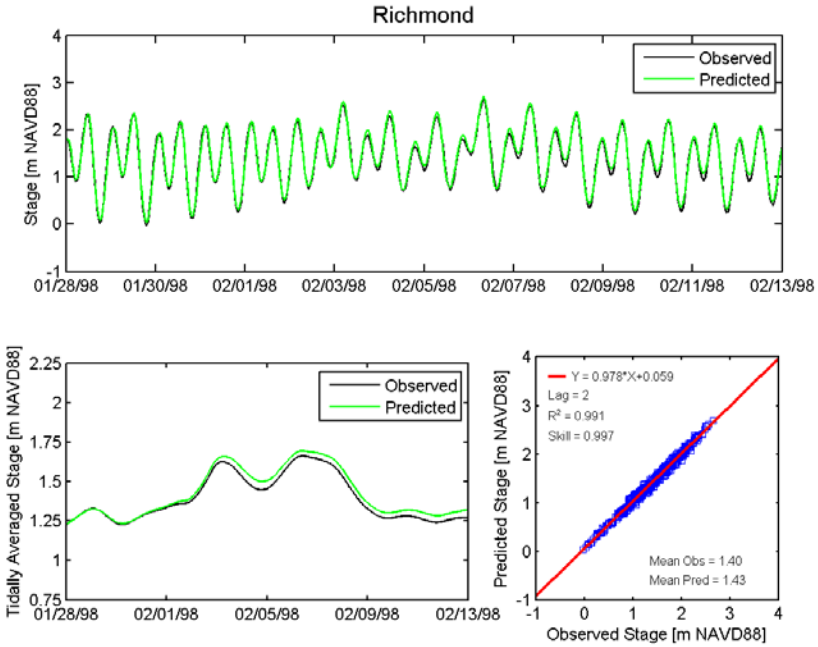

Figure 4.5-14 Observed and predicted stage at Richmond NOAA tide station (9414863) during the February 1998 simulation period.

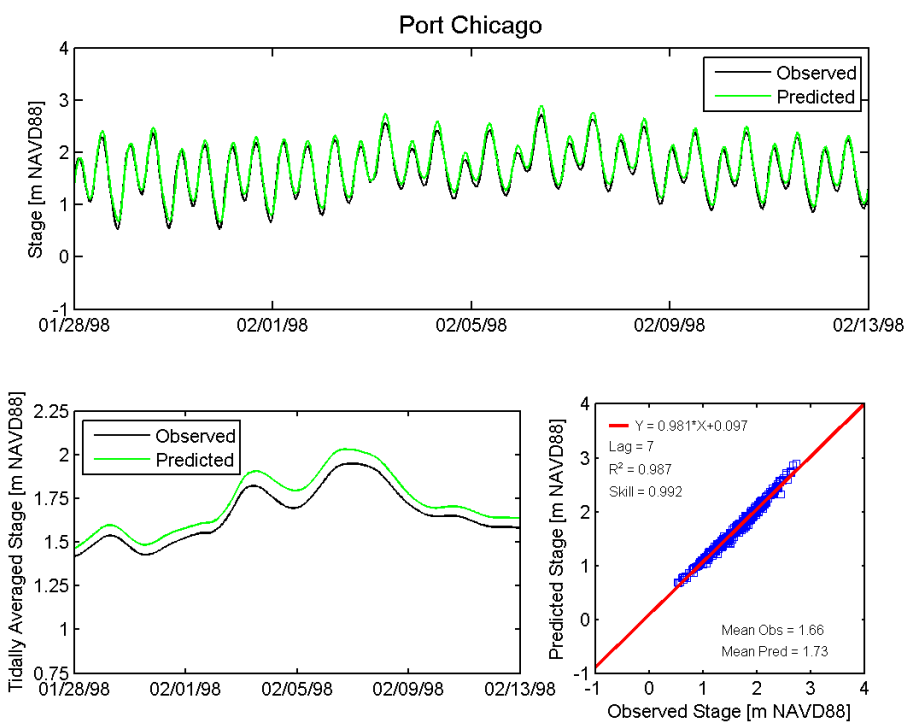

Figure 4.5-15 Observed and predicted stage at Port Chicago NOAA tide station (9415144) during the February 1998 simulation period.

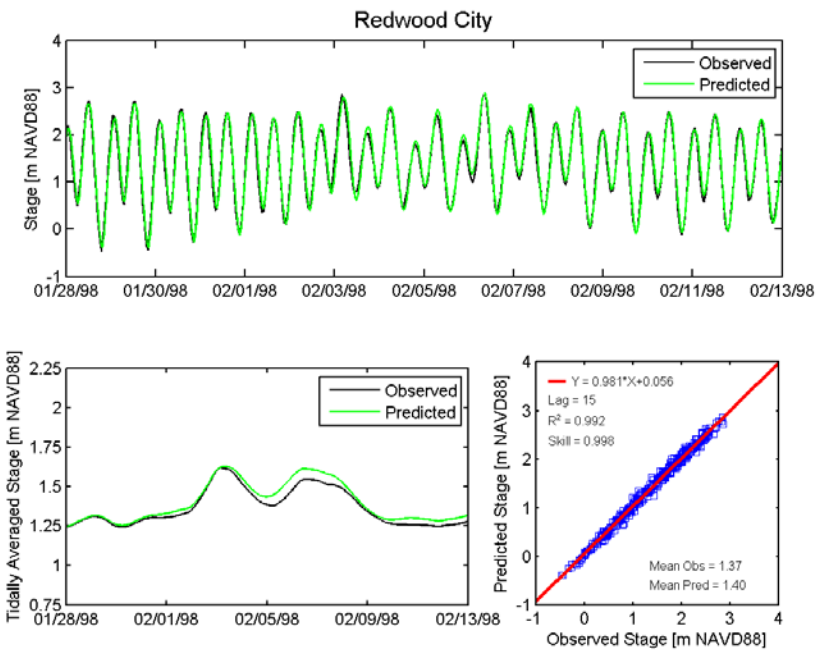

Figure 4.5-16 Observed and predicted stage at Redwood City NOAA tide station (9414523) during the February 1998 simulation period.

4.5.5 Model Verification for December 2006 Storm

The December 2006 simulation period spans from December 20, 2006 to December 30, 2006. This simulation period does not include any of the 47 ranked events listed in Table 4.4-1. The peak observed water level at San Francisco (9414290) during this period occurred on December 21, 2006. A storm surge of approximately 25 cm occurred between December 26 and December 28. Water level comparisons were made at San Francisco (9414290) (Figure 4.5-17), Alameda (9414750) (Figure 4.5-18), Port Chicago (9415144) (Figure 4.5-19), and Redwood City (9414523) (Figure 4.5-20). The results of the cross-correlation analysis at each station are summarized in Table 4.5-5. With the exception of Port Chicago, the predicted mean water levels during the December 2006 simulation period are within 0.03 m of observed mean water levels at all stations. The values of the coefficient of determination between observed and predicted water levels are between 0.994 and 0.998, and the model skill values are between 0.995 and 0.999.

The maximum observed water level at San Francisco during this simulation period occurred on December 21, 2006. The maximum observed water level at San Francisco (9414290) was 2.00 m (6.56 ft) and the corresponding predicted peak water level is 2.01 m (6.59 ft), a difference of 0.01 m (0.03 ft). At Redwood City (9414523), the maximum observed water level during this simulation period occurred during the storm surge on December 27, 2006. The maximum observed water level at Redwood City (9414523) was 2.47 m (8.10 ft) and the corresponding predicted peak water level was 2.37 m (7.78 ft), a difference of 0.10 m (0.32 ft). Comparisons of observed and predicted water levels for this event from the F3 study at the San Francisco and Redwood City stations are shown in Figures 4-19 and 4-20 of Letter and Sturm (2010). Based on Figure 4-20 in the F3 study (Letter and Sturm, 2010), the peak water level on December 27, 2006 was under predicted by about 1 ft (0.30 m) when wind was included in the simulation and by slightly less than 1 ft when wind was not used in the simulation. Thus the current results show significant improvement in the accuracy of the prediction of this peak water level relative to the F3 model verification simulations.

Table 4.5-5 Model verification results for the December 2006 storm.

Station Location	Mean Water Level			Amplitude Ratio	Lag (min)	Coefficient of Determination	Skill	Figure Number
	Observed (m)	Predicted (m)	Difference (m)					
San Francisco	0.92	0.93	0.01	1.02	-1	0.998	0.999	4.5-17
Alameda	0.93	0.96	0.03	1.03	15	0.997	0.999	4.5-18
Port Chicago	1.06	1.11	0.05	0.99	11	0.994	0.995	4.5-19
Redwood City	0.99	1.00	0.01	1.00	10	0.994	0.998	4.5-20

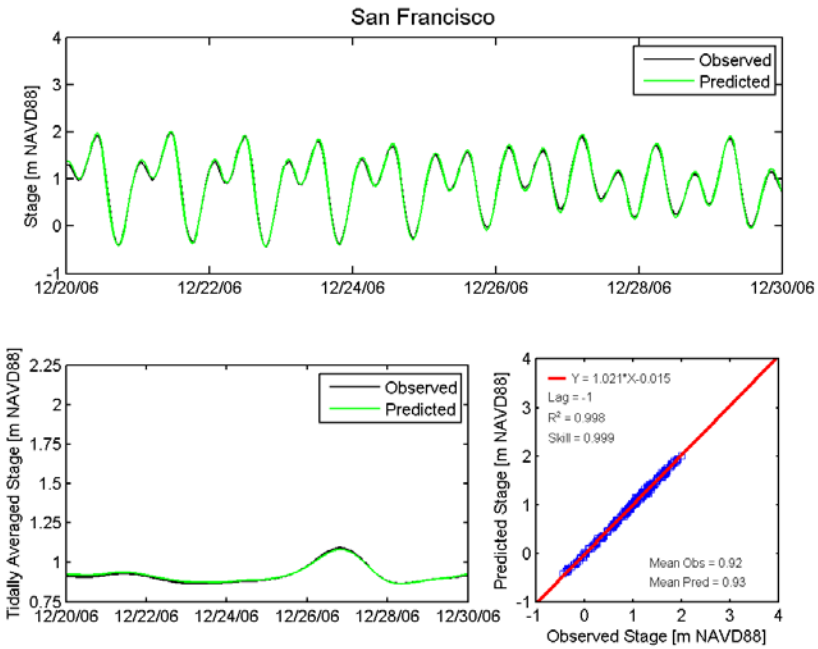

Figure 4.5-17 Observed and predicted stage at San Francisco NOAA tide station (9414290) during the December 2006 Storm simulation period.

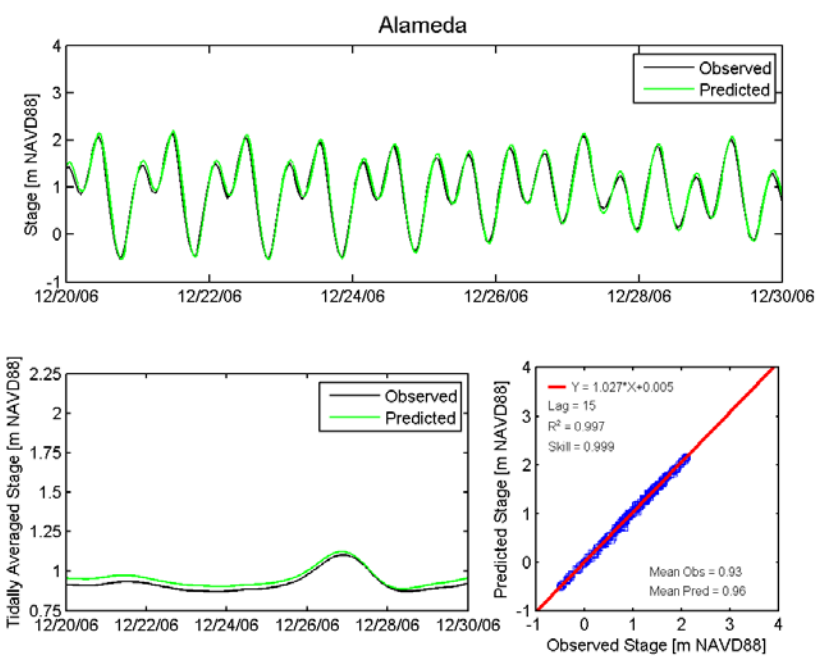

Figure 4.5-18 Observed and predicted stage at Alameda NOAA tide station (9414750) during the December 2006 Storm simulation period.

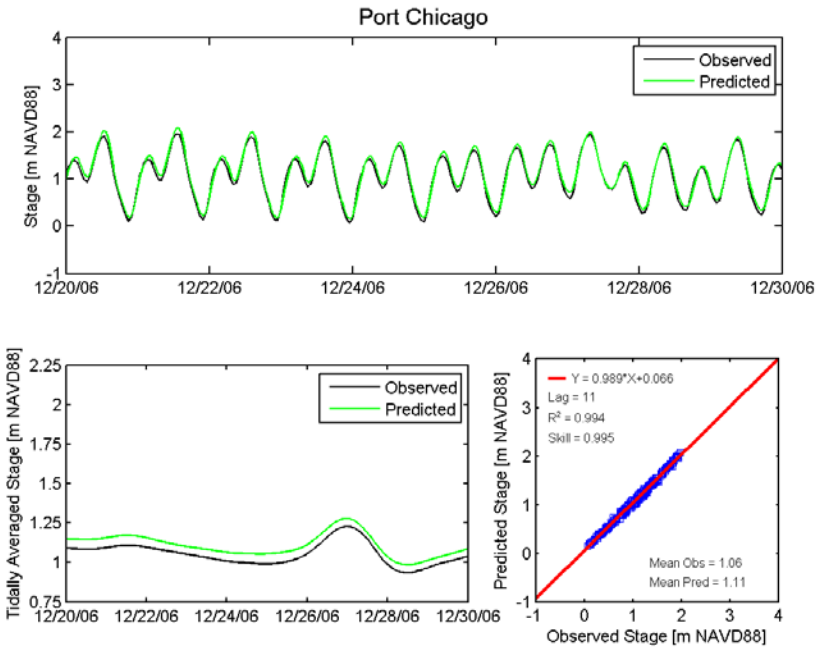

Figure 4.5-19 Observed and predicted stage at Port Chicago NOAA tide station (9415144) during the December 2006 simulation period.

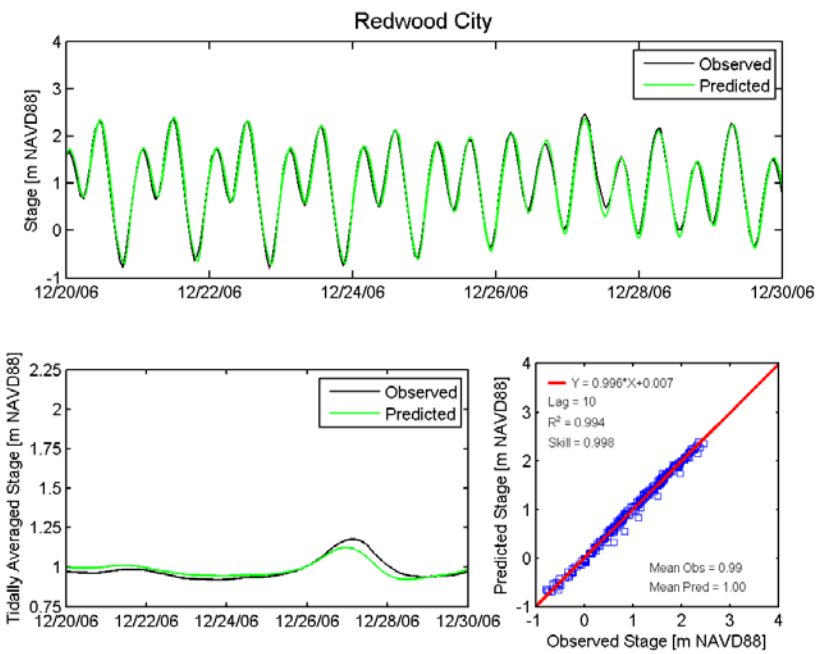

Figure 4.5-20 Observed and predicted stage at Redwood City NOAA tide station (9414523) during the December 2006 simulation period.

4.6 Assessment of Model Accuracy for All Simulated Storm Peaks

This section provides an assessment of the accuracy of the predicted peak water levels for each of the ten ranked events which occurred during the model validation simulations. Model accuracy was evaluated at the San Francisco tide station (9414290), and at all South Bay tide stations for which either hourly water level observation data or maximum event water level data were available.

For each event, the maximum observed water level was calculated using both the hourly water level observation data from NOAA and using the maximum monthly water level reported by NOAA at each station. In some cases, the maximum monthly water level reported by NOAA exceeded the maximum water level in the hourly time series data. This can occur if the hourly data does not exactly capture the peak tidal water level at high tide. For events where the reported maximum monthly water level exceeded the maximum hourly data at a given station, the maximum monthly water level was used for the highest peak observed water level for that storm event rather than using the maximum of the hourly data, as indicated in Tables 4.6-1 and 4.6-2. This approach helps to ensure that the maximum measured peak water level was used for each event. When the maximum monthly data was used, this approach resulted in a 0.02 to 0.05 m higher maximum water level than the maximum water level that was reported in the hourly data.

Table 4.6-1 shows the difference between the observed and predicted peak water level at San Francisco (9414290) for each of the ten ranked events during the model validation simulations. The predicted peak water level is within 0.10 m (0.33 ft) of the observed peak water level for all ten events, and within 0.04 m (0.13 ft) of the observed peak water level for nine of the ten events. The maximum difference of 0.10 m at San Francisco station (9414290) occurred for the December 3, 1983 peak water level. This difference can be partially explained because the observed wind from SFO was applied uniformly over the model domain for the 1983 storm events. When wind is not included in the simulation(see Table 4.7-3) the difference between the predicted and observed water level for this event is only 0.05 m (0.16 ft). In the January 1983 storm, wind has a much smaller effect on peak water levels in South San Francisco Bay (see Table 4.7-4). In the 1997 and 1998 storm events when better geographic coverage of wind observation data were available, the maximum difference between the predicted and observed water levels at San Francisco was 0.04 m (0.13 ft).

Table 4.6-2 shows the difference between the observed and predicted peak water levels at three South San Francisco Bay tide stations for each of the ten ranked events during the model validation simulations. For the four ranked events during January 1983, the only water level observation data available in South San Francisco Bay is at San Mateo Bridge (9414458). The predicted peak water level is within 0.04 m (0.13 ft) of the observed peak water level at San Mateo Bridge for all four of these events. For the ranked event during December 1983, hourly water level observations are available at Redwood City (9414523) and a single maximum observed water level is reported at Coyote Creek (9414575).

The highest water level recorded by NOAA within the project area occurred at the Coyote Creek (9414575) station on December 3, 1983 (NOAA, 1990). This event was also reported by the USACE (1984) as 12.5 ft MLLW. Using the conversion from MLLW to NAVD88 (Table 4.1-2) reported by Foxgrover et al. (2007), this observed peak water level corresponds to a maximum observed water level of 11.01 ft NAVD88 (3.36 m NAVD88)[2]. At Coyote Creek (9414575), the predicted peak water level of 3.35 m (10.99 ft)on December 3, 1983 is within 0.01 m (0.02 ft) of the peak observed water level. For this same event, the predicted peak water level at Redwood City (9414523) is 0.11 m (0.36 ft) higher than the peak observed water level at Redwood City. For the five ranked events during 1997 and 1998, the only water level observation data available in South San Francisco Bay is at Redwood City (9414523). The predicted peak water level is within 0.06 m (0.20 ft) of the observed peak water level at Redwood City for all five of these events.

For the twenty-one comparisons of peak water level shown in Tables 4.6-1 and 4.6-2, the predicted peak water level is within 0.06 m (0.20 ft) of the observed peak water level for nineteen of the twenty-one comparisons and within 0.04 m (0.13 ft) for seventeen of the twenty-one comparisons.

The cross-correlation for each of the two calibration periods (Table 4.3-1 and Table 4.3-3), and each of the model validation periods (Table 4.5-1, Table 4.5-2, Table 4.5-3, Table 4.5-4, and Table 4.5-5) show the calculated phase difference between observed and predicted water level time series at each of the stations where time series comparisons were made. The maximum phase difference between observed and predicted time series identified in the cross-correlation analysis occurred during the January 1983 storm event at the Alameda (9414750), where the predicted tides lagged the observed tides by 17 minutes. At all other stations and for all other events simulated, the phase difference between observed and predicted time series was 15 minutes or less. In each simulation, the largest phase differences typically occurred at the Alameda (9414575) station. This phase difference may result because the NOAA water level station at Alameda (9414750) is located behind a breakwater that cannot be fully resolved in the model grid. Given that hourly observation data was used for the comparisons between observed and predicted water levels, the calculated phase error is much smaller than the data

[2] Because NOAA does not report a datum conversion between MLLW and NAVD88 at the Coyote Creek station, multiple different peak water levels for this event have been reported in NAVD88. PWA (2007) reports this peak water level as 10.88 ft MLLW (page 3.3-10) and lists a conversion from MLLW to NAVD of -1.52 ft (Page 3.3-5). PWA (2006) reports this same event as 3.35 m (10.99 ft) using a conversion between MLLW and NAVD88 of -0.46 m (page 20-21). In both cases this event is cited as USACE (1984) which lists the event as 12.5 ft MLLW. DHI (2010) report this same event as 11.55 ft NAVD88, however their conversion between MLLW and NAVD88 was based on V-Datum. It is widely recognized that V-Datum does a poor job of converting between geodetic and tidal datums in far South San Francisco Bay. Foxgrover et al. (2011b) report that V-Datum consistently underestimates the offset between NAVD88 and MLLW for regions south of Dumbarton Bridge. Thus the peak water level reported in NAVD88 by DHI (2010) is likely to be significantly overstated. Using the water level data collected at Coyote Creek during 2011, the USACE estimated the conversion between MLLW and NAVD88 to be -0.41 m (-1.345 ft), which would suggest a peak water level of 11.17 ft NAVD88 (3.40 m NAVD88). Based on the best available datum conversion data currently available from Foxgrover et al. (2007), the peak water level of 12.51 ft MLLW for this event corresponds to 11.01 ft NAVD88 (3.36 m NAVD88). This is the value used for the comparisons to predicted water levels for the December 1983 event in this study.

frequency suggesting that the model is accurately predicting the propagation of tidal phase throughout the model domain.

Table 4.6-1 Model verification results for all storm peaks at San Francisco tide station (9414290).

Simulation	Rank	Start Date	End Date	Maximum Observed Water Level (m NAVD88)	Maximum Predicted Water Level (m NAVD88)	Difference (m)
January 1983	1	1/26/1983	1/29/1983	2.71	2.68	-0.03
January 1983	5	1/28/1983	1/31/1983	2.54	2.58	0.04
January 1983	16	1/22/1983	1/25/1983	2.31	2.30	-0.01
January 1983	39	1/17/1983	1/20/1983	2.01	2.05	0.04
December 1983	2	12/2/1983	12/5/1983	2.67	2.57	-0.10
November 1997	17	11/26/1997	11/28/1997	2.34†	2.31	-0.03
December 1997	32	12/5/1997	12/8/1997	2.15	2.14	-0.01
February 1998	3	2/4/1998	2/7/1998	2.59	2.57	-0.02
February 1998	4	2/6/1998	2/9/1998	2.59	2.57	-0.02
February 1998	12	2/2/1998	2/5/1998	2.44	2.48	0.04

† Maximum observed water level is from the monthly maximum reported by NOAA.

Table 4.6-2 Model verification results for all storm peaks at South Bay tide stations.

Simulation	Rank	Start Date	End Date	Maximum Observed Water Level (m NAVD88)	Maximum Predicted Water Level (m NAVD88)	Difference (m)
January 1983*	1	1/26/1983	1/29/1983	3.04†	3.02	-0.02
January 1983*	5	1/28/1983	1/31/1983	2.98	2.94	-0.04
January 1983*	16	1/22/1983	1/25/1983	2.56	2.56	0.00
January 1983*	39	1/17/1983	1/20/1983	2.30	2.31	0.01
December 1983**	2	12/2/1983	12/5/1983	2.97†	3.08	0.11
December 1983***	2	12/2/1983	12/5/1983	3.36†	3.35	-0.01
November 1997**	17	11/26/1997	11/28/1997	2.70†	2.69	-0.01
December 1997**	32	12/5/1997	12/8/1997	2.40	2.45	0.05
February 1998**	3	2/4/1998	2/7/1998	2.85	2.89	0.04
February 1998**	4	2/6/1998	2/9/1998	2.85	2.89	0.04
February 1998**	12	2/2/1998	2/5/1998	2.85	2.79	-0.06

*San Mateo Bridge (9414458)
** Redwood City (9414523)
*** Coyote Creek (9414575)
† Maximum observed water level is from the monthly maximum reported by NOAA.

4.7 Evaluation of Storm Surge Propagation and Effect of Wind

This section evaluates storm surge propagation in South San Francisco Bay and the effects of wind on predicted peak water levels during storms. A series of additional sensitivity simulations were made to isolate the effects of wind, the propagation of and amplification of astronomical tides, and the propagation of storm surge. A total of six different simulations were compared in this analysis as shown in Table 4.7-1.

Four simulations of the December 1983 validation period (Table 4.7-1) were compared in this analysis. The first simulation used observed tides from San Francisco (9414290) for the tidal boundary condition and observed SFO wind is applied uniformly over the model domain. This simulation is identical to the simulation shown in Section 4.5.2. An additional simulation was made using identical parameters, except without wind. This simulation allows for an evaluation of wind effects during the December 1983 storm event. The third simulation for the December 1983 used astronomical tides developed from tidal harmonic constituents from San Francisco (9414290) as the ocean boundary condition rather than observed tides and does not use wind. This simulation allows for an assessment of how well the model predicts the propagation of astronomical tides in the absence of storm or wind forcing. The results of this simulation are presented in section 4.7.1. The final simulation for the December 1983 used astronomical tides developed from tidal harmonic constituents from San Francisco (9414290) with observed SFO is wind applied uniformly over the model domain. This simulation allows for an evaluation of the effects of wind without storm surge. When astronomical tides from San Francisco are used for the ocean boundary condition, the amplification factor and phase shift described in Section 3.6 were applied to account for the difference in tidal range between observed San Francisco tides and tides along the model ocean boundary and to account for the phase difference of tides between the San Francisco (9414290) station and the model boundary.

Two simulations of the January 1983 validation period (Table 4.7-1) were compared in this analysis. The first simulation uses observed tides from San Francisco (9414290) for the tidal boundary condition and observed SFO wind is applied uniformly over the model domain. This simulation is identical to the simulation shown in Section 4.5.1. The second simulation of the January 1983 period was made using identical parameters, except without wind. This simulation allows for an evaluation of the effects of wind during the January 1983 storm event.

Table 4.7-1 Simulations used in evaluation of storm surge propagation and effects of wind.

Simulation Period	Scenario Number	Scenario Name	Tidal Boundary Condition	Wind
December 1983	1	Predicted*	Observed	Observed SFO
	2	Predicted (No Wind)	Observed	None
	3	Predicted (Astronomical BC)	Astronomical	None
	4	Predicted (Astronomical+Wind)	Astronomical	Observed SFO
January 1983	5	Predicted*	Observed	Observed SFO
	6	Predicted (No Wind)	Observed	None

* These simulations are identical to the model validation simulations presented in Section 4.5.

4.7.1 Simulation of December 1983 using Astronomical Tides

The December 1983 simulation period spans from November 26, 1983 to December 8, 1983. A simulation of the December 1983 validation period was made using astronomical tides from San Francisco (9414290) for the ocean boundary condition rather than observed tides, and wind forcing was not used in this simulation (Scenario 3 in Table 4.7-1). The predicted water levels in this simulation represent the propagation of the astronomical tides in San Francisco Bay in the absence of storm surge or wind forcing. The predicted water levels from this simulation at five stations in San Francisco Bay were compared with astronomical tides from NOAA at each station which are derived from the harmonic constituents at each respective station.

Predicted water levels from this simulation were compared to astronomical tides at San Francisco (9414290) (Figure 4.7-1), San Mateo Bridge (9414458) (Figure 4.7-2), Redwood City (9414523) (Figure 4.7-3), Dumbarton Bridge (9414509) (Figure 4.7-4), and at Coyote Creek (9414575) (Figure 4.7-5). The results of the cross-correlation analysis at these five stations are summarized in Table 4.7-2. The predicted mean water levels during the December 1983 simulation period are within 0.03 m of observed mean water levels at all five stations. With the exception of Coyote Creek, the values of the coefficient of determination between observed and predicted water levels are between 0.996 and 0.997, and the model skill is 0.999 at all four station.

In general the predicted tidally averaged stage is relatively flat at all five stations, with slightly larger deviations for stations in the south end of South Bay. At Coyote Creek, there is relatively poor agreement between the predicted (modeled) water levels and the astronomical tides generated from tidal harmonic constituents. Since the comparison at Dumbarton Bridge indicates very good agreement between predicted (modeled) tides and astronomical tides, this suggests that the astronomical tides from NOAA at Coyote Creek are suspect[3]. Thus, the use of astronomical tides at Coyote Creek and San Francisco to develop transfer functions between water levels at San Francisco and Coyote Creek is not likely to produce accurate results.

[3]The astronomical tides developed using tidal harmonic constituents may not be accurate if the time series used to extract the tidal constituents was not representative. In this case, based on the comparisons shown in Figure 4.7-5, NOAA CO-OPS has confirmed (Gill, email comm., March, 22 2012) that a significant error was found in the Accepted Harmonic Constants for NOAA station 9414575 that were posted prior to March 21, 2012. NOAA reported that this resulted due to a conversion error which affected original numbers which were within a certain negative range. This error predominantly affected lower low water values during spring tide, which is consistent with the discrepancy seen in Figure 4.7-5.

Table 4.7-2 Cross-correlation results from December 1983 simulation using astronomical tides at the ocean boundary and astronomical tides at each station.

Station Location	Mean Water Level			Amplitude Ratio	Lag (min)	Coefficient of Determination	Skill	Figure Number
	Astronomical (m)	Predicted (m)	Difference (m)					
San Francisco (9414290)	0.97	0.97	0.00	0.98	2	0.997	0.999	4.7-1
San Mateo Br. (9414458)	1.02	1.02	0.01	1.01	0	0.997	0.999	4.7-2
Redwood City (9414523)	1.01	1.03	0.02	0.99	5	0.996	0.999	4.7-3
Dumbarton Br. (9414509)	1.01	1.03	0.02	0.99	-7	0.996	0.999	4.7-4
Coyote Creek (9414575)	1.08	1.05	-0.03	1.18	3	0.907	0.964	4.7-5

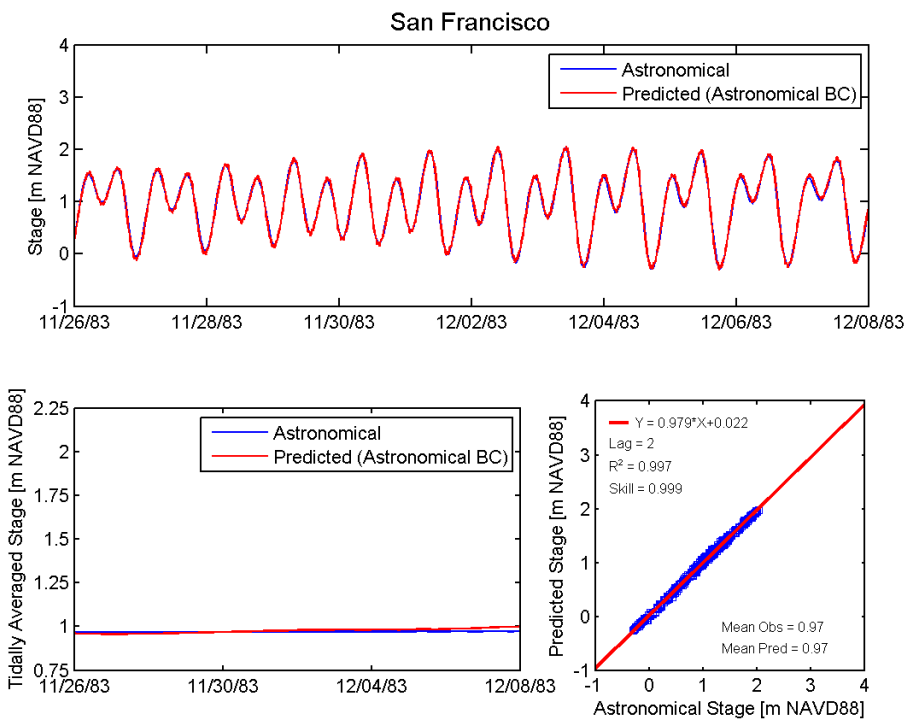

Figure 4.7-1 Astronomical tide and predicted tide at San Francisco NOAA tide station (9414290) for December 1983 simulation using astronomical tides for the ocean boundary condition.

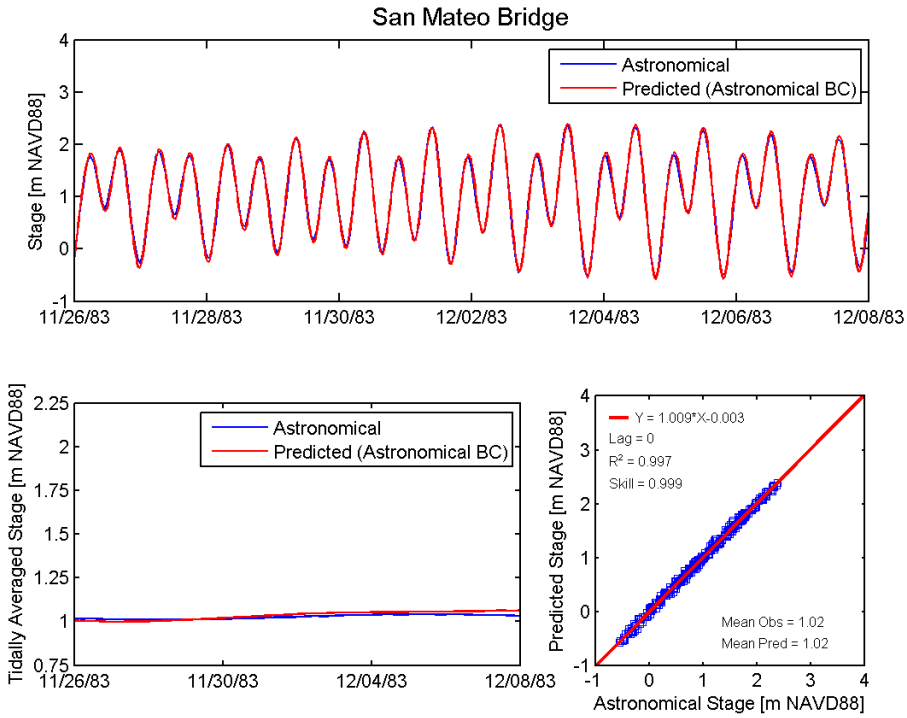

Figure 4.7-2 Astronomical tide and predicted tide at San Mateo Bridge NOAA tide station (9414458) for December 1983 simulation using astronomical tides for the ocean boundary condition.

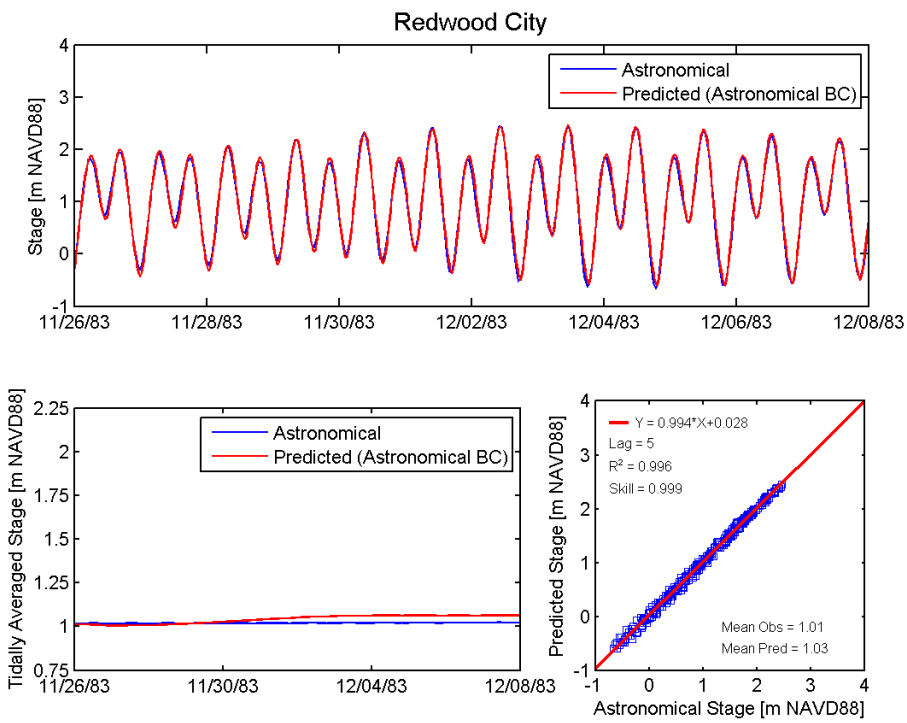

Figure 4.7-3 Astronomical tide and predicted tide at Redwood City NOAA tide station (9414523) for December 1983 simulation using astronomical tides for the ocean boundary condition.

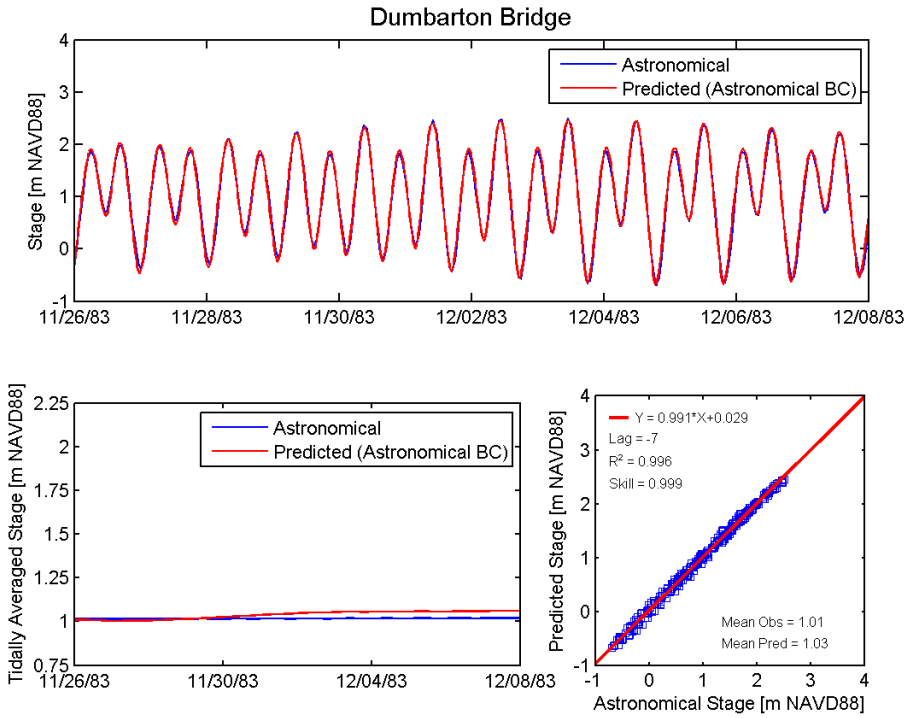

Figure 4.7-4 Astronomical tide and predicted tide at Dumbarton Bridge NOAA tide station (9414509) for December 1983 simulation using astronomical tides for the ocean boundary condition.

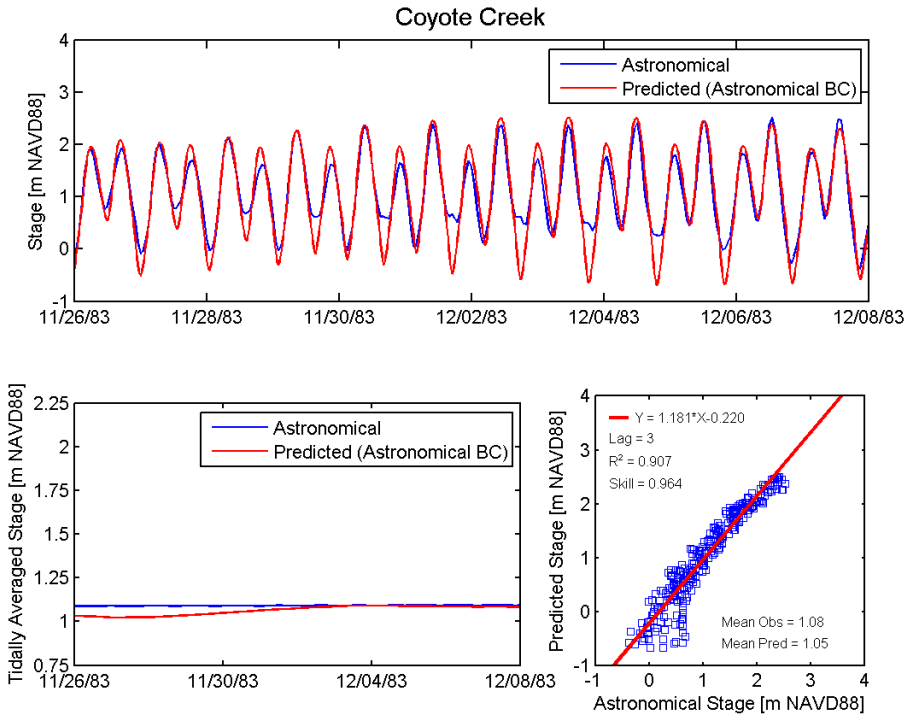

Figure 4.7-5 Astronomical tide and predicted tide at the Coyote Creek NOAA tide station (9414575) for December 1983 simulation using astronomical tides for the ocean boundary condition.

4.7.2 Evaluation of Storm Surge Propagation during December 1983 Storm

This section evaluates storm surge propagation during the December 1983 storm. Predicted water levels for the December 1983 storm presented in Section 4.5.2 (Scenario 1 in Table 4.7-1) were compared to predicted water levels from a simulation which used identical parameters except that astronomical tides from San Francisco (9414290) were used for the ocean boundary condition rather than observed tides (Scenario 4 in Table 4.7-1). Identical wind forcing was applied in these two simulations. An additional comparison was made between predicted water levels for a simulation made using observed water levels at the ocean boundary without wind (Scenario 2 in Table 4.7-1) and a simulation without wind that used astronomical tides from San Francisco (9414290) for the ocean boundary (Scenario 3 in Table 4.7-1). The purpose of these two comparisons is to evaluate whether the storm surge observed at the San Francisco tide station amplifies in South San Francisco Bay. Storm surge propagation was evaluated for simulations both with and without wind.

Figure 4.7-6 shows the difference between predicted water levels at five stations in San Francisco Bay from the simulation using observed tides and wind and the simulation using astronomical tides and wind. The difference between these two simulations represents the residual storm surge for the two simulations with wind. The top panel shows the raw difference, and the bottom panel shows the difference when filtered with a 4th order Butterworth filter with a cutoff frequency of 1/3 $hours^{-1}$ to remove the high frequency noise from the comparison. The filtered comparison shows that the tidal surge is not amplified significantly as it propagates into South Bay. The difference between the maximum filtered storm surge at San Francisco and the maximum filtered storm surge at San Mateo Bridge, Dumbarton Bridge, and Coyote Creek is less than 0.04 m (0.13 ft). The maximum filtered storm surge at Redwood City is approximately 0.05 m (0.16 ft) higher than at San Francisco.

Figure 4.7-7 shows the difference between predicted water levels at five stations in San Francisco Bay from the simulation using observed tides without wind and the simulation using astronomical tides without wind. The difference between these two simulations represents the residual storm surge for the two simulations without wind. The top panel shows the raw difference, and the bottom panel shows the difference when filtered with a 4th order Butterworth filter with a cutoff frequency of 1/3 $hours^{-1}$ to remove the high frequency noise from the comparison. The filtered comparison shows that the tidal surge is not amplified significantly as it propagates into South Bay. The difference between the maximum filtered storm surge at San Francisco and the maximum filtered storm surge at San Mateo Bridge, Redwood City, and Dumbarton Bridge is less than 0.02 m (0.07 ft). The maximum filtered storm surge at Dumbarton Bridge is approximately 0.04 m (0.13 ft) higher than at San Francisco.

These two comparisons demonstrate that storm surge does not amplify significantly as it propagates into South San Francisco Bay in the same way that the astronomical tides amplify. The similarities between the storm surge propagation for the simulations with and without wind suggests that the propagation of the storm surge observed at San Francisco into the South Bay is not strongly influenced by wind. However, wind forcing can have a strong influence on peak water levels in the Far South Bay as seen in the following section.

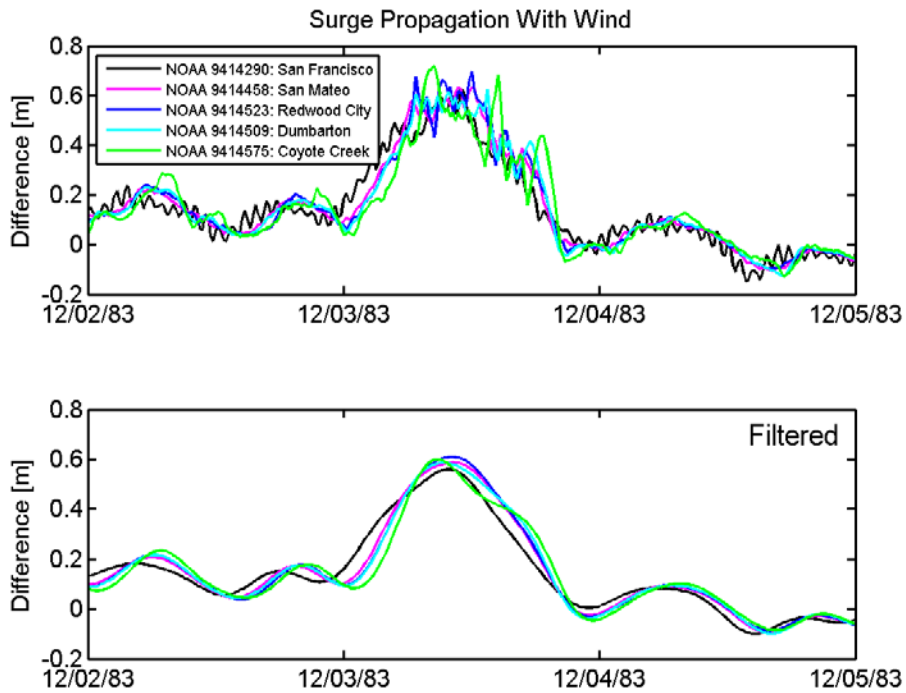

Figure 4.7-6 Difference between predicted water levels at five stations in San Francisco Bay from simulations using observed tides and astronomical tides at ocean boundary. In both cases, wind forcing was applied. The top panel shows the raw difference and the bottom panel shows the filtered difference.

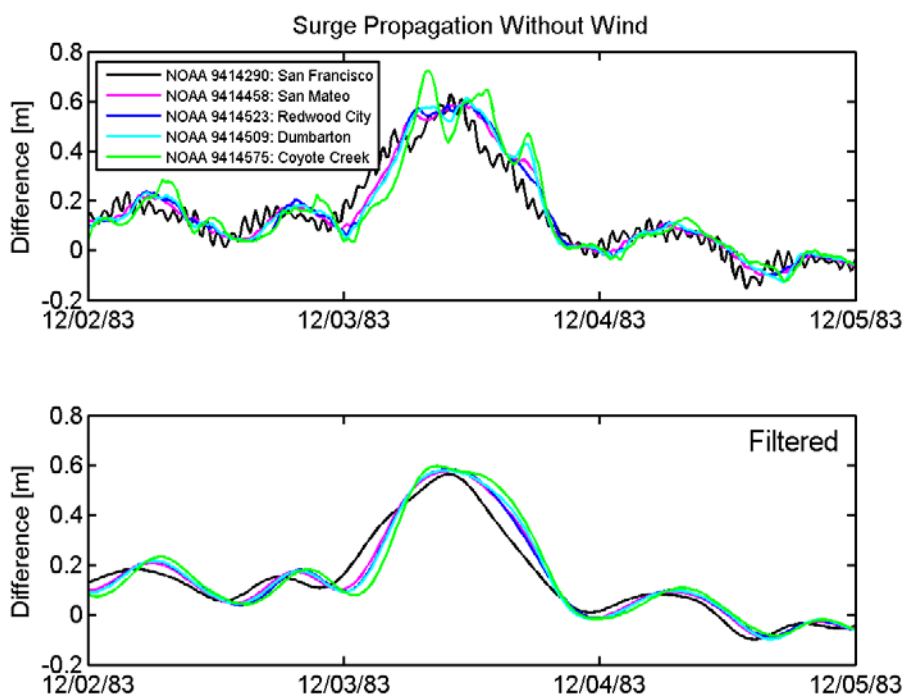

Figure 4.7-7 Difference between predicted water levels at five stations in San Francisco Bay from simulations using observed tides and astronomical tides at ocean boundary. In both cases, no wind forcing was applied. The top panel shows the raw difference and the bottom panel shows the filtered difference.

4.7.3 Evaluation of Effect of Wind during December 1983 Storm

This section evaluates the effect of wind on predicted water levels during the December 1983 storm event. Predicted water levels from the December 1983 storm presented in Section 4.5.2 (Scenario 1 in Table 4.7-1) which used observed wind speed and direction from SFO uniformly over the model domain were compared to predicted water levels from a simulation using identical model parameters except that it did not include wind forcing (Scenario 2 in Table 4.7-1).

On December 3, when the peak water levels occurred in South San Francisco Bay, the observed wind direction was between 270 degrees and 360 degrees and the observed wind speed at SFO was more than 20 m/s (44.7 mph) as seen in Figure 4.7-8. When the wind direction is between 270 and 360 degrees, the wind direction is from the north-northwest. This wind direction is generally aligned with the axis of South San Francisco Bay which tends to increase water levels in the south end of South San Francisco Bay.

Predicted water levels were compared between these two simulations at five stations. At two of these stations (San Francisco and Redwood City) hourly water level data were also available for comparison, and at one station (Coyote Creek) only the peak water level observation was available. At two stations (San Mateo Bridge and Dumbarton Bridge), no observation data were available for comparison. Comparisons of water levels were made at San Francisco (9414290) (Figure 4.7-9), San Mateo Bridge (9414458) (Figure 4.7-10), Redwood City (9414523) (Figure 4.7-11), Dumbarton Bridge (9414509) (Figure 4.7-12), and Coyote Creek (9414575) (Figure 4.7-13). The maximum predicted water level at each station from the simulations with and without wind are shown in Table 4.7-3.

At San Francisco (9414290) and San Mateo Bridge (9414458), the maximum predicted water levels for the simulation with wind are 0.05 m (0.16 ft) and 0.07 m (0.25 ft) lower than the maximum predicted water levels for the simulation without wind, respectively. However, at Redwood City (9414523) and Dumbarton Bridge (9414509), the maximum predicted water levels for the simulation with wind are 0.04 m (0.13 ft) and 0.05 m (0.15 ft) higher than the maximum predicted water levels for the simulation without wind, respectively. At Redwood City, wind also has a significant effect on the tidal phase. The timing of the peak water level for the simulation with wind much more closely matches the timing of the peak observed water level than the simulation without wind (Figure 4.7-11).

The largest effect of wind is evident at Coyote Creek, where the maximum predicted water level from the simulation with wind is 0.25 m (0.82 ft) higher than the maximum predicted water level from the simulation without wind (Figure 4.7-13). The maximum predicted water level from the simulation with wind is within 0.01 m (0.03 ft) of the maximum observed water level at Coyote Creek, whereas the maximum predicted water level from the simulation without wind is 0.26 m (0.85 ft) less than the maximum observed water level at Coyote Creek. Wind also results in a shift in the timing of the peak water level at Coyote Creek. This demonstrates the potential influence of wind speed and direction on maximum water levels in the project area during a period with relative strong winds aligned with the axis of South San Francisco Bay.

Table 4.7-3 Maximum observed water level and maximum predicted water level from simulations with and without wind forcing for December 1983 simulation period.

Name	NOAA Station	Maximum Water Level (m NAVD88)			Maximum Water Level (ft NAVD88)		
		Observed	Predicted with SFO Wind	Predicted without Wind	Observed	Predicted with SFO Wind	Predicted without Wind
San Francisco	9414290	2.67	2.57	2.62	8.76	8.43	8.59
San Mateo Br.	9414458	-	2.90	2.97	-	9.51	9.76
Redwood City	9414523	2.97	3.08	3.04	9.74	10.10	9.97
Dumbarton Br.	9414509	-	3.11	3.06	-	10.20	10.05
Coyote Creek	9414575	3.36	3.35	3.10	11.01	10.99	10.19

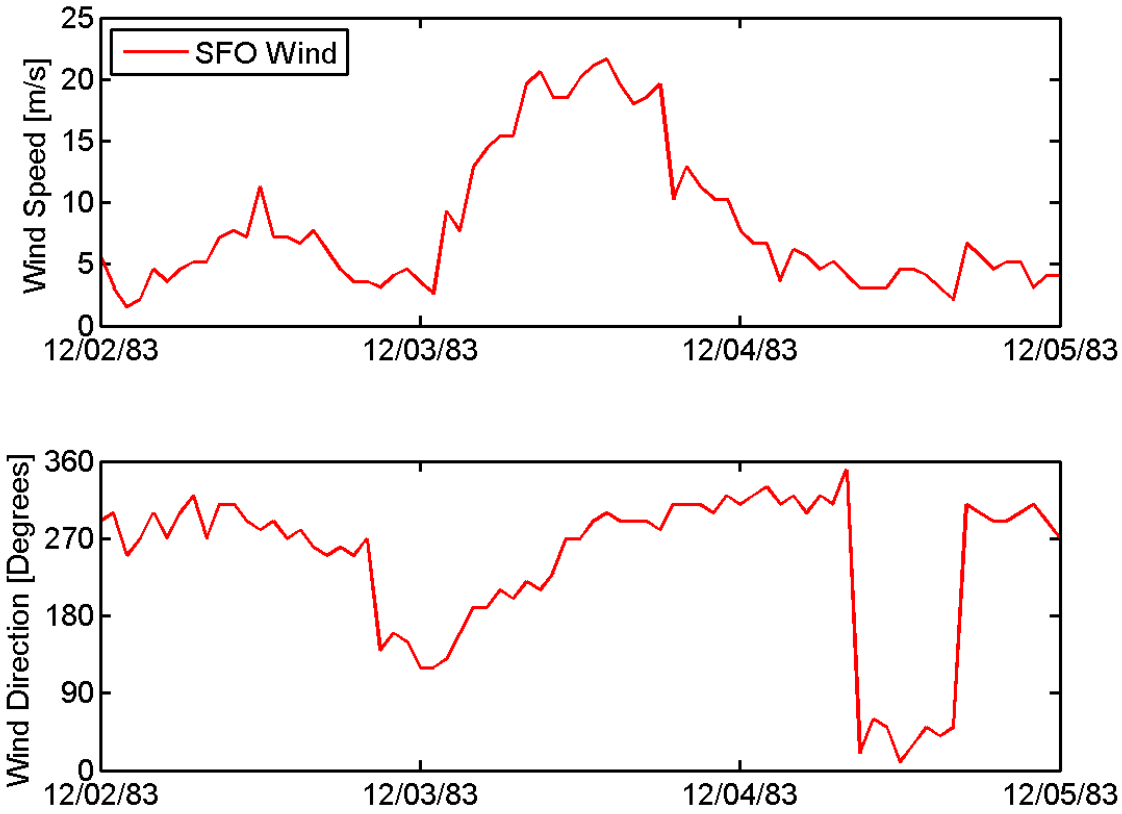

Figure 4.7-8 Observed wind speed and direction at San Francisco International Airport (SFO) from December 2, 1983 to December 5, 1983 (Source: NOAA, 1993).

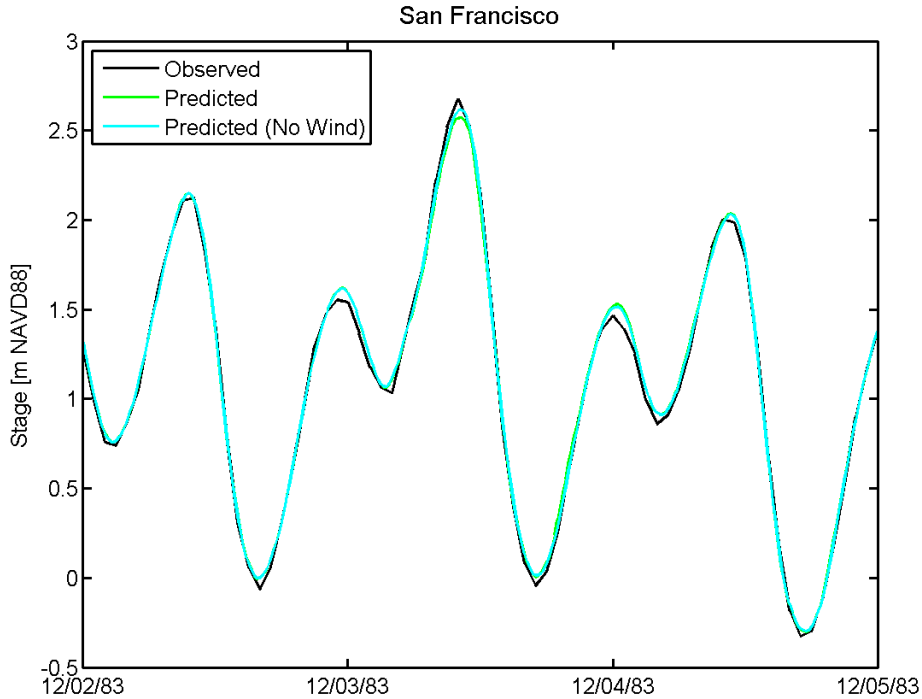

Figure 4.7-9 Observed and predicted stage at the San Francisco NOAA tide station (9414290) from December 1983 storm simulations made with and without wind forcing.

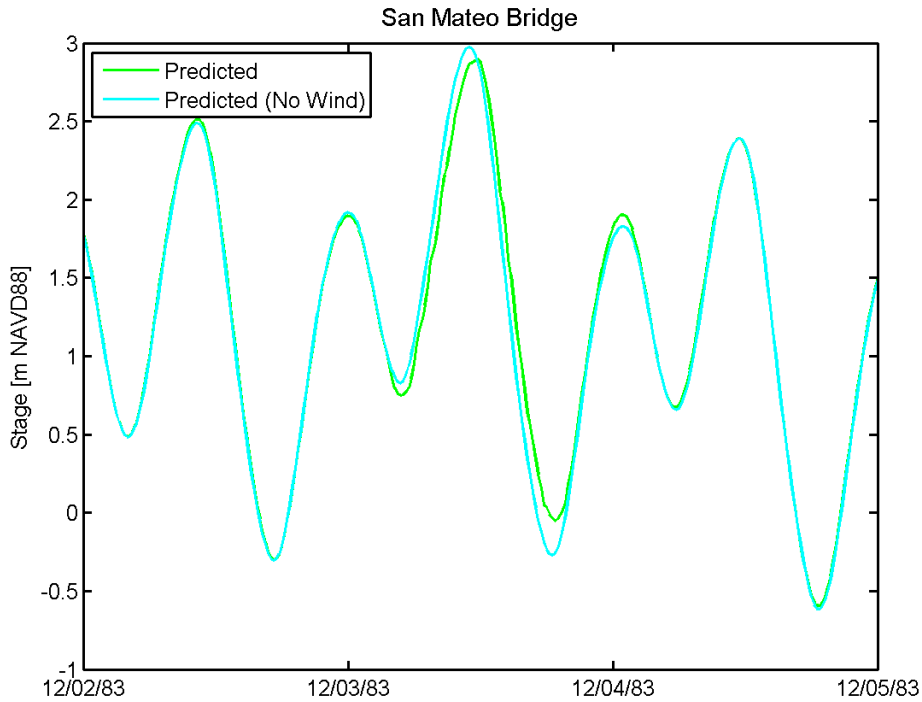

Figure 4.7-10 Predicted stage at the San Mateo Bridge NOAA tide station (9414458) from December 1983 storm simulations made with and without wind forcing.

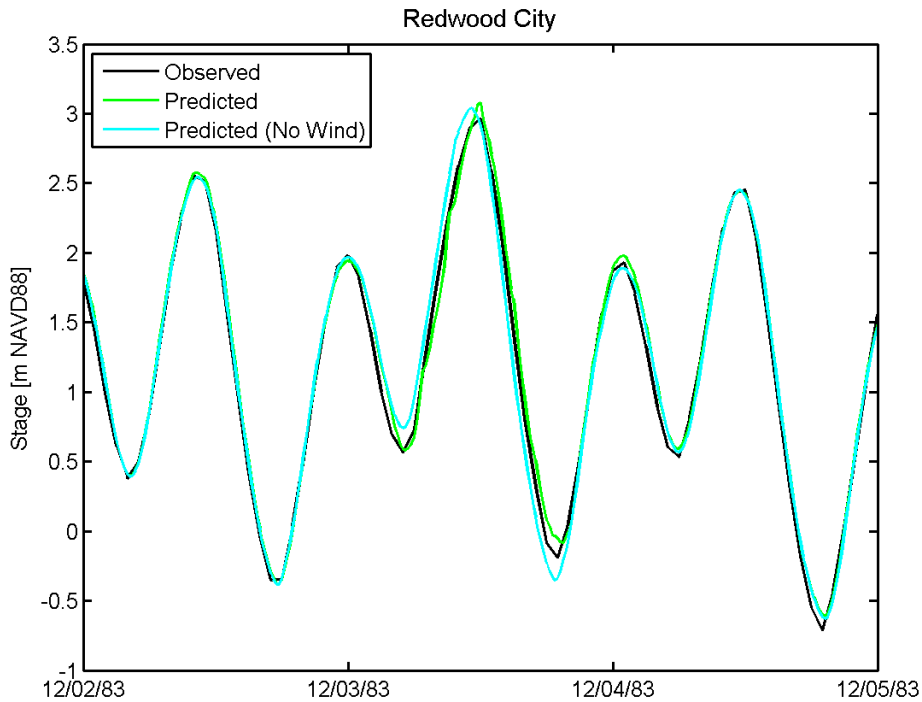

Figure 4.7-11 Observed and predicted stage at the Redwood City NOAA tide station (9414523) from December 1983 storm simulations made with and without wind forcing.

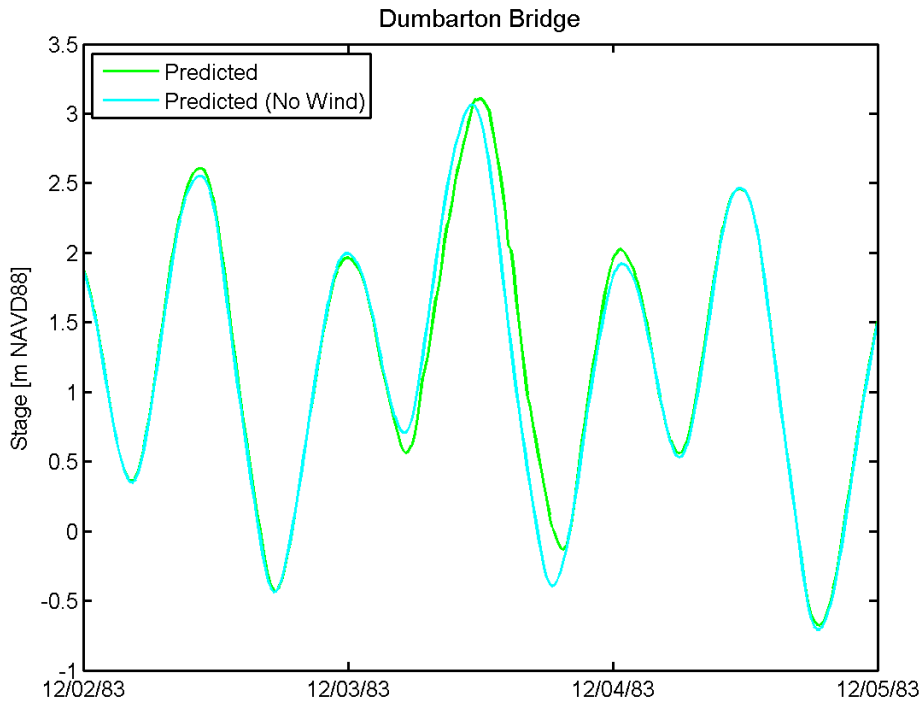

Figure 4.7-12 Predicted stage at the Dumabrton Bridge NOAA tide station (9414509) from December 1983 storm simulations made with and without wind forcing.

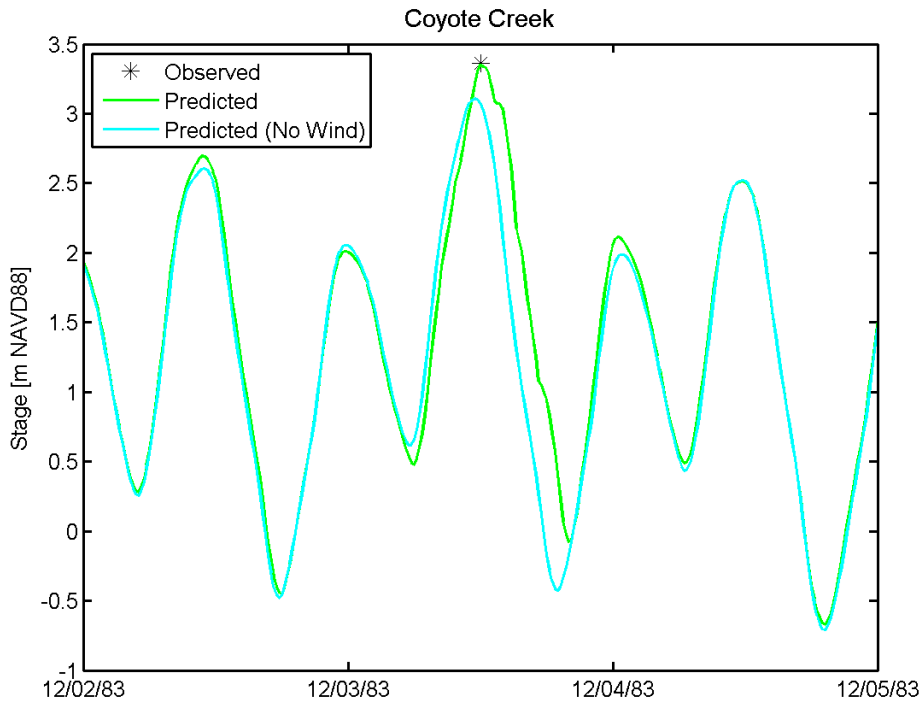

Figure 4.7-13 Predicted stage at the Coyote Creek NOAA tide station (9414575) from December 1983 storm simulations made with and without wind forcing, shown with peak observed water level for December 3, 1983.

4.7.4 Evaluation of Effect of Wind during January 1983 Storm

This section evaluates the effect of wind on predicted water levels during the January 1983 storm. Predicted water levels for the January 1983 storm presented in Section 4.5.1 (Scenario 5 in Table 4.7-1) which used observed wind speed and direction from SFO uniformly over the model domain were compared to predicted water levels for a simulation using identical model parameters except that it did not include wind forcing (Scenario 6 in Table 4.7-1).

On January 27, when the peak water levels occurred in South San Francisco Bay, the maximum observed hourly wind speed at SFO was 14.9 m/s (33.3 mph) as seen in Figure 4.7-14. During the first half of the day when the peak water level occurred, the wind speed was relatively low and the wind direction was between 90 and 180 degrees. On January 26, when higher wind speeds were observed, the wind direction was around 180 degrees indicating winds from the south.

Predicted water levels were compared for these two simulations at five stations. At two of these stations (San Francisco and San Mateo Bridge) hourly water level data were also available for comparison. At three stations (Redwood City, Dumbarton Bridge, and Coyote Creek), no observation data were available for comparison. Comparisons of water levels were made at San Francisco (9414290) (Figure 4.7-15), San Mateo Bridge (9414458) (Figure 4.7-16), Redwood City (9414523) (Figure 4.7-17), Dumbarton Bridge (9414509) (Figure 4.7-18), and Coyote Creek (9414575) (Figure 4.7-19). The maximum predicted water level at each station for the simulations with and without wind are shown in Table 4.7-4. During the January 1983 simulation period, wind has a much smaller influence on predicted water levels than during the December 1983 simulation period (Section 4.7.3). In addition, the wind during the January 1983 simulation results in a decrease in maximum predicted water level at all five stations relative to the simulation without wind.

At the San Francisco station (9414290) and San Mateo Bridge (9414458), the maximum predicted water levels from the simulation with wind are 0.00 m (0.02 ft) and 0.01 m (0.05 ft) lower than the maximum predicted water levels from the simulation without wind, respectively. At Redwood City (9414523) and Dumbarton Bridge (9414509), the maximum predicted water levels from the simulation with wind are 0.02 m (0.07 ft) and 0.02 m (0.06 ft) lower than the maximum predicted water levels from the simulation without wind, respectively. At Coyote Creek, the maximum predicted water level from the simulation with wind is 0.03 m (0.09 ft) lower than maximum the predicted water level from the simulation without wind.

Unlike the December 1983 simulation, wind does not result in a significant difference in tidal phase at any of the stations at on January 27, the day of the maximum water level during the January 1983 simulation. However on January 26, 1983 wind has a somewhat large effect on tidal phase, and also results in a larger decrease in maximum water level relative to the simulation without wind, especially at Redwood City (9414523) (Figure 4.7-17), Dumbarton Bridge (9414509) (Figure 4.7-18), and Coyote Creek (9414575) (Figure 4.7-19). At San Mateo

Bridge (9414458) (Figure 4.7-16), the maximum predicted water level for the simulation with wind very closely matches the observed peak water level on January 26, indicating that the observed water levels are being similarly influenced by wind. This simulation demonstrates that when the wind direction is from the south, wind can result in a decrease rather than an increase in maximum water levels in the project area during some storms (the reverse of wind setup).

Table 4.7-4 Maximum observed water level and maximum predicted water level for simulations with and without wind forcing for January 1983 simulation period.

Name	NOAA Station	Maximum Water Level (m NAVD88)			Maximum Water Level (ft NAVD88)		
		Observed	Predicted with SFO Wind	Predicted without Wind	Observed	Predicted with SFO Wind	Predicted without Wind
San Francisco	9414290	2.71	2.68	2.68	8.89	8.78	8.80
San Mateo Br.	9414458	3.02	3.02	3.03	9.91	9.89	9.94
Redwood City	9414523	-	3.08	3.10	-	10.11	10.18
Dumbarton Br.	9414509	-	3.11	3.13	-	10.20	10.26
Coyote Creek	9414575	-	3.16	3.19	-	10.37	10.46

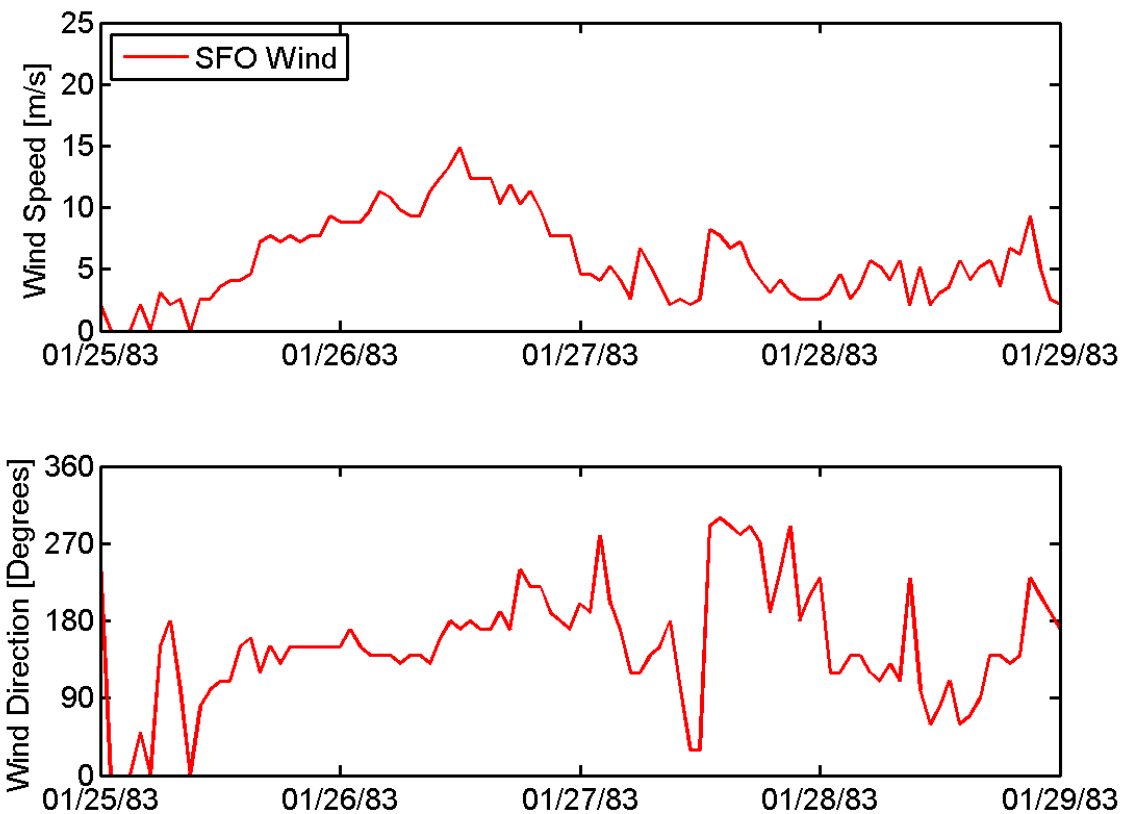

Figure 4.7-14 Observed wind speed and direction at San Francisco International Airport (SFO) from January 25, 1983 to January 29, 1983 (Source: NOAA, 1993).

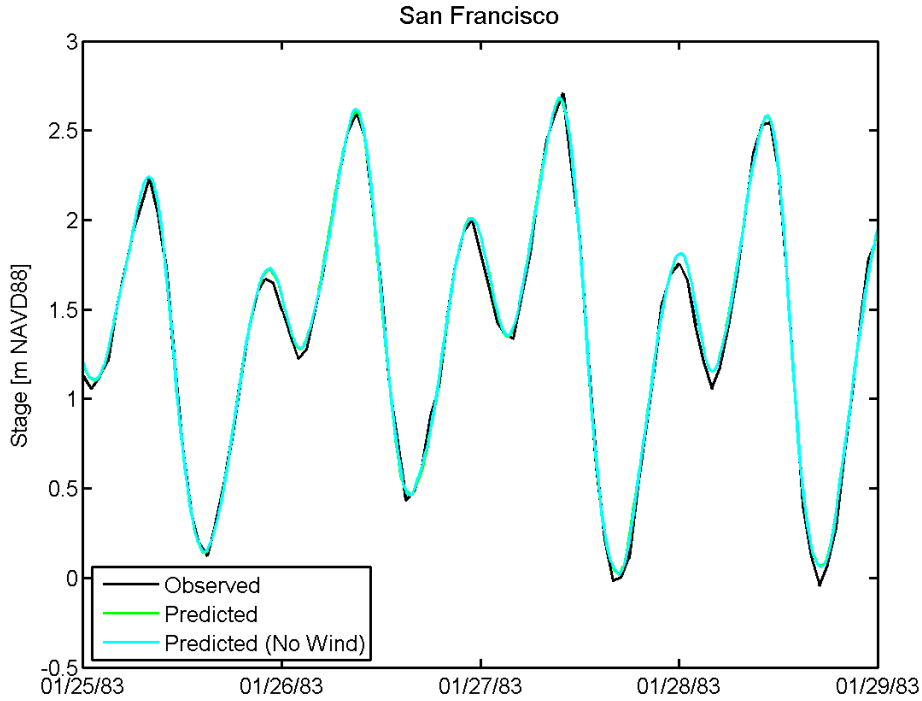

Figure 4.7-15 Observed and predicted stage at the San Francisco NOAA tide station (9414290) from January 1983 storm simulations made with and without wind forcing.

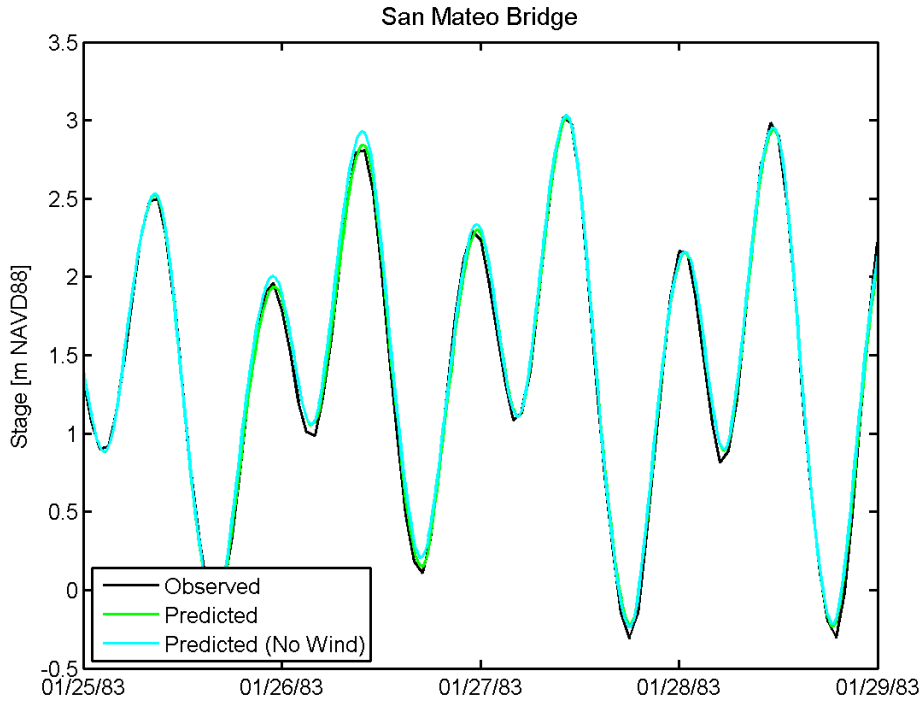

Figure 4.7-16 Observed and predicted stage at the San Mateo Bridge NOAA tide station (9414458) from January 1983 storm simulations made with and without wind forcing.

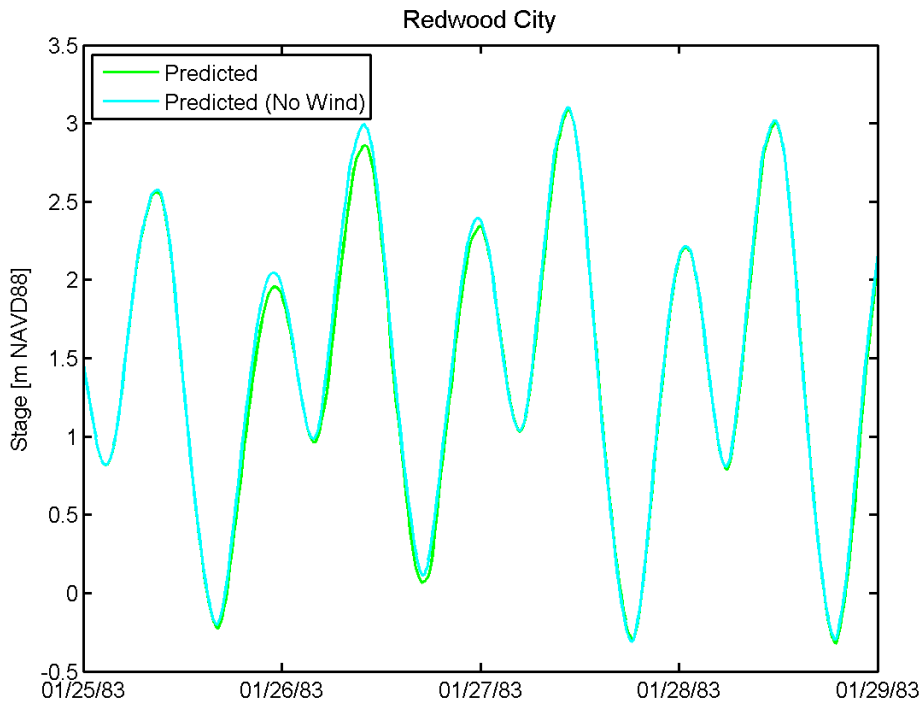

Figure 4.7-17 Predicted stage at the Redwood City NOAA tide station (9414523) from January 1983 storm simulations made with and without wind forcing.

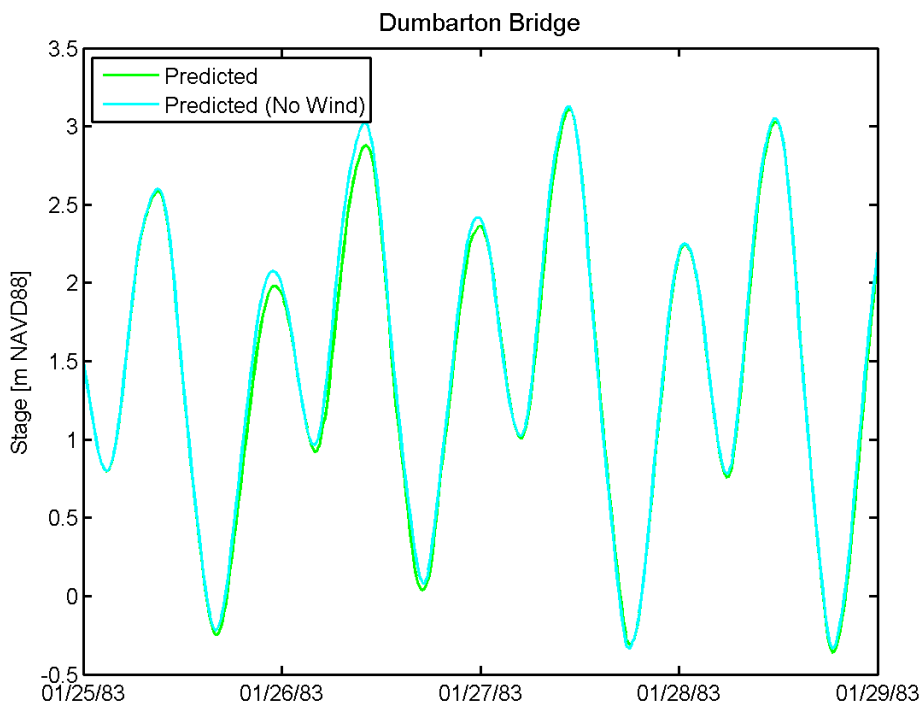

Figure 4.7-18 Predicted stage at the Dumabrton Bridge NOAA tide station (9414509) from January 1983 storm simulations made with and without wind forcing.

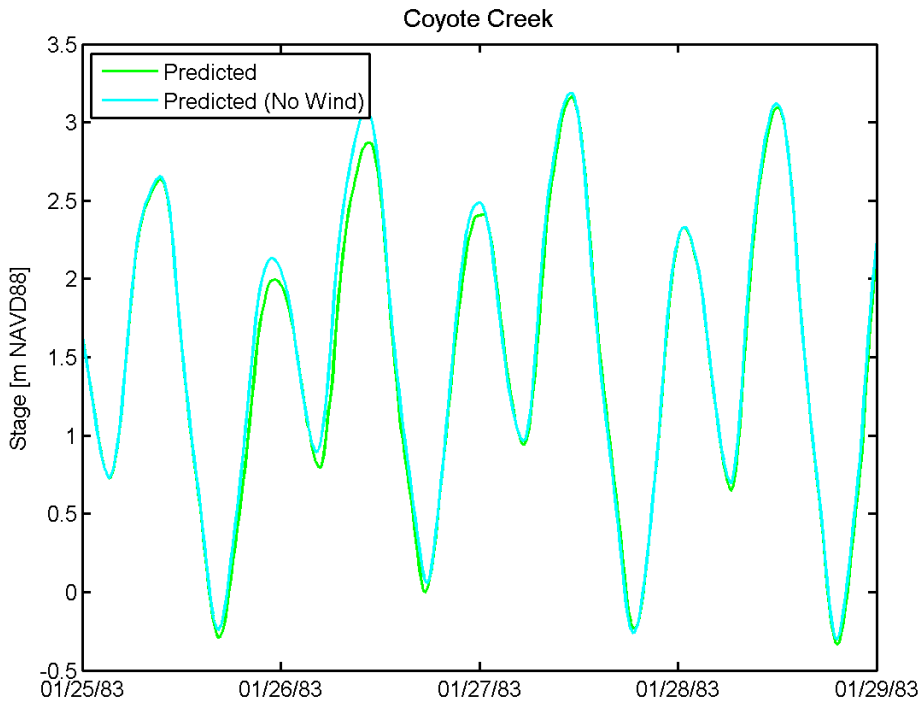

Figure 4.7-19 Predicted stage at the Coyote Creek NOAA tide station (9414575) from January 1983 storm simulations made with and without wind forcing.

5. Screening of Preliminary Alternatives

The ecosystem restoration and flood damage reduction alternatives consist of a combination of measures from managed pond habitats, tidal habitats and flood protection plans. A set of six preliminary alternatives were developed from a range of conceptual alternatives of FRM alignments (HDR, 2011) and ER designs (ESA PWA, 2012) based on feedback from the Project Delivery Team (PDT) and the project sponsors.

5.1 Description of Preliminary Alternatives

Six preliminary alternatives were developed by combining the two most likely Flood Risk Management (FRM) levee alignments, with a suite of ecosystem restoration (ER) options, as shown in Table 5.1-1. The ecosystem restoration options (ESA PWA, 2012) assume a phased approach to pond restoration and were developed using two different assumptions about the sediment deposition rate within the restored ponds, which depends on the ambient suspended sediment concentration (SSC). The ecosystem restoration options also include variations based on the level of upland fill incorporated into the project design. Schematics showing the layout for the six screening alternatives are shown in Figures 5.1-1 through 5.1-6. The Habitat Zones for 2067 shown on these schematics were developed by ESA PWA (2012).

In order to facilitate the selection of the two final alternatives which will be used for production simulations under year 0 (Section 6) and year 50 (Section 7) conditions, the six preliminary alternatives were evaluated using the high resolution UnTRIM model of Far South San Francisco Bay, which is described in Section 3. Instead of performing a detailed R&U analysis on each of the six alternatives, a single flood event, corresponding to approximately a 100-year return interval event, was selected from the set of storm events used in the model calibration under the without project conditions (Section 4). The January 1983 storm event (Section 4.5.1) was selected for this analysis, and will be used to test and compare the 6 preliminary alternatives presented in this section. The purpose of these event driven analyses is to eliminate undesirable alternatives, thereby reducing the number of alternatives which will undergo a detailed R&U analysis. Based on the results of these analyses, a maximum of two alternatives will be selected for further consideration.

Table 5.1-1 Description of six preliminary alternatives which combine two FRM alignments with a range of ecosystem restoration options.

Alternative	FRM Alignment	Sedimentation Rate	Upland Fill	Figure
Alternative 1	Option 1	Low (100 mg/l SSC)	None	5.1-1
Alternative 2	Option 1	Low (100 mg/l SSC)	1:30	5.1-2
Alternative 3	Option 1	High (200 mg/l SSC)	None	5.1-3
Alternative 4	Option 1	High (200 mg/l SSC)	1:30	5.1-4
Alternative 5	Option 2 (Existing)	Low (100 mg/l SSC)	None	5.1-5
Alternative 6	Option 2 (Existing)	High (200 mg/l SSC)	None	5.1-6

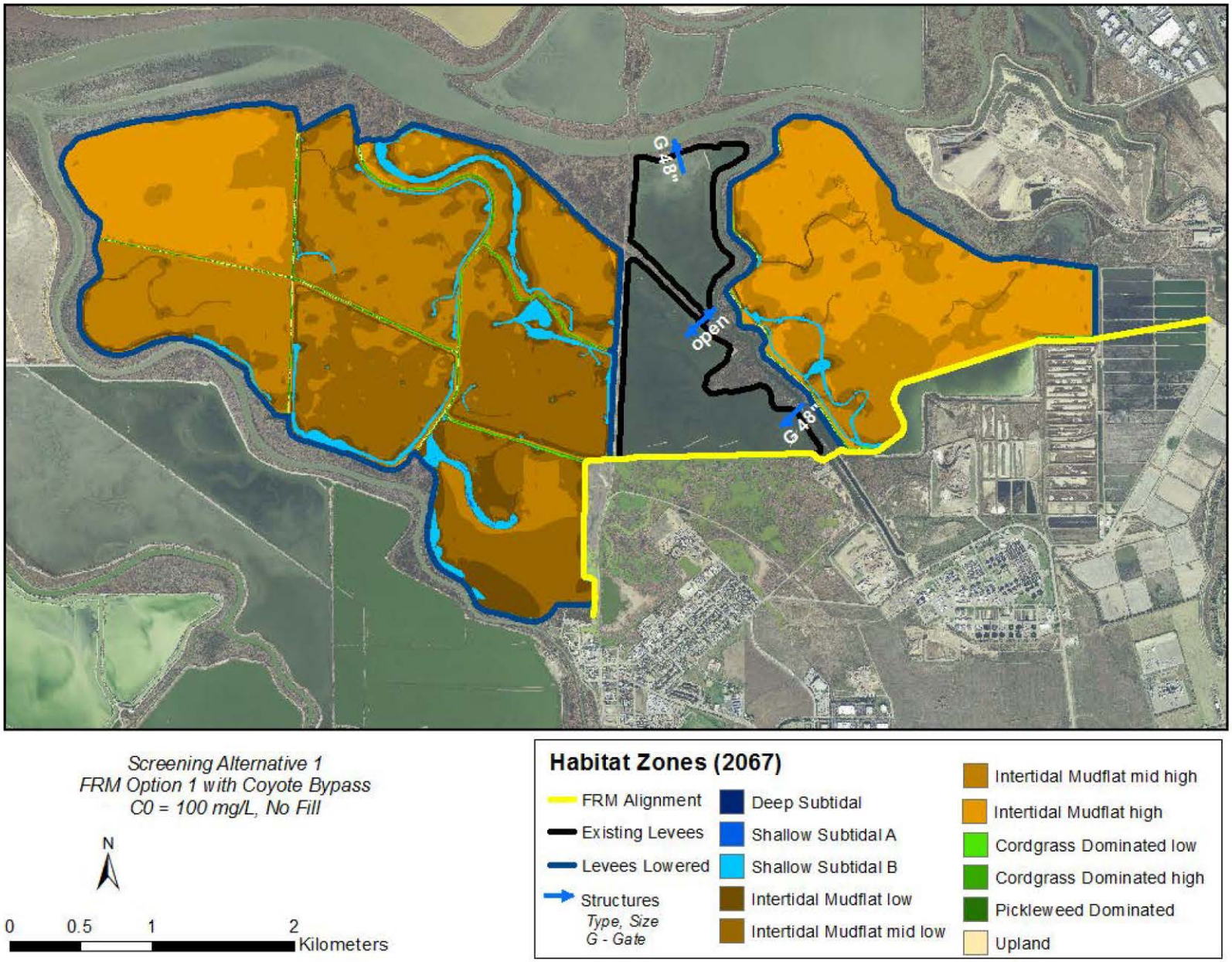

Figure 5.1-1 Layout for Screening Alternative 1 which combines FRM Option 1 with the Coyote Bypass Extension, a low sedimentation rate based on a SSC of 100 mg/l, and no upland fill.

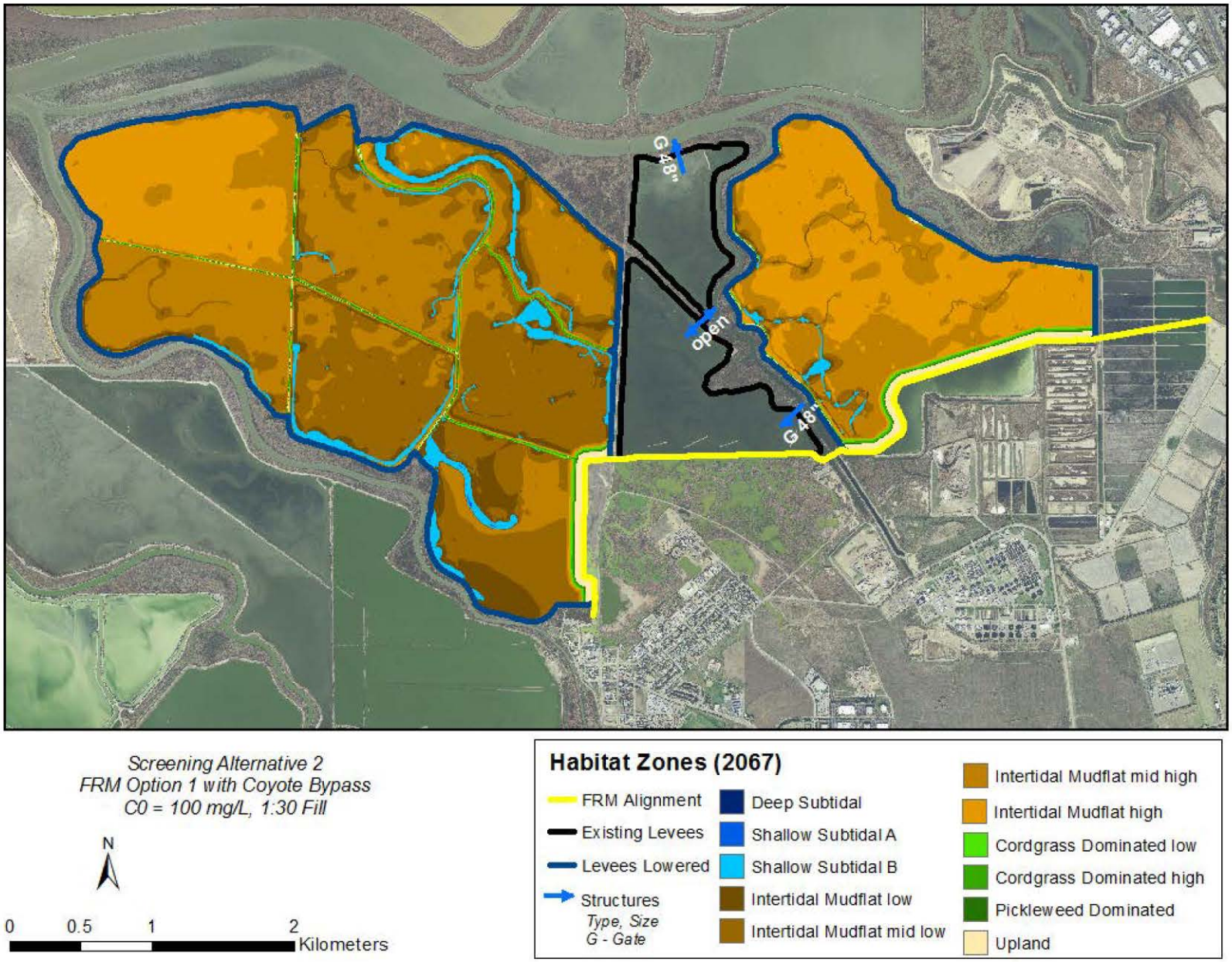

Figure 5.1-2 Layout for Screening Alternative 2 which combines FRM Option 1 with the Coyote Bypass Extension, a low sedimentation rate based on a SSC of 100 mg/l, and upland fill with a 1:30 slope.

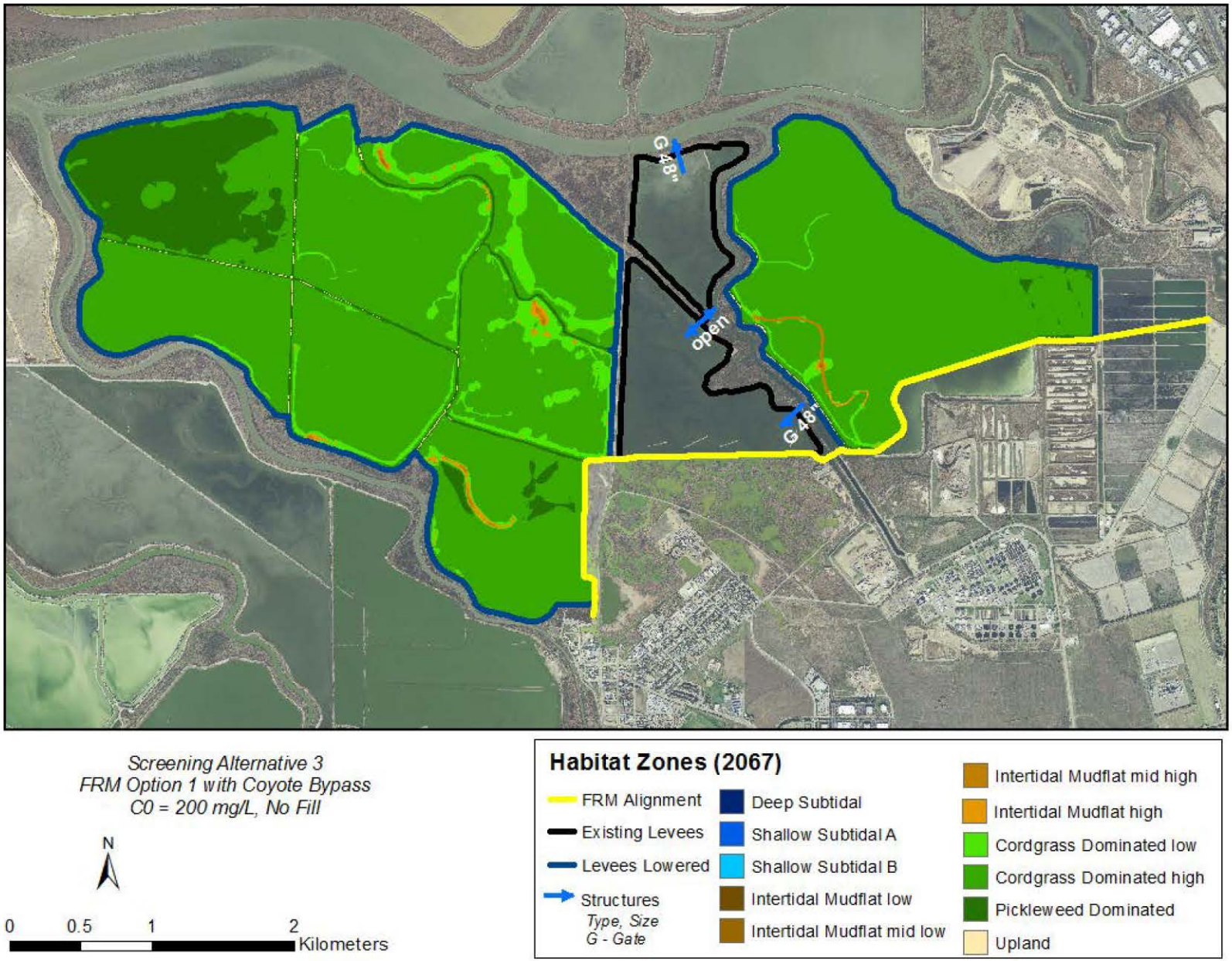

Figure 5.1-3 Layout for Screening Alternative 3 which combines FRM Option 1 with the Coyote Bypass Extension, a high sedimentation rate based on a SSC of 200 mg/l, and no upland fill.

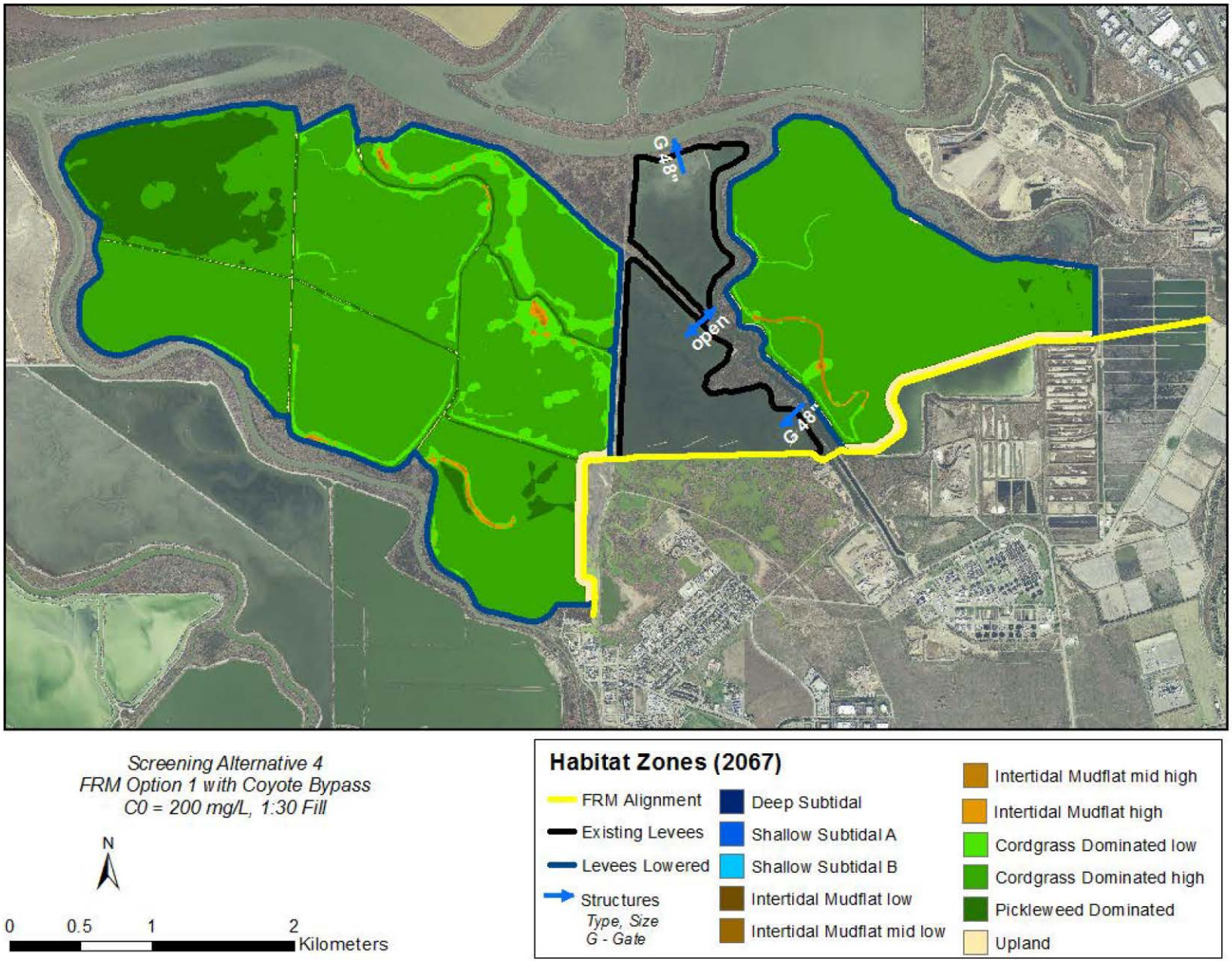

Figure 5.1-4 Layout for Screening Alternative 4 which combines FRM Option 1 with the Coyote Bypass Extension, a high sedimentation rate based on a SSC of 200 mg/l, and upland fill with a 1:30 slope.

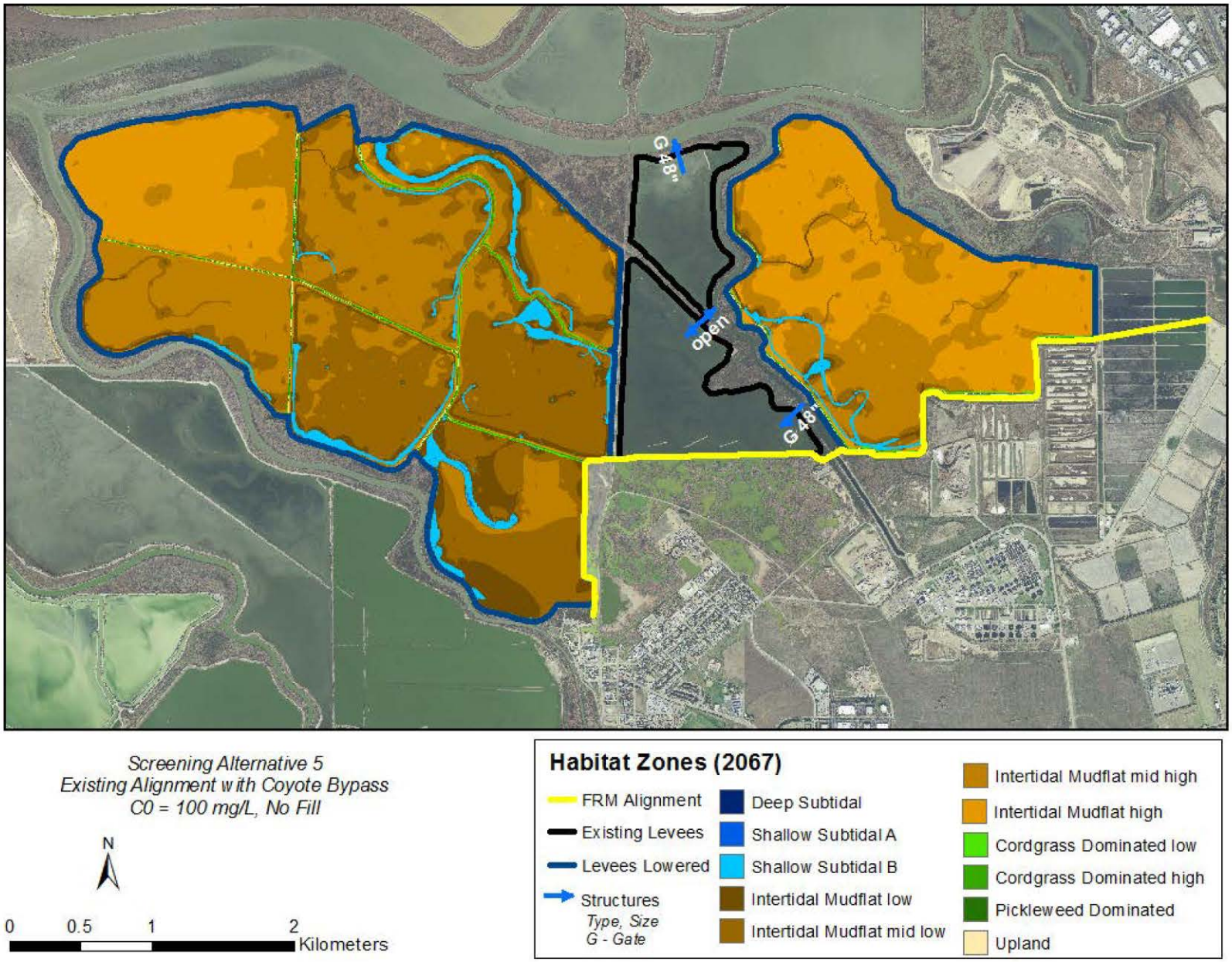

Figure 5.1-5 Layout for Screening Alternative 5 which combines the existing levee alignment (FRM Option 2) with the Coyote Bypass Extension, a low sedimentation rate based on a SSC of 100 mg/l, and no upland fill.

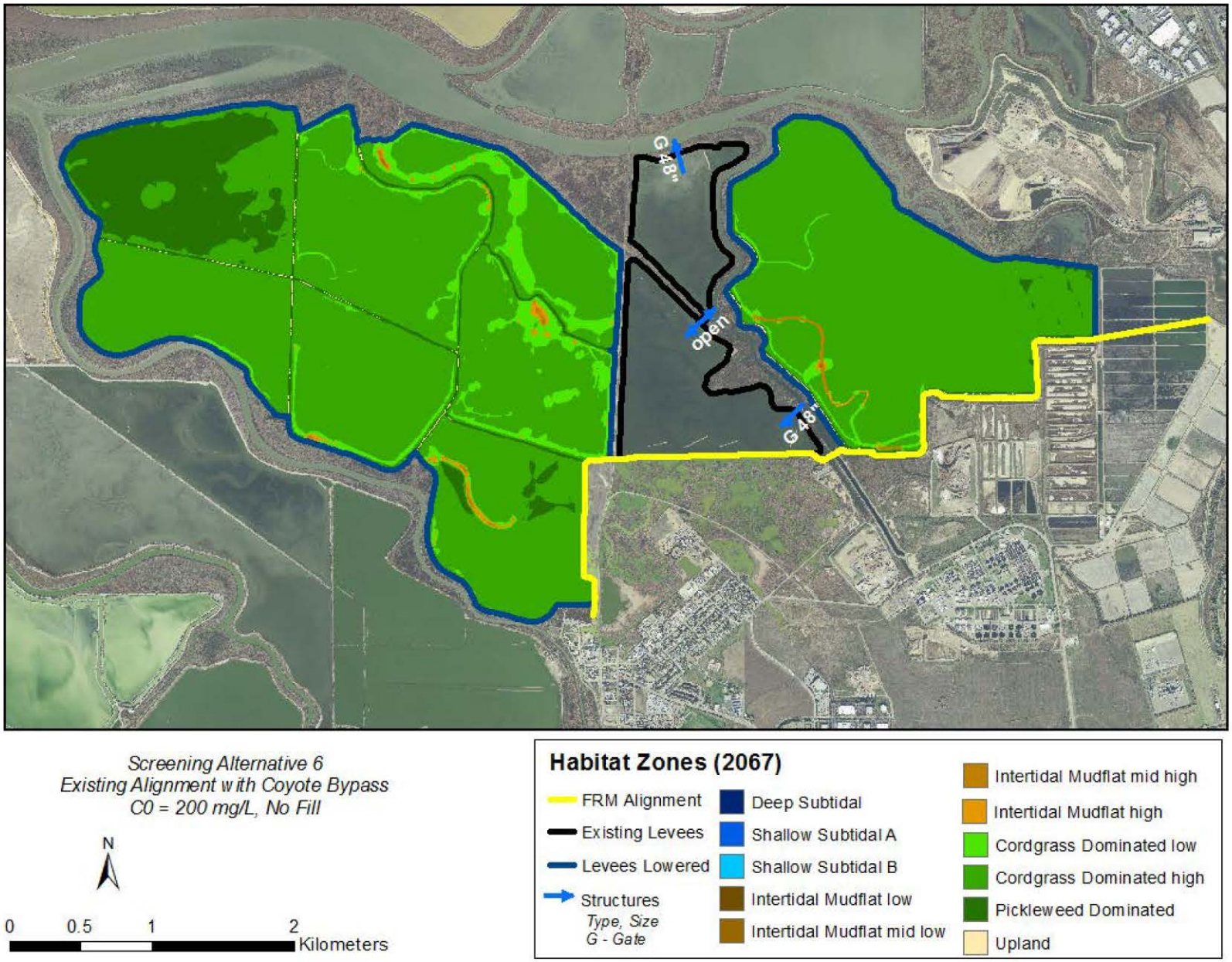

Figure 5.1-6 Layout for Screening Alternative 6 which combines the existing levee alignment (FRM Option 2) with the Coyote Bypass Extension, a high sedimentation rate based on a SSC of 200 mg/l, and no upland fill.

5.2 Evaluation Approach for Preliminary Alternatives

Each of the six preliminary alternatives was evaluated under year 50 (2067) conditions. For each alternative, the January 1983 storm event (Section 4.5.1) was simulated, using an estimate of sea level rise within the study area based on the modified NRC Curve III (USACE, 2011).

5.2.1 Model Boundary Conditions

Based on the modified NRC Curve III (USACE, 2011), 0.649 m (2.13 ft) of sea level rise was applied at the model ocean boundary relative to the sea level of the historic 1983 storm. With the exception of the sea level rise offset, all other model boundary conditions were identical to those simulated for the January 1983 storm simulation presented in Section 4.5.1

5.2.2 Ponds A9 through A15

The year 50 conditions assume a phased restoration of ponds A9 through A15, beginning in 2017 (See Figure 2.1-1 for pond locations). Under this scenario (ESA PWA, 2012) Pond A12 would be restored to tidal conditions in 2017, followed by the restoration of the western most ponds (A9 through A11) in 2022. The central ponds (A13 through A15) would be restored in 2030. The marsh accretion for ponds A9 through A15 shown in Figures 5.1-1 through 5.1-6 was developed by ESA PWA (2012) assuming this phasing of the restoration for two different assumed sedimentation rates. The intent of this phased alternative is to restore tidal action to Pond A12 as soon as possible to maximize accretion in this pond, since it is the lowest pond in the project area (ESA PWA, 2012).

5.2.3 Ponds A16 and A17

The current ecosystem restoration options under consideration for the South San Francisco Bay Shoreline Study do not include restoration actions for Pond A16 or Pond A17. However, Ponds A16 and A17 are currently being restored as part of the South Bay Salt Pond (SBSP) Restoration Phase I projects. Pond A16 and Pond A17 are surrounded by external and internal salt pond levees. Pond A16 is connected to Artesian Slough through a 48-inch culvert with an adjustable tidal gate located in the southeastern corner of the pond. Pond A17 is hydraulically connected to Coyote Creek via a 48-inch culvert with an adjustable tidal gate, located in the northeast corner of the pond. Water within Alviso System A16 flows between the two ponds through an existing gap between the Pond A16 and Pond A17 levees. A siphon exists between Ponds A17 and A18 that is planned to be plugged and closed (Mruz pers. comm., 2006).

During summer operations in 2006, the tidal gates on both the Pond A16 and Pond A17 water control structures were opened to allow muted tidal exchanges between Pond A16 and Artesian Slough, and between Pond A17 and Coyote Creek, to manage dissolved oxygen (DO) levels (Mruz pers. comm., 2006). During typical winter operations, Pond System A16 is operated to take in water from Artesian Slough and discharge to Coyote Creek through Pond A17 to avoid the entrainment of fish in Coyote Creek.

Ponds A16 and A17 are treated identically in all six of the preliminary alternatives (Figures 5-1 through 5-6), however several assumptions are made for the representation of Ponds A16 and A17 in 2067. First, it is assumed that by 2067, the existing siphon between Ponds A17 and A18 has been plugged and closed. Second, it is assumed that during a storm event such as the January 1983 event that the ponds will be managed in the current winter configuration with flow entering Pond A16 from Artesian Slough through a 48-inch culvert, and Pond A17 is discharging to Coyote Creek through a 48-inch culvert. Lastly, it is assumed that Ponds A16 and A17 remain hydraulically connected, and no changes are made to the existing levees surrounding ponds A16 and A17, with the exception of the levee separating Pond A16 from New Chicago Marsh, which is part of the FRM levee alignment.

5.2.4 Pond A18

The year 50 conditions assume a phased restoration of salt ponds in the project area, beginning in 2017. Under this scenario (ESA PWA, 2012) Pond A18 would be restored to tidal action in 2027. The marsh accretion for Pond A18 shown in Figures 5.1-1 through 5.1-6 was developed by ESA PWA (2012) assuming the restoration of Pond A18 to tidal action in 2027 for two different assumed sedimentation rates.

5.2.5 Artesian Slough Tide Gate

The current FRM design assumes the installation of a tide gate on Artesian Slough. The specific details of this tide gate have not yet been determined. Based on data collected by Santa Clara Valley Water District (SCVWD), it was assumed that there will be a side hinged restrained tide gate (96”x96”) with an aluminum and steel frame and door with a steel hinge assembly, and hydraulic controls (Sergio Jimenez, HDR, pers. comm.). It is expected that the structure will match the invert of the existing outflow from the San Jose Water Pollution Control Plant (WPCP). The size of the gate will be designed to accommodate San Jose WPCP plant discharge on maximum load, with some sort of automated closure. With the gate open, discharge would continue as it does under existing conditions. However, under flood conditions the gate would be closed and act as a continuation of the levee (Sergio Jimenez, HDR, pers. comm.). The screening alternative simulations assume that the Artesian Slough tide gate will be closed, and no discharge from the San Jose WPCP will be released into Artesian Slough.

5.2.6 New Chicago Marsh Tide Gate

The current FRM design assumes the installation of a new tide gate between ponds A16 and A13. The specific details of this tide gate have not yet been determined. The screening alternative simulations assume that the New Chicago Marsh tide gate will be closed, and no flow between New Chicago Marsh and Coyote Creek will occur along the existing marsh channel adjacent to the Railroad tracks.

5.2.7 Evaluation Locations

Predicted water levels for each of the screening alternatives were evaluated at sixteen stations located along the project levee (Figure 5.2-1). The locations of each of the evaluation locations are provided in Table 5.2-1. Each evaluation point is located approximately 40 m away from the project levee. Because two different levee alignments were considered in the screening alternatives (Table 5.1-1), alternate points were selected for stations 10 through 14 when the two alignments are different.

Table 5.2-1 Location of Screening Alternative Evaluation Stations.

Station Number	Station Name	Location UTM [m]	
		Easting	Northing
1	A12 Levee 1	590366.1	4143258.0
2	A12 Levee 2	590288.5	4143711.5
3	A12 Levee 3	590298.4	4144033.1
4	A13 Levee 1	590421.9	4144260.2
5	Warm Springs Marsh Tide Gate	590577.1	4144228.5
6	A16 Levee 1	590961.6	4144287.4
7	A16 Levee 2	591719.3	4144304.5
8	Artesian Slough Tide Gate	592110.6	4144267.8
9	A18 Levee 1	592281.7	4144318.0
10	A18 Levee 2 (FRM Alignment 1)	592490.1	4144388.4
10b	A18 Levee 2b (Existing Alignment)	592558.0	4144295.8
11	A18 Levee 3 (FRM Alignment 1)	592516.0	4144510.7
11b	A18 Levee 3b (Existing Alignment)	592676.2	4144538.3
12	A18 Levee 4 (FRM Alignment 1)	592504.4	4144728.9
12b	A18 Levee 4b (Existing Alignment)	592704.3	4144707.1
13	A18 Levee 5 (FRM Alignment 1)	592979.2	4144925.2
13b	A18 Levee 5b (Existing Alignment)	593188.1	4144700.5
14	A18 Levee 6 (FRM Alignment 1)	593367.9	4145049.9
14b	A18 Levee 6b (Existing Alignment)	593480.8	4144854.5
15	A18 Levee 7	593781.4	4145106.2
16	Coyote Bypass Levee 1	594332.6	4145187.3

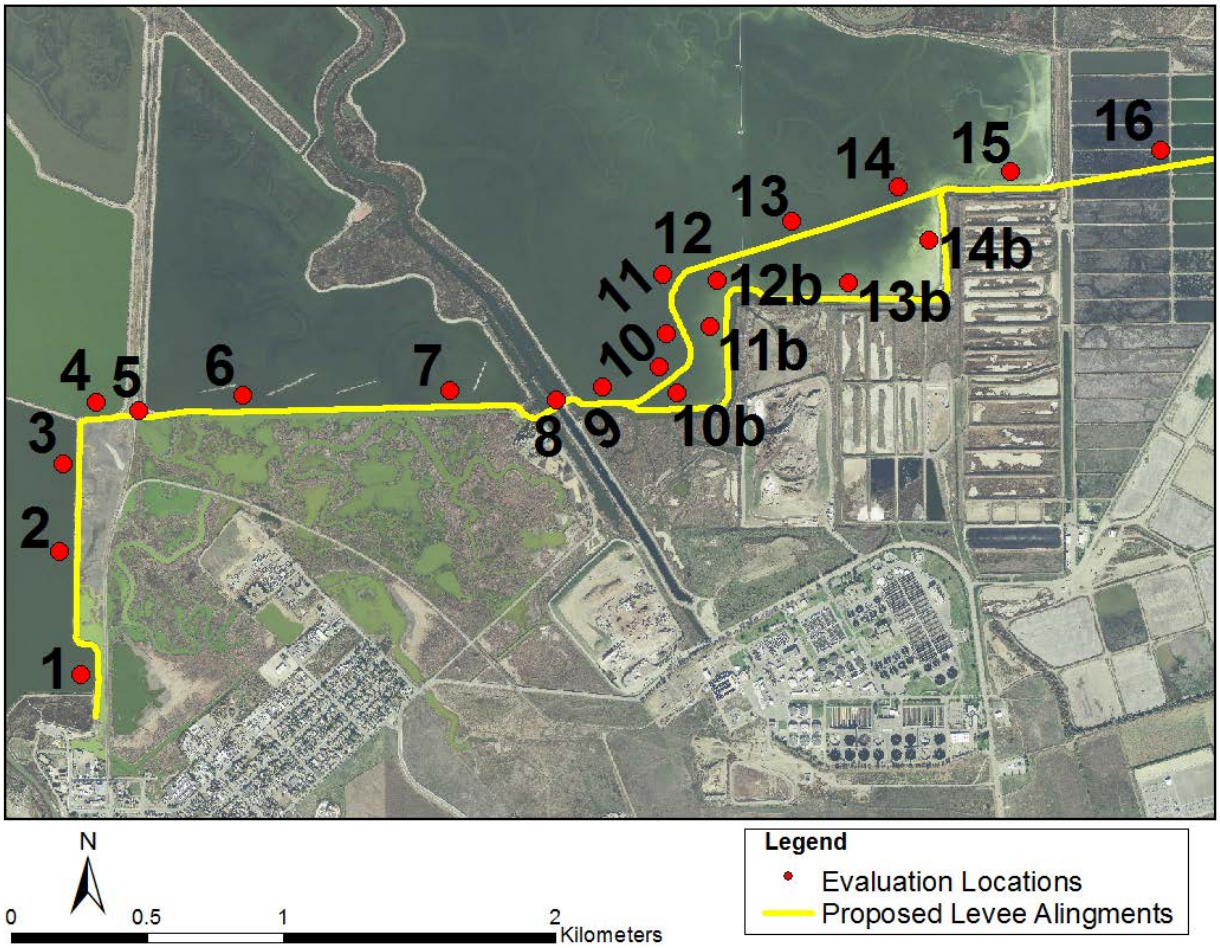

Figure 5.2-1. Station locations for screening alternatives.

5.3 Results of Preliminary Alternative Evaluation

For each alternative simulation, the maximum predicted water level at each of the sixteen evaluation locations is listed in Tables 5.3-1-2 and 5.3-2. The predicted water level at evaluation location 16 is listed as "dry" for all of the scenarios because this station was at a higher elevation than the maximum water level and remained dry during all six simulations.

The predicted maximum water levels range from 3.744 m to 3.774 m (12.285 to 12.381 ft) at all locations and for all scenarios. Thus the difference between the highest and lowest water level predicted at the 16 locations for all scenarios is 0.03 m (0.096 ft). This suggests that neither the specific alignment of the levee nor the rate of marsh accretion assumed in the restored ponds is likely to have a significant impact on the predicted water level along the FRM levee during a storm event equivalent to the January 1983 event with 0.649 m (2.13 ft) of sea level rise.

One of the reasons for the similarity between the different locations and scenarios is that the predicted water levels for this event are significantly above any of the existing salt pond levees. For example, the average elevation of the external salt levee that separates Pond A16 from Artesian Slough is 3.25 m NAVD88 (10.7 ft) which is approximately 0.5 m (1.64) ft below the lowest predicted peak water levels at station 6 and 7 in Pond A16. Since the existing pond

levees are overtopped by more than 0.5 m under this scenario, the resulting water levels along the project levee are relatively uniform.

5.3.1 Effect of FRM Alignment

The effect of the FRM alignment on the maximum predicted water levels can be evaluated by comparing Alternative 1 to Alternative 5 and Alternative 3 to Alternative 6 (Table 5.1-1). A comparison of Alternative 1 and Alternative 5 provides an assessment of the effect of the FRM alignment for the lower sedimentation rate (100 mg/l SSC). With the low sedimentation rate, FRM2 (existing alignment) results in a lower peak flood level along the levee than FRM of between 0.002 and 0.011 m (0.008 and 0.034 ft). A comparison of Alternative 3 and Alternative 6 provides an assessment of the effect of the FRM alignment for the higher sedimentation rate (200 mg/l SSC). With the high sedimentation rate, FRM2 (existing alignment) also results in a lower peak flood level along the levee than FRM of between 0.002 and 0.011 m (0.006 and 0.036 ft). For both sedimentation rates, the biggest differences in peak water levels that result from the two different FRM alignments occur at stations 9 through 15 in Pond A18 and the smallest differences occur in Ponds A12, A13, and A16 (stations 1 through 7). Overall, the maximum predicted difference in peak water level that can be attributed to the differences between the FRM alternatives used in the screening analysis was 0.011 m (0.036 ft). Thus, the choice of FRM alignment is not expected to have a significant impact on the maximum predicted water levels under year 50 conditions.

5.3.2 Effect of Sedimentation Rate

The effect of the FRM alignment on the maximum predicted water levels can be evaluated by comparing Alternatives 1, 2, and 5 to Alternatives 3, 4, and 6 (Table 5.1-1). For the three alternatives with the low sedimentation rate (100 mg/l SSC), predicted peak water levels range from 3.745 to 3.7744 m (12.287 to 12.381 ft) at all locations. For the three alternatives with the high sedimentation rate (200 mg/l SSC), predicted peak water levels range from 3.744 to 3.760 m (12.285 to 12.335 ft) at all locations. At stations 1 through 7, the low sedimentation rate results in a maximum water level up to 0.022 m (0.072 ft) higher than the high sedimentation rate. In Pond A18, the difference in sedimentation rate has a smaller effect on peak water levels during the screening simulations. Thus, assumed sedimentation rate has a larger influence on the maximum predicted water levels under year 50 conditions than the FRM alignment.

5.3.3 Effect of Upland Fill

The effect of the upland fill on the maximum predicted water levels can be evaluated by comparison of Alternative 1 to Alternative 2 and Alternative 3 to Alternative 4 (Table 5.1-1). The upland fill results in in slightly higher peak water levels than the simulation without upland fill. A comparison of Alternative 1 and Alternative 2 shows a 0.000 to 0.004 m (0.002 to 0.013 ft) increase in peak water levels. A similar comparison of Alternative 3 and Alternative 4 shows a 0.001 to 0.004 m (0.003 to 0.013 ft) increase in peak water levels. Thus, the upland fill is not expected to have a significant impact on the maximum predicted water levels under year 50 conditions.

Table 5.3-1 Peak Flood Levels for six Screening Alternatives in meters [NAVD 88].

Station Number	Station Name	Peak Flood Levels [m NAVD88]					
		Alt1	Alt2	Alt3	Alt4	Alt5	Alt6
1	A12 Levee 1	3.773	3.774	3.758	3.759	3.770	3.756
2	A12 Levee 2	3.770	3.771	3.756	3.757	3.767	3.754
3	A12 Levee 3	3.770	3.771	3.755	3.756	3.767	3.753
4	A13 Levee 1	3.770	3.770	3.753	3.755	3.767	3.751
5	Warm Springs Marsh Tide Gate	3.769	3.771	3.753	3.754	3.767	3.750
6	A16 Levee 1	3.769	3.770	3.749	3.752	3.767	3.747
7	A16 Levee 2	3.769	3.771	3.747	3.749	3.766	3.744
8	Artesian Slough Tide Gate	3.759	3.762	3.756	3.760	3.749	3.747
9	A18 Levee 1	3.758	3.762	3.756	3.759	3.749	3.746
10/10b	A18 Levee 2/2b	3.758	3.761	3.755	3.758	3.748	3.746
11/11b	A18 Levee 3/3b	3.758	3.761	3.755	3.758	3.748	3.746
12/12b	A18 Levee 4/4b	3.759	3.761	3.755	3.759	3.748	3.746
13/13b	A18 Levee 5/5b	3.758	3.761	3.755	3.759	3.747	3.745
14/14b	A18 Levee 6/6b	3.756	3.760	3.756	3.759	3.746	3.745
15	A18 Levee 7	3.755	3.759	3.756	3.760	3.745	3.745
16	Coyote Bypass Levee 1	dry	dry	dry	dry	dry	dry

Table 5.3-2 Peak Flood Levels for six Screening Alternatives in feet [NAVD 88].

Station Number	Station Name	Peak Flood Levels [ft NAVD88]					
		Alt1	Alt2	Alt3	Alt4	Alt5	Alt6
1	A12 Levee 1	12.378	12.381	12.329	12.332	12.368	12.323
2	A12 Levee 2	12.369	12.373	12.323	12.327	12.360	12.316
3	A12 Levee 3	12.370	12.372	12.319	12.323	12.359	12.312
4	A13 Levee 1	12.367	12.370	12.313	12.321	12.359	12.306
5	Warm Springs Marsh Tide Gate	12.366	12.370	12.312	12.316	12.358	12.303
6	A16 Levee 1	12.366	12.369	12.301	12.309	12.358	12.295
7	A16 Levee 2	12.364	12.371	12.292	12.301	12.356	12.285
8	Artesian Slough Tide Gate	12.332	12.343	12.323	12.335	12.301	12.293
9	A18 Levee 1	12.330	12.341	12.321	12.333	12.299	12.291
10/10b	A18 Levee 2/2b	12.330	12.341	12.319	12.330	12.297	12.290
11/11b	A18 Levee 3/3b	12.330	12.339	12.318	12.329	12.298	12.289
12/12b	A18 Levee 4/4b	12.331	12.341	12.320	12.333	12.298	12.289
13/13b	A18 Levee 5/5b	12.328	12.341	12.320	12.333	12.294	12.287
14/14b	A18 Levee 6/6b	12.323	12.336	12.322	12.334	12.289	12.286
15	A18 Levee 7	12.321	12.332	12.322	12.335	12.287	12.287
16	Coyote Bypass Levee 1	dry	dry	dry	dry	dry	dry

6. Year 0 Model Production Simulations and Analysis

The year 0 (2017) production simulations were developed to predict peak water levels for a set of synthesized events that cover the ranges of all the controlling parameters, such as tide, residual surge, wind speed, and wind direction for two project alternatives. This section presents the model boundary conditions and assumptions used in the development of the year 0 long wave production simulations and the resulting lookup tables which provide the peak water level for each of the events at a set of evaluation locations in the project area. The lookup tables will allow the interpretation of the responses of all the synthesized events randomly selected by the Monte Carlo Simulation (MCS) process during statistical analysis of year 0 conditions.

6.1 Boundary Conditions for Year 0 Model Production Simulations

This section describes the model boundary conditions used in the year 0 production simulations. The model boundary conditions were developed to cover a range of tide, river inflow, and wind conditions.

6.1.1 Tidal Boundary Conditions for Year 0 Production Simulations

A suite of tidal boundary conditions were developed to span the range of astronomical and residual (surge) tides observed at San Francisco (9414290). Based on an analysis of historic astronomic tides generated from tidal harmonic constituents and hourly water level observations at San Francisco (Lisa Andes, USACE, pers. comm.), the peak astronomic tides ranged from 5.15 to 7.25 ft MLLW. The coincident surge associated with these peaks ranged from 0 to 2.4 ft, whereas the non-coincident tidal surge ranged from 0 to 3.5 ft. In order to provide a look-up table spanning the full range of possible conditions, four peak astronomic tides between 5.15 ft and 7.25 ft MLLW and four peak surge heights between 0.5 and 3.5 ft were selected, resulting in a total of sixteen event permutations with peak water levels at San Francisco (9414290) shown in Table 6-1 in feet referenced to MLLW. Table 6-2 shows the resulting water surface elevations for the same sixteen events in meters referenced to NAVD88.

For each astronomical tide peak, a historical event period was selected from the astronomical tides generated from tidal harmonic constituents at San Francisco (9414290) from the period between 1901 and 2005 such that the peak astronomical tide matched the target and the peak astronomical tide for the preceding three days did not exceed this peak water level. This ensured that a peak water level during the spin-up period prior to the event did not exceed the event peak. These astronomical tides generated from tidal harmonic constituents were used to develop the synthetic events.

Each synthetic event spans a period of five days, from January 1, 2017 through January 5, 2017. For each event, the peak astronomical tide from the corresponding time series generated from the tidal harmonic constituents was shifted in time to occur at 12:00 on 1/4/2017. Each storm event spans a 48 hour period from 1/3/2017 at 12:00 to 1/5/2017 at 12:00 with the peak surge for each event occurring at 12:00 on January 4, 2017 which is coincident with the peak

astronomical tide. The storm surge was represented by the first half cycle of a sine function with a period of 4 days and amplitude of between 0.5 and 3.5 ft. Figure 6.1-1 shows the resulting tides for events 1 through 4 (Table 6-1) developed using a peak astronomical tide of 5.15 ft. The resulting tides for events 5 through 8 (Table 6-1) developed using a peak astronomical tide of 5.85 ft are shown on Figure 6.1-2. Figure 6.1-3 shows the resulting tides for events 9 through 12 (Table 6-1) developed using a peak astronomical tide of 6.55 ft. The resulting tides for events 13 through 16 (Table 6-1) developed using a peak astronomical tide of 5.85 ft are shown on Figure 6.1-4. For each of the 16 events simulated, the synthetic tides developed for San Francisco (9414290) were multiplied by an amplification factor to account for the difference in tidal range between observed San Francisco tides and tides along the model ocean boundary, and a phase lead was applied to account for the phase difference between the San Francisco tide station and the model boundary, as described in Section 3.6. These adjustments ensured that the resulting peak water elevation at San Francisco predicted for each of the scenarios was within 0.005 ft of the peak values shown in Table 6-2.

Twelve of the resulting events were simulated for each of the year 0 FRM alternatives considered. Only the twelve events with peak residuals between 0.5 ft and 2.5 ft were used for the year 0 production simulations since those events covered the full range needed for the MCS analysis based on coincident sampling approach adopted for this study (Noble Consultants, 2012). The four events which included 3.5 ft of surge (Events 4, 8, 12, and 16) were not simulated under year 0 conditions.

Table 6-1 Peak water level in ft referenced to MLLW at San Francisco station (9414290) for sixteen events derived from combining four peak astronomical tides with four peak residual tides.

Peak Residual (ft MLLW)	Peak Astronomical Tide (ft MLLW)			
	5.15	**5.85**	**6.55**	**7.25**
0.5	Event 1: 5.65	Event 5: 6.35	Event 9: 7.05	Event 13: 7.75
1.5	Event 2: 6.65	Event 6: 7.35	Event 10: 8.05	Event 14: 8.75
2.5	Event 3: 7.65	Event 7: 8.35	Event 11: 9.05	Event 15: 9.75
3.5	Event 4: 8.65	Event 8: 9.35	Event 12: 10.05	Event 16: 10.75

Table 6-2 Peak water level in m referenced to NAVD88 at San Francisco station (9414290) for sixteen events derived from combining four peak astronomical tides with four peak residual tides.

Peak Residual (m)	Peak Astronomical Tide (m NAVD88)			
	1.59	**1.80**	**2.01**	**2.23**
0.15	Event 1: 1.74	Event 5: 1.95	Event 9: 2.17	Event 13: 2.38
0.46	Event 2: 2.04	Event 6: 2.26	Event 10: 2.47	Event 14: 2.68
0.76	Event 3: 2.35	Event 7: 2.56	Event 11: 2.78	Event 15: 2.99
1.07	Event 4: 2.65	Event 8: 2.87	Event 12: 3.08	Event 16: 3.29

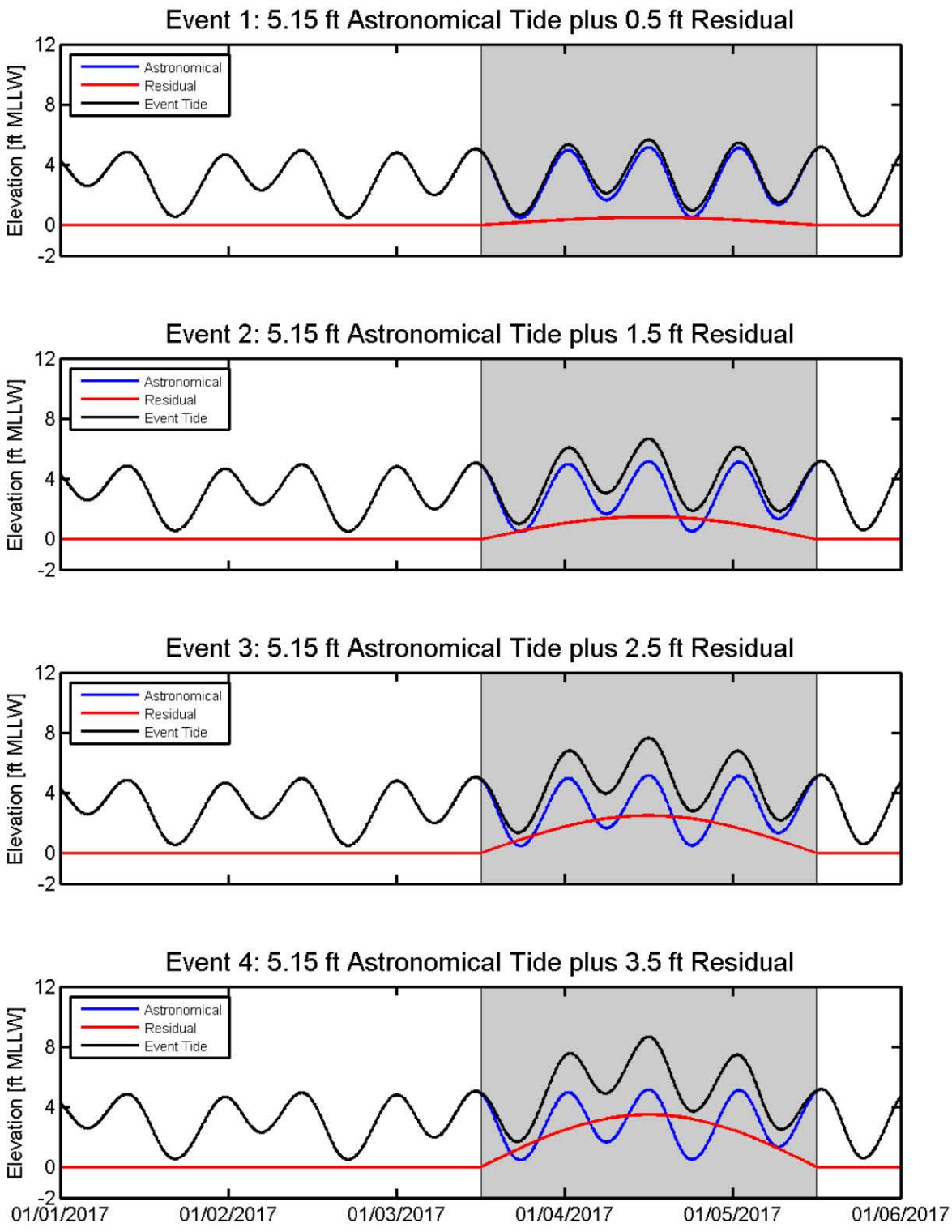

Figure 6.1-1 Astronomical tides generated from tidal harmonics, residual (surge), and resulting event water surface elevations in ft referenced to MLLW at San Francisco for Event 1 through Event 4.

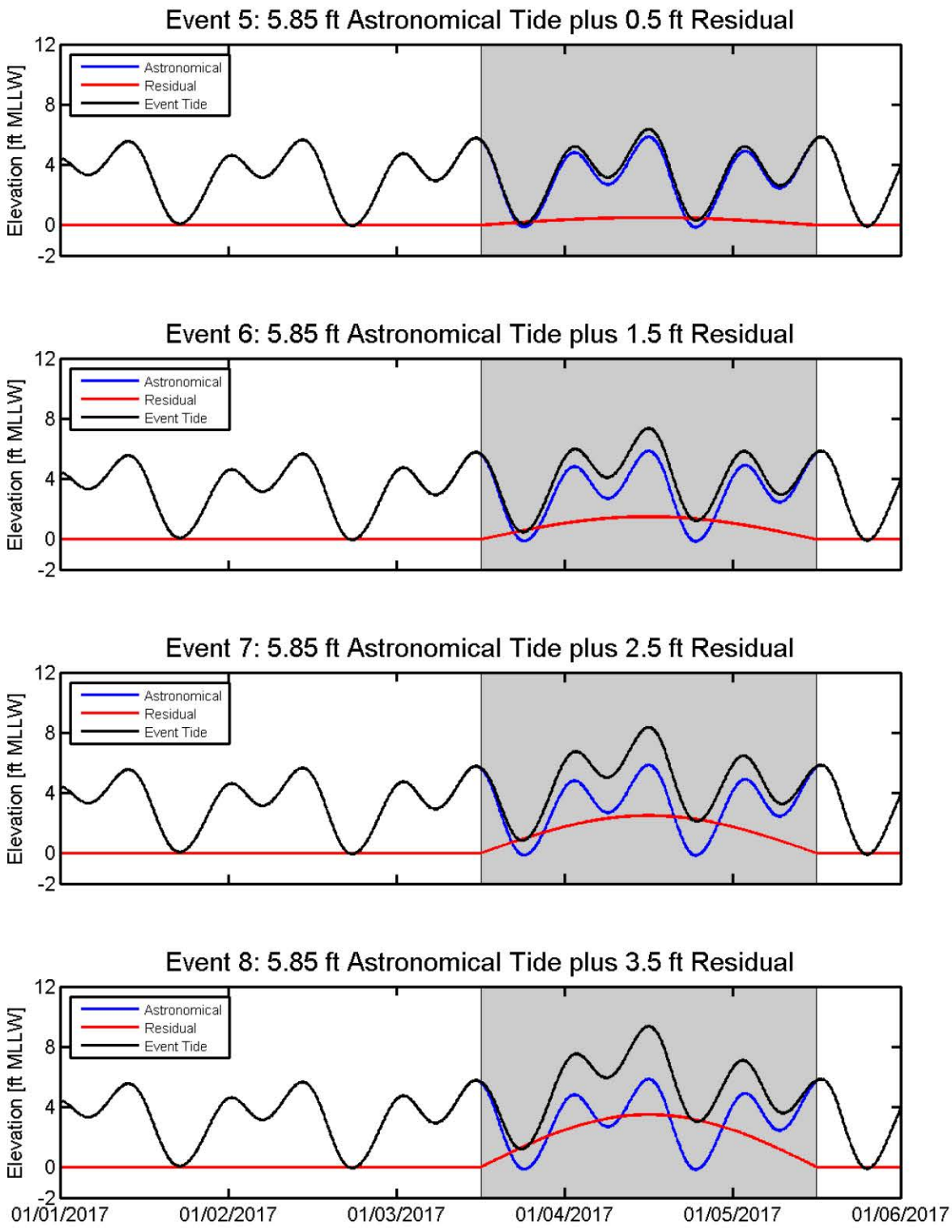

Figure 6.1-2 Astronomical tides generated from tidal harmonics, residual (surge), and resulting event water surface elevations in ft referenced to MLLW at San Francisco for Event 5 through Event 8.

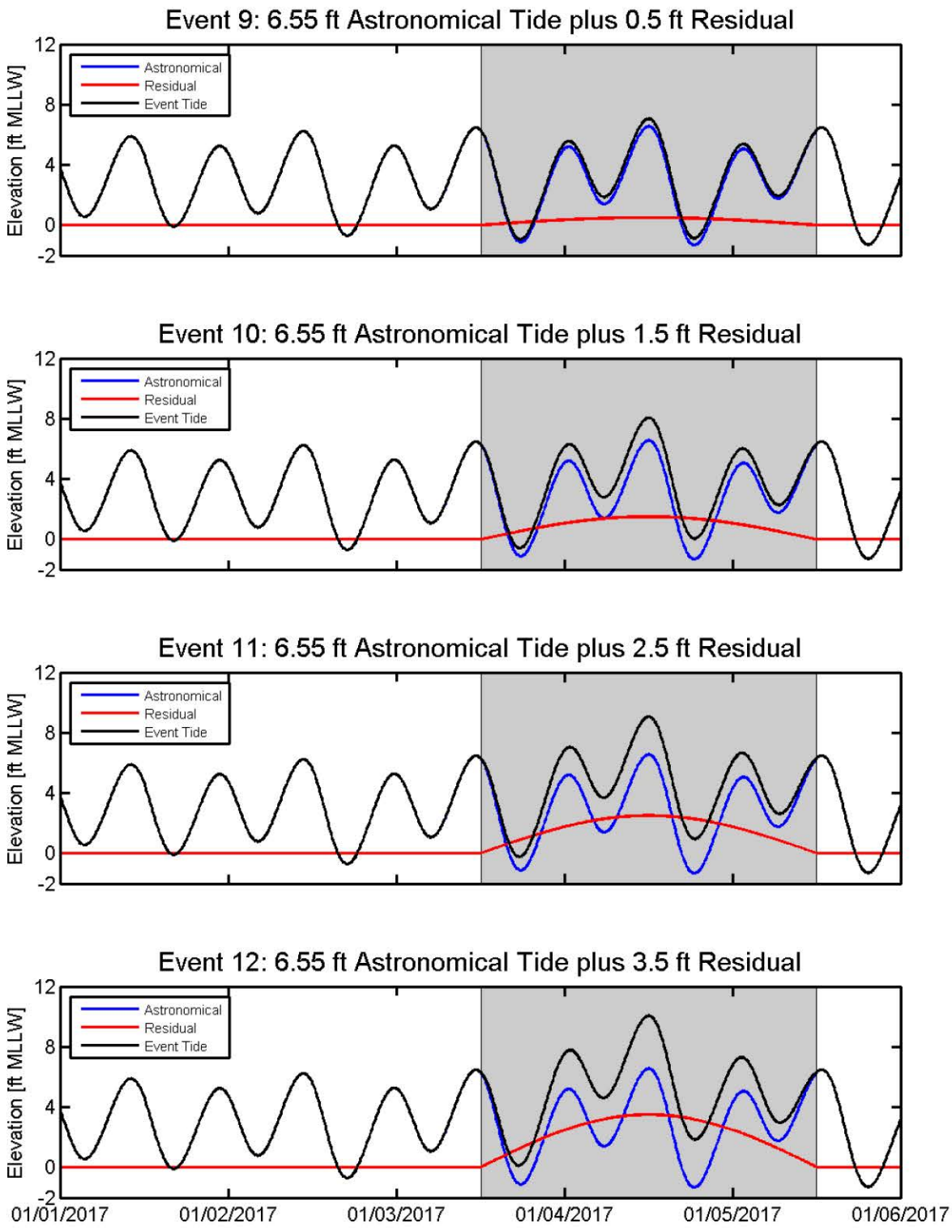

Figure 6.1-3 Astronomical tides generated from tidal harmonics, residual (surge), and resulting event water surface elevations in ft referenced to MLLW at San Francisco for Event 9 through Event 12.

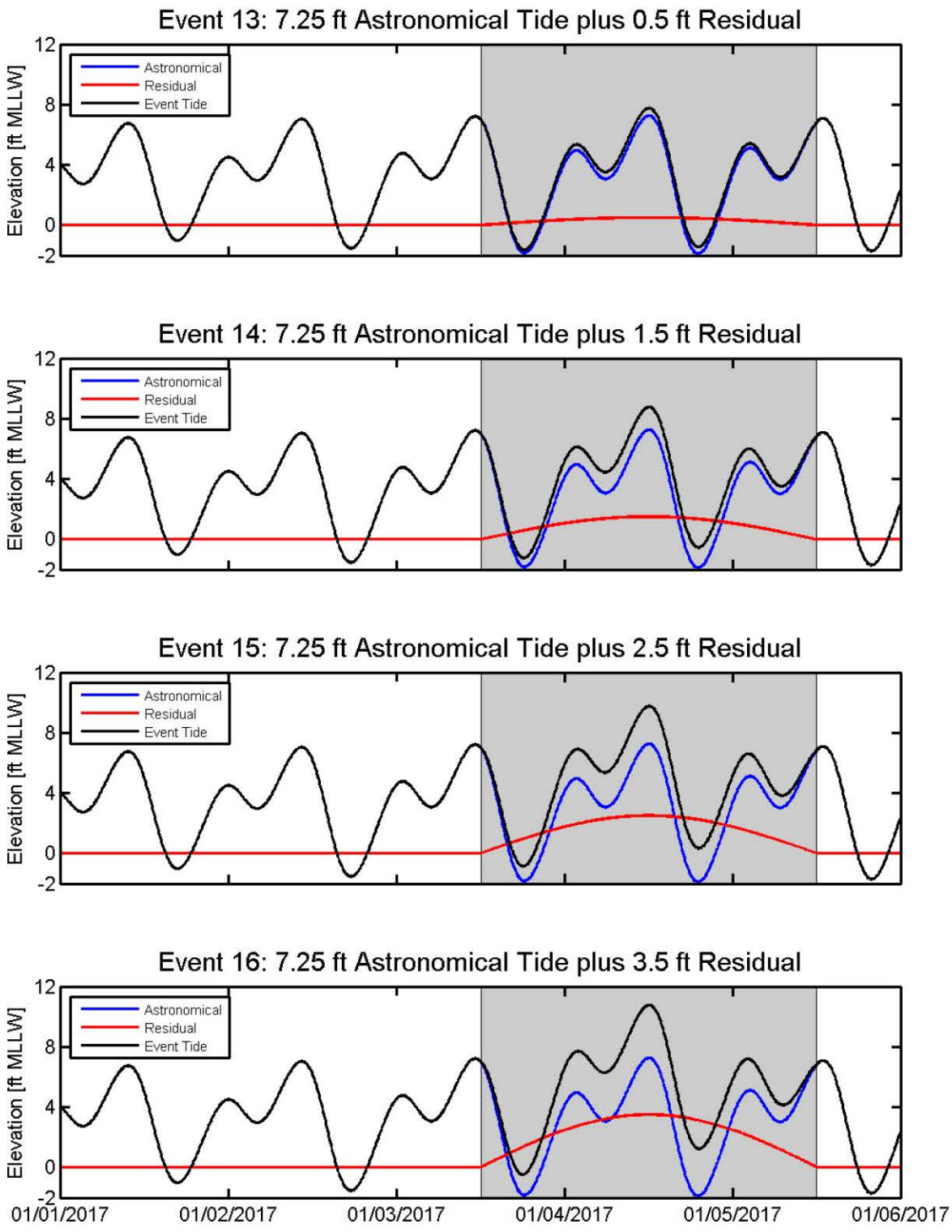

Figure 6.1-4 Astronomical tides generated from tidal harmonics, residual (surge), and resulting event water surface elevations in ft referenced to MLLW at San Francisco for Event 13 through Event 16.

6.1.2 River Inflows for Year 0 Production Simulations

The UnTRIM San Francisco Bay-Delta model includes freshwater inflows from the Sacramento-San Joaquin Delta, and tributaries which flow directly into San Francisco Bay as described in Section 3.6. A sensitivity analysis by Letter and Sturm (2010) found that raising the Delta outflow from 11,000 cfs to 300,000 cfs resulted in only a 0.03 ft increase in the peak residual water level at Coyote Creek, whereas the impact of increasing South Bay inflows from 278 cfs to 20,000 cfs raised the peak residual water level at the mouth of Coyote Creek by 0.16 ft. This suggests that peak water levels within the project area are likely to be sensitive to local tributary inflows but not sensitive to changes in inflows from North Bay or the Delta.

A constant inflow rate was used for all year 0 simulation events for all river inflows with the exception of Coyote Creek and Guadalupe River. The average January flow was calculated for each river inflow and each export using available daily flow data for all days during January from 1980 to 2011. The resulting average January flows represent elevated flows typical of winter conditions, but not extreme flood peaks, and were applied as constant inflow rates for each of the year 0 event simulations.

For Coyote Creek and Guadalupe River, a relationship was developed between coastal surge and peak fluvial flow using historical flow data from the USGS and historic surge (residual) data observed at San Francisco (9414290). Figure 6.1-5 shows the correlation between peak fluvial flow measured on Guadalupe River and the coincident tidal residual observed at San Francisco (9414290). The linear trend line indicates increasing peak fluvial flow correlates with increasing tidal residual. Figure 6.1-6 shows the correlation between peak fluvial flow measured on Coyote Creek and the coincident tidal residual observed at San Francisco (9414290). The linear trend line indicates that on Coyote Creek there is not a strong correlation between peak fluvial flow and tidal residual. The lacking of a correlation may be due to the regulation of peak flows in Coyote Creek by upstream reservoirs (Lisa Andes, USACE, pers. comm.).

For Guadalupe River, the linear relationship shown on Figure 6.1-5 was used to develop four peak flow hydrographs based on the four peak residual events simulated for year 0 (see Table 6-1). Based on an evaluation of historic flood hydrographs on Coyote Creek and Guadalupe River most flow events last for about 12 hours (Lisa Andes, USACE, pers. comm.). On average, the peak flow on Guadalupe River occurred 5.7 hours after the peak residual tide at the San Francisco NOAA station (9414290), and the peak flow on Coyote Creek occurred 11.1 hours after the peak residual tide at the San Francisco NOAA station (9414290). As a result, the duration of each synthetic flow event on the Guadalupe River was assumed to be 12 hours, with the peak flow 5.7 hours after peak surge. Prior to and subsequent to the peak flow event, the average January flow calculated for Guadalupe River was used. For Coyote Creek, the peak flow was assumed to be identical for all events. The y-intercept value of 1,650 cfs (46.7 m^3/s) from the linear fit as shown on Figure 6.1-6 was used as the peak flow on Coyote Creek for all events, with the peak flow 11.1 hours after peak surge, and all events were assumed to last 12 hours. Prior to and subsequent to the peak flow event, the average January flow calculated for Coyote Creek was used. The resulting inflow hydrographs used in the year 0 simulations for Coyote Creek and Guadalupe River are shown in Figure 6.1-7.

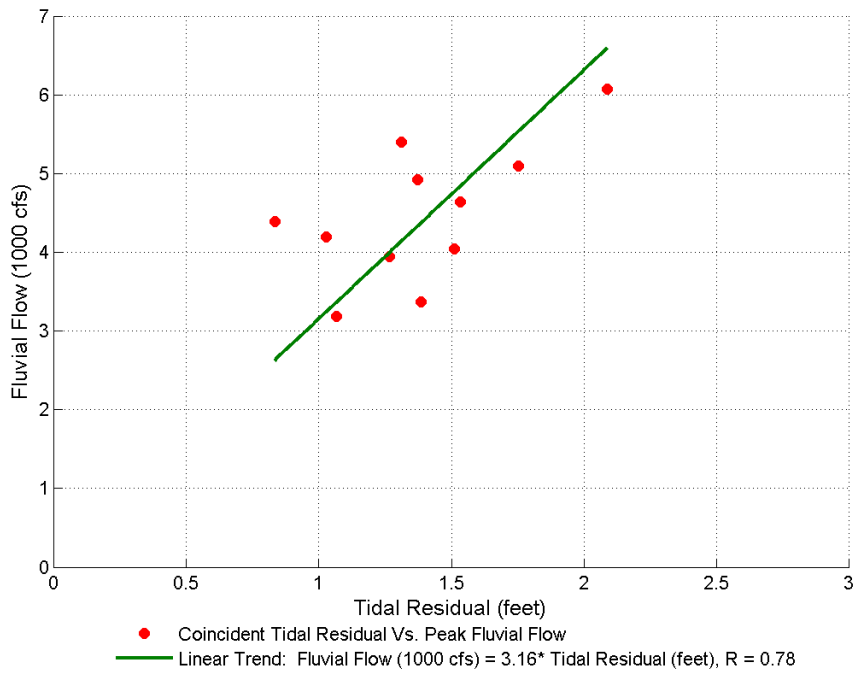

Figure 6.1-5 Relationship between peak fluvial flow and coincident tidal residual for Guadalupe River (from Lisa Andes, USACE).

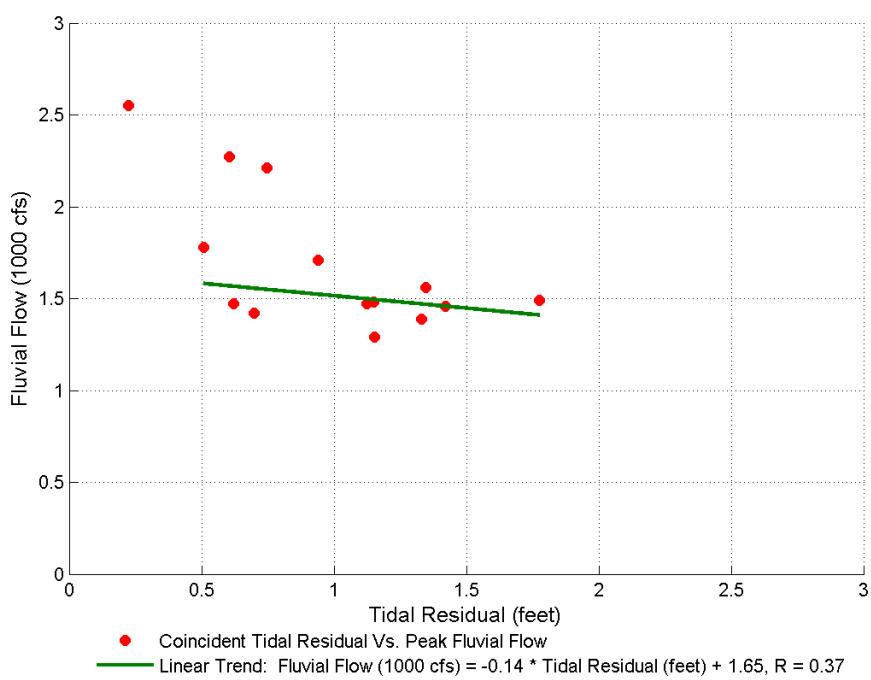

Figure 6.1-6 Relationship between peak fluvial flow and coincident tidal residual for Coyote Creek (from Lisa Andes, USACE).

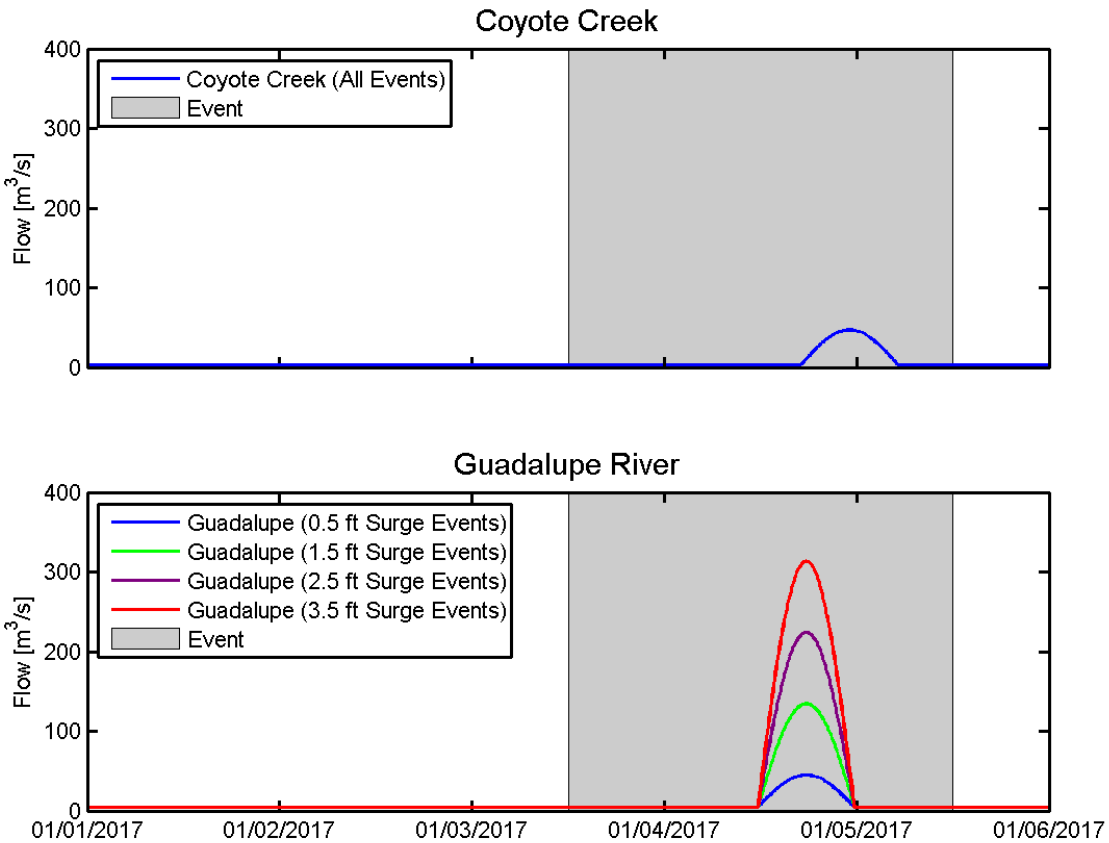

Figure 6.1-7 Inflow hydrograph for Coyote Creek (top) and Guadalupe River (bottom) used for year 0 simulations.

6.1.3 Wind Boundary Conditions for Year 0 Production Simulations

A set of synthetic wind events were developed to represent the range of potential wind conditions that are likely to result in significant wind induced setup in the project area. As seen in Section 4.7.3, wind can result in a significant increase in the maximum predicted water level in the project area during period with relative strong winds aligned with the axis of South San Francisco Bay. Conversely, during a period of weaker winds from the south (Section 4.7.4), wind can result in a decrease in water levels in the south end of South San Francisco Bay.

Based on an analysis of historic wind data at San Francisco International Airport (SFO), the most frequently occurring wind directions which lead to significant wind setup in the South Bay are 292.5 and 315 degrees (Frank Wu, USACE, pers. comm.). These two wind directions are approximately aligned with the axis of South San Francisco Bay, similar to the wind direction during December 1983 (Section 4.7.3). Analysis of wind events in San Francisco Bay suggests a typical duration of approximately 20 hours (Frank Wu, USACE, pers. comm.). For the synthetic events, three non-zero wind speeds and two wind directions were simulated, as shown in Table 6-3.

Six different wind conditions (Table 6-3) were simulated to evaluate wind setup for Event 1, Event 3, Event 13, and Event 15 (Table 6-1). The wind setup for each of the six non-zero wind scenarios were simulated for each of these four tidal events, and the wind setup for each wind scenario was calculated as the difference between the peak water surface elevation from the simulation with wind and the peak water surface elevation from the corresponding simulation without wind. This approach assumes that the wind set-up can be decoupled from the surge events and allows for two-dimensional interpolation of wind effects based on surge and stage in the MCS analysis. Figure 6.1-8 shows the wind speed and direction spanning the five day simulation period for the six wind events. In each event, the wind speed ramps up for two hours, remains constant for 16 hours, and ramps down for 2 hours. It is assumed that the wind event is coincident with the surge event such that the peak winds occur for 8 hours before and after the peak surge.

Table 6-3 Synthetic wind events used in the simulations to develop wind setup look-up tables.

Wind Direction (degrees)	Maximum Sustained Wind Speed (mph)			
	0 mph	**20 mph**	**30 mph**	**40 mph**
292.5	0 mph from 292.5 degrees	20 mph from 292.5 degrees	30 mph from 292.5 degrees	40 mph from 292.5 degrees
315.0	0 mph from 315.0 degrees	20 mph from 315.0 degrees	30 mph from 315.0 degrees	40 mph from 315.0 degrees

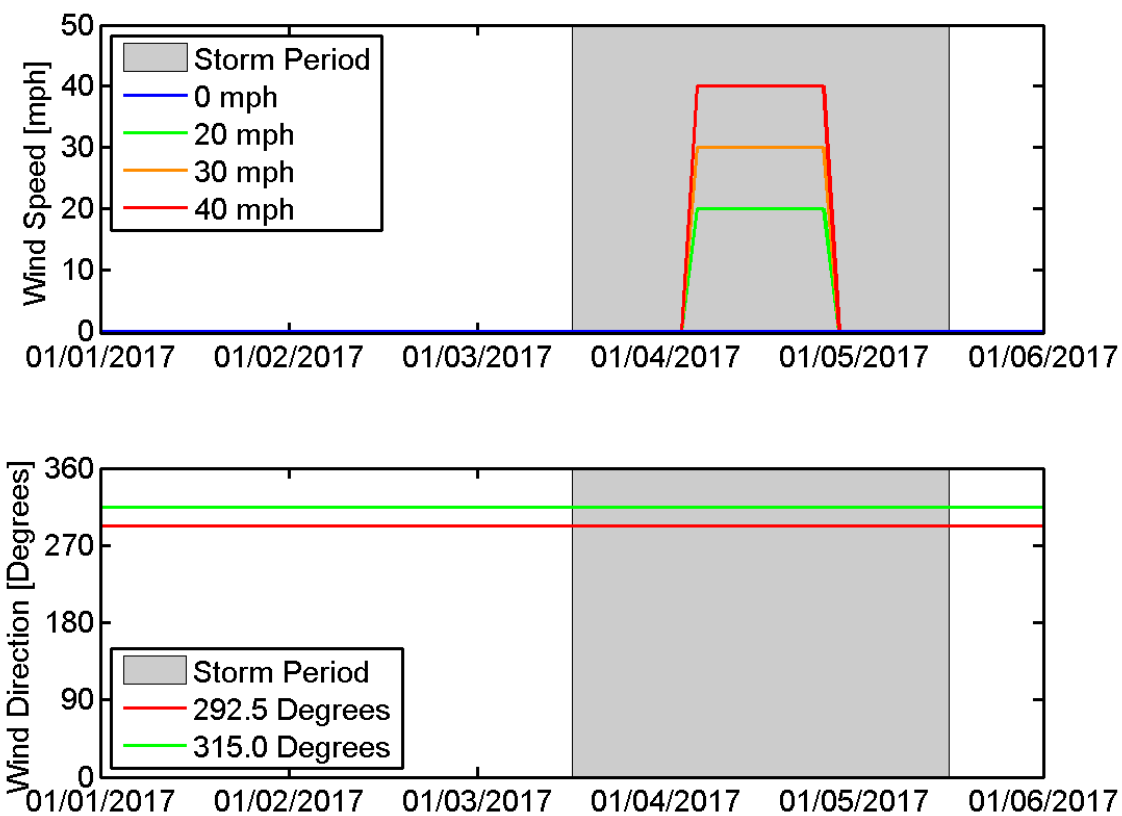

Figure 6.1-8 Predicted wind speed for four maximum sustained wind speeds (top); and wind direction for two wind directions (bottom) used in the simulations to develop wind look-up tables.

6.2 Description of Year 0 Flood Risk Management Alternatives

This section describes the Flood Risk Management (FRM) alternatives evaluated under year 0 conditions. Two different FRM alignments were considered: the Locally Preferred Alignment (LPA) and a tentative National Economic Development (NED) alignment. For each alignment, the pond operations for ponds A9 through A18 were developed based on typical winter operating conditions (See Figure 2.1-1 for pond locations). The initial water surface elevations for each of the ponds used in the year 0 simulations are shown in Table 6-4.

Table 6-4 Initial water surface elevations for winter conditions used in year 0 simulations.

Location	Initial Water Surface Elevation [ft NGVD]	Initial Water Surface Elevation [ft NAVD]
Pond A9	1.5	4.2
Pond A10	1.5	4.2
Pond A11	1.4	4.1
Pond A14	1.3	4.0
Pond A12	1.4	4.1
Pond A13	1.2	3.9
Pond A15	2.8	5.5
Pond A16	2.3	5.0
Pond A17	2.3	5.0
Pond A18	1.5	4.2
New Chicago Marsh	-3.0	-0.3

6.2.1 LPA and NED FRM Alignments

The LPA alignment follows the existing levee alignment along the eastern side of Pond A12, the southern side of Pond A13 and Pond A16, and follows a new alignment through Pond A18 and across the existing waste water treatment plant settling ponds to connect to the existing Coyote bypass levee (Figure 6.2-1). The tentative NED alignment follows the existing levee alignment along the eastern side of Pond A12, the railroad spur through New Chicago Marsh (NCM), an existing levee around the south and east side of NCM, and the same alignment as the LPA through Pond A18 and across the existing waste water treatment plant settling ponds to connect to the existing Coyote bypass levee (Figure 6.2-2).

6.2.2 Ponds A9 through A15

The year 0 simulations assume that Ponds A9 through A15 are operated similar to how they are currently operated during winter, and that restoration of these ponds has not yet begun in year 0. Ponds A9, A10, A11, and A14 are operated to maintain tidal circulation, while Ponds A12, A13, and A15 are operated as batch ponds. The intake for the A14 system is located at the northwest corner of Pond A9 and consists of two 48-inch gates. A single 48-inch gate allows for flow from Pond A9 into Pond A10, from Pond A10 into Pond A11, and from pond A11 to Pond A14. Two 48-inch gates allow for outflow from pond A14 to Coyote Creek near low water. A

48-inch gate allows for flow from Pond A12 to A13. Initial water levels in Pond A9 through A15 were based on assumed winter design operations (Table 6-5). Design water surface elevations in the ponds which were given relative to NGVD were converted to NAVD88 by adding 2.7 feet. The year 0 operation of Ponds A9 through A15 are identical for both the LPA (Figure 6.2-1) and NED (Figure 6.2-2) FRM designs.

6.2.3 Ponds A16 and A17

The current ecosystem restoration options under consideration for the South San Francisco Bay Shoreline Study do not include restoration actions for Pond A16 or Pond A17. However, Ponds A16 and A17 are currently being restored as part of the South Bay Salt Pond (SBSP) Restoration Phase I projects. Pond A16 and Pond A17 are surrounded by external and internal salt pond levees. Pond A16 is connected to Artesian Slough through a 48-inch culvert with an adjustable tidal gate located in the southeastern corner of the pond. Pond A17 is hydraulically connected to Coyote Creek via a 48-inch culvert with an adjustable tidal gate, located in the northeast corner of the pond. Water within Alviso System A16 flows between the two ponds through an existing gap between the Pond A16 and Pond A17 levees. A siphon exists between Ponds A17 and A18 that is planned to be plugged and closed (Mruz pers. comm., 2006).

Under winter operating conditions, flow enters Pond A16 from Artesian Slough through a 48-inch gate, and a 48-inch gate allows for outflow from Pond A17 to Coyote Creek to avoid the entrainment of fish in Coyote Creek. It is assumed that the siphon between A17 and A18 is closed. Initial water levels in Pond A16 and Pond A17 were based on assumed winter design operations (Table 6-5). The year 0 operation of Ponds A16 and A17 are identical for both the LPA (Figure 6.2-1) and NED (Figure 6.2-2) FRM designs.

6.2.4 Pond A18

The year 0 simulations assume that Pond A18 is operated similar to how it is currently operated during winter, and that restoration of Pond A18 has not yet begun in year 0. Pond A18 is currently managed by the City of San Jose under continuous discharge operations (City of San Jose, 2011). A 48-inch gate near the northwest corner of Pond A18 is operated to allow flow into Pond A18 from Artesian Slough. A 48-inch gate near the southwest corner of Pond A18 allows for outflow from pond A18 to Artesian Slough. The initial water level in Pond A18 was based on assumed winter design operations (Table 6-5). The year 0 operation of Pond A18 is identical for both the LPA (Figure 6.2-1) and NED (Figure 6.2-2) FRM designs.

6.2.5 New Chicago Marsh

New Chicago Marsh (NCM) is managed by the U.S. Fish & Wildlife Service (Mruz and Albertson, 2008). Water levels are maintained within NCM so that it does not get too dry, and also does not flood the salt marsh harvest mouse habitat. Flow into NCM is managed by a 48-inch tide gate located at the south end of Triangle Marsh, along the southeast side of the Railroad Tracks between Pond A15 and A16. NCM is also connected to Pond A16 by a siphon which allows flow from A16 into NCM. A pump station located at the northeastern edge of NCM allows for water

to be pumped out of the marsh when elevated water levels threaten salt marsh harvest mouse habitat within the marsh.

During winter, the tide gate at the south end of Triangle Marsh is closed to prevent excessive high tide flows into the marsh (Mruz and Albertson, 2008), the siphon from pond A16 is closed, and the pumps are off but left in ready position in case too much water gets into the system and threatens mouse habitat (Mruz, pers. comm., 2012). Under these conditions, the only water coming into NCM will be from rain, run-off, or levee overtopping. The initial water level in NCM was assumed to be -3.0 ft NGVD (-0.3 ft NAVD88), which is at the low end of the ideal water level range within the marsh to allow for inputs from heavy rains without flooding the marsh habitat.

The LPA FRM design (Figure 6.2-1) assumes the installation of a tide gate between ponds A16 and A13. The specific details of this tide gate have not yet been determined. The year 0 simulations of the LPA FRM alignment assume that the New Chicago Marsh tide gate will be closed, and no flow between New Chicago Marsh and Coyote Creek will occur along the existing marsh channel adjacent to the Railroad tracks.
The tentative NED FRM design (Figure 6.2-2) assumes the levee alignment follows the existing railroad spur through NCM. For the tentative NED FRM design, it is assumed that no flow structures which allow flow through this levee are open during winter conditions.

6.2.6 Artesian Slough Tide Gate

Both the LPA and NED FRM designs assume the installation of a tide gate on Artesian Slough at the location where the FRM levee alignment crosses Artesian Slough. The specific details of this tide gate have not yet been determined. Based on data collected by Santa Clara Valley Water District (SCVWD), it was assumed that there will be a side hinged restrained tide gate (96”x96”) with an aluminum and steel frame and door with a steel hinge assembly, and hydraulic controls (Sergio Jimenez, HDR, pers. comm.). It is expected that the structure will match the invert of the existing outflow from the San Jose Water Pollution Control Plant (WPCP). The size of the gate will be designed to accommodate San Jose WPCP plant discharge on maximum load, with some sort of automated closure. With the gate open, discharge would continue as it does under existing conditions. However, under flood conditions the gate would be closed and act as a continuation of the levee (Sergio Jimenez, HDR, pers. comm.). The screening alternative simulations assume that the Artesian Slough tide gate will be closed, and no discharge from the San Jose WPCP will be released into Artesian Slough.

6.2.7 Evaluation Locations

Predicted water levels for each of the year 0 simulation events were evaluated at twenty-three stations located along the project levees (Figure 6.2-3). The locations of each of the evaluation stations are provided in Table 6-5. The first ten evaluation stations are located along the outer levee of the existing salt ponds. Five stations are located along the inner levee along Pond A12, Pond A13, Pond A16, and Pond A18. One station (P14) is located in Artesian Slough and one station is located in the connection to the Coyote Bypass (P17). Five stations are located inside

NCM, and one station (P23) is located at the tide gate between Ponds A15 and A16 at the south end of Triangle Marsh.

6.2.8 Outer Levee Failure Conditions

An additional set of simulations was made using both the LPA FRM alignment and the tentative NED alignment to evaluate peak water levels under conditions when the outer levees surrounding the existing ponds are breached. A total of six levee failure locations were considered for both the LPA alignment (Figure 6.2-4) and the tentative NED alignment (Figure 6.2-5). The breach invert for each levee failure was determined based on the approximate elevation of the inner toe of the levee. The breach width for each levee failure was calculated using the approach developed by Nagy (2006) and described by Hubel (2012).

Table 6-5 Locations of evaluation stations used to evaluate peak water levels for year 0 simulations.

Station Number	Station Location	Location UTM [m]	
		Easting	Northing
P1	Outer Levee	593233.3	4145676.4
P2	Outer Levee	591908.3	4146684.9
P3	Outer Levee	591654.1	4146446.6
P4	Outer Levee	591018.6	4146425.5
P5	Outer Levee	589835.7	4146432.1
P6	Outer Levee	588429.4	4146619.6
P7	Outer Levee	586954.3	4146563.6
P8	Outer Levee	586874.5	4144942.8
P9	Outer Levee	589140.5	4144135.9
P10	Outer Levee	590187.3	4143119.5
P11	Inner Levee	590288.5	4143711.5
P12	Inner Levee	590421.9	4144260.2
P13	Inner Levee	591227.1	4144290.6
P14	Artesian Slough Tide Gate	592110.6	4144267.8
P15	Inner Levee	592504.4	4144728.9
P16	Inner Levee	592979.2	4144925.2
P17	Coyote Bypass	594332.1	4145187.4
P18	New Chicago Marsh	590377.9	4144050.7
P19	New Chicago Marsh	591262.2	4143832.2
P20	New Chicago Marsh	591801.4	4143465.6
P21	New Chicago Marsh	592193.0	4143827.3
P22	New Chicago Marsh	591899.7	4144113.3
P23	New Chicago Marsh Tide Gate	590642.5	4145613.0

6.3 Year 0 Model Production Simulation Results

Twelve of the sixteen tidal events shown on Table 6-1 were simulated for both the LPA FRM design (Figure 6.2-1) and the tentative NED FRM design (Figure 6.2-2). The predicted peak water level for each event was evaluated at the twenty-three evaluation locations shown on Figure 6.2-3.

6.3.1 Peak Water levels for Year 0 Production Simulations without Wind

The predicted peak water surface elevations for the twelve year 0 event simulations for the LPA FRM design without wind at the twenty-three evaluation locations are listed in Table 6-6. The predicted peak water surface elevation for the sixteen year 0 event simulations for the tentative NED FRM design without wind at the twenty-three evaluation locations are listed in Table 6-7. The levee alignments for the LPA and tentative NED FRM designs are identical with the exception of the levee along New Chicago Marsh. Because there is no levee overtopping which results in flow into New Chicago Marsh under any of the scenarios without wind, the resulting water surface elevations are identical for both alignments for the year 0 simulations that do not include wind.

Peak water surface elevations along the outer levees (Point 1 through Point 10) range from 7.28 ft under Scenario 1 to as high as 11.85 ft under Scenario 15. Along the inner levees, water surface elevations in Ponds A12 and A13 (Point 11 and Point 12) remain at the initial water surface of 4.10 ft in all twelve year 0 scenarios which do not include wind. Inside Ponds A16 (Point 13), peak water levels range from 4.89 ft to 5.29 ft. Inside Pond A18 (Point 15 and Point 16), peak water levels range from 4.25 ft to 4.62 ft. Water levels in A16 and A18 are controlled by inflow through the tide gates which are increased by higher water levels on the outer levees and outflow through tide gates which is reduced by elevated water levels along the outer levee. However this effect is muted by the tide gates which restrict the flow rates into or out of the ponds. In Artesian Slough (Point 14), peak water levels range from 7.52 ft to 11.51 ft. Point 17, which is located on the existing settling ponds is at a higher elevation and is not wet for any of the scenarios. Inside New Chicago Marsh (Point 18 through Point 22), the water surface remains at the initial water surface of -0.3 ft in all scenarios, since local precipitation and runoff is not simulated, and no overtopping of the levees surrounding New Chicago Marsh is predicted.

6.3.2 Effect of Wind on Peak Water levels for Year 0 Production Simulations

Six wind scenarios (Table 6-3) were simulated for Event 1, Event 4, Event 13, and Event 16 (Table 6-1) using the LPA FRM alignment, resulting in a total of twenty-four simulations with wind. It is expected that wind would also have an identical effect for the tentative NED FRM alignment. The wind setup for each wind simulation event was calculated as the difference between the peak water surface elevation from the simulation with wind and the peak water surface elevation from the corresponding simulation without wind. As a result, the calculated wind setup at locations within the ponds includes both wind induced setup as well as any additional wind induced overtopping of the outer pond levees that results from the wind setup

along the outboard levees as described below. The contribution of wind to peak water surface elevation at twenty-three evaluation locations for the LPA FRM alignment are listed in Table 6-8.

Along the outer levees (Point 1 through Point 10), wind setup results in an increase in peak water level of between 0.06 and 1.89 ft. The largest increase in water surface elevation due to wind occurs at Point 1 and Points 8 through Point 10 along Alviso Slough. Wind has a larger effect on peak water level in Alviso Slough (Point 8 through Point 10) for Events 1 and 13 (0.5 ft peak residual) when the peak Guadalupe River inflow into Alviso Slough is lower than the for Events 3 and 15 (2.5 ft peak residual) when the Guadalupe River inflow into Alviso Slough is higher. In Artesian Slough (Point 14), wind setup results in an increase in peak water level of between 0.33 and 1.47 ft. The six wind simulations for Event 15 typically result in a smaller increase in peak water surface elevation than the wind simulations for Event 1, 3, and 13, particularly along the outer levees.

Inside the ponds (Point 11 through 13, Point 15 and Point 16), wind results in an increase in peak water level of between 0.01 and 0.41 ft, for Events 1, 4, and 13. For Event 15, which has the highest predicted water levels of the events simulated without wind, wind setup results in some overtopping of the outer levees leading to increases in peak water levels in Pond A12, A13, and A16 of up to 3.80 ft. Since the wind setup is calculated as the difference between the peak water surface elevation from the simulation with wind and the peak water surface elevation from the corresponding simulation without wind, the calculated wind setup shown in Table 6-8 at locations within the ponds includes both wind induced setup as well as any additional wind induced overtopping of the outer pond levees that results from the wind setup along the outboard levees.

Figure 6.3-1 shows the predicted water surface elevation at Coyote Creek NOAA station (9414575) for the Event 15 simulation without wind, and the six Event 15 simulations with wind. The wind speed and direction time series simulated for each of the wind events is shown in Figure 6.1-8. For the events with wind, the wind setup results in a higher Lower High Water on January 4 than without wind, a significantly higher water surface elevation during the subsequent Higher Low Water as draining of the Far South Bay during ebb tide is inhibited by the wind setup, and a higher peak event water level at the following Higher High Water. This pattern of wind setup predicted at the Coyote Creek NOAA station (9414575) is similar to that predicted for the December 1983 storm event (Figure 4.7-13). The predicted wind setup along the outer levees along the outer levees (Point 1 through Point 10) also shows a similar pattern.

The wind setup along the outer levees increases the head difference between the water level in Coyote Creek near high water which increased flow through the pond structures into the managed ponds, and decreases the head difference between the pond and Coyote Creek at low water (due to the higher water surface at low water in Coyote Creek) which reduces outflow from the managed ponds near low water. Figure 6.3-2 shows the predicted water surface elevation inside Pond A16 (Point 13 on Figure 6.2-3) for the Event 15 simulation without wind, and six Event 15 simulations with wind. Without wind, the pond operates a muted tidal system as flow into and out of the pond is controlled by the tidal gates. For the two events with 20 mph peak winds, the increase in water level in Coyote Creek at both higher high water and

lower high water results in increased inflow into Pond A16 and decreased outflow from Pond A16 during the storm event. Thus the "wind setup" inside Pond A16 (Point 13) for the 20 mph wind event can be largely attributed to the effect of the wind setup at the outer levees on the flows through the pond control structures. For the events with 40 mph peak winds, the wind setup on the outer levees results in a large enough increase in water levels that overtopping of the levee into Pond A16 occurs, which raises the water level inside Pond A16 by up to 1.66 ft for the wind event with peak winds of 40 mph at 292.5 degrees. Similar overtopping into Pond A12 (Point 11) and Pond A13 (Point 12) results in an increase in peak water level of up to 3.80 ft in Pond A13 (Point 12) for the wind event with peak winds of 40 mph at 292.5 degrees.

Overtopping of the levee around Pond A18 (Points 15 and Point 16) is not predicted and the "wind setup" of up to 0.41 ft inside Pond A18 can be largely attributed to the effect of the wind setup at the outer levees on the flows through the pond control structures. Inside New Chicago Marsh (Point 18 through Point 22), wind setup results in only very small changes in peak water surface elevation, with maximum increases in peak water surface elevation due to wind between 0.00 and 0.05 ft.

6.3.3 Peak Water levels for Year 0 Production Simulations with Levee Failures

The predicted peak water surface elevation for the twelve year 0 event simulations for the LPA FRM design with outer levee failures and without wind at the twenty-three evaluation locations are listed in Table 6-9. Six wind scenarios (Table 6-3) were simulated for Event 1, Event 3, Event 13, and Event 15 (Table 6-1) using the LPA FRM alignment with outer levee failures, resulting in a total of twenty-four simulations with wind. The wind setup for each event with wind was calculated as the difference between the peak water surface elevation from the simulation with wind and the peak water surface elevation from the corresponding simulation without wind. The contribution of wind to peak water surface elevation at twenty-three evaluation locations for the LPA FRM alignment with outer levee failures are listed in Table 6-10. As described in Section 6.3.2, the contribution of wind to peak water surface elevation inside the managed ponds includes the influence of wind setup on flow through pond control structures and wind induced overtopping.

The predicted peak water surface elevation for the twelve year 0 event simulations for the tentative NED FRM design with outer levee failures and without wind at the twenty-three evaluation locations are listed in Table 6-11. Six wind scenarios (Table 6-3) were simulated for Event 1, Event 3, Event 13, and Event 15 (Table 6-1) using the tentative NED FRM alignment with outer levee failures, resulting in a total of twenty-four simulations with wind. The wind setup for each event with wind was calculated as the difference between the peak water surface elevation from the simulation with wind and the peak water surface elevation from the corresponding simulation without wind. The contribution of wind to peak water surface elevation at twenty-three evaluation locations for the tentative NED FRM alignment with outer levee failures are listed in Table 6-12. As described in Section 6.3.2, the contribution of wind to peak water surface elevation inside the managed ponds includes the influence of wind setup on flow through pond control structures and wind induced overtopping. For the tentative NED FRM alignment breach scenarios (Figure 6.2-5), overtopping of the levees between Ponds A12, A13, and A16 into New Chicago Marsh (NCM) results in significant increase in peak water levels

inside NCM (Points 18 through 22) in the NED breach scenarios both without wind (Table 6-11) and with wind (Table 6-12). This suggests that any FRM alignments on the landward side of NCM are likely to result in increased flood risk to salt marsh harvest mouse habitat in NCM.

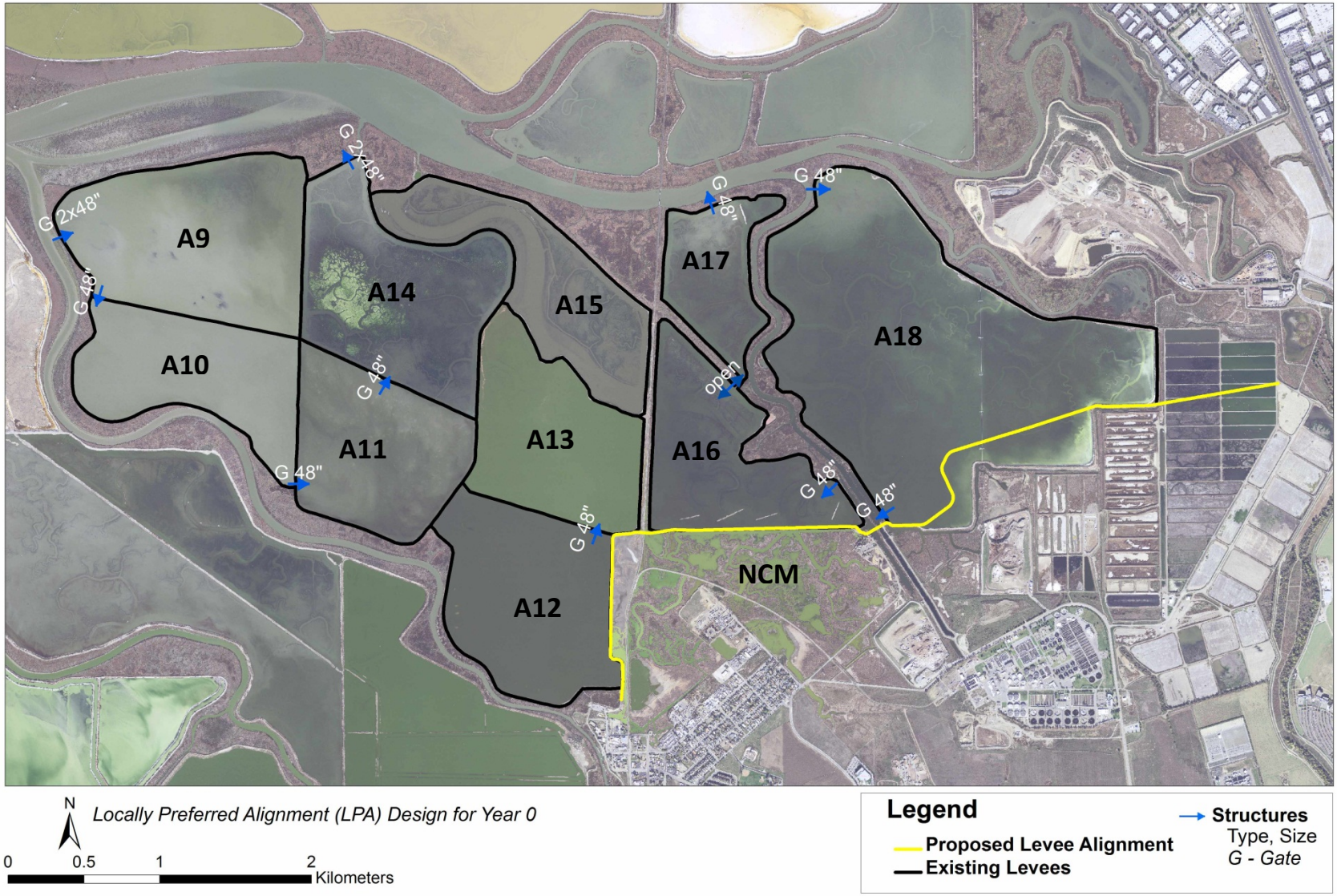

Figure 6.2-1 Locally Preferred Alignment (LPA) FRM Levee alignment and pond operations for year 0.

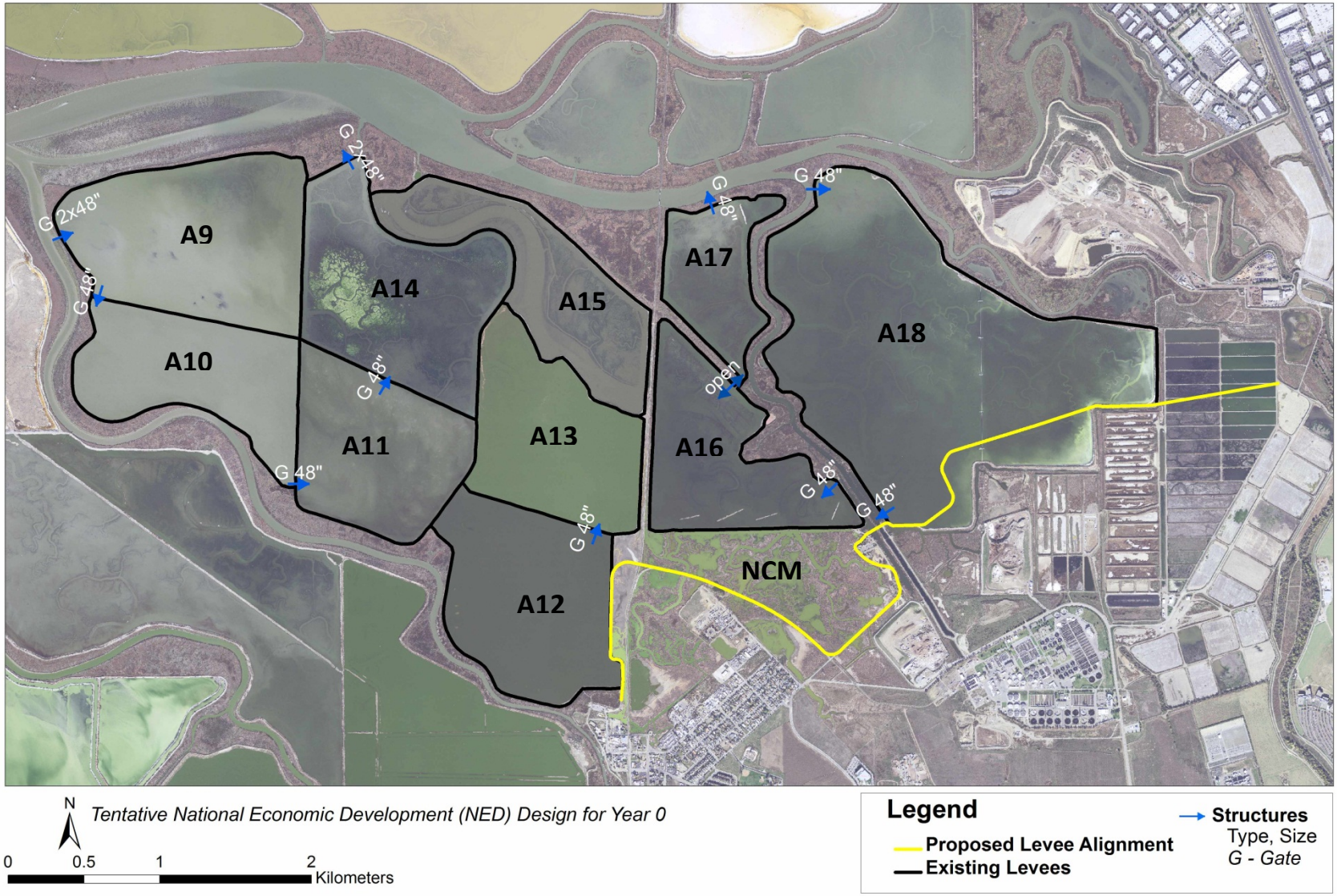

Figure 6.2-2 Tentative National Economic Development (NED) FRM Levee alignment and pond operations for year 0.

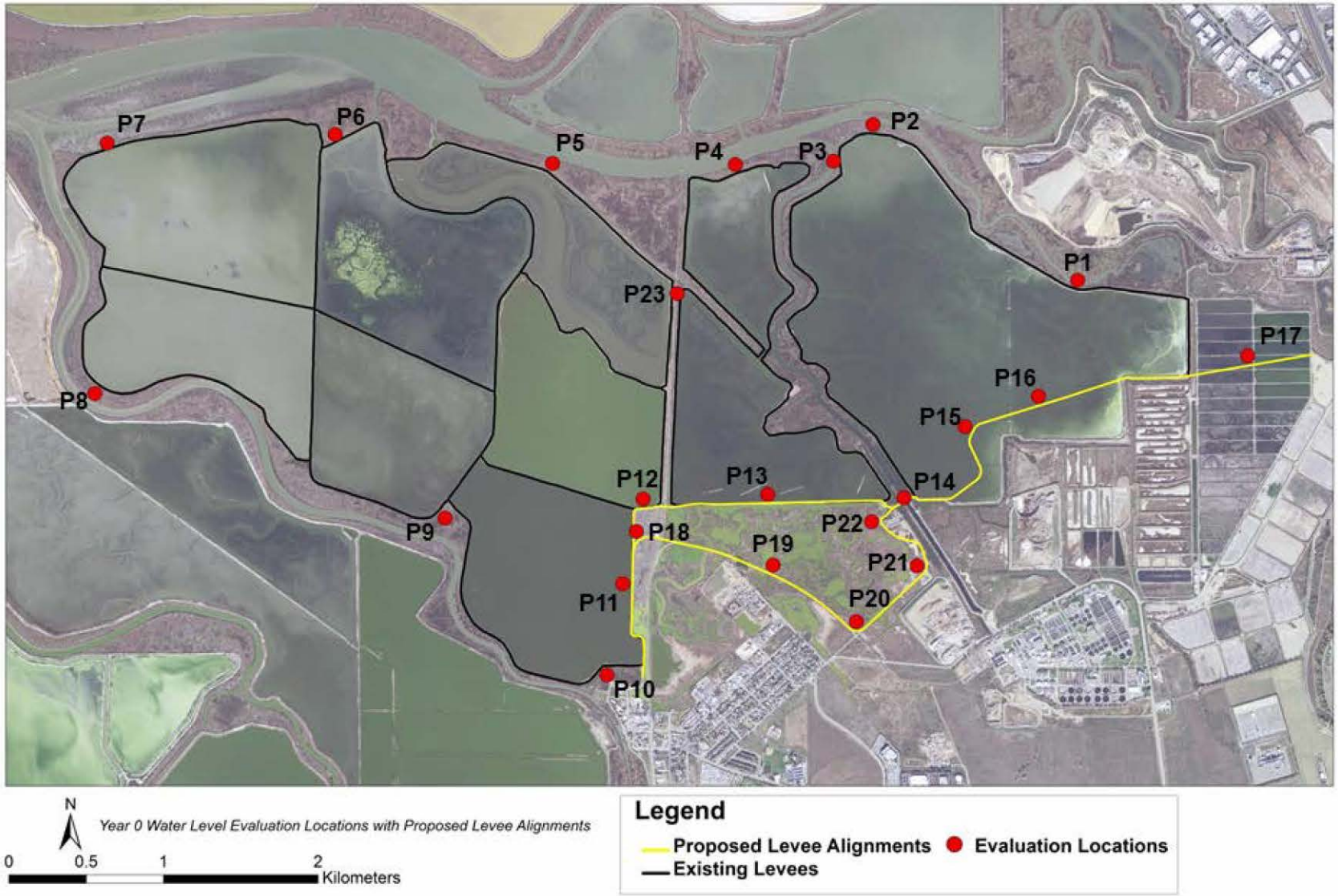

Figure 6.2-3 Locations used for evaluation of peak water levels for year 0 model simulations.

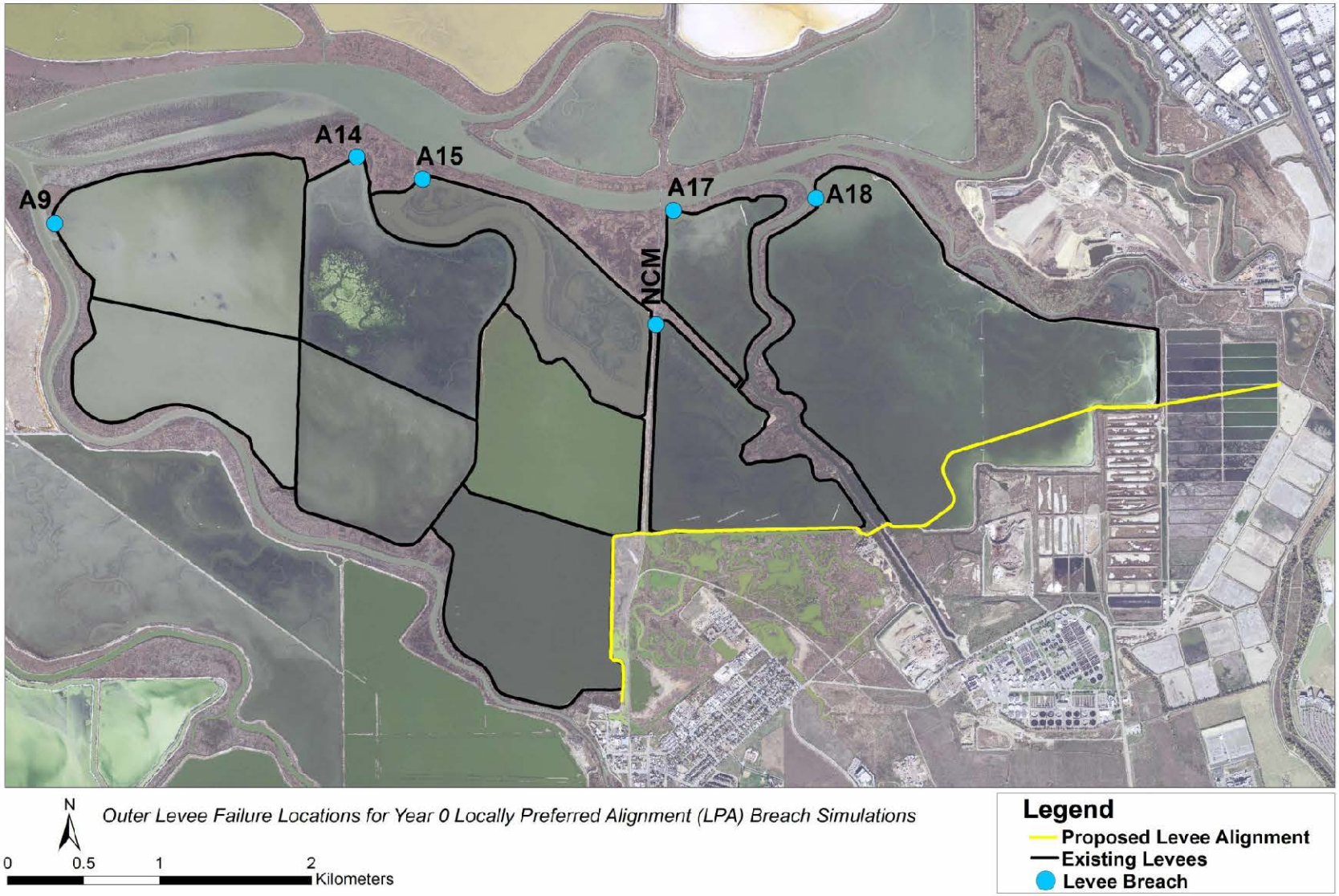

Figure 6.2-4 Locations of levee failures simulated for the evaluation of peak water levels for year 0 Locally Preferred Alignment (LPA) model simulations with levee breaches.

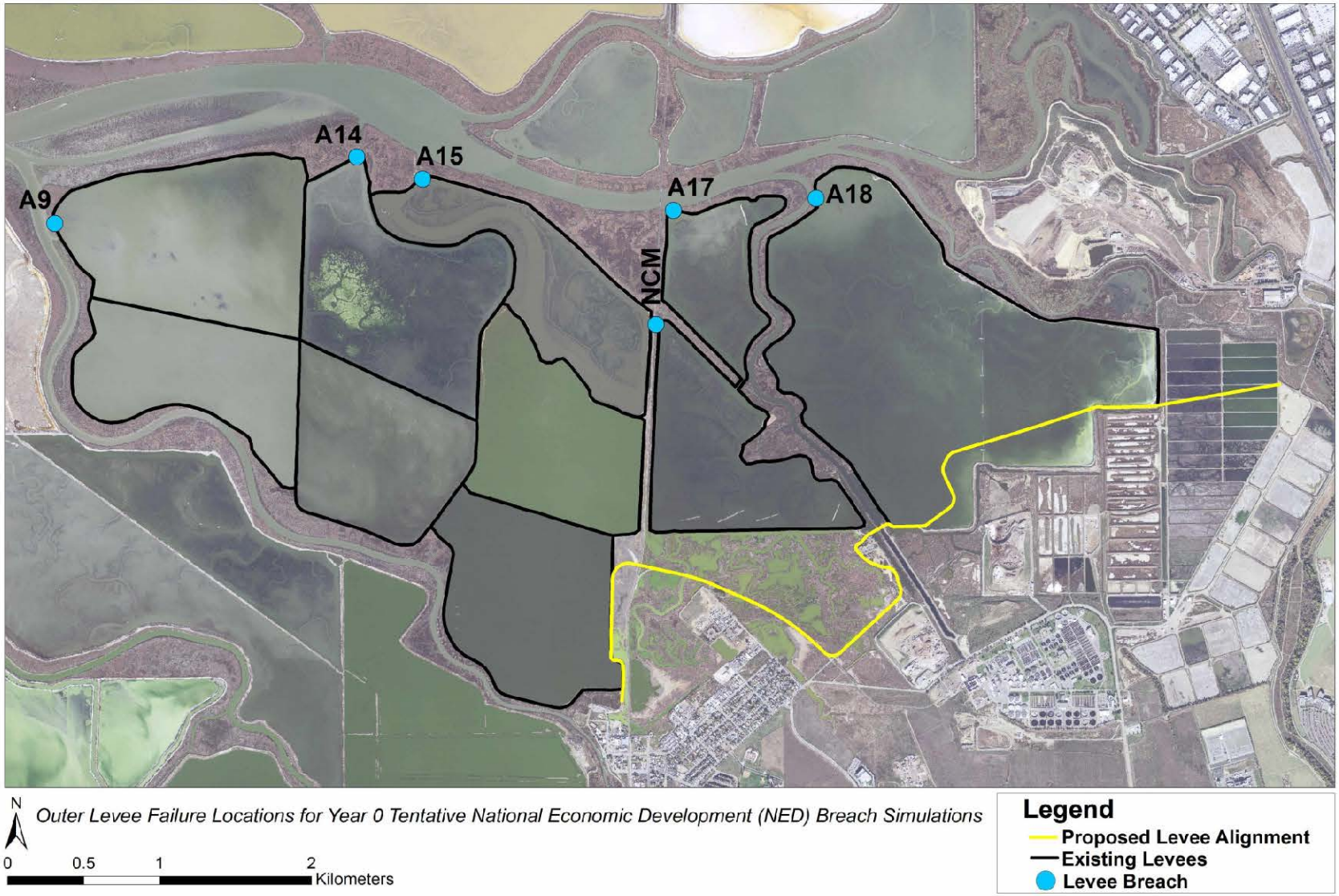

Figure 6.2-5 Locations of levee failures simulated for the evaluation of peak water levels for year 0 tentative National Economic Development (NED) model simulations with levee breaches.

Table 6-6 Predicted peak water surface elevation [ft NAVD88] for year 0 LPA FRM scenarios at twenty-three evaluation locations.

Event	Tide		Evaluation Location																						
	Astronomical [ft MLLW]	Surge [ft]	1	2	3	4	5	6	7	8	9	10	11	12	13	14	15	16	17	18	19	20	21	22	23
1	5.15	0.5	7.57	7.52	7.49	7.45	7.39	7.33	7.28	7.32	7.49	7.56	4.10	4.10	4.89	7.52	4.25	4.25	dry	-0.30	-0.30	-0.30	-0.30	-0.30	7.43
2	5.15	1.5	8.40	8.36	8.34	8.32	8.27	8.22	8.17	8.22	8.51	8.72	4.10	4.10	4.98	8.36	4.32	4.32	dry	-0.30	-0.30	-0.30	-0.30	-0.30	8.31
3	5.15	2.5	9.25	9.27	9.27	9.24	9.22	9.20	9.16	9.23	9.61	11.00	4.10	4.10	5.08	9.31	4.39	4.39	dry	-0.30	-0.30	-0.30	-0.30	-0.30	8.59
4	5.15	3.5	-	-	-	-	-	-	-	-	-	-	-	-	-	-	-	-	-	-	-	-	-	-	-
5	5.85	0.5	8.24	8.20	8.17	8.14	8.08	8.02	7.97	7.99	8.19	8.31	4.10	4.10	4.94	8.21	4.34	4.34	dry	-0.30	-0.30	-0.30	-0.30	-0.30	8.12
6	5.85	1.5	9.06	9.04	9.04	9.02	8.98	8.96	8.92	8.97	9.27	9.48	4.10	4.10	5.03	9.09	4.41	4.41	dry	-0.30	-0.30	-0.30	-0.30	-0.30	9.01
7	5.85	2.5	9.91	9.98	9.98	9.95	9.92	9.91	9.88	9.96	10.28	11.05	4.10	4.10	5.12	10.01	4.49	4.49	dry	-0.30	-0.30	-0.30	-0.30	-0.30	9.76
8	5.85	3.5	-	-	-	-	-	-	-	-	-	-	-	-	-	-	-	-	-	-	-	-	-	-	-
9	6.55	0.5	8.98	8.96	8.95	8.92	8.88	8.85	8.80	8.83	9.01	9.19	4.10	4.10	5.02	9.00	4.38	4.38	dry	-0.30	-0.30	-0.30	-0.30	-0.30	8.91
10	6.55	1.5	9.74	9.87	9.86	9.84	9.81	9.80	9.77	9.84	10.08	10.38	4.10	4.10	5.10	9.91	4.44	4.44	dry	-0.30	-0.30	-0.30	-0.30	-0.30	9.48
11	6.55	2.5	10.97	10.84	10.82	10.79	10.78	10.78	10.76	10.83	11.09	11.42	4.10	4.10	5.18	10.86	4.51	4.51	dry	-0.30	-0.30	-0.30	-0.30	-0.30	10.82
12	6.55	3.5	-	-	-	-	-	-	-	-	-	-	-	-	-	-	-	-	-	-	-	-	-	-	-
13	7.25	0.5	9.48	9.54	9.54	9.51	9.47	9.45	9.42	9.45	9.59	9.81	4.10	4.10	5.09	9.60	4.48	4.48	dry	-0.30	-0.30	-0.30	-0.30	-0.30	8.99
14	7.25	1.5	10.61	10.49	10.47	10.44	10.41	10.40	10.39	10.45	10.65	10.92	4.10	4.10	5.18	10.50	4.55	4.55	dry	-0.30	-0.30	-0.30	-0.30	-0.30	10.46
15	7.25	2.5	11.58	11.49	11.46	11.41	11.38	11.43	11.36	11.41	11.60	11.85	4.10	4.10	5.29	11.51	4.62	4.62	dry	-0.30	-0.30	-0.30	-0.30	-0.30	11.40
16	7.25	3.5	-	-	-	-	-	-	-	-	-	-	-	-	-	-	-	-	-	-	-	-	-	-	-

Table 6-7 Predicted peak water surface elevation [ft NAVD88] for year 0 tentative NED FRM scenarios at twenty-three evaluation locations.

Event	Tide		Evaluation Location																						
	Astronomical [ft MLLW]	Surge [ft]	1	2	3	4	5	6	7	8	9	10	11	12	13	14	15	16	17	18	19	20	21	22	23
1	5.15	0.5	7.57	7.52	7.49	7.45	7.39	7.33	7.28	7.32	7.49	7.56	4.10	4.10	4.89	7.52	4.25	4.25	dry	-0.30	-0.30	-0.30	-0.30	-0.30	7.43
2	5.15	1.5	8.40	8.36	8.34	8.32	8.27	8.22	8.17	8.22	8.51	8.72	4.10	4.10	4.98	8.36	4.32	4.32	dry	-0.30	-0.30	-0.30	-0.30	-0.30	8.31
3	5.15	2.5	9.25	9.27	9.27	9.24	9.22	9.20	9.16	9.23	9.61	11.00	4.10	4.10	5.08	9.31	4.39	4.39	dry	-0.30	-0.30	-0.30	-0.30	-0.30	8.59
4	5.15	3.5	-	-	-	-	-	-	-	-	-	-	-	-	-	-	-	-	-	-	-	-	-	-	-
5	5.85	0.5	8.24	8.20	8.17	8.14	8.08	8.02	7.97	7.99	8.19	8.31	4.10	4.10	4.94	8.21	4.34	4.34	dry	-0.30	-0.30	-0.30	-0.30	-0.30	8.12
6	5.85	1.5	9.06	9.04	9.04	9.02	8.98	8.96	8.92	8.97	9.27	9.48	4.10	4.10	5.03	9.09	4.41	4.41	dry	-0.30	-0.30	-0.30	-0.30	-0.30	9.01
7	5.85	2.5	9.91	9.98	9.98	9.95	9.92	9.91	9.88	9.96	10.28	11.05	4.10	4.10	5.12	10.01	4.49	4.49	dry	-0.30	-0.30	-0.30	-0.30	-0.30	9.76
8	5.85	3.5	-	-	-	-	-	-	-	-	-	-	-	-	-	-	-	-	-	-	-	-	-	-	-
9	6.55	0.5	8.98	8.96	8.95	8.92	8.88	8.85	8.80	8.83	9.01	9.19	4.10	4.10	5.02	9.00	4.38	4.38	dry	-0.30	-0.30	-0.30	-0.30	-0.30	8.91
10	6.55	1.5	9.74	9.87	9.86	9.84	9.81	9.80	9.77	9.84	10.08	10.38	4.10	4.10	5.10	9.91	4.44	4.44	dry	-0.30	-0.30	-0.30	-0.30	-0.30	9.48
11	6.55	2.5	10.97	10.84	10.82	10.79	10.78	10.78	10.76	10.83	11.09	11.42	4.10	4.10	5.18	10.86	4.51	4.51	dry	-0.30	-0.30	-0.30	-0.30	-0.30	10.82
12	6.55	3.5	-	-	-	-	-	-	-	-	-	-	-	-	-	-	-	-	-	-	-	-	-	-	-
13	7.25	0.5	9.48	9.54	9.54	9.51	9.47	9.45	9.42	9.45	9.59	9.81	4.10	4.10	5.09	9.60	4.48	4.48	dry	-0.30	-0.30	-0.30	-0.30	-0.30	8.99
14	7.25	1.5	10.61	10.49	10.47	10.44	10.41	10.40	10.39	10.45	10.65	10.92	4.10	4.10	5.18	10.50	4.55	4.55	dry	-0.30	-0.30	-0.30	-0.30	-0.30	10.46
15	7.25	2.5	11.58	11.49	11.46	11.41	11.38	11.43	11.36	11.41	11.60	11.85	4.10	4.10	5.29	11.51	4.62	4.62	dry	-0.30	-0.30	-0.30	-0.30	-0.30	11.40
16	7.25	3.5	-	-	-	-	-	-	-	-	-	-	-	-	-	-	-	-	-	-	-	-	-	-	-

Table 6-8 Contribution of wind to peak water surface elevation [ft] at twenty-three evaluation locations for year 0 LPA design.

Event	Wind		Evaluation Location																						
	Dir [deg]	Speed [mph]	1	2	3	4	5	6	7	8	9	10	11*	12*	13*	14	15*	16*	17	18	19	20	21	22	23
1	292.5	20	0.39	0.38	0.37	0.37	0.37	0.35	0.34	0.34	0.39	0.42	0.01	0.02	0.01	0.36	0.02	0.05	0.00	0.00	0.00	0.00	0.01	0.00	0.37
1	292.5	30	0.85	0.84	0.85	0.83	0.81	0.78	0.75	0.75	0.86	0.92	0.03	0.06	0.06	0.90	0.07	0.18	0.00	0.00	0.00	0.00	0.02	0.01	0.82
1	292.5	40	1.50	1.42	1.44	1.43	1.42	1.36	1.37	1.43	1.57	1.76	0.06	0.13	0.16	1.47	0.18	0.40	0.00	0.00	0.00	0.00	0.05	0.03	1.43
1	315.0	20	0.36	0.35	0.35	0.36	0.35	0.35	0.35	0.34	0.39	0.42	0.01	0.03	0.02	0.32	0.03	0.06	0.00	0.00	0.00	0.00	0.01	0.00	0.36
1	315.0	30	0.76	0.76	0.77	0.77	0.75	0.73	0.73	0.75	0.85	0.91	0.02	0.07	0.08	0.83	0.12	0.19	0.00	0.00	0.00	0.00	0.02	0.00	0.76
1	315.0	40	1.46	1.40	1.42	1.42	1.42	1.39	1.43	1.54	1.67	1.89	0.05	0.15	0.20	1.47	0.27	0.41	0.00	0.00	0.00	0.00	0.04	0.01	1.42
3	292.5	20	0.34	0.38	0.38	0.37	0.35	0.34	0.33	0.36	0.36	0.06	0.01	0.02	0.02	0.39	0.02	0.02	0.00	0.00	0.00	0.00	0.01	0.00	0.54
3	292.5	30	0.93	0.82	0.83	0.84	0.83	0.84	0.78	0.84	0.74	0.16	0.03	0.06	0.06	0.81	0.06	0.14	0.00	0.00	0.00	0.00	0.02	0.01	1.50
3	292.5	40	1.43	1.12	1.14	1.13	1.06	1.13	1.14	1.14	1.25	0.51	0.06	0.13	0.18	1.23	0.17	0.37	0.00	0.00	0.00	0.00	0.05	0.03	1.89
3	315.0	20	0.31	0.34	0.35	0.34	0.33	0.33	0.33	0.37	0.34	0.05	0.01	0.03	0.02	0.37	0.02	0.02	0.00	0.00	0.00	0.00	0.01	0.00	0.57
3	315.0	30	0.92	0.77	0.78	0.79	0.79	0.77	0.74	0.81	0.72	0.15	0.02	0.07	0.08	0.74	0.09	0.15	0.00	0.00	0.00	0.00	0.02	0.00	1.51
3	315.0	40	1.47	1.12	1.13	1.10	1.06	1.13	1.05	1.11	1.21	0.52	0.04	0.15	0.23	1.28	0.26	0.39	0.00	0.00	0.00	0.00	0.04	0.01	2.00
13	292.5	20	0.56	0.37	0.37	0.36	0.34	0.34	0.32	0.34	0.44	0.41	0.01	0.02	0.03	0.37	0.02	0.02	0.00	0.00	0.00	0.00	0.01	0.00	0.66
13	292.5	30	0.94	0.66	0.66	0.65	0.66	0.66	0.66	0.66	0.71	0.76	0.03	0.06	0.09	0.65	0.05	0.11	0.00	0.00	0.00	0.00	0.02	0.01	1.17
13	292.5	40	1.70	1.33	1.32	1.25	1.17	1.21	1.22	1.20	1.45	1.56	0.06	0.13	0.21	1.41	0.13	0.33	0.00	0.00	0.00	0.00	0.05	0.03	1.95
13	315.0	20	0.54	0.34	0.35	0.35	0.34	0.33	0.33	0.37	0.46	0.41	0.01	0.03	0.04	0.36	0.02	0.02	0.00	0.00	0.00	0.00	0.01	0.00	0.70
13	315.0	30	0.93	0.65	0.62	0.63	0.65	0.65	0.65	0.66	0.67	0.72	0.02	0.07	0.12	0.65	0.07	0.13	0.00	0.00	0.00	0.00	0.02	0.00	1.17
13	315.0	40	1.55	1.14	1.15	1.10	1.10	1.21	1.18	1.21	1.42	1.53	0.04	0.15	0.27	1.31	0.22	0.35	0.00	0.00	0.00	0.00	0.04	0.01	1.90
15	292.5	20	0.34	0.30	0.31	0.30	0.28	0.24	0.26	0.27	0.28	0.25	0.02	0.02	0.05	0.33	0.02	0.02	0.00	0.00	0.00	0.00	0.01	0.00	0.31
15	292.5	30	0.70	0.65	0.67	0.65	0.63	0.55	0.56	0.59	0.60	0.55	0.11	0.07	0.28	0.69	0.05	0.08	0.00	0.00	0.00	0.00	0.02	0.01	0.68
15	292.5	40	1.16	1.04	1.06	1.05	1.00	0.91	1.00	1.00	0.94	0.93	0.84	3.80	1.66	1.08	0.09	0.27	0.00	0.00	0.00	0.00	0.05	0.03	1.08
15	315.0	20	0.35	0.30	0.31	0.30	0.29	0.26	0.29	0.31	0.33	0.28	0.01	0.03	0.05	0.33	0.02	0.02	0.00	0.00	0.00	0.00	0.01	0.00	0.32
15	315.0	30	0.66	0.59	0.60	0.59	0.57	0.50	0.54	0.59	0.61	0.56	0.10	0.08	0.28	0.65	0.05	0.09	0.00	0.00	0.00	0.00	0.02	0.00	0.64
15	315.0	40	1.07	0.92	0.94	0.94	0.91	0.80	0.92	0.94	0.90	0.88	0.73	2.00	1.37	1.03	0.16	0.28	0.00	0.00	0.00	0.00	0.04	0.01	1.03

* Contribution of wind to peak water surface elevation inside the managed ponds includes the influence of wind setup on flow through pond control structures and wind induced overtopping as described in Section 6.3.2.

Table 6-9 Predicted peak water surface elevation [ft NAVD88] for year 0 LPA design scenarios with outer levee failures at twenty-three evaluation locations.

Event	Tide		Evaluation Location																						
	Astronomical [ft MLLW]	Surge [ft]	1	2	3	4	5	6	7	8	9	10	11	12	13	14	15	16	17	18	19	20	21	22	23
1	5.15	0.5	7.02	7.00	6.09	6.96	6.95	6.95	7.03	7.13	7.30	7.35	4.10	4.10	5.65	6.11	5.74	5.74	dry	-0.30	-0.30	-0.30	-0.30	-0.30	6.66
2	5.15	1.5	7.94	7.91	6.84	7.88	7.88	7.88	7.94	8.04	8.32	8.59	4.10	4.10	6.25	6.86	6.70	6.70	dry	-0.30	-0.30	-0.30	-0.30	-0.30	7.43
3	5.15	2.5	8.83	8.80	7.84	8.77	8.80	8.81	8.91	9.04	9.45	11.01	4.10	4.37	6.96	7.87	7.76	7.76	dry	-0.30	-0.30	-0.30	-0.30	-0.30	8.42
4	5.15	3.5	-	-	-	-	-	-	-	-	-	-	-	-	-	-	-	-	-	-	-	-	-	-	-
5	5.85	0.5	7.70	7.66	6.54	7.63	7.63	7.63	7.70	7.79	7.98	8.08	4.10	4.10	5.98	6.57	6.35	6.36	dry	-0.30	-0.30	-0.30	-0.30	-0.30	7.27
6	5.85	1.5	8.61	8.56	7.53	8.54	8.57	8.55	8.68	8.80	9.13	9.31	4.10	4.13	6.68	7.55	7.41	7.41	dry	-0.30	-0.30	-0.30	-0.30	-0.30	7.89
7	5.85	2.5	9.35	9.40	8.57	9.37	9.43	9.48	9.63	9.78	10.15	11.07	4.10	7.01	7.56	8.59	8.50	8.50	dry	-0.30	-0.30	-0.30	-0.30	-0.30	9.09
8	5.85	3.5	-	-	-	-	-	-	-	-	-	-	-	-	-	-	-	-	-	-	-	-	-	-	-
9	6.55	0.5	8.43	8.39	7.04	8.36	8.39	7.98	8.53	8.61	8.80	8.93	4.10	4.10	6.51	7.06	6.88	6.88	dry	-0.30	-0.30	-0.30	-0.30	-0.30	7.78
10	6.55	1.5	9.20	9.21	8.00	9.18	9.25	9.28	9.47	9.60	9.86	10.14	4.10	5.41	7.25	8.02	7.91	7.91	dry	-0.30	-0.30	-0.30	-0.30	-0.30	8.94
11	6.55	2.5	9.98	10.00	9.08	9.98	10.09	10.17	10.43	10.62	10.91	11.25	5.03	9.38	8.13	9.11	9.02	9.02	dry	-0.30	-0.30	-0.30	-0.30	-0.30	9.54
12	6.55	3.5	-	-	-	-	-	-	-	-	-	-	-	-	-	-	-	-	-	-	-	-	-	-	-
13	7.25	0.5	8.97	8.95	7.72	8.92	8.97	8.98	9.14	9.22	9.36	9.58	4.10	4.68	7.01	7.74	7.61	7.61	dry	-0.30	-0.30	-0.30	-0.30	-0.30	8.70
14	7.25	1.5	9.64	9.75	8.78	9.73	9.81	9.88	10.09	10.23	10.45	10.73	4.27	8.96	7.83	8.82	8.72	8.72	dry	-0.30	-0.30	-0.30	-0.30	-0.30	9.37
15	7.25	2.5	10.64	10.53	9.98	10.50	10.61	10.67	11.00	11.21	11.43	11.72	8.90	9.85	9.05	10.08	9.90	9.90	dry	-0.30	-0.30	-0.30	-0.30	-0.30	10.14
16	7.25	3.5	-	-	-	-	-	-	-	-	-	-	-	-	-	-	-	-	-	-	-	-	-	-	-

Table 6-10 Contribution of wind to peak water surface elevation [ft] at twenty-three evaluation locations for year 0 LPA design with outer levee failures.

Event	Wind		Evaluation Location																						
	Dir [deg]	Speed [mph]	1	2	3	4	5	6	7	8	9	10	11*	12*	13*	14	15*	16*	17	18	19	20	21	22	23
1	292.5	20	0.36	0.33	0.24	0.33	0.32	0.31	0.31	0.32	0.33	0.37	0.01	0.02	0.10	0.24	0.36	0.38	0.00	0.00	0.00	0.00	0.01	0.00	0.40
1	292.5	30	0.81	0.78	0.58	0.78	0.75	0.72	0.71	0.72	0.80	0.85	0.03	0.06	0.36	0.62	0.92	0.96	0.00	0.00	0.00	0.00	0.02	0.01	0.71
1	292.5	40	1.63	1.55	1.50	1.55	1.52	1.45	1.39	1.42	1.57	1.72	0.06	0.14	0.96	1.59	1.88	1.92	0.00	0.00	0.00	0.00	0.05	0.03	1.25
1	315.0	20	0.33	0.32	0.20	0.31	0.32	0.32	0.32	0.33	0.35	0.36	0.01	0.03	0.10	0.22	0.38	0.39	0.00	0.00	0.00	0.00	0.01	0.00	0.42
1	315.0	30	0.71	0.69	0.54	0.70	0.69	0.67	0.68	0.70	0.77	0.82	0.02	0.07	0.38	0.59	0.92	0.94	0.00	0.00	0.00	0.00	0.02	0.00	0.70
1	315.0	40	1.49	1.44	1.41	1.44	1.44	1.39	1.37	1.46	1.60	1.77	0.04	0.15	0.98	1.53	1.83	1.85	0.00	0.00	0.00	0.00	0.04	0.01	1.24
3	292.5	20	0.31	0.30	0.36	0.30	0.32	0.32	0.34	0.36	0.39	0.06	0.01	0.96	0.28	0.36	0.41	0.42	0.00	0.00	0.00	0.00	0.01	0.00	0.44
3	292.5	30	0.69	0.73	0.93	0.72	0.72	0.75	0.78	0.85	0.83	0.16	0.03	3.61	0.74	0.95	1.04	1.06	0.00	0.00	0.00	0.00	0.02	0.01	0.78
3	292.5	40	1.33	1.28	1.95	1.29	1.24	1.20	1.12	1.09	1.25	0.45	2.71	5.28	1.78	2.02	2.13	2.18	0.00	0.00	0.00	0.00	0.05	0.03	1.43
3	315.0	20	0.28	0.28	0.38	0.29	0.31	0.32	0.33	0.36	0.38	0.05	0.01	1.02	0.29	0.37	0.43	0.44	0.00	0.00	0.00	0.00	0.01	0.00	0.44
3	315.0	30	0.64	0.68	0.93	0.67	0.69	0.72	0.73	0.82	0.80	0.15	0.02	3.57	0.77	0.94	1.04	1.07	0.00	0.00	0.00	0.00	0.02	0.00	0.75
3	315.0	40	1.34	1.25	1.92	1.26	1.22	1.14	1.11	1.09	1.25	0.44	2.60	5.25	1.81	2.05	2.12	2.17	0.00	0.00	0.00	0.00	0.04	0.01	1.39
13	292.5	20	0.28	0.29	0.37	0.29	0.30	0.32	0.32	0.33	0.43	0.45	0.01	1.15	0.27	0.38	0.43	0.45	0.00	0.00	0.00	0.00	0.01	0.00	0.26
13	292.5	30	0.66	0.70	0.94	0.68	0.70	0.74	0.75	0.85	0.81	0.89	0.04	3.78	0.70	0.97	1.07	1.10	0.00	0.00	0.00	0.00	0.02	0.01	0.60
13	292.5	40	1.19	1.12	1.93	1.13	1.07	1.08	1.25	1.19	1.40	1.53	2.58	4.98	1.59	2.04	2.12	2.18	0.00	0.00	0.00	0.00	0.05	0.03	1.17
13	315.0	20	0.27	0.28	0.40	0.29	0.30	0.33	0.32	0.35	0.44	0.46	0.01	1.29	0.30	0.41	0.47	0.48	0.00	0.00	0.00	0.00	0.01	0.00	0.27
13	315.0	30	0.62	0.67	1.01	0.66	0.69	0.72	0.72	0.85	0.81	0.88	0.04	3.90	0.77	1.04	1.14	1.16	0.00	0.00	0.00	0.00	0.02	0.00	0.58
13	315.0	40	1.20	1.09	1.94	1.10	1.07	1.04	1.25	1.14	1.33	1.46	2.57	4.98	1.67	2.09	2.17	2.21	0.00	0.00	0.00	0.00	0.04	0.01	1.13
15	292.5	20	0.31	0.26	0.38	0.23	0.23	0.23	0.23	0.25	0.26	0.25	0.55	0.08	0.36	0.38	0.38	0.39	0.00	0.00	0.00	0.00	0.01	0.00	0.31
15	292.5	30	0.72	0.69	0.96	0.65	0.53	0.53	0.59	0.61	0.62	0.58	1.43	0.48	1.34	0.98	0.99	1.01	0.00	0.00	0.00	0.00	0.02	0.01	0.81
15	292.5	40	1.54	1.44	1.92	1.40	1.21	1.00	1.06	1.07	1.04	1.01	2.91	1.96	2.80	1.97	2.04	2.08	0.00	0.00	0.00	0.00	0.05	0.03	1.79
15	315.0	20	0.31	0.25	0.38	0.22	0.24	0.24	0.27	0.30	0.32	0.30	0.59	0.08	0.38	0.39	0.37	0.38	0.00	0.00	0.00	0.00	0.01	0.00	0.31
15	315.0	30	0.63	0.60	0.89	0.57	0.46	0.48	0.54	0.58	0.62	0.55	1.39	0.42	1.28	0.93	0.91	0.93	0.00	0.00	0.00	0.00	0.02	0.00	0.75
15	315.0	40	1.33	1.21	1.69	1.19	1.03	0.82	0.94	0.97	0.96	0.93	2.64	1.69	2.50	1.82	1.80	1.84	0.00	0.00	0.00	0.00	0.04	0.01	1.59

* Contribution of wind to peak water surface elevation inside the managed ponds includes the influence of wind setup on flow through pond control structures and wind induced overtopping as described in Section 6.3.2.

Table 6-11 Predicted peak water surface elevation [ft NAVD88] for year 0 tentative NED design scenarios with outer levee failures at twenty-three evaluation locations.

Event	Tide		Evaluation Location																						
	Astronomical [ft MLLW]	Surge [ft]	1	2	3	4	5	6	7	8	9	10	11	12	13	14	15	16	17	18	19	20	21	22	23
1	5.15	0.5	7.03	7.00	6.12	6.96	6.95	6.95	7.03	7.13	7.29	7.35	4.10	4.10	5.65	6.12	5.73	5.73	dry	-0.30	-0.30	-0.30	-0.30	-0.30	6.72
2	5.15	1.5	7.93	7.91	6.84	7.88	7.88	7.88	7.94	8.04	8.31	8.59	4.10	4.10	6.25	6.86	6.70	6.70	dry	-0.30	-0.15	-0.30	-0.30	-0.30	7.44
3	5.15	2.5	8.83	8.80	7.84	8.77	8.80	8.81	8.91	9.04	9.46	11.01	4.10	4.30	6.96	7.88	7.75	7.75	dry	3.67	0.84	0.84	0.84	0.84	8.04
4	5.15	3.5	-	-	-	-	-	-	-	-	-	-	-	-	-	-	-	-	-	-	-	-	-	-	-
5	5.85	0.5	7.70	7.66	6.55	7.63	7.63	7.62	7.70	7.79	7.98	8.08	4.10	4.10	5.98	6.57	6.35	6.35	dry	-0.30	-0.30	-0.30	-0.30	-0.30	7.27
6	5.85	1.5	8.61	8.56	7.51	8.54	8.57	8.56	8.68	8.80	9.12	9.31	4.10	4.13	6.68	7.55	7.42	7.42	dry	2.70	0.25	-0.30	-0.30	0.24	7.89
7	5.85	2.5	9.35	9.40	8.56	9.37	9.43	9.48	9.63	9.78	10.15	11.07	4.10	6.14	7.56	8.57	8.49	8.49	dry	4.22	2.38	2.38	2.38	2.38	8.52
8	5.85	3.5	-	-	-	-	-	-	-	-	-	-	-	-	-	-	-	-	-	-	-	-	-	-	-
9	6.55	0.5	8.43	8.39	7.03	8.36	8.39	7.98	8.53	8.61	8.80	8.93	4.10	4.10	6.51	7.06	6.88	6.88	dry	0.28	0.23	-0.30	-0.30	0.18	7.77
10	6.55	1.5	9.20	9.20	7.99	9.18	9.25	9.28	9.47	9.60	9.86	10.14	4.10	5.00	7.24	8.02	7.91	7.91	dry	4.20	1.57	1.57	1.54	1.54	8.30
11	6.55	2.5	9.98	9.99	9.08	9.97	10.08	10.16	10.43	10.62	10.91	11.25	4.23	8.89	8.10	9.11	9.00	9.00	dry	5.54	5.54	5.54	5.54	5.54	9.31
12	6.55	3.5	-	-	-	-	-	-	-	-	-	-	-	-	-	-	-	-	-	-	-	-	-	-	-
13	7.25	0.5	8.97	8.95	7.71	8.92	8.97	8.98	9.14	9.22	9.36	9.58	4.10	4.41	7.00	7.73	7.60	7.61	dry	3.90	1.45	1.45	1.39	1.39	8.12
14	7.25	1.5	9.63	9.75	8.77	9.72	9.81	9.87	10.09	10.23	10.45	10.72	4.10	7.84	7.82	8.81	8.71	8.71	dry	4.51	3.82	3.82	3.82	3.82	8.94
15	7.25	2.5	10.62	10.51	9.96	10.48	10.60	10.66	11.00	11.21	11.43	11.72	6.32	9.51	8.79	10.05	9.88	9.88	dry	8.85	8.85	8.86	8.87	8.86	10.00
16	7.25	3.5	-	-	-	-	-	-	-	-	-	-	-	-	-	-	-	-	-	-	-	-	-	-	-

Table 6-12 Contribution of wind to peak water surface elevation [ft] at twenty-three evaluation locations for year 0 tentative NED design with outer levee failures.

Event	Wind		Evaluation Location																						
	Dir [deg]	Speed [mph]	1	2	3	4	5	6	7	8	9	10	11*	12*	13*	14	15*	16*	17	18*	19*	20*	21*	22*	23
1	292.5	20	0.35	0.33	0.17	0.32	0.31	0.31	0.31	0.32	0.34	0.37	0.01	0.02	0.10	0.21	0.37	0.38	0.00	0.00	0.00	0.00	0.01	0.00	0.34
1	292.5	30	0.80	0.78	0.55	0.77	0.75	0.72	0.71	0.72	0.80	0.85	0.03	0.06	0.36	0.61	0.93	0.96	0.00	0.00	0.07	0.00	0.02	0.01	0.64
1	292.5	40	1.64	1.55	1.46	1.55	1.52	1.45	1.40	1.42	1.58	1.74	0.07	0.14	0.96	1.57	1.88	1.93	0.00	2.73	0.49	0.00	0.05	0.49	1.18
1	315.0	20	0.33	0.32	0.18	0.31	0.31	0.31	0.32	0.33	0.36	0.37	0.01	0.03	0.10	0.23	0.39	0.40	0.00	0.00	0.00	0.00	0.01	0.00	0.35
1	315.0	30	0.71	0.70	0.50	0.70	0.70	0.68	0.68	0.71	0.79	0.83	0.02	0.07	0.38	0.58	0.92	0.94	0.00	0.00	0.05	0.00	0.02	0.00	0.64
1	315.0	40	1.50	1.45	1.40	1.46	1.45	1.40	1.38	1.48	1.63	1.80	0.04	0.15	0.99	1.52	1.82	1.85	0.00	2.21	0.39	0.00	0.04	0.48	1.17
3	292.5	20	0.31	0.30	0.36	0.30	0.31	0.32	0.34	0.36	0.39	0.06	0.01	0.64	0.27	0.36	0.41	0.42	0.00	0.38	0.72	0.72	0.72	0.72	0.18
3	292.5	30	0.69	0.73	0.93	0.71	0.72	0.75	0.78	0.85	0.83	0.17	0.03	2.45	0.74	0.94	1.03	1.06	0.00	0.67	2.13	2.13	2.13	2.13	0.57
3	292.5	40	1.33	1.29	1.93	1.29	1.24	1.19	1.11	1.09	1.25	0.44	0.83	4.96	1.68	2.01	2.11	2.17	0.00	4.32	7.16	7.21	7.21	7.18	1.57
3	315.0	20	0.28	0.28	0.37	0.29	0.31	0.32	0.33	0.35	0.38	0.05	0.01	0.69	0.29	0.36	0.43	0.44	0.00	0.36	0.76	0.76	0.76	0.76	0.17
3	315.0	30	0.64	0.68	0.92	0.67	0.68	0.72	0.73	0.83	0.79	0.15	0.02	2.43	0.77	0.94	1.04	1.06	0.00	0.68	2.08	2.08	2.08	2.08	0.53
3	315.0	40	1.34	1.24	1.89	1.25	1.21	1.14	1.10	1.09	1.25	0.46	0.71	4.91	1.72	2.02	2.11	2.15	0.00	4.15	6.97	6.97	6.97	6.97	1.47
13	292.5	20	0.28	0.29	0.38	0.28	0.30	0.32	0.31	0.33	0.43	0.46	0.01	0.78	0.27	0.39	0.43	0.44	0.00	0.23	0.71	0.71	0.71	0.71	0.20
13	292.5	30	0.66	0.70	0.96	0.68	0.70	0.74	0.75	0.85	0.82	0.88	0.03	2.65	0.69	0.98	1.06	1.09	0.00	0.56	1.99	1.99	2.00	2.00	0.63
13	292.5	40	1.20	1.12	1.93	1.12	1.06	1.08	1.26	1.18	1.39	1.52	0.70	4.84	1.48	2.05	2.10	2.16	0.00	3.85	6.29	6.30	6.36	6.35	1.46
13	315.0	20	0.27	0.28	0.41	0.29	0.30	0.33	0.32	0.35	0.44	0.46	0.01	0.87	0.30	0.43	0.47	0.48	0.00	0.25	0.77	0.77	0.77	0.77	0.21
13	315.0	30	0.62	0.67	1.02	0.66	0.68	0.72	0.72	0.84	0.81	0.87	0.02	2.79	0.76	1.04	1.13	1.15	0.00	0.57	2.09	2.09	2.09	2.09	0.62
13	315.0	40	1.19	1.08	1.94	1.11	1.06	1.04	1.26	1.15	1.34	1.48	0.64	4.82	1.57	2.08	2.15	2.19	0.00	3.79	6.23	6.23	6.29	6.29	1.41
15	292.5	20	0.31	0.28	0.39	0.25	0.22	0.21	0.23	0.25	0.25	0.25	1.86	0.14	0.36	0.41	0.40	0.40	0.00	0.53	0.56	0.57	0.58	0.57	0.37
15	292.5	30	0.71	0.67	0.94	0.63	0.54	0.53	0.57	0.60	0.61	0.58	3.39	0.28	0.96	0.97	0.97	1.00	0.00	0.89	0.92	0.94	0.95	0.94	0.91
15	292.5	40	1.47	1.36	1.82	1.32	1.12	0.95	1.06	1.07	1.04	1.00	5.07	1.88	2.65	1.89	1.95	1.99	0.00	2.55	2.59	2.62	2.63	2.61	1.72
15	315.0	20	0.33	0.29	0.39	0.26	0.24	0.24	0.27	0.30	0.31	0.30	2.22	0.17	0.39	0.42	0.40	0.40	0.00	0.58	0.61	0.62	0.62	0.61	0.41
15	315.0	30	0.65	0.59	0.87	0.57	0.49	0.48	0.54	0.58	0.62	0.55	3.35	0.26	0.92	0.93	0.91	0.92	0.00	0.87	0.90	0.92	0.92	0.91	0.85
15	315.0	40	1.29	1.15	1.61	1.12	0.96	0.78	0.94	0.97	0.96	0.92	4.78	1.59	2.34	1.74	1.72	1.75	0.00	2.26	2.29	2.31	2.29	2.28	1.53

* Contribution of wind to peak water surface elevation inside the managed ponds includes the influence of wind setup on flow through pond control structures and wind induced overtopping as described in Section 6.3.2.

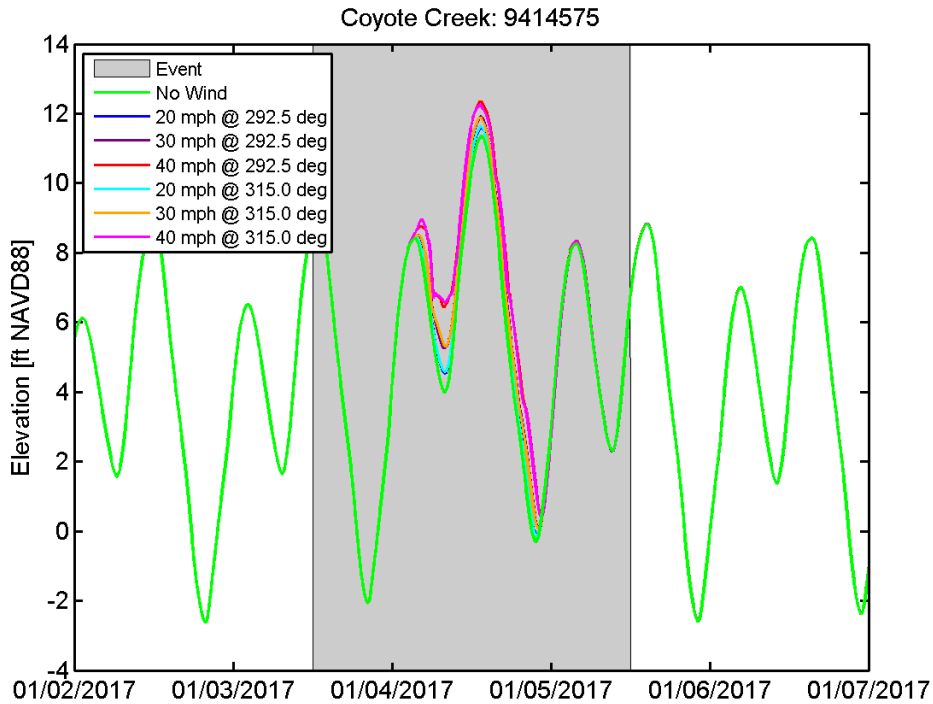

Figure 6.3-1 Predicted water surface elevation at Coyote Creek NOAA station (9414575) for Event 15 simulation without wind, and six Event 15 simulations with wind.

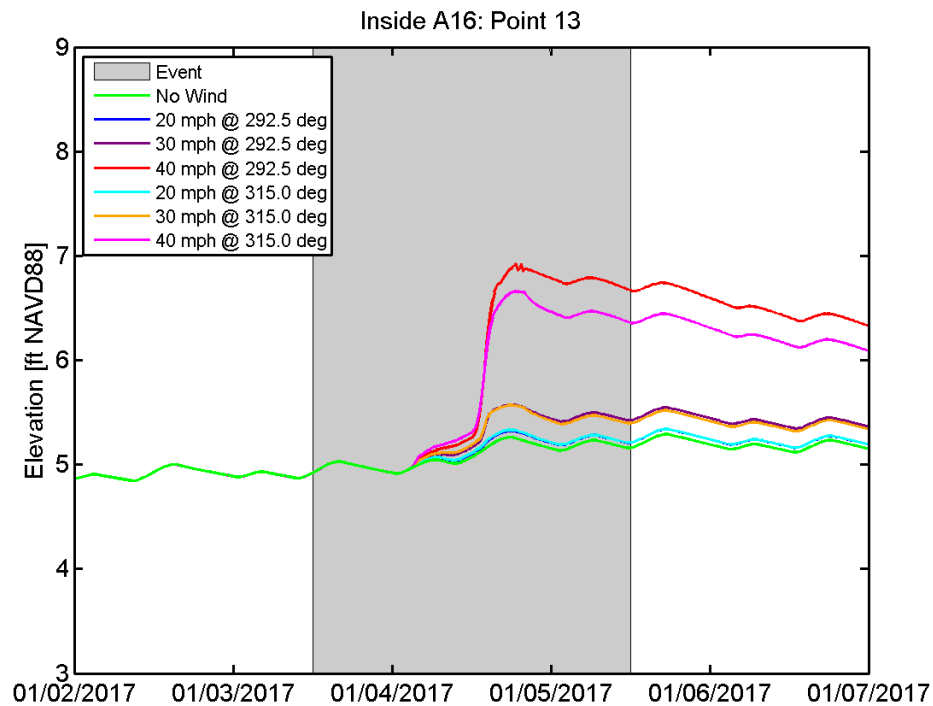

Figure 6.3-2 Predicted water surface elevation inside Pond A16 (Point 13 on Figure 6.2-3) for Event 15 simulation without wind, and six Event 15 simulations with wind.

7. Development of Year 50 Project Conditions

The model bathymetry for the year 50 (2067) simulations incorporate both the expected accretion within the project ponds which has been estimated as part of the ecosystem design (ESA PWA, 2012), as well as estimated channel evolution in the vicinity of the project area. It is expected that the channel and mudflat bathymetry in the project area may evolve in response to both sea level rise and due to channel adjustment which will occur following the opening of the salt ponds to tidal action. The analysis presented in the section makes use of three different methods of evaluation which use a combination of modeling and historical data analysis to estimate channel evolution in the vicinity of the project area for year 50 conditions.

First, a comparison between bathymetric and LiDAR data collected in 2004 and 2010 allowed for an assessment of the channel evolution which has occurred in the Coyote Creek region following the breaching of the three island ponds in March 2006. This analysis (Section 7.1) considered the channel evolution in the project area for subtidal, intertidal and marsh areas. Second, sediment deposition patterns in mudflat and marsh areas in the Coyote region were evaluated through a short sediment transport simulation (Section 7.2) during a period when a strong net sediment flux into the far South San Francisco Bay was observed at Dumbarton Bridge. Third, the expected channel scour resulting from the restoration of Ponds A9 through A15 and Pond A18 to tidal action were investigated through simulations of channel shear stress and velocity under existing conditions and under future conditions with SLR and projected year 50 pond bathymetry (Section 7.3). Finally, the results of the three separate analyses were combined into a single estimate of bathymetric change in the project area to establish year 50 (2067) conditions which included 0.649 m (2.13 ft) of sea level rise and the planned restoration of Ponds A9 through A15 and Pond A18 (Section 7.4).

7.1 Evaluation of Bathymetric Evolution Following Island Pond Breaches

The purpose of this analysis is to evaluate the bathymetric evolution in the Coyote Creek region which occurred following the breaching of the three island ponds in March 2005. Through the comparison of bathymetric and LiDAR data collected prior to 2005 and bathymetric and LiDAR data collected in 2010, geomorphic evolution of the channels and mudflats in Coyote Creek can be evaluated.

Gross and Schaaf & Wheeler (2003) predicted on the order of 0.6 to 0.8 m (2 to 2.5 ft) of scour in Coyote Creek following the island pond (Ponds A19-A21) breaches based on an analysis of the predicted change in cross-sectional average peak velocity resulting from the increase in tidal prism from opening the island ponds to tidal action (see Section 7.3 for a more detailed discussion of this analysis). The analysis presented in this section quantifies the observed scour which has occurred in the five years following the opening of the three island ponds to tidal action. This analysis is used both to provide an assessment of the assumptions used by Gross and Schaaf & Wheeler (2003) and to guide a similar analysis to predict the additional scour that is likely to occur in the channel of Coyote Creek and adjacent sloughs as a result of the increase in tidal prism associated with the restoration of Ponds A9 through A15 and Pond A18 (See Section 7.3).

7.1.1 Bathymetric Data Sources

All data sources were provided or converted into the North American Datum of 1983 (NAD83), UTM Zone 10 horizontal datum, and NGVD88 vertical datum. All analysis of historic bathymetry was conducted in meters relative to NAVD88.

Four primary bathymetric data sets were used in this analysis. Two LiDAR data sets were used to provide good coverage of mudflat and marsh areas, but these data sets do not provide information about subtidal bathymetric changes. The two LiDAR data sets used in this analysis were:

- 2004 LiDAR – Bare earth processed LiDAR point data that were available for the South San Francisco Bay for the year 2004. This data set was collected by TerraPoint USA, and reprocessed by the USACE Joint Airborne LiDAR Bathymetry Technical Center of Expertise (JALBTCX). The reprocessed points were reprojected to the UTM datum and then cropped to two subsections—one centered at Alviso, and the second covering the shoreline of the South Bay between Dumbarton Bridge and Calaveras Point (See Figure 7.1-1 for location). Points in these two sections were used to create two 1 m resolution DEMs using the USGS tool, las2dem. The documentation for JALBTCX states that the post-processed data has a potential error of about ± 20 cm in addition to the survey accuracies already reported by the USGS.

- 2010 LiDAR – Bare earth (with vegetation removed) Digital Elevation Models (DEMs) created from a LiDAR overflight in 2010 of the San Francisco Coast, funded by an American Recovery and Reinvestment Act (ARRA) project, were downloaded from the USGS Click Holdings database (http://lidar.cr.usgs.gov) in .las format. Images (rasters) created from these files were mosaicked (with blending) into a geodatabase in ArcMap 10 to cover the project area of the South San Francisco Bay. Two sections were then clipped from this mosaic for further comparison — one centered at Alviso, and the second covering the shoreline of the South Bay between Dumbarton Bridge and Calaveras Point.

In addition, two composite bathymetric data sets which combine bathymetric and LiDAR data from a range of available sources were used within a smaller region of Coyote Creek. The two composite bathymetric data sets used in the analysis were:

- 2005 SFEI DEM – A continuous DEM of the South San Francisco Bay created from sonar soundings from Foxgrover et al. (2007) in the channels merged with 2005 bare earth LiDAR elevations and other data sources covering the marshes and tidal areas which was developed for the San Francisco Estuary Institute (SFEI) was provided by U.C. Berkeley (Stacey et al., 2011). Although this DEM was developed in 2011, for the purpose of comparison it is referred to as the 2005 DEM since the primary bathymetric soundings from Foxgrover et al. (2007) and the bare earth LiDAR data used to develop this DEM were from 2005. However, some components of this DEM, such as the cross-sections in Artesian Slough surveyed by Fremont Engineers for Cargill, Inc. were collected prior to 2005.

- 2010 USGS DEM from Continuous LiDAR and Sonar – A continuous DEM of Coyote Creek and Alviso Slough was provided by the USGS, created from sonar soundings in the channel merged with the 2010 LiDAR elevations covering the marshes and tidal areas (Foxgrover et al., 2011b).

The comparison of these bathymetric data sources which are derived from a combination of LiDAR, soundings, surveys, and other data sources is subject to the inherent uncertainty of each data set used to develop the data sources. In a study of Corte Madera Marsh, Foxgrover et al. (2011a) report that the "bare earth" LiDAR data in Corte Madera Marsh were on average 0.23 m (0.75 ft) higher than elevations obtained by RTK GPS measurements. Thus it is likely that both the 2004 and 2010 LiDAR data are likely to indicate higher elevations than would be obtained by ground based surveys due in a large part to the difficulty in removing the influence of vegetation on LiDAR measurements. In addition, the accuracy of the LiDAR surveys is on the same order as the observed differences between the subsequent surveys. Due to these uncertainties, the comparative bathymetry evaluation cannot provide a precise measure of bathymetric change, but can be used to assess qualitative change where patterns exist. However, in areas where subsequent multibeam bathymetry surveys are available, such as in the channel areas of Coyote Creek, the error in the comparisons is likely to be much smaller than in the LiDAR comparisons.

7.1.2 Coyote Creek Cross-Sections

Six cross-sections were extracted from the continuous 2005 SFEI DEM and 2010 USGS DEMs along Coyote Creek between Calaveras Point and the Railroad Bridge between Pond A20 and A21 (Figure 7.1-1). Elevations were extracted from the 2005 SFEI DEM and 2010 USGS DEM at 2 m intervals along each of the six cross-sections.

Figures 7.1-2 through 7.1-7 show the bathymetry from 2005 SFEI DEM compared to 2010 USGS DEM along six cross-sections in Coyote Creek (Figure 7.1-1). Almost all of the cross-sections show incision in Coyote Creek of up to about a meter in the five-year interval between the successive bathymetric surveys of Coyote Creek. However, since the levees surrounding ponds A19, A20, and A21 were breached in March 2006, any scour that is attributed to breaching of the island ponds would have occurred over four years.

The restoration of ponds A19, A20, and A21 to tidal action in March 2006 was expected to result in scour in Coyote Creek as a result of the increased tidal prism of the restored ponds. Gross and Schaaf & Wheeler (2003) estimated that the due to this increased tidal prism, channel deepening of between 2 and 2.5 feet could be expected in Coyote Creek following the breaching of ponds A19, A20, and A21. As seen in Figure 7.1-2, the channel at the location of the Railroad Bridge over Coyote Creek (Section 0 on Figure 7.1-1) scoured by more than 1 m between 2005 and 2010, which is slightly more than was predicted by Gross and Schaaf & Wheeler (2003). Similar scour of the thalweg in Coyote Creek is evident at Section 2 (Figure 7.1-4), Section 3 (Figure 7.1-5), and Section 4 (Figure 7.1-6). In addition to channel deepening, some widening of the channel between 2005 and 2010 is observed at Section 0 (Figure 7.1-2),

Section 1 (Figure 7.1-3), Section 2 (Figure 7.1-4), and Section 3 (Figure 7.1-5). Additional comparisons between these two DEMs (see top panel of Figure 7.1-10 and discussion in Section 7.1.5) also indicates both deepening and widening of some reaches of Coyote Creek between 2005 and 2010.

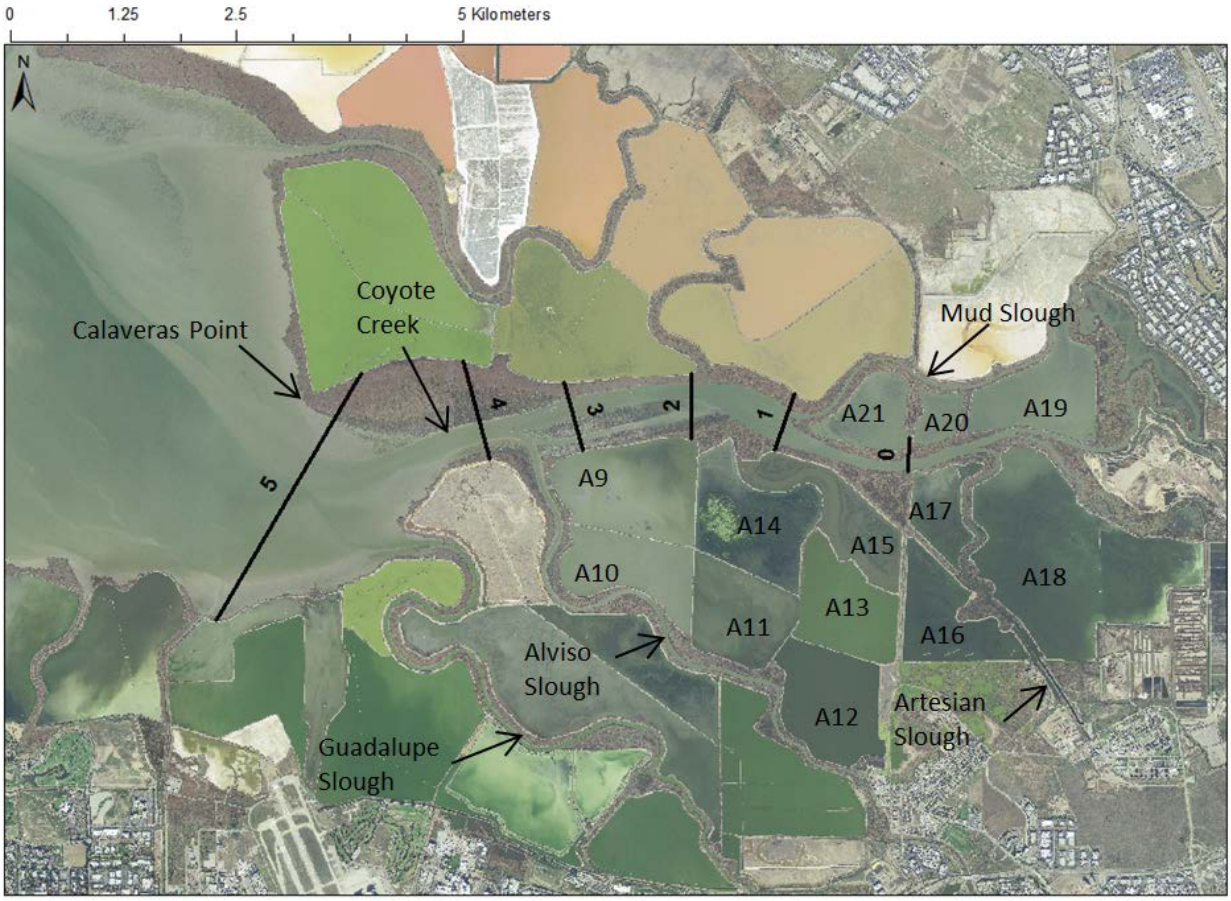

Figure 7.1-1 Locations of six cross-sections of Coyote Creek between the Railroad Bridge between Pond A20 and A21 (Section 0) and Calaveras Point (Section 5).

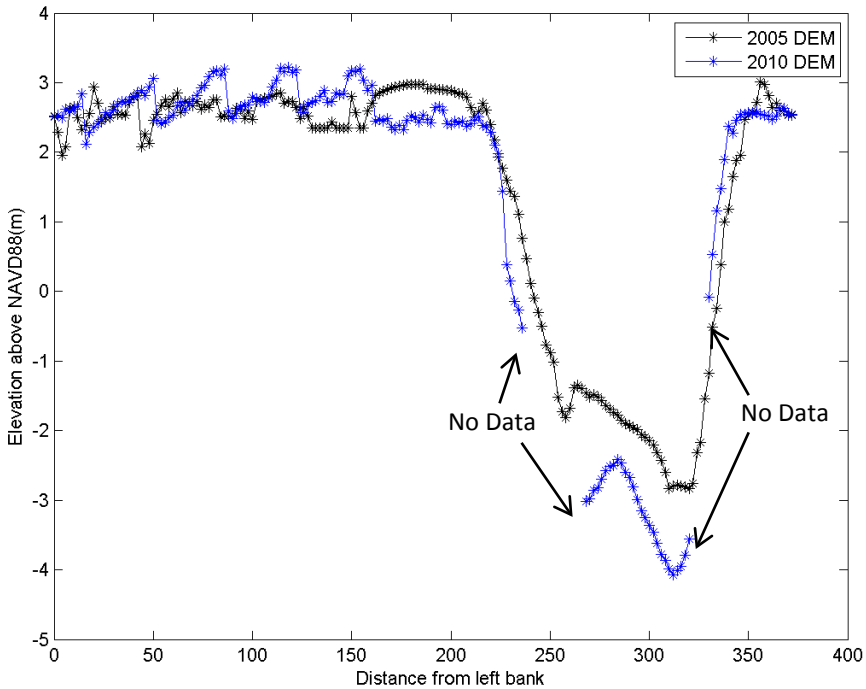

Figure 7.1-2 Change in the bathymetry at cross-section 0 from 2005 to 2010.

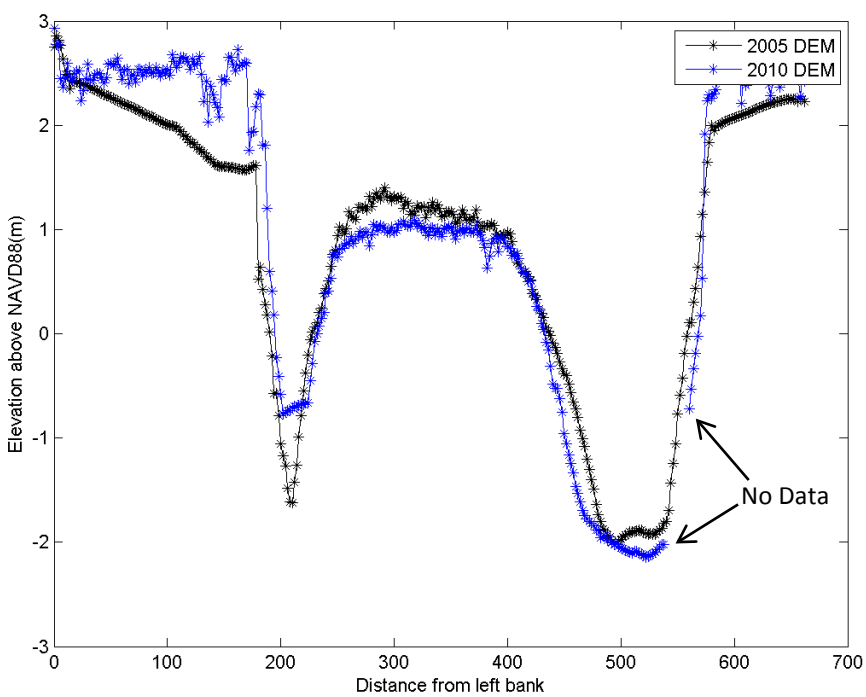

Figure 7.1-3 Change in the bathymetry at cross-section 1 from 2005 to 2010.

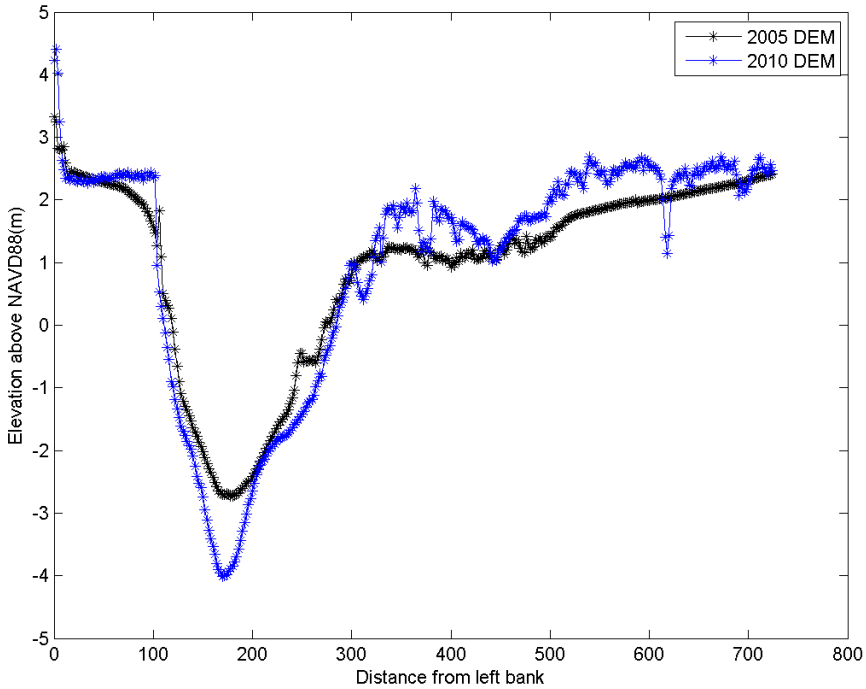

Figure 7.1-4 Change in the bathymetry at cross-section 2 from 2005 to 2010.

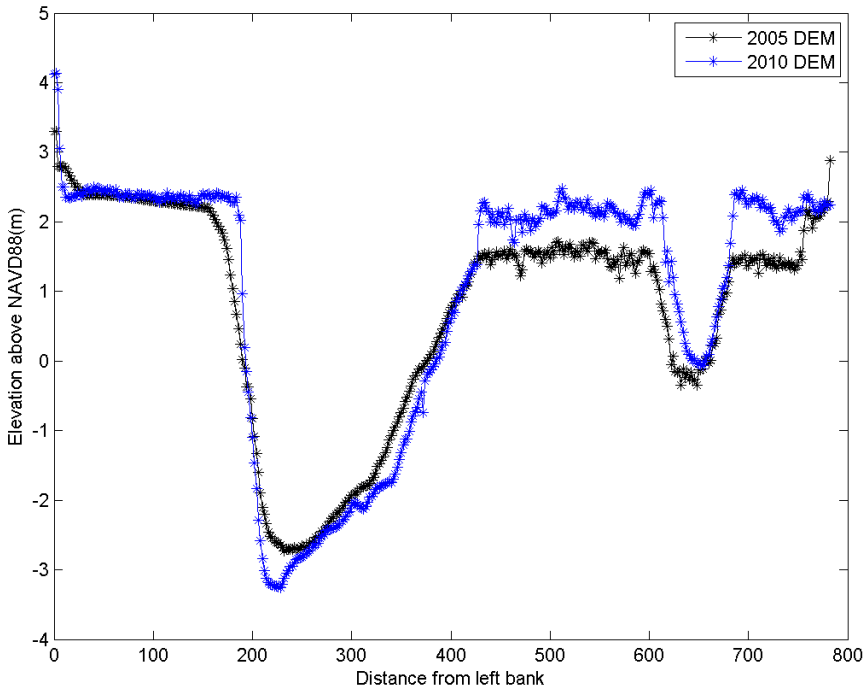

Figure 7.1-5 Change in the bathymetry at cross-section 3 from 2005 to 2010.

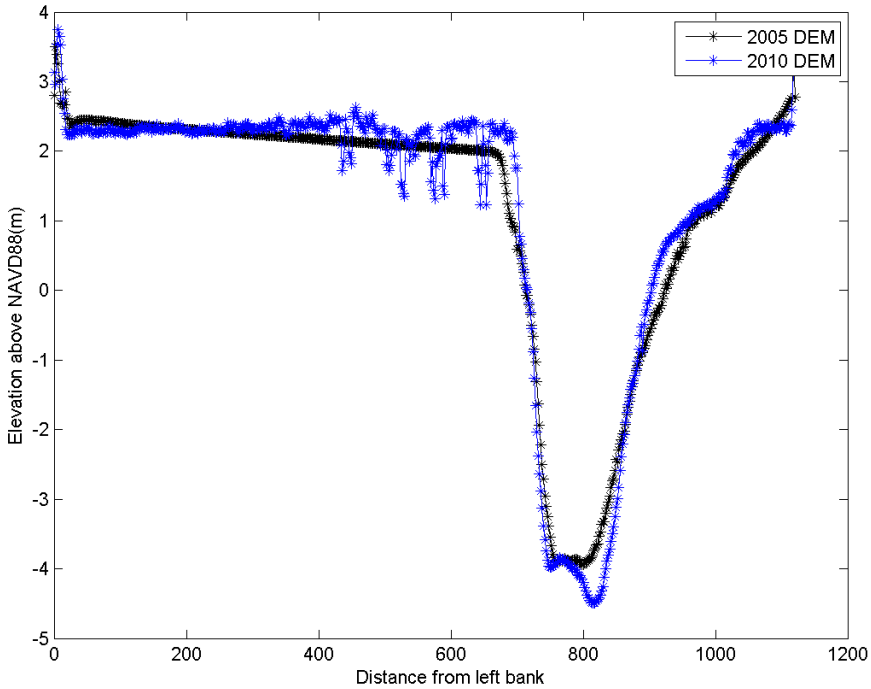

Figure 7.1-6 Change in the bathymetry at cross-section 4 from 2005 to 2010.

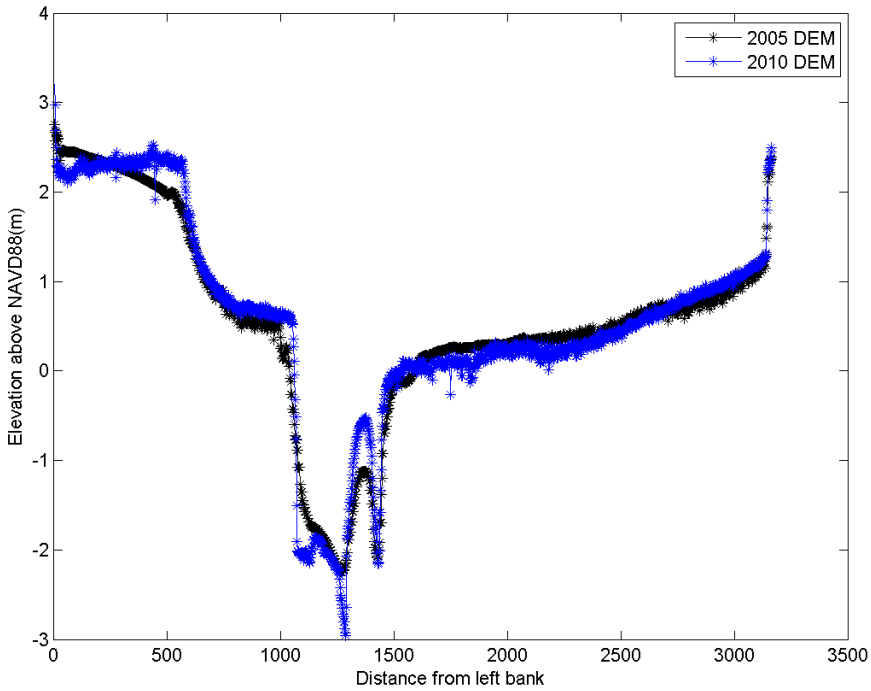

Figure 7.1-7 Change in the bathymetry at cross-section 5 from 2005 to 2010.

7.1.3 Evaluation of Bathymetric Change by Geomorphic Zone

Using the tidal datums calculated from the water-level data measured in 2011 at the NOAA Coyote Creek (9414575) tide station (Table 7.1-1), four "geomorphic zones" were defined. Figure 7.1-8 illustrates these four zones—Subtidal, Intertidal Mudflat, Marsh, and Upland—and the elevations used to define these zones. Figure 7.1-9 shows the geomorphic classification regions on the 2005 SFEI DEM.

Table 7.1-1 Tidal Datums for NOAA Coyote Creek station (9414575) calculated using 2011 water level observations.

Parameter	Value (m, NAVD88)
MHHW	2.33
MHW	2.13
MTL	1.06
MLW	-0.02
MLLW	-0.41

7.1.4 Masking

Multiple data sources, with varying degrees of coverage and accuracy, comprise the two continuous DEMs described in Section 7.1.1. In order to remain consistent in the cross-year comparisons, areas that showed artificial change due to known data biases or gaps in one of the data sets were masked out of the bathymetric change analysis. In particular, Mud Slough, the borrow ditch surrounding pond A21 (Figure 7.1-1), and the managed ponds were excluded from the comparisons. Mud Slough bathymetry was defined in the 2005 DEM from the 2005 bathymetric survey, but only LiDAR covers Mud Slough in 2010. Thus, only the elevation of the slough water surface over the subtidal channel was mapped in 2010. The 2005 DEM also has a hand-drawn representation of the A21 borrow ditch that is not present in the 2010 dataset. Thus, a comparison of these two datasets without applying a mask would show artificial accretion of both Mud Slough and the borrow ditch between 2005 and 2010. Elevations of the managed ponds in the LiDAR datasets represent the water surface, rather than the underlying bathymetry, so these ponds were also excluded from the comparisons.

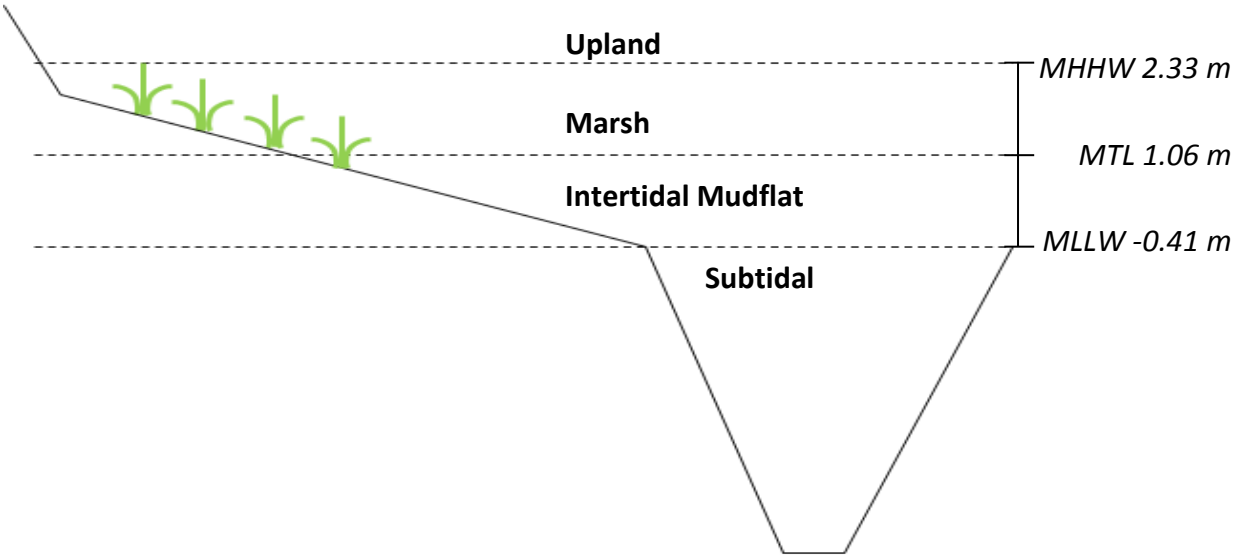

Figure 7.1-8 Classification of geomorphic zones by water levels.

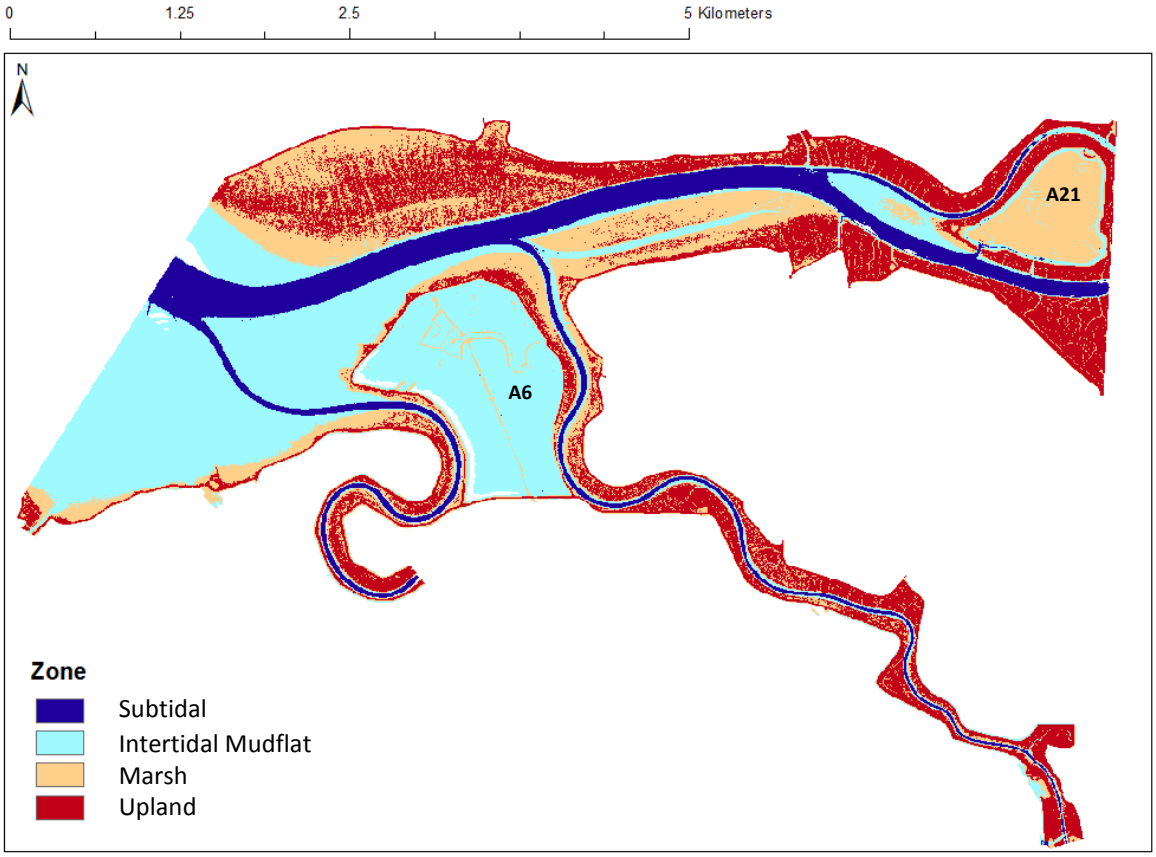

Figure 7.1-9 Geomorphic classification of the Alviso area based upon 2011 tidal datums at Coyote Creek.

7.1.5 Results

Two additional comparisons were made between the elevation maps at Alviso, approximately over the same time period, but using data from a range of sources. Figure 7.1-10 shows a map of change due to deposition or erosion between 2005 and 2010 comparing the mixed-source 2005 dataset to the 2010 LiDAR, as well as the change between 2004 and 2010 comparing LiDAR to LiDAR. Both of these three-dimensional analyses of the data show little change across the tidal flats, and aggradation of the high marsh areas, with similar rates and patterns of change between the two comparisons. Subtidal areas are incorporated into the 2005 and 2010 elevation maps, and the comparison between these two datasets also confirms the incision of Coyote Creek observed in the cross-section analysis. As previously mentioned, Mud Slough and the borrow ditch surrounding Alviso pond A21 have been masked out of these analyses, and the managed ponds were masked out of the 2004 to 2010 comparison. Areas which showed less-than about ±5 cm of change have also been masked out. Thus, the resulting figure shows a conservative estimate of marsh and channel evolution.

Changes measured from the two DEMs are also shown for three geomorphic zones—Subtidal, Intertidal Mudflat, and Marsh—as Figures 7.1-11 to 7.1-13. As with Figure 7.1-10, areas showing change of less-than about ±5 cm have been masked out. Figure 7.1-11 is useful for illustrating where Coyote Creek has scoured the most, as well as highlighting aggradation near the confluence with Guadalupe Slough. Figure 7.1-12 shows that almost no measurable change occurred within the intertidal mudflat areas, while Figure 7.1-13 highlights locations of aggradation on the marsh plain surface.

A third representation of the data is given as a plot of the average change, within a range of elevations, against the initial elevation in 2005. Figure 7.1-14 shows the mean calculated for each 10 cm interval between MLLW and MHHW measured at the Coyote Creek (9414575) station, as well as the standard deviation around the mean. Figures 7.1-15 to 7.1-17 show similar plots to Figure 7.1-14, but are broken out by geomorphic zone.

Comparison of bathymetric data in the subtidal (below MLLW) portions of Coyote Creek from 2005 to 2010 shows channel scour of up to 0.6 m in the Coyote Creek region over this period, with average channel scour on the order of 0.20 m. This result suggests that additional scour is likely to occur in the channel of Coyote Creek and adjacent sloughs as a result of the increase in tidal prism associated with the restoration of Ponds A9 through A15 and Pond A18. The magnitude of the expected channel scour resulting from these restoration efforts is investigated further in Section 7.3.

Comparison of elevation in intertidal mudflat areas (between MLLW and MTL) between Dumbarton Bridge and Calaveras Point show relatively little change between 2005 and 2010 (Figure 7.1-18 and Figure 7.1-19). Comparison of marsh areas (between MTL and MHHW) show some deposition (Figure 7.1-19), however definitive conclusions about the bathymetric change in marsh areas are more difficult to discern from the data comparison based on differences in the data sources available for marsh areas in 2005 and 2010.

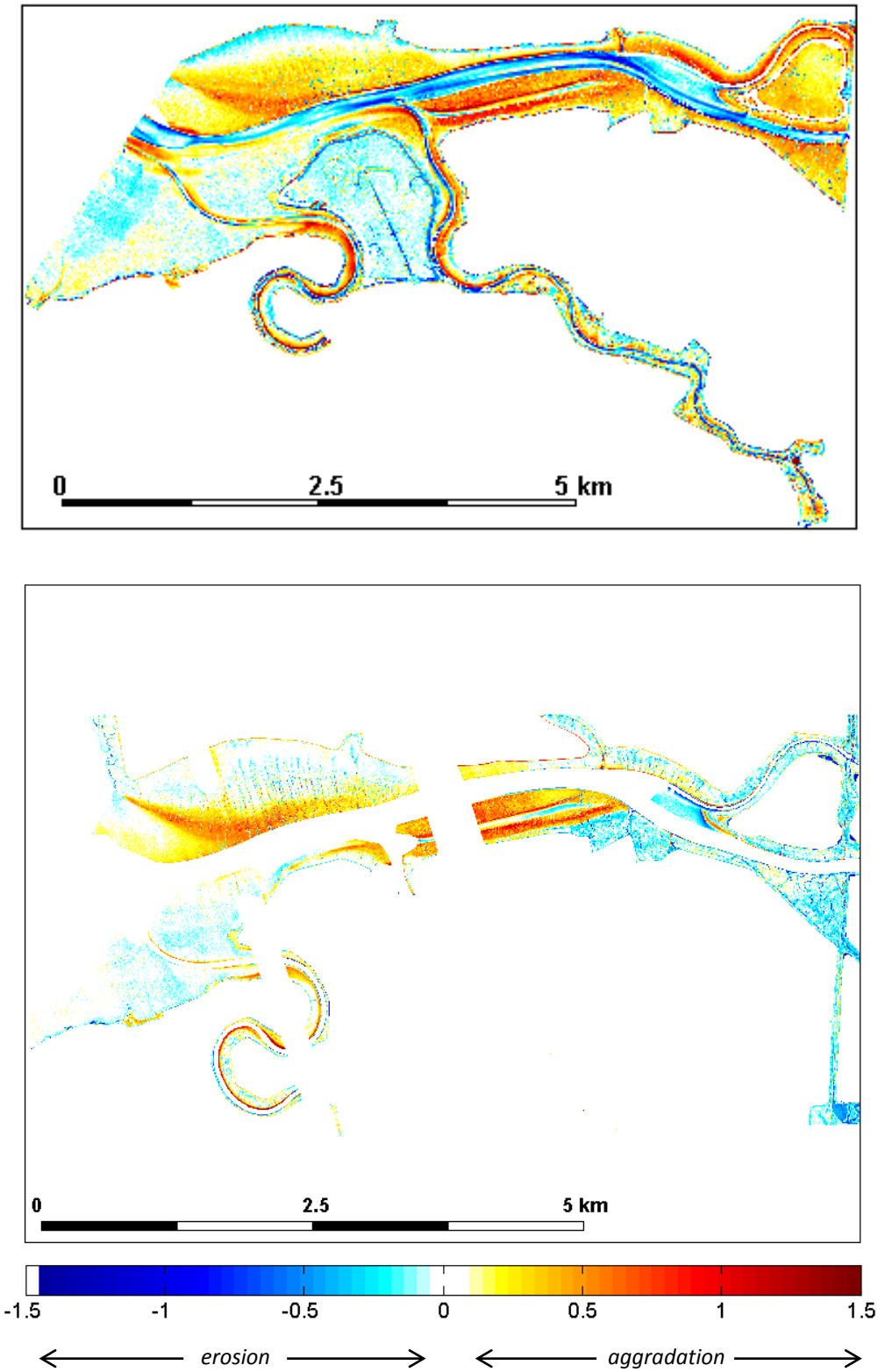

Figure 7.1-10 Change in elevation in Alviso region. Top panel shows the difference between the combined 2005 sonar and LiDAR dataset and the 2010 DEM. Bottom panel shows the difference between the 2004 and 2010 LiDAR surveys.

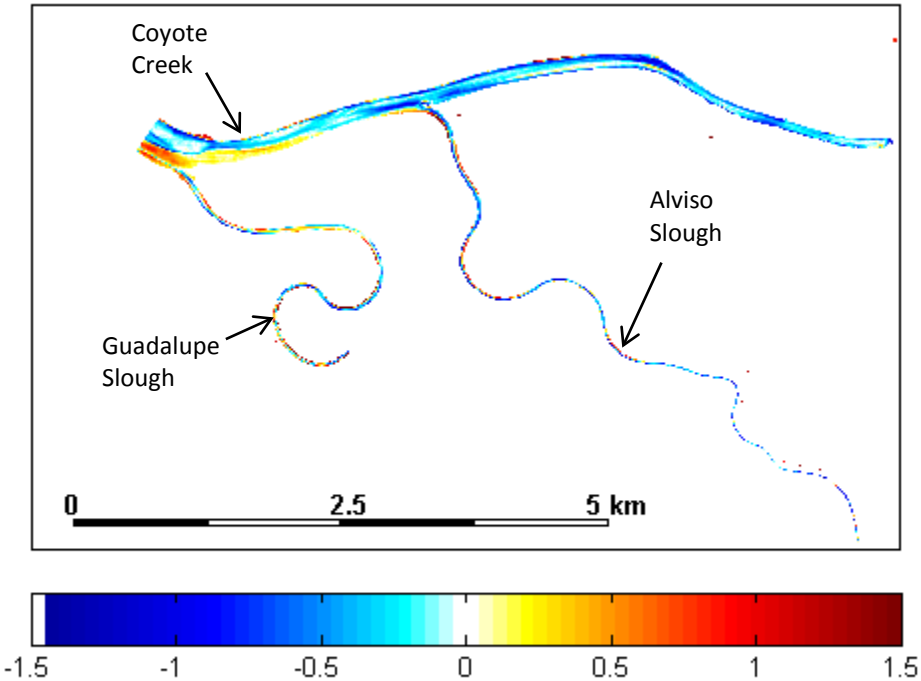

Figure 7.1-11 Subtidal change in elevation at Alviso from 2005 to 2010 from comparison of the combined 2005 sonar and LiDAR dataset and the 2010 DEM. The 2004 LiDAR data comparison is not shown here, since the dataset only covers areas above MLLW.

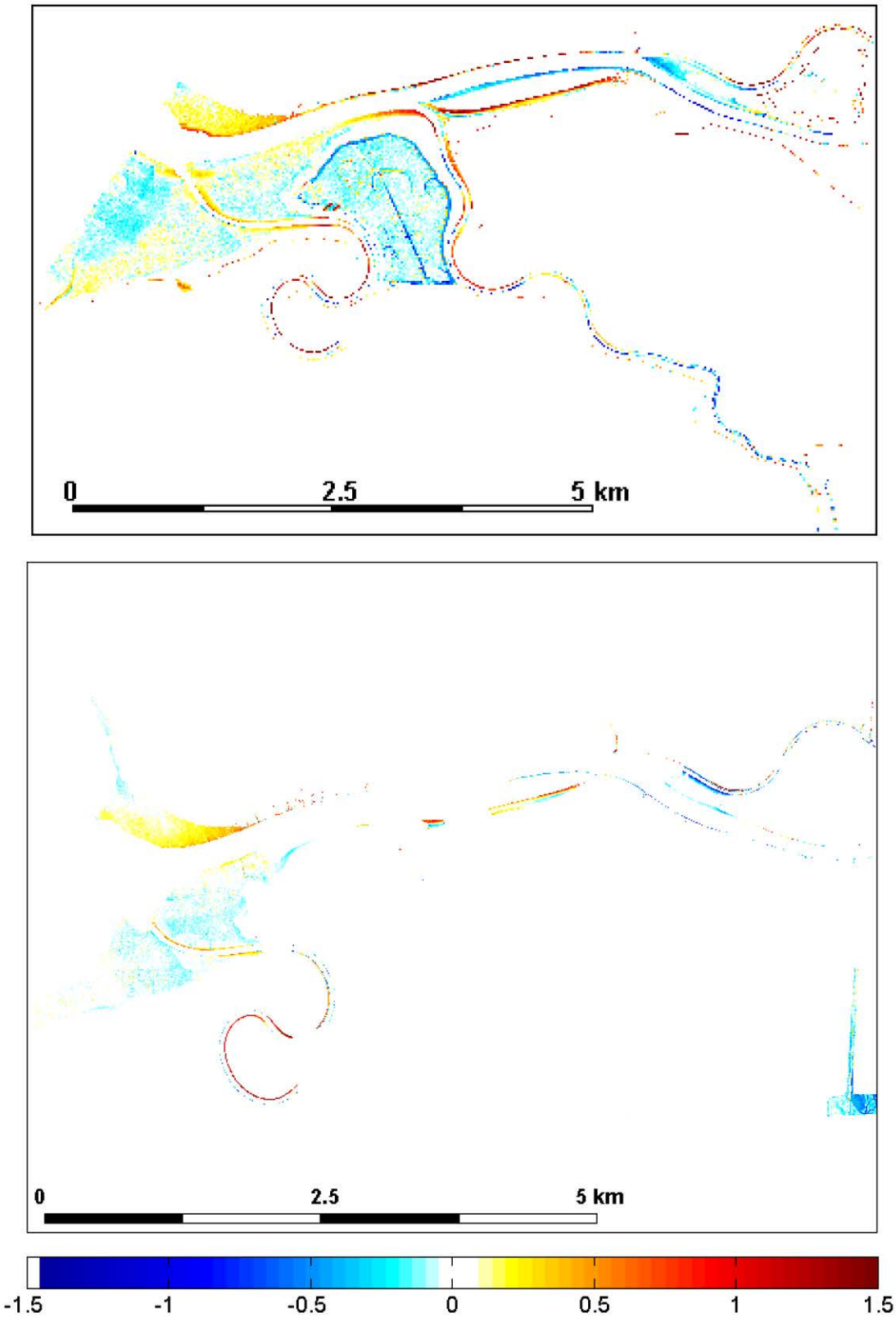

Figure 7.1-12 Intertidal mudflat change in elevation at Alviso from 2005 to 2010. Top panel shows the difference between the combined 2005 sonar and LiDAR dataset and the 2010 DEM. Bottom panel shows the difference between the 2004 and 2010 LiDAR surveys.

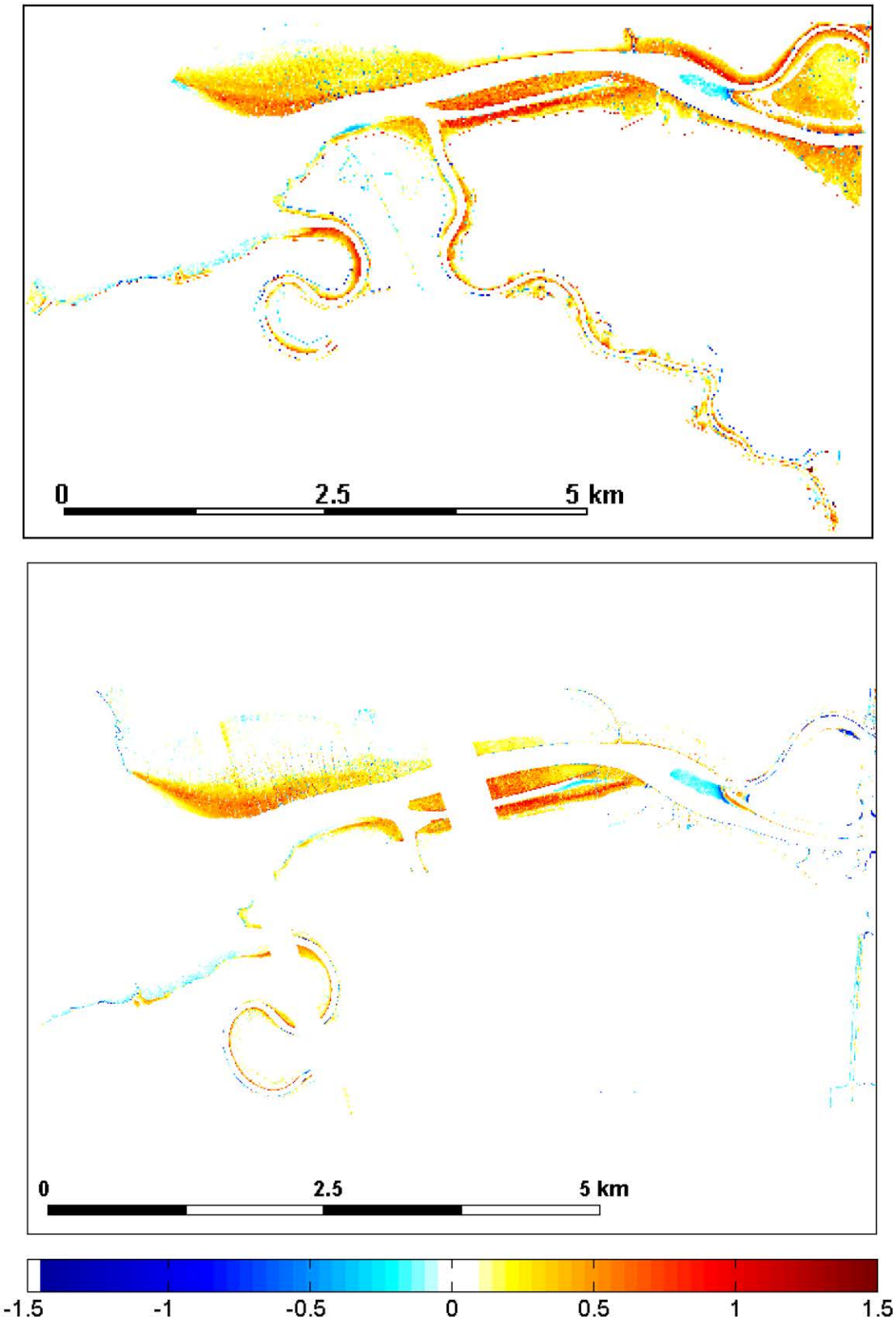

Figure 7.1-13 Marsh plain change in elevation at Alviso from 2005 to 2010. Top panel shows the difference between the combined 2005 sonar and LiDAR dataset and the 2010 DEM. Bottom panel shows the difference between the 2004 and 2010 LiDAR surveys.

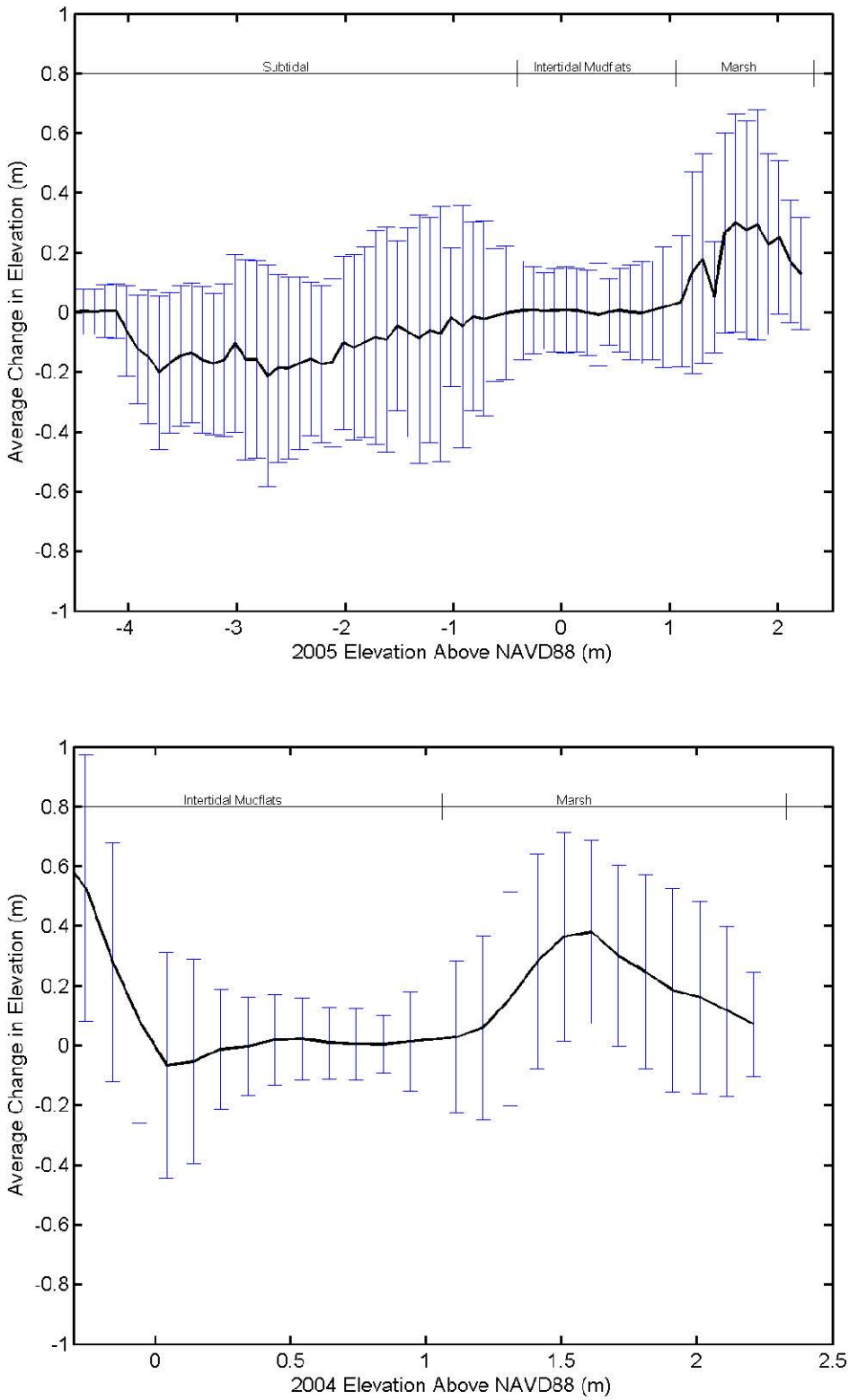

Figure 7.1-14 Average change in elevation with the standard deviation in each 10 cm bin against the initial elevation. Top panel shows change between the 2005 to the 2010 DEMs. Bottom panel shows change between the 2004 and 2010 LiDAR surveys.

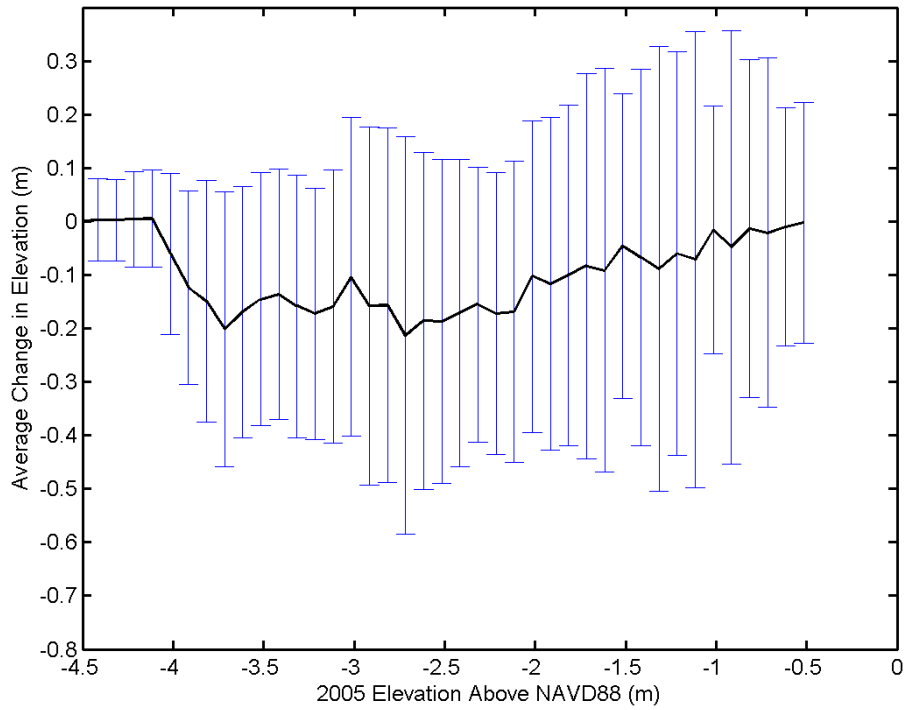

Figure 7.1-15 Average change in elevation with the standard deviation in each 10 cm bin between the 2005 to the 2010 DEMs, with the initial elevation in 2005, in the areas classified as Subtidal.

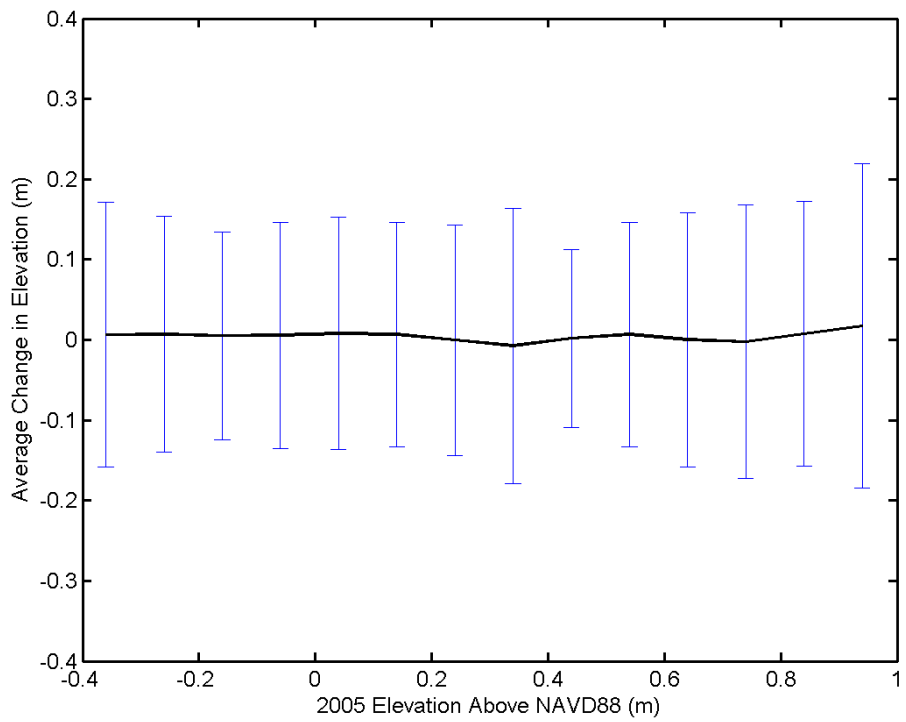

Figure 7.1-16 Average change in elevation with the standard deviation in each 10 cm bin between the 2005 to the 2010 DEMs, with the initial elevation in 2005, in the areas classified as Intertidal Mudflats.

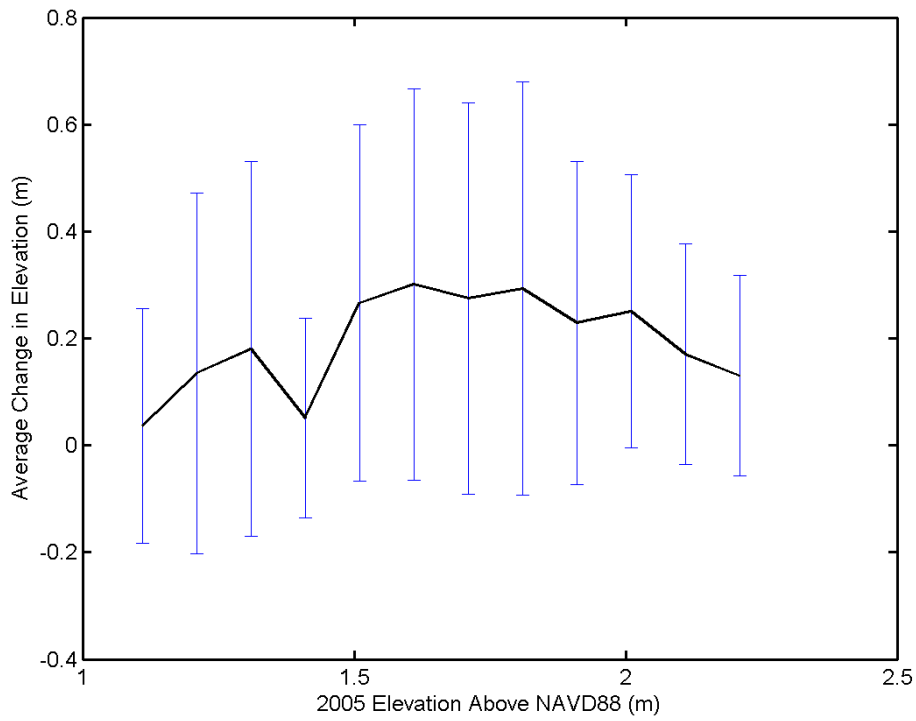

Figure 7.1-17 Average change in elevation from the 2005 to the 2010 DEMs, with the initial elevation in 2005, in the areas classified as Marsh.

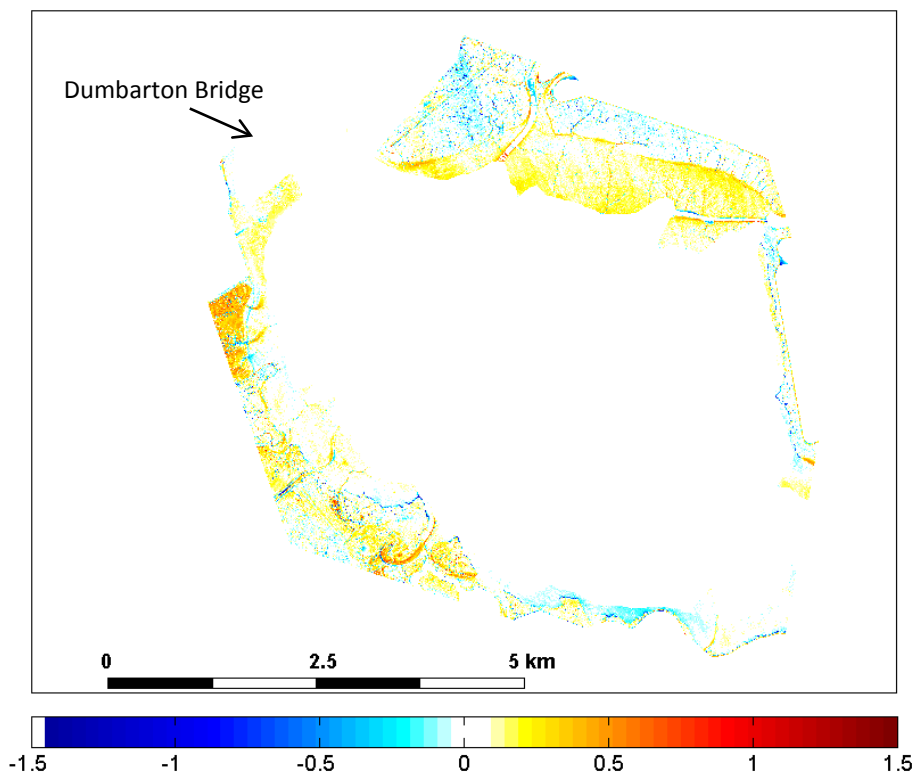

Figure 7.1-18 Change in elevation around the shoreline of South San Francisco Bay south of Dumbarton Bridge and north of Alviso between the 2004 and 2010 LiDAR surveys.

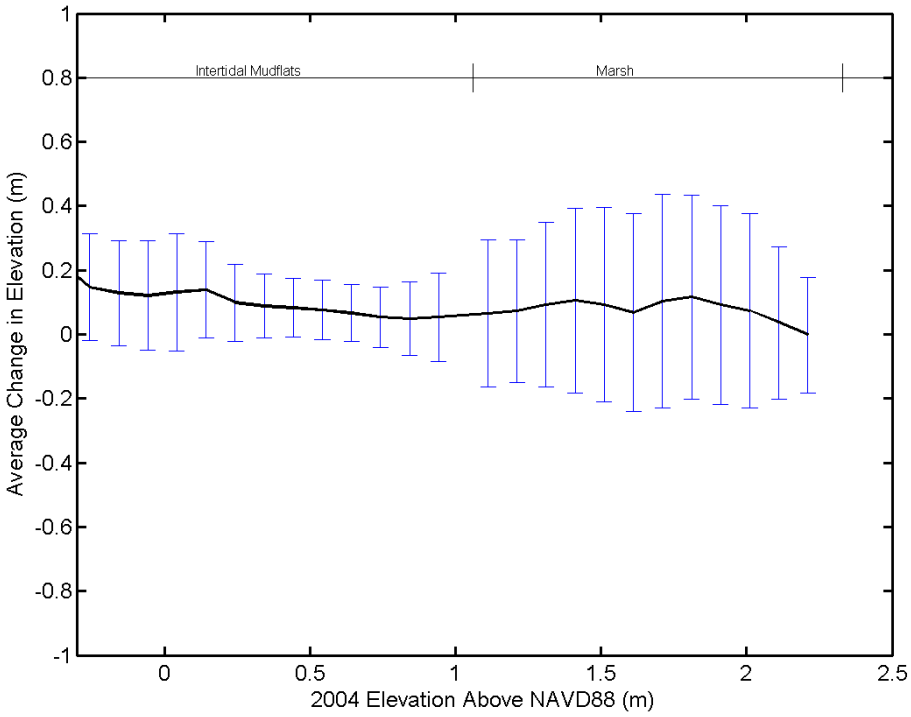

Figure 7.1-19 Average change in elevation around the shoreline of South San Francisco Bay between the 2004 and the 2010 LiDAR surveys against the initial elevation in 2004.

7.2 Evaluation of Deposition Patterns in Mudflat and Marsh Areas

Sediment deposition patterns in mudflat and marsh areas in the Coyote region were evaluated through a four week sediment transport simulation using the UnTRIM hydrodynamic model coupled to the SediMorph morphologic model. The model simulation spans a period when there was a large observed net sediment flux past Dumbarton Bridge into the Far South Bay. The predicted sediment deposition patterns in mudflat and marsh areas were evaluated to inform projections of morphologic change in mudflat and marsh areas for the development of Year 50 bathymetric conditions.

7.2.1 UnTRIM – SediMorph model coupling

The UnTRIM San Francisco Bay-Delta model has been coupled to the SediMorph seabed morphologic model to create a fully three-dimensional hydrodynamic and sediment transport modeling system (Bever and MacWilliams, 2012; MacWilliams et al., 2012, in prep). SediMorph is a morphologic model that calculates erosion, deposition, net sediment flux to/from the sea bed, the adjustment and tracking of sediment parameters in the seabed, and the change in seabed elevation due to sediment erosion and deposition. The physics modeled in SediMorph are described in detail by Malcherek (2001). A full description of the governing equations for the SediMorph model is presented by BAW (2005).

SediMorph simulates the transport of multiple sediment grain classes, each with different characteristics, such as settling velocity, critical shear stress, diameter, and density. SediMorph keeps track of multiple seabed sediment layers, each of which can be composed of different fractions of each sediment class. Erosion from a surface exchange layer, in this study equal to five times the maximum grain diameter on the seabed in any given cell, is calculated according to Partheniades (1965). The deposition flux is calculated by multiplying the suspended sediment concentration times the sediment settling velocity.

The UnTRIM and SediMorph models run concurrently on identical model grids and pass information between one another to create a fully three-dimensional hydrodynamic and sediment transport modeling framework. SediMorph uses the currents, waves, and suspended sediment concentration from UnTRIM to calculate the erosion and deposition fluxes, and then passes the net flux between the seabed and the water column back to UnTRIM for use in updating the suspended sediment concentration and adjusts the bed elevation to account for erosion and deposition within each grid cell. SediMorph then updates the fractions of each sediment class within the seabed. The suspended sediment advection, mixing, and settling, are calculated in UnTRIM, which incorporates the suspended sediment concentration in the equation of state following Warner et al. (2008). A complete description of the UnTRIM-SediMorph coupled modeling system and the application to San Francisco Bay is described in MacWilliams et al. (2012).

7.2.2 Far South San Francisco Bay Hydrodynamic and Sediment Simulation

The UnTRIM-SediMorph coupled modeling system was applied to the high-resolution portion of San Francisco Bay south of Dumbarton Bridge. A period spanning from January 12, 2009 through April 12, 2009 was simulated using the full model domain (Figure 3.4-2 and Figure 3.5-1) in order to save predicted water level and salinity at Dumbarton Bridge (Figure 4.1-1). A separate model simulation of Far South San Francisco Bay was then made using only the portion of the model grid south of Dumbarton Bridge (Figure 3.5-1). This simulation spans from March 15, 2009 through April 12, 2009, a period with a large observed net sediment input to the South Bay past Dumbarton Bridge (Figure 7.2-1).

In the Far South San Francisco Bay simulation the open boundary was located at Dumbarton Bridge, and the predicted water level and salinity at Dumbarton Bridge from the full-bay simulation together with the observed sediment concentration at Dumbarton Bridge were applied at the open boundary in order to simulate sediment deposition in the Far South Bay. Suspended sediment concentration at the open boundary was specified based on observed cross sectional average concentrations measured by the USGS (Greg Shellenbarger, pers. comm., 2012). Setting a suspended sediment concentration on the open boundary allowed sediment to enter the model domain on an incoming tide. However, sediment exiting the model domain on ebb tide was lost from the model domain. Freshwater input to the Far South Bay for this simulation was identical to that described in Section 3.6. However, sediment input from the South Bay tributaries was neglected in this simulation because, based on the available data, sediment input from the South Bay tributaries represented only 0.15% of the sediment flux from the open boundary over the simulated time-period.

The suspended sediment concentration at Dumbarton Bridge was partitioned into three sediment classes, representing slit, flocculated material, and sand (Table 7.2-1). Observations of the size distribution of suspended sediment within the Far South Bay were not available, so the suspended sediment concentration was partitioned into the three sediment grain classes based on the predicted suspended sediment concentrations at Dumbarton Bridge from full bay model runs which incorporated a realistic initial sediment bed and current and wave induced sediment resuspension and transport (Bever and MacWilliams, 2012). In this simulation, the time-averaged partitioning of the three classes in suspension at Dumbarton Bridge was 76, 23.5, and 0.5% silt, flocs, and sand, respectively. For the Far South San Francisco Bay simulation, the suspended sediment concentration set at the model open boundary was partitioned into the three sediment classes using these percentages.

The model simulation did not use an initial sediment bed to allow for the direct tracking and analysis of the sediment entering the model domain at Dumbarton Bridge, however all sediment that entered the domain was subject to erosion and deposition throughout the simulation. Sediment entering the model domain through the open boundary is transported throughout the Far South Bay by the modeled currents. Sediment was deposited on the seabed as it settled out of the water column. Upon settling a porosity of 0.85 was used to determine the sediment depositional thickness. This porosity was at the high end of porosity values reported for the San Francisco Bay in Caffrey (1995), because the simulated sediment

deposition was assumed to be unconsolidated over the course of this short model run. Once the seabed shear stress exceeded the critical shear stress of a sediment grain class the sediment began to erode and underwent further transport throughout the Bay. The sediment undergoes depositional and erosional cycles with the tidal current speeds and ultimately started accumulating in regions favoring sediment deposition, with less deposition in regions of higher current speeds.

The predicted cumulative sediment flux into the Far South Bay was compared to the observed cumulative sediment flux at Dumbarton Bridge. The simulation approach specified the water level and sediment concentration at the model open boundary at Dumbarton Bridge, but not the resulting sediment flux which is the cumulative summation of sediment entering the model domain on flood tide and leaving the model domain during ebb tide. Figure 7.2-1 shows the observed and predicted cumulative sediment flux past Dumbarton Bridge for three water years. In this figure, the predicted cumulative sediment flux at the start of the model simulation was set to be equal to the observed cumulative sediment flux at the time that the simulation started in order to allow for direct comparison during the simulation period. Figure 7.2-2 shows the observed and predicted cumulative sediment flux into the far South Bay over the simulation period. In this figure, the observed and predicted cumulative sediment fluxes were set to 0 at the start of the model simulation period. Figure 7.2-3 shows the observed and predicted instantaneous and tidally-averaged sediment flux past Dumbarton Bridge into the far South Bay, as well as the cross-correlation statistics described in Section 4.1. The predicted sediment flux shows a similar pattern to the observed sediment flux, with relatively small sediment fluxes during the first week of the simulation and the largest sediment fluxes during the final week of the simulation. For this period, the value of the coefficient of determination between the observed and predicted sediment flux is 0.820, and the model skill value is 0.943. In general, the Far South San Francisco Bay simulation reproduced the net sediment flux past Dumbarton Bridge that was calculated based on field observations by the USGS (Figures 7.2-1 through 7.2-3) indicating that the model is accurately representing the net transport of sediment into the Far South Bay during this period.

Table 7.2-1. Sediment grain class parameters used in the model simulation.

Sediment class	Settling Velocity (mm s^{-1})	Critical Shear Stress (Pa)	Diameter (µm)	Density (kg m^{-3})	Erosion Rate Parameter (kg m^{-2} s^{-1})
Silt	0.038	0.022	7.8	2650	$5x10^{-5}$
Flocculated Silt and Clay	0.9	0.1	125	1300	$5x10^{-5}$
Sand	2	0.094	62.5	2650	$5x10^{-5}$

7.2.3 Results of Sediment Deposition Simulations

In order to investigate spatial patterns in sediment deposition, the model domain was subdivided into subtidal, intertidal and mudflat, marsh and upland morphological zones based on the seabed elevation, following the approach described in Section 7.1.3. Only model grid cells that were wet during the simulation were considered in the analysis (Figure 7.2-4). The

model predicted more sediment deposition in the shallow portions of the model domain than in the deeper channels. The greatest depositional thicknesses were above about -1.5 m NAVD88 with little sediment deposition below -1.5 m NAVD88 (Figure 7.2-5). Most of the predicted sediment deposition, and the overall thickest sediment deposits, occurred in the intertidal mudflat and marsh depth ranges.

The depositional pattern of increasing sediment deposition out of the channels is highlighted in 2D spatial plots of sediment depositional thicknesses (Figure 7.2-6). Separating the spatial sediment deposition by geomorphic classification further shows the lack of sediment deposition in the subtidal classification (Figure 7.2-7) compared to the intertidal (Figure 7.2-8) and marsh (Figure 7.2-9) elevation ranges. Other than right near the open boundary the subtidal regions show very little sediment deposition. Mudflat and marsh regions, however, show sediment deposition throughout the model domain, albeit decreasing thicknesses at the eastern side of the model domain at the farthest distance from the open boundary and the sediment source.

The modeled sediment deposition patterns compare favorably with the historic bathymetric changes derived from comparing subsequent bathymetric and LiDAR surveys presented in Section 7.1. As two examples, both the observed historic change (Figure 7.1-13) and the model (Figure 7.2-9) show sediment deposition on the north side of Coyote Creek near Calaveras Point and on the South side of Coyote Creek north of Ponds A9 (see Figure 7.1-1 for locations). Additionally, in the regions of Coyote Creek which have been erosional since the breaching of the Island ponds (Figures 7.1-10) the model predicts almost no sediment deposition (Figure 7.2-7). The potential for further scour in these regions is evaluated in Section 7.3.

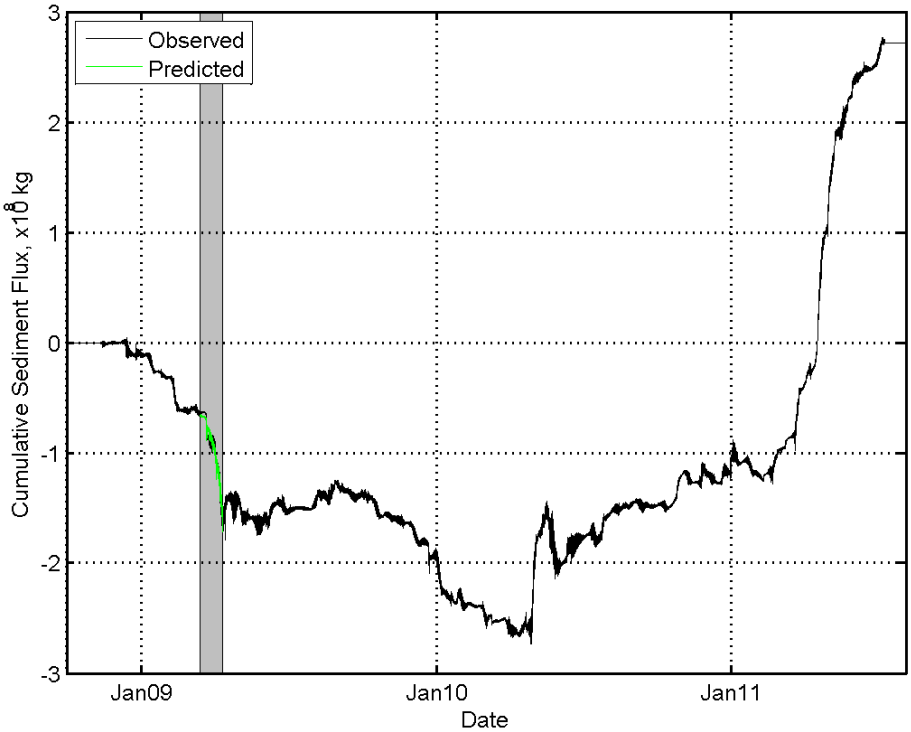

Figure 7.2-1. Observed and predicted cumulative sediment flux past Dumbarton Bridge. The shaded area highlights the simulation period. A negative sediment flux is toward the south into the Far South Bay.

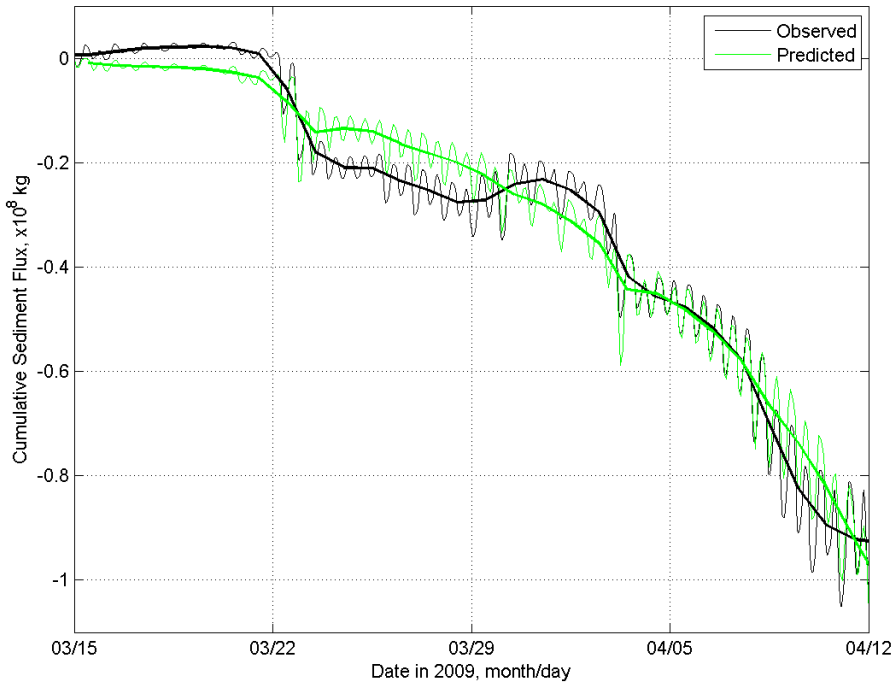

Figure 7.2-2 Observed and predicted cumulative sediment flux into the far South Bay over the simulation period. A negative sediment flux is toward the south into the Far South Bay. The thick lines show the daily averaged cumulative sediment flux.

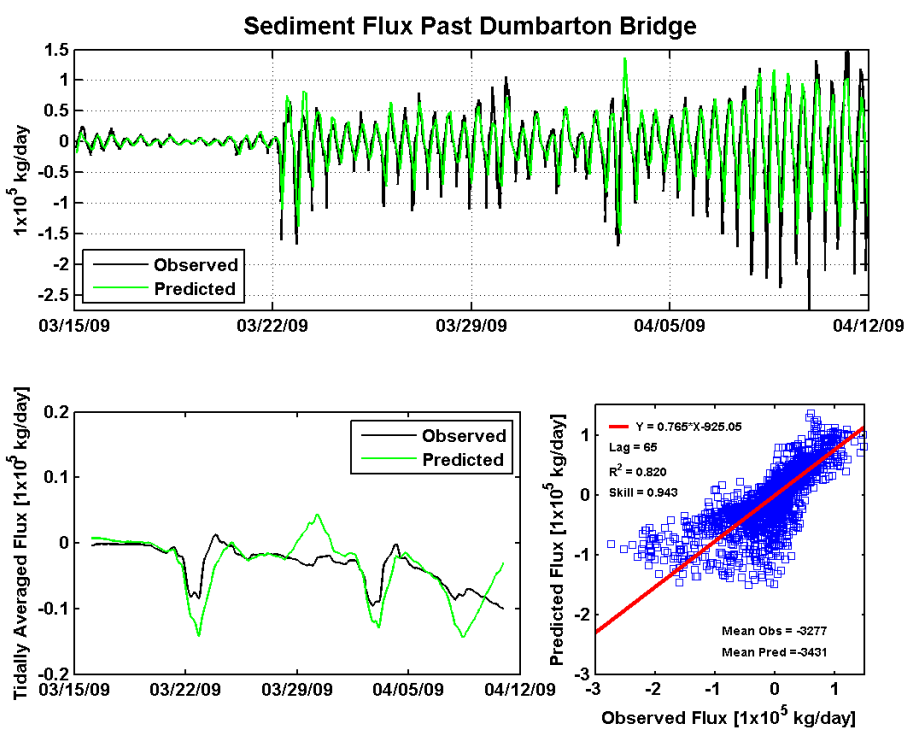

Figure 7.2-3 Observed and predicted sediment flux past Dumbarton Bridge into the far South Bay over the 2009 sediment simulation period.

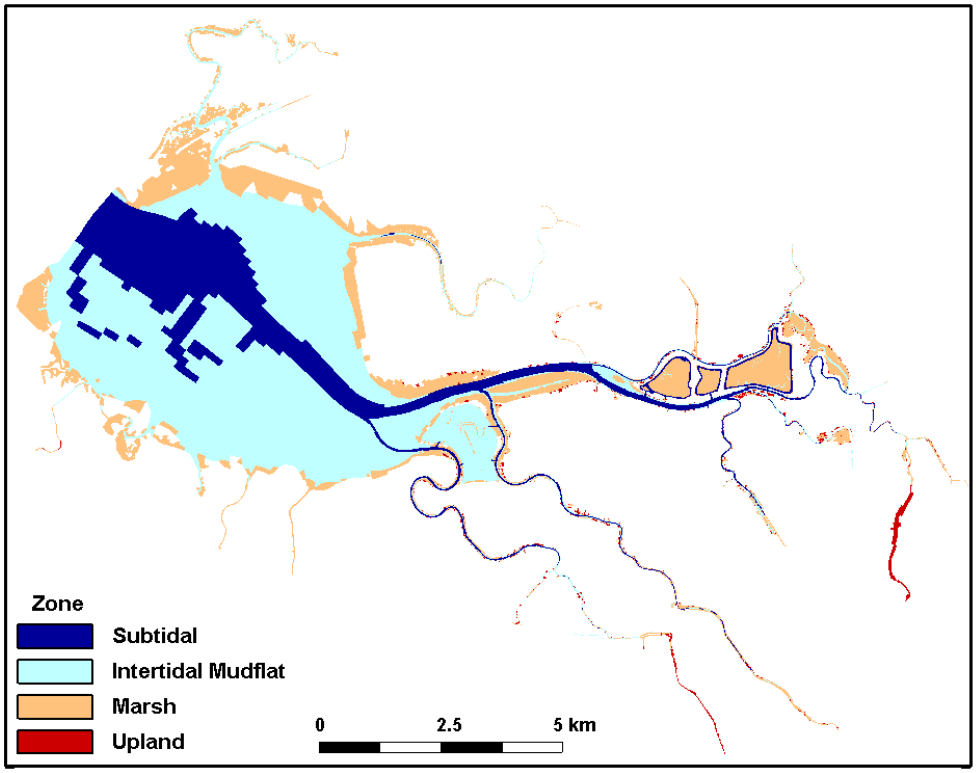

Figure 7.2-4. The geomorphic classification of each grid cell in the model simulation. Only grid cells that were wet during the simulation were considered.

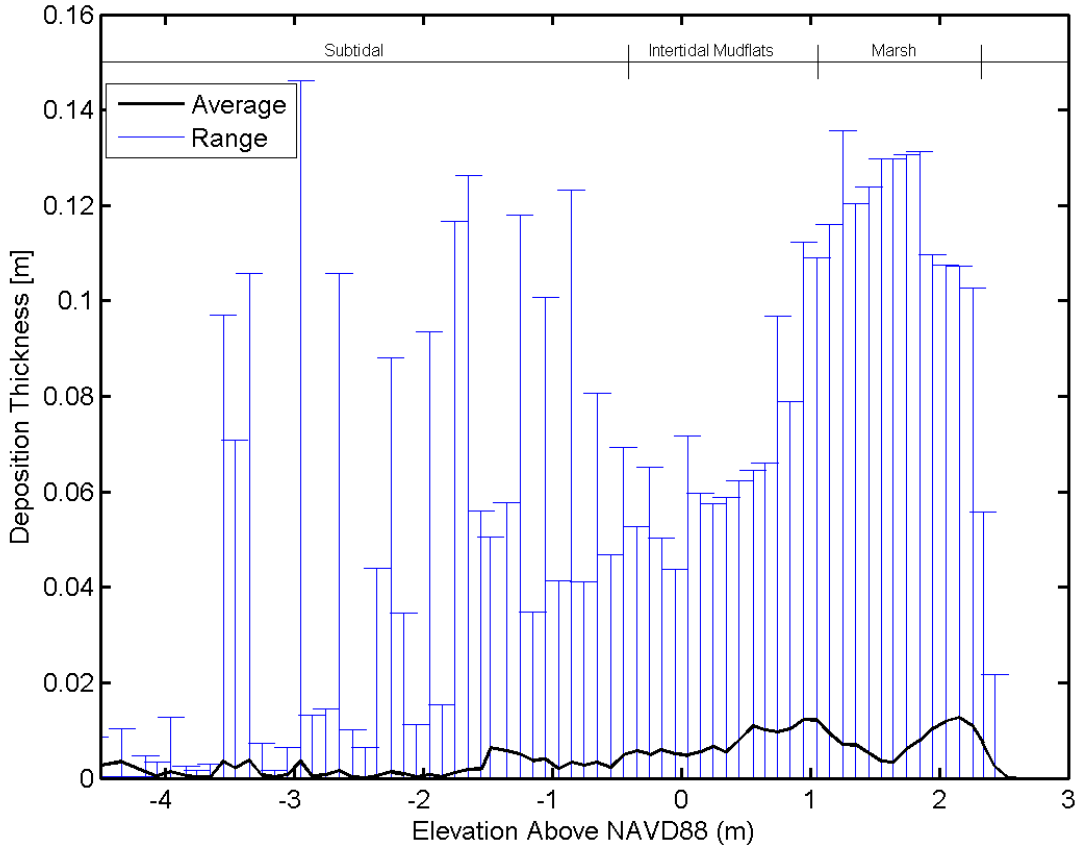

Figure 7.2-5. Sediment deposition thickness as a function of elevation. The black line shows the average seabed elevation change for all grid cells within the 10 cm depth bins and the blue bars show the maximum and minimum deposition thickness within each bin.

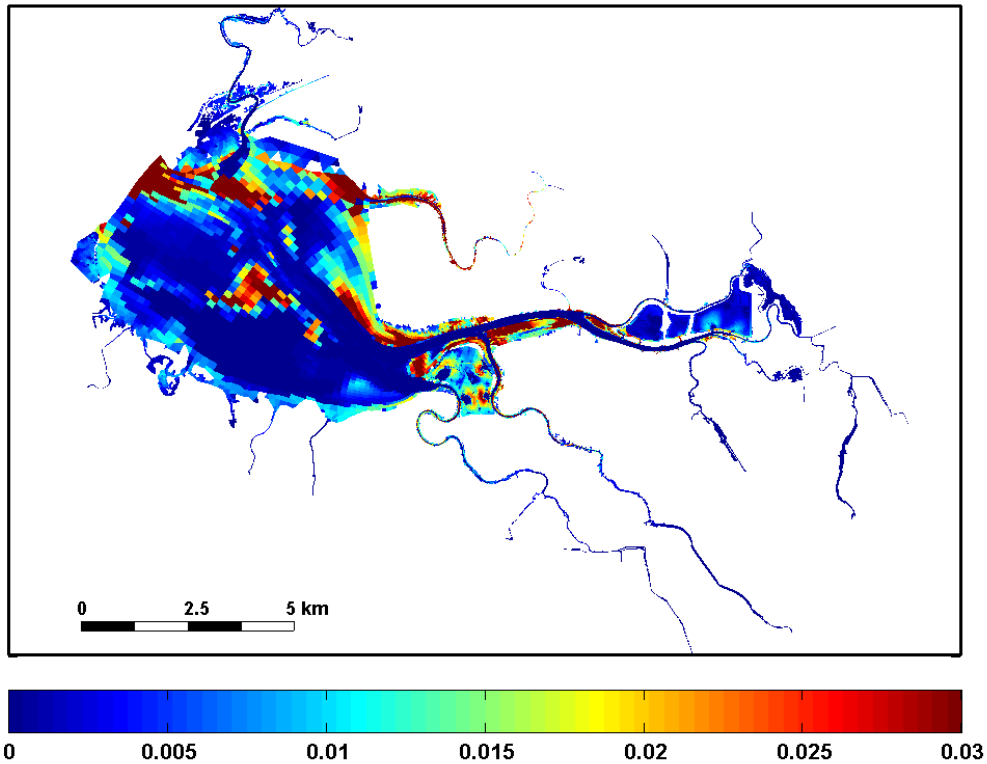

Figure 7.2-6. Sediment depositional thicknesses in meters at the end of the four week simulation.

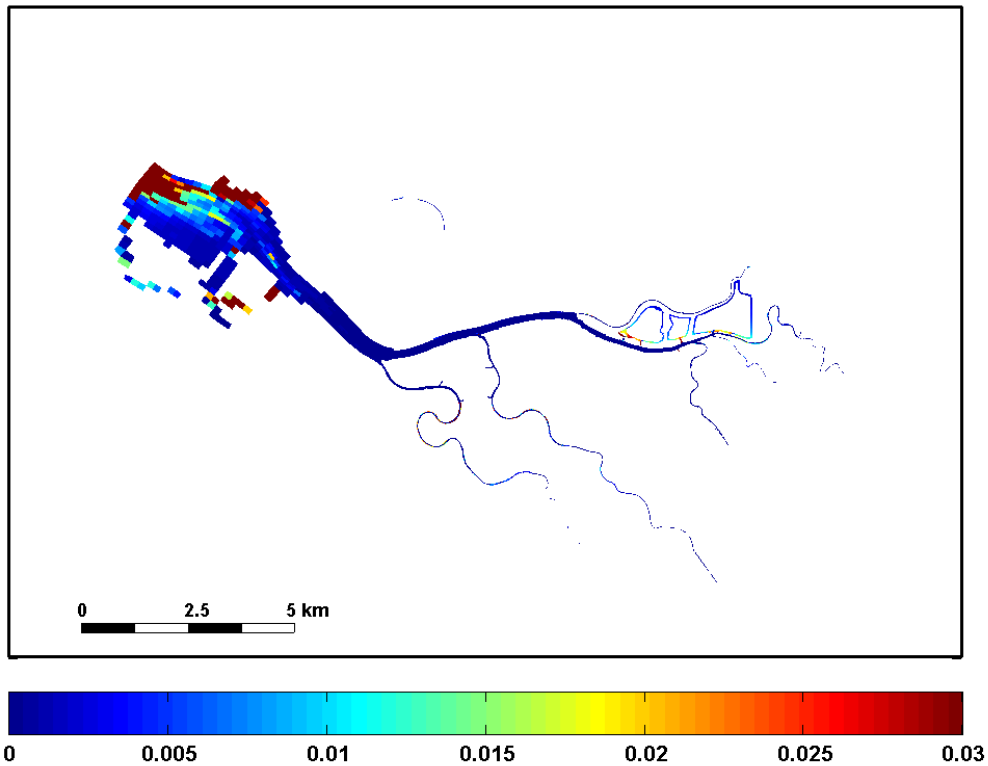

Figure 7.2-7. Sediment depositional thicknesses in meters for the subtidal geomorphic classification.

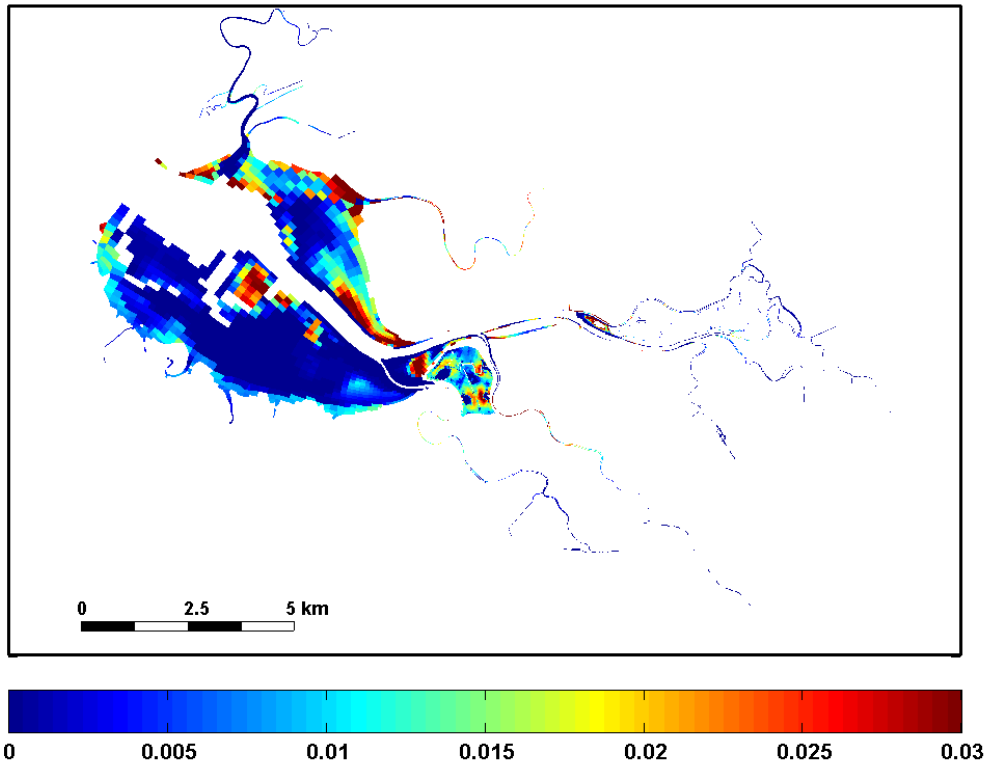

Figure 7.2-8. Sediment depositional thicknesses in meters for the intertidal and mudflat geomorphic classification.

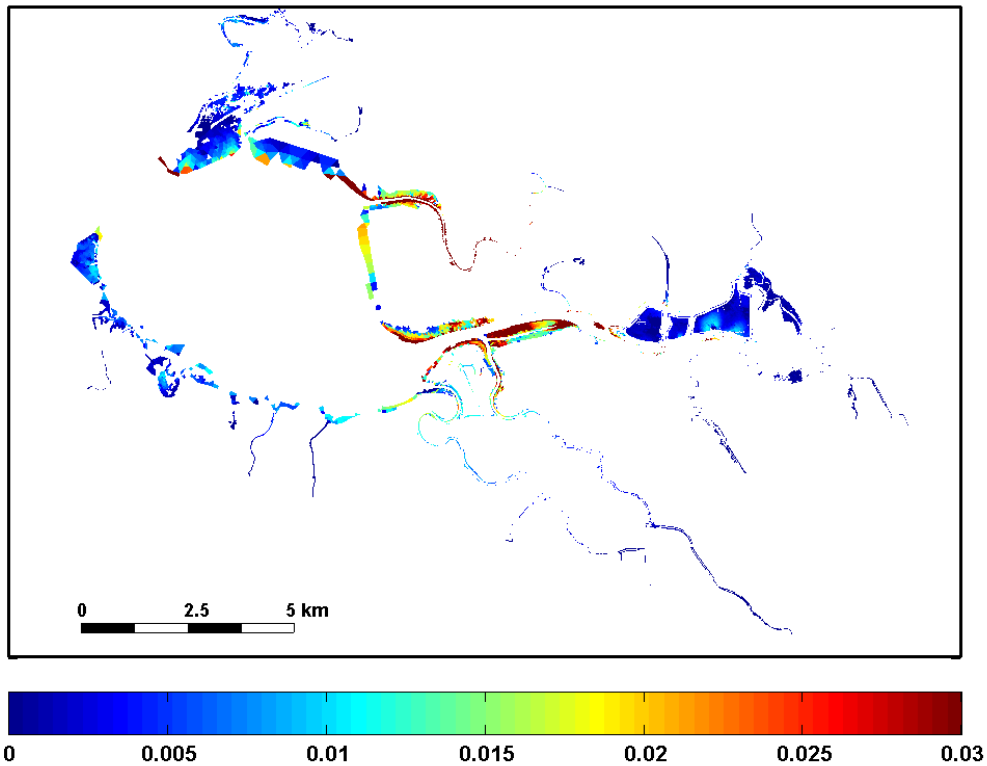

Figure 7.2-9. Sediment depositional thicknesses in meters for the marsh geomorphic classification.

7.3 Evaluation of the Potential for Channel Scour Following Pond Restoration

As part of the South Bay Salt Pond Initial Stewardship Plan, Gross and Schaaf & Wheeler (2003) evaluated the potential for scour in Coyote Creek following the restoration of the three island ponds (Pond A19, Pond A20, and Pond A21) to tidal action. Their analysis evaluated RMS velocity in Coyote Creek (Figure 7.3-1) and cross-sectional averaged velocity at the Railroad Crossing on Coyote Creek between Pond A20 and A21 (Figure 7.3-2). Based on the increase in cross-sectional averaged velocity due to the increased tidal prism of the restored ponds, Gross and Schaaf & Wheeler (2003) estimated the increase in cross-sectional area during peak flood tide velocity (Figure 7.3-3) and peak ebb tide velocity (Figure 7.3-4) necessary to reduce the cross-sectional average velocity following the pond restoration to be equal to the cross-sectional averaged velocity under the baseline conditions. This approach predicted on the order of 0.6 to 0.8 m (2 to 2.5 ft) of scour could occur in Coyote Creek following the restoration of the three island ponds to tidal action. This estimate is similar to the observed magnitude of scour which occurred in Coyote Creek (Figure 7.1-4). Additionally, the region in which the RMS velocity was predicted to increase (Figure 7.3-1) is similar to the region where scour was observed (Figure 7.1-10, top panel) based on a comparison of the 2005 and 2010 bathymetric surveys of Coyote Creek. This suggests that the potential for scour can be reasonably predicted through an analysis of regions where velocity or bed shear stress is likely to increase due to increases in tidal prism following restoration.

The magnitude of the expected channel scour resulting from the restoration of Ponds A9 through A15 and Pond A18 was investigated through simulations of velocity and bed shear stress under existing conditions and under future conditions with sea level rise (SLR) and projected Year 50 pond bathymetry. Using a similar approach as that used by Gross and Schaaf & Wheeler (2003), the predicted scour was estimated by assuming that the existing channels are in equilibrium with the existing tidal prism, and allowing for scour under future with project conditions and SLR when the resulting daily RMS shear stress is higher than the peak existing shear stress.

Rather than predicting scour at specific cross-sections (i.e., Gross and Schaaf & Wheeler, 2003), the goal of this study was to predict the spatial distribution and magnitude of scour that could result from the combined effects of the restoration of Ponds A9 through A15 and Pond A18, and from sea level rise. As a result, an iterative approach was developed to allow for scouring until the daily RMS shear stress under future conditions, with pond restoration and sea level rise, was reduced to the daily RMS shear stress under existing conditions. First, the existing conditions were simulated for a thirty day period. The existing conditions assumed that the island ponds, which were breached in 2006, were open to tidal action, but that Pond A6, which was breached in December 2010, was not yet open to tidal action. The reason for excluding A6 from the existing conditions was that the bathymetry used in the region surrounding A6 was collected in 2010 prior to the breaching of A6, so it was more reasonable to assume that the bathymetry was in equilibrium with pre-breach conditions and that some scour in the channels around A6 would likely to occur between 2010 and 2067 in response to the restoration of Pond A6 to tidal action.

On each of the thirty days of the scour analysis simulation, the daily RMS shear stress under existing conditions was saved for comparison with the daily RMS shear stress under future conditions. Next, the future conditions with 0.649 m (2.13 ft) of SLR were simulated assuming that A6 was opened to tidal action and Ponds A9 through A15 and Pond A18 were restored with the bathymetry developed for screening Alternative 2 (Figure 5.1-2). Additionally it was assumed that 50 cm (1.64 ft) of additional accretion occurred in Pond A6 and Ponds A19-21 between 2010 and 2067. This accretion rate was estimated based on average rate of accretion in the restored ponds (Figure 5.1-2) that was estimated by ESA-PWA (2012).

The daily RMS shear stress in the Coyote Creek region on the first day of the scour analysis under existing conditions (Figure 7.3-5) and future with project conditions which include sea level rise show a significant increase in daily RMS shear stress in some regions of Coyote Creek (Figure 7.3-6). In grid cells where the daily RMS shear stress under future conditions was greater than 0.1 N/m^2, the channel bed was allowed to scour based on the magnitude of the increase in daily RMS shear stress relative to existing conditions. In grid cells where the future daily RMS shear stress was less than 0.1 N/m^2 or the increase in daily RMS shear stress relative to existing conditions was less than 0.05 N/m^2, it was assumed that no scour occurred on that step in those cells. Within each grid cell, the scour for each iterative step (day) was specified as 0.025 m, 0.05 m, and 0.10 m for daily RMS shear stress increases of 0.05 N/m^2, 0.5 N/m^2, and 1.0 N/m^2, respectively. These scour amounts are greater than would be expected in a single day, however the goal of the approach was to develop the equilibrium end-state of the scour rather than the time that the scour would take. At the end of each simulation day, the scour in each grid cell was calculated, and the bathymetry was adjusted prior to the start of the next day. This process was repeated for 29 additional days, spanning two-spring-neap cycles, with a maximum of 2 m of scour allowed in each grid cell. The resulting scour at the completion of this analysis period is shown in Figure 7.3-7.

The results of the scour analysis (Figure 7.3-7) indicate that significant scour of up to 2 m or more is expected in Coyote Creek between Calaveras Point and Pond A9, primarily as the result of restoring Ponds A9 through A15 to tidal action. Some scour is also predicted between the mouth of Guadalupe Slough and the south west breach of A6, primarily resulting from the restoration of A6 to tidal action in December 2010. Between 0.4 and 1.6 m of additional scour is predicted in Coyote Creek between the mouth of Mud Slough and Pond A18. Some scour is also predicted in the channels of Mud Slough, Mowry Slough, and Newark Slough. This scour is likely the result of increased tidal prism of these sloughs due to sea level rise. The patterns and magnitude of scour predicted through this analysis are consistent with the scour observed following the breach of the Island Ponds (Figure 7.1-10, top panel).

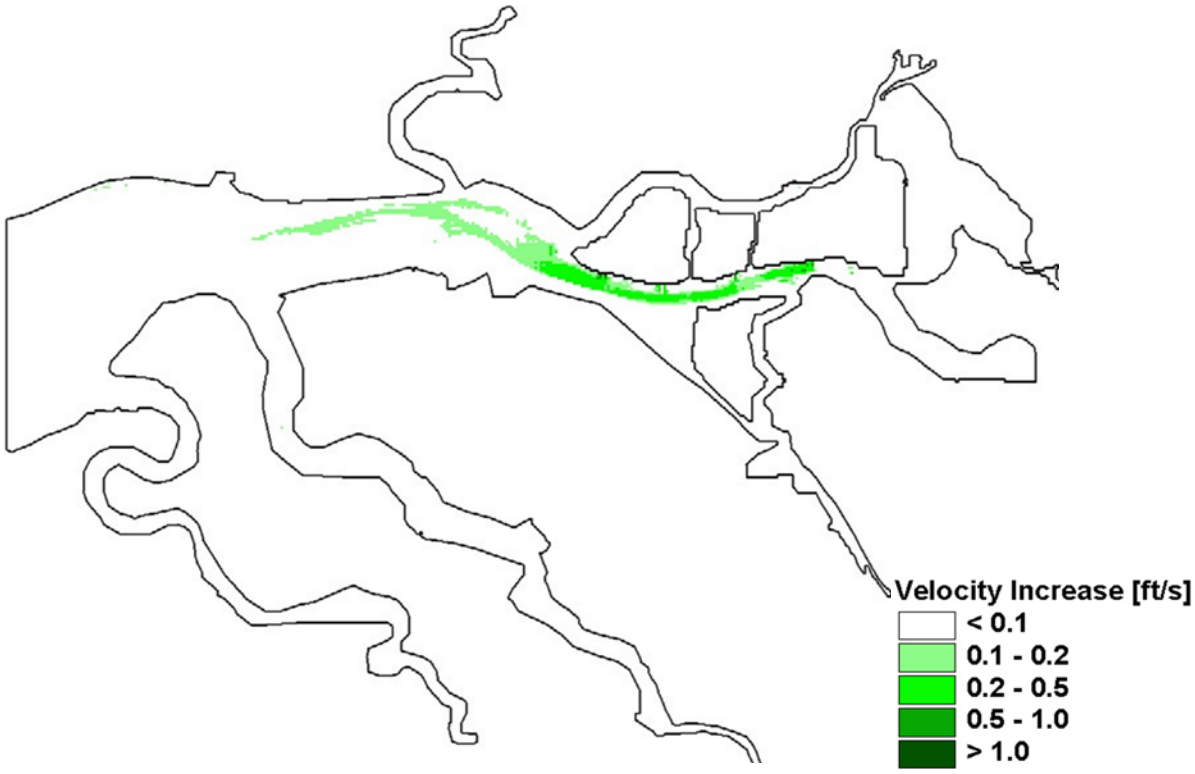

Figure 7.3-1 Predicted increase in RMS velocity resulting from restoration of Ponds A19-A21 to tidal action (from Gross and Schaaf & Wheeler, 2003).

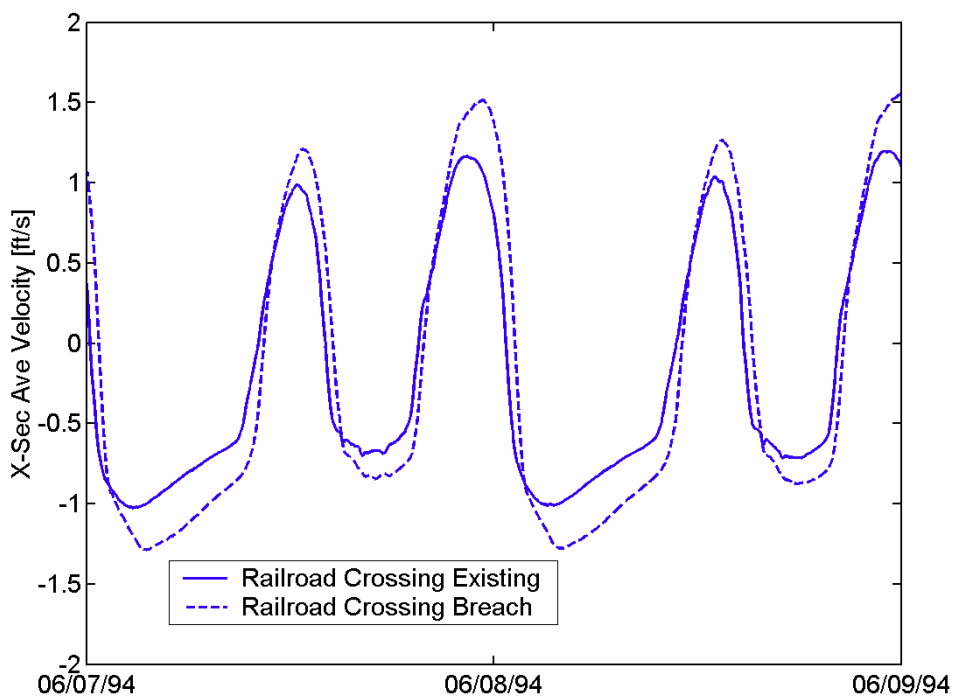

Figure 7.3-2 Cross-sectional average velocity at Railroad Bridge over Coyote Creek between Pond A20 and A21 for existing (pre-restoration) and Pond A19-21 restoration (breach) conditions (from Gross and Schaaf & Wheeler, 2003).

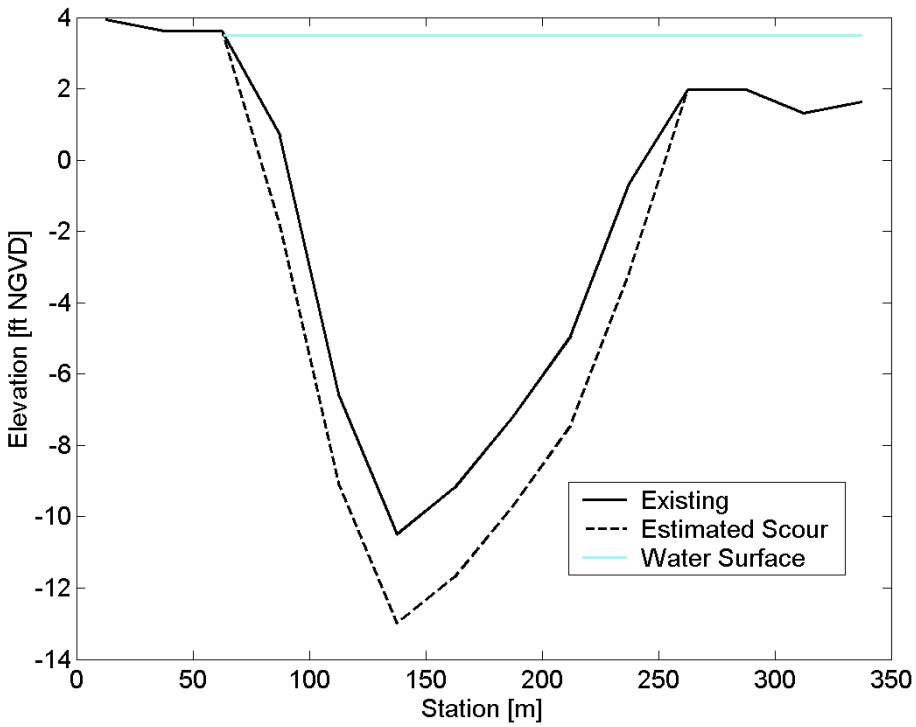

Figure 7.3-3 Existing cross-section geometry and estimated scour at the Railroad Bridge over Coyote Creek between Pond A20 and A21 based on peak flood tide velocity (from Gross and Schaaf & Wheeler, 2003).

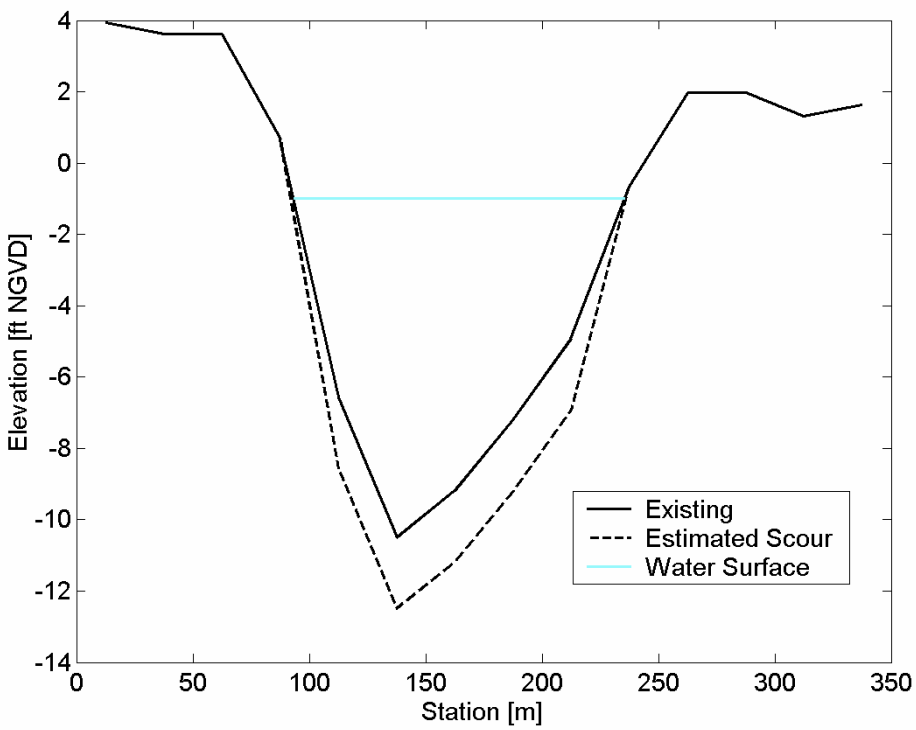

Figure 7.3-4 Existing cross-section geometry and estimated scour at the Railroad Bridge over Coyote Creek between Pond A20 and A21 based on peak ebb tide velocity (from Gross and Schaaf & Wheeler, 2003).

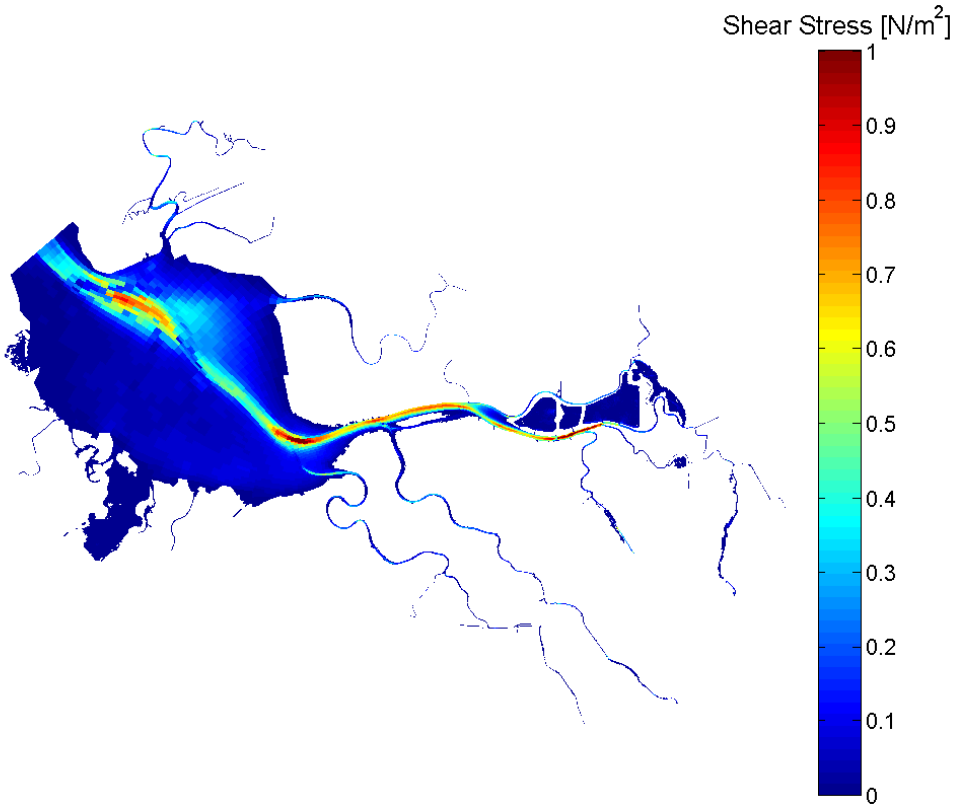

Figure 7.3-5 Predicted daily RMS shear stress in Coyote Creek region on first day of scour analysis simulation under existing (baseline conditions).

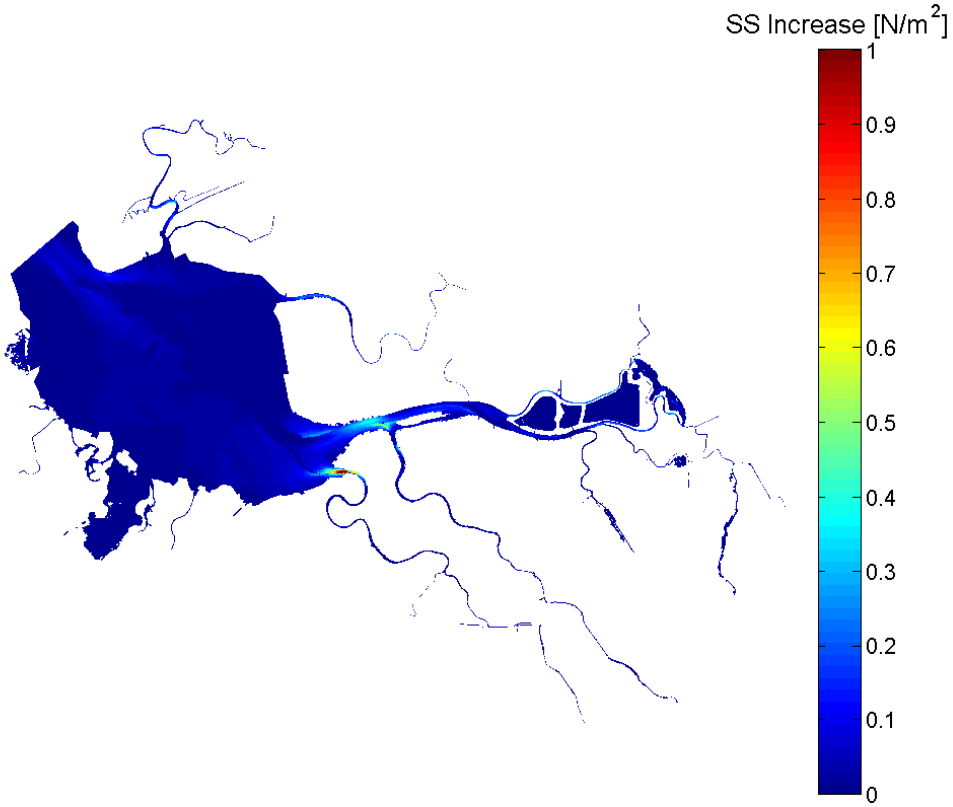

Figure 7.3-6 Predicted increases in daily RMS shear stress in Coyote Creek region under future (2067) with project conditions relative to existing (baseline) conditions on first day of scour analysis simulation.

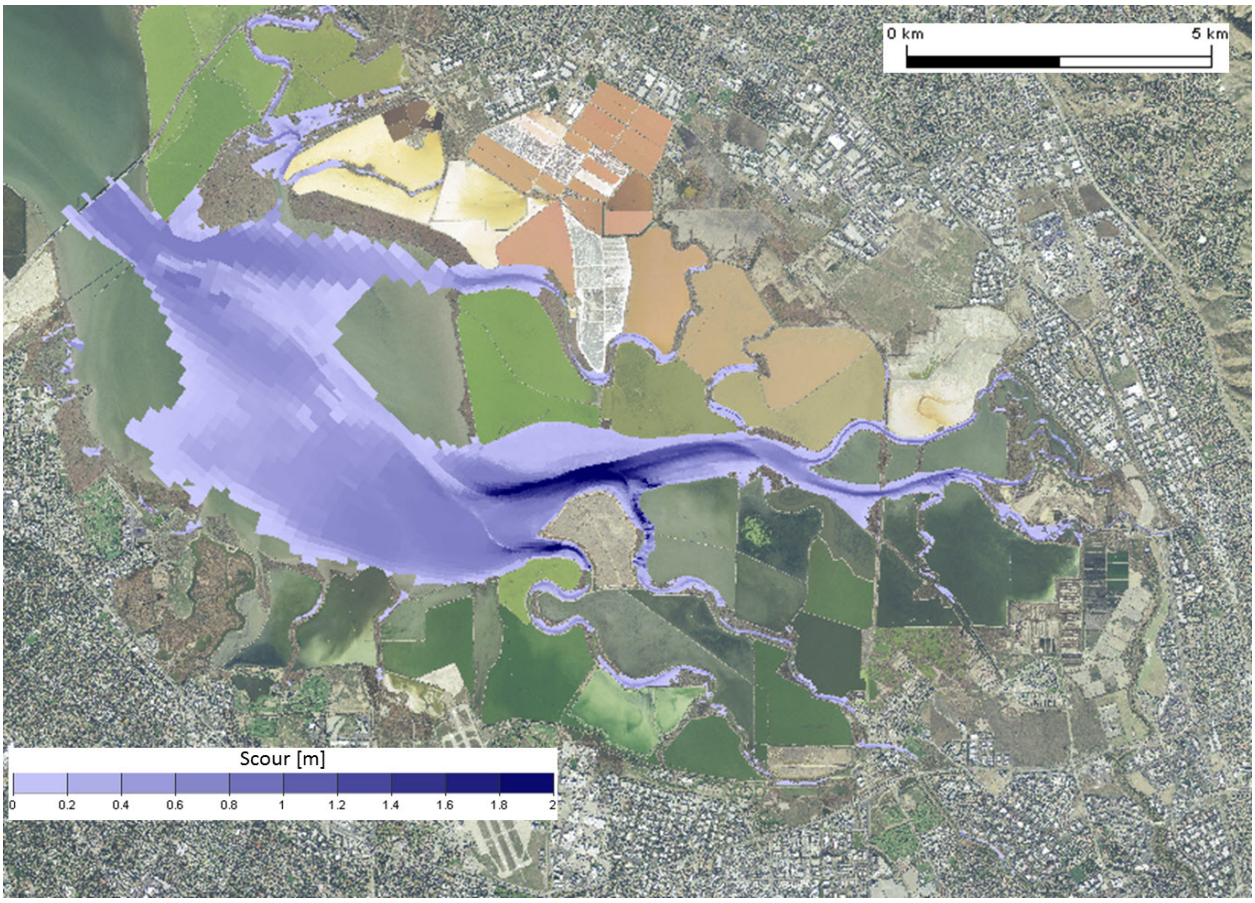

Figure 7.3-7 Predicted cumulative scour at completion of scour analysis simulation which indicates the potential scour expected to occur in the Coyote Creek region under future (2067) with project conditions in response to 0.649 m (2.13 ft) of sea level rise and the restoration of Ponds A6, A9 through A15, and A18.

7.4 Development of Projected Bathymetry in the Project Area for Year 50

The projection of bathymetry for 2067 within the project area is subject to significant uncertainty resulting from future weather and climate conditions, changes to the available sediment supply, sea level rise, the timing and design of the restoration of the former salt ponds to tidal action (including both the ponds in the project area and the adjacent ponds being restored as part of the South Bay Salt Pond Restoration Project), and the subsequent morphologic evolution of the restored ponds. The approached used in this study to develop the year 50 bathymetry was developed based on the results of the analysis of recent historic bathymetric change (Section 7.1), a projection of areas within the project area most likely to remain accretional under future conditions with sea level rise (Section 7.1 and Section 7.2), and analysis of the potential for channel scour resulting from increased tidal prism from the restored pond areas (Section 7.3). This section describes how the results of these three analyses were combined to project bathymetric conditions for year 50 (2067).

The results of the historic bathymetric change analysis (Figure 7.1-14) suggest that the majority of the sediment accretion will occur in marsh areas, that relatively little deposition will occur in

mudflat areas, and that channel areas are likely to scour downstream of pond areas that are restored to tidal action. The predicted scour which was estimated to occur in order to reduce the daily RMS bed shear stress under 2067 conditions with sea level rise and the restoration of ponds A6, A9 through A15, and Pond A18 to be similar to the daily RMS shear stress under pre-2010 conditions is applied to the channel areas to account for scour. It is assumed that relatively little change occurs in mudflat areas, based on the relatively small observed average change to mudflat elevations (Figure 7.1-16). Marsh areas are assumed to be accretional over time based on the accretional pattern of observed (Figure 7.1-14) and predicted deposition within the project area (Figure 7.2-5).

Based on observed (Figure 7.1-14) and predicted (Figure 7.2-5) deposition within the project area, an empirical geomorphic relationship (Figure 7.4-1) was developed to estimate accretion in the project area over 67 years from 2010 to 2067. This analysis covers the period between the most recent bathymetric and LiDAR surveys (2010) and the start of the project (2017) as well as the 50 year time horizon of the project, which spans from 2017 to 2067. The empirical geomorphic relationship shown in Figure 7.4-1 was applied on an annual time step in order to estimate accretion in the project area for regions other than the restored ponds, for which accretion estimates were developed by ESA PWA (2012). Based on the Modified Curve III (Figure 7.4-2) the annual rate of sea level rise increases from approximately 0.006 m/year in 2010 to 0.0185 m/year in 2067. For each year, the tidal datums (MLLW, MTL, MHHW) were adjusted for sea level rise, and the accretion rate within each cell was calculated based on the elevation in each cell using the empirical geomorphic relationship shown in Figure 7.4-1. An additional accretion of 5 cm/year was assumed in Pond A6 and A17 for the first five years following restoration, based on observations of rapid accretion rates in both A6 and the island ponds following the initial restoration to tidal action. Lastly, accretion was assumed to be zero in the areas which were predicted to be erosional in the scour analysis (Figure 7.3-7).

The resulting accretion predicted in the project area is shown in Figure 7.4-3. The low SSC scenario (ESA PWA, 2012) was selected as a conservative estimate for the accretion in Ponds A9 through A15 and Pond A18. Figure 7.4-4 shows the predicted accretion in the project area based on empirical accretion rate analysis together with the predicted accretion in Ponds A9 through A15 and Pond A18 based on the low SSC scenario developed by ESA PWA (2012). The predicted bathymetric change south of Dumbarton Bridge used in the year 50 (2067) scenarios relative to 2010 conditions is shown in Figure 7.4-5.

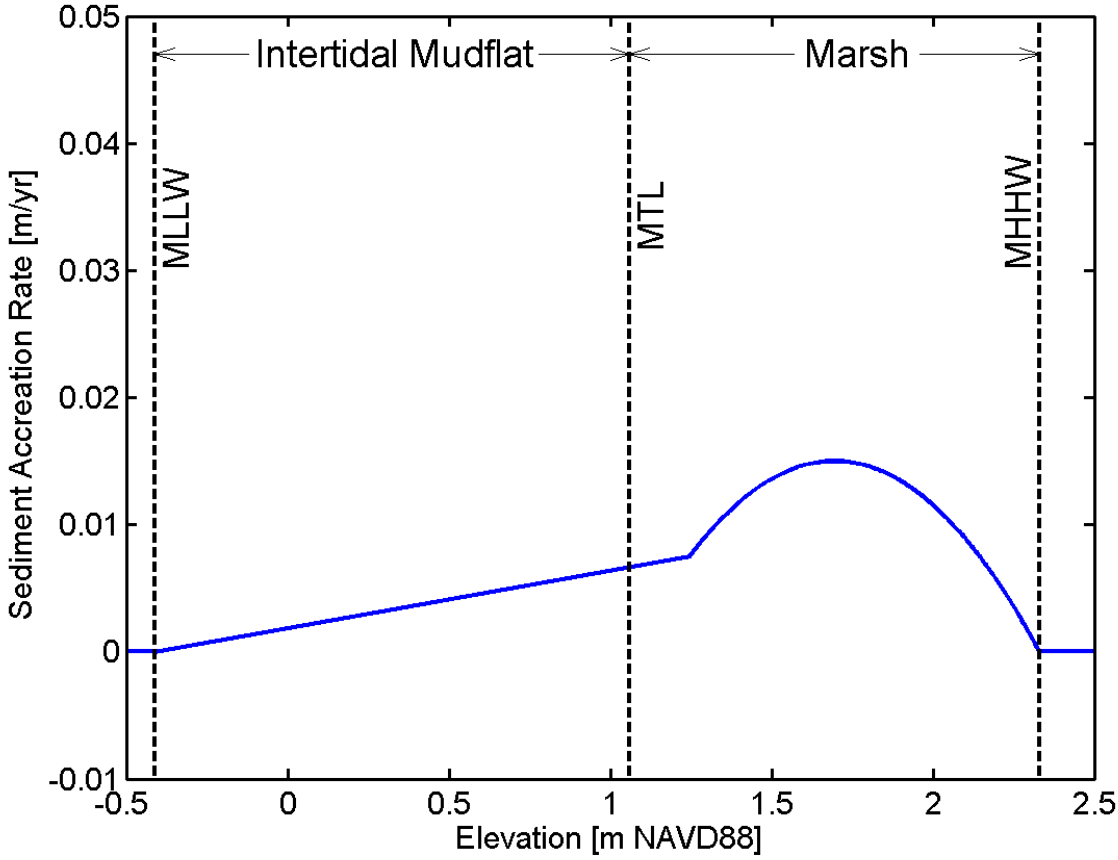

Figure 7.4-1 Empirical accretion rate curve used in accretion analysis.

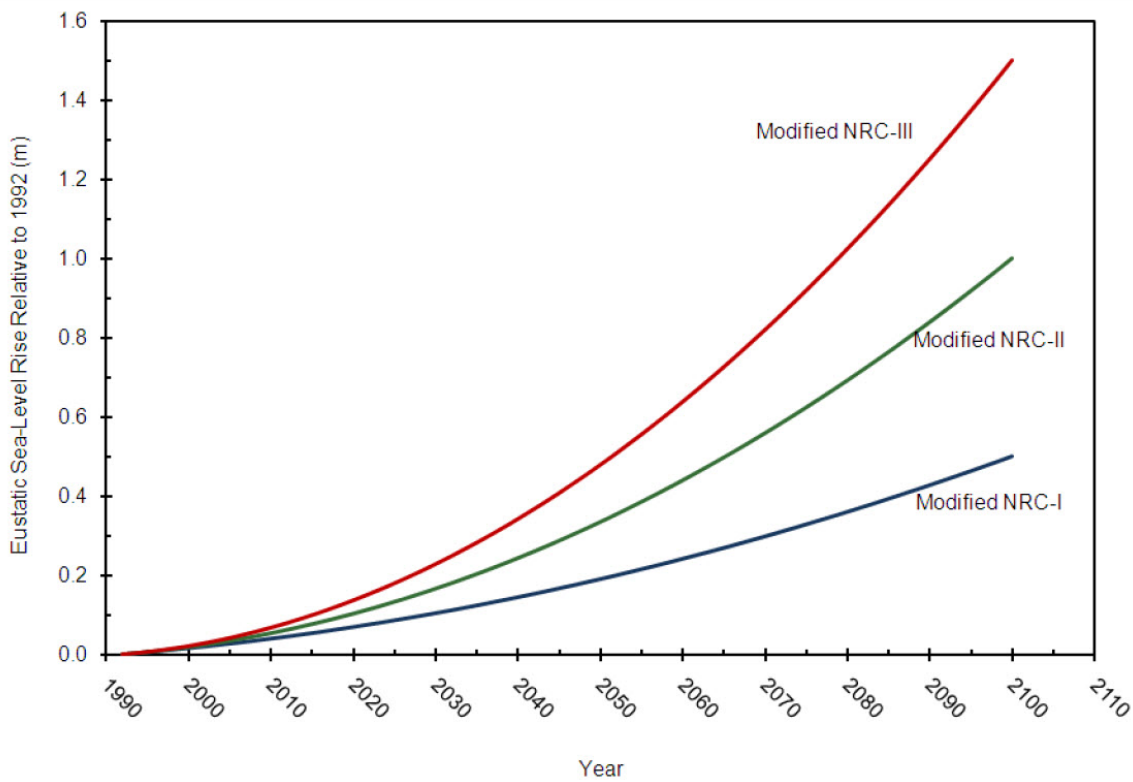

Figure 7.4-2 Modified scenarios for Global Mean Sea Level Rise based on updates to the NRC (1987) equation (from USACE, 2011).

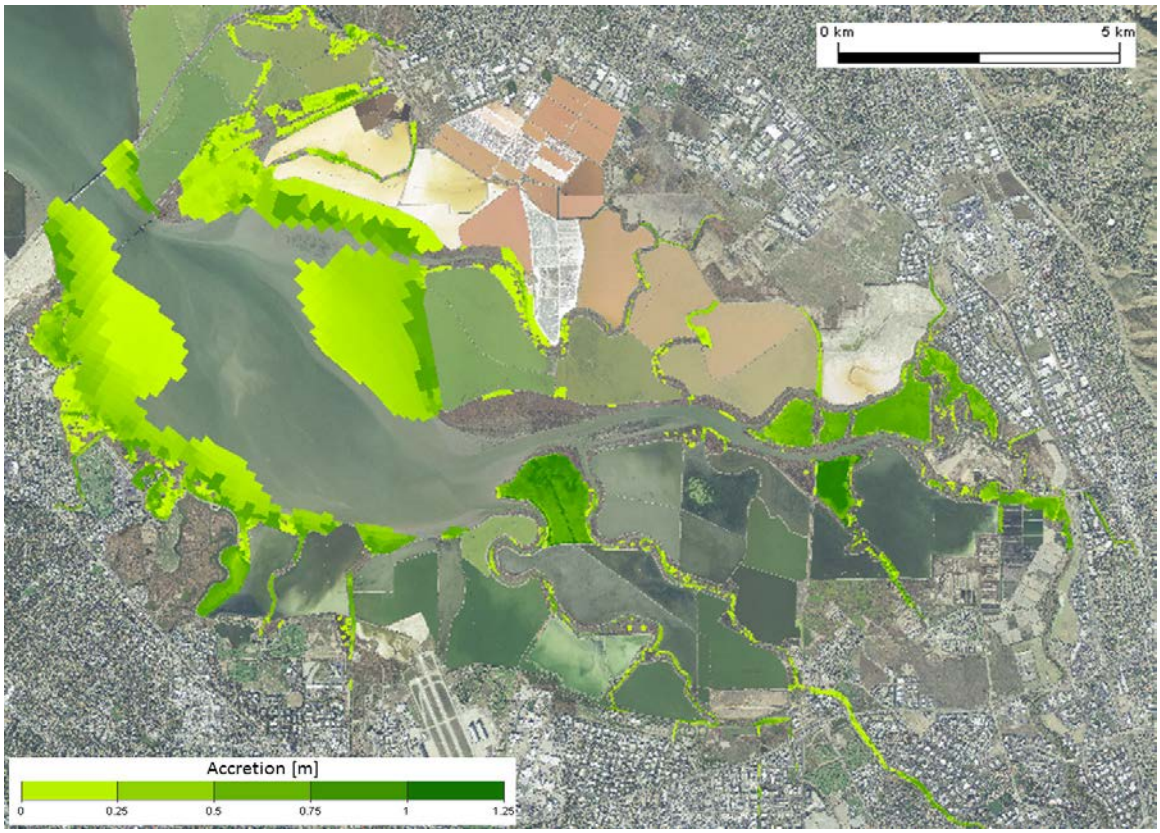

Figure 7.4-3 Predicted accretion in the project area based on empirical accretion rate analysis.

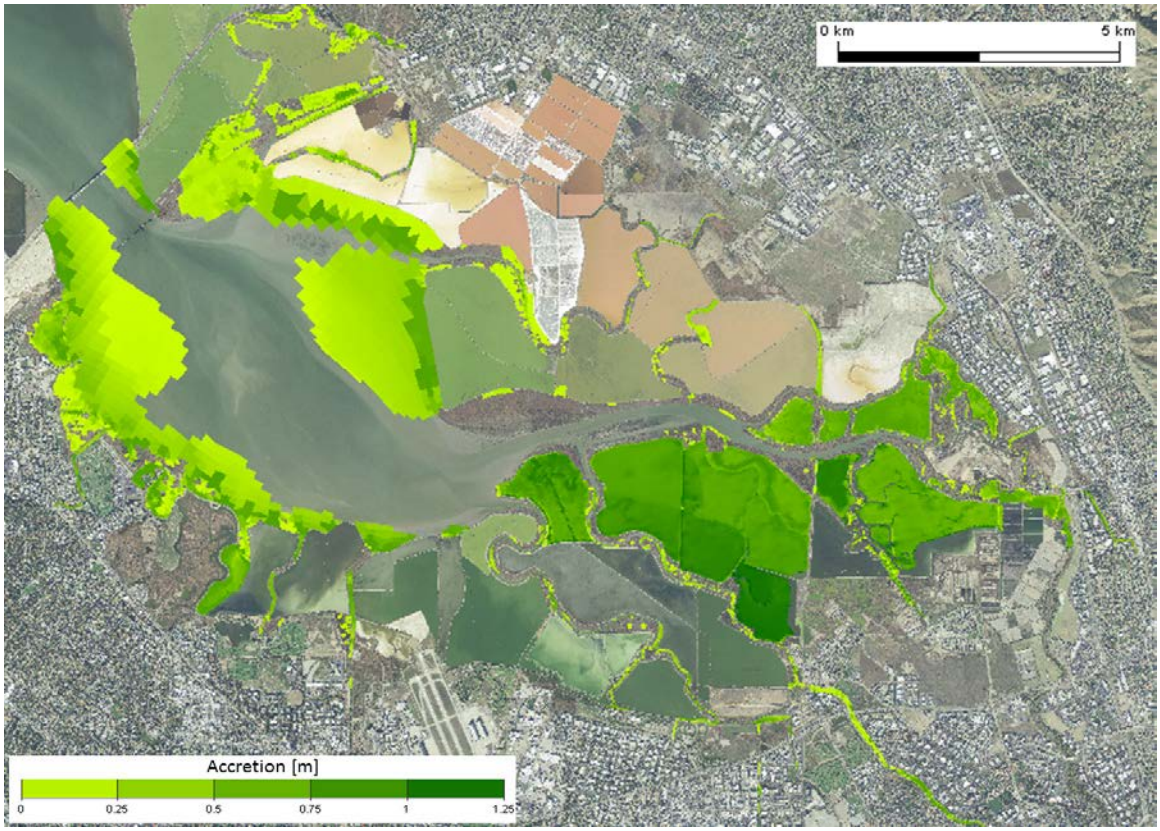

Figure 7.4-4 Predicted accretion in the project area based on empirical accretion rate analysis, shown with predicted accretion in Ponds A9 through A15 and A18 for low SSC scenario (ESA PWA, 2012).

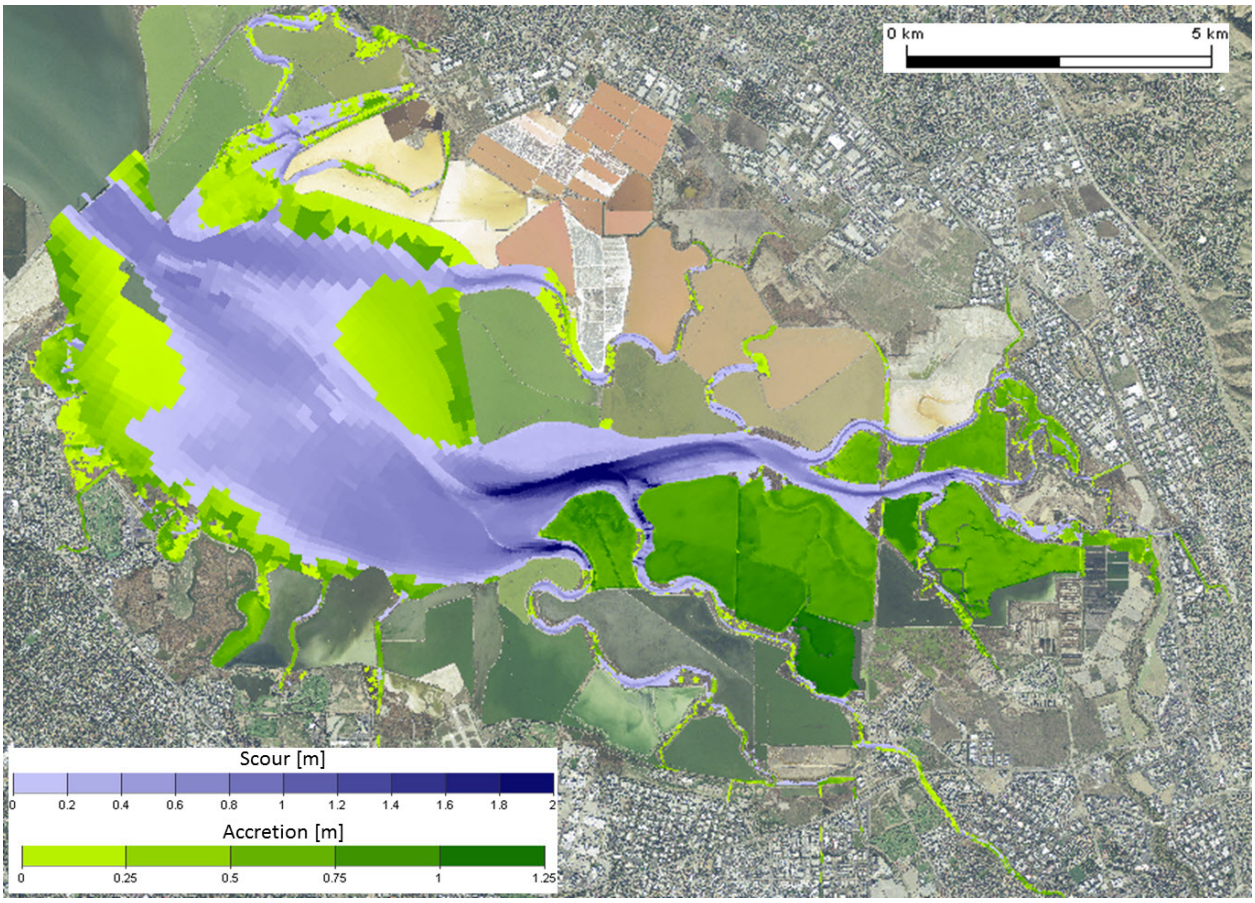

Figure 7.4-5 Predicted bathymetric change south of Dumbarton Bridge for year 50 (2067) scenarios relative to 2010 conditions.

8. Year 50 Model Production Simulations and Analysis

The year 50 (2617) production simulations were developed to predict peak water levels for a set of synthesized events that cover the ranges of all the controlling parameters, such as tide, residual surge, wind speed, and wind direction for one project alternative. This section presents the model boundary conditions and assumptions used in the development of the year 50 long wave production simulations and the resulting lookup tables which provide the peak water level for each of the events at a set of evaluation locations in the project area. The lookup tables will allow the interpretation of the responses of all the synthesized events randomly selected by the Monte Carlo Simulation (MCS) process during statistical analysis of year 50 conditions.

8.1 Boundary Conditions for Year 50 Model Production

This section describes the model boundary conditions used in the year 50 production simulations. The model boundary conditions were developed to cover a range of tide, river inflow, and wind conditions.

8.1.1 Tidal Boundary Conditions for Year 50 Production Simulations

As described in section 6.1.1, a suite of sixteen tidal boundary conditions (Table 6-1) were developed for the year 0 production simulations to span the range of astronomical and residual (surge) tides observed at the San Francisco NOAA tide station (9414290). For the year 50 production simulations, these sixteen events were adjusted to include 0.649 m (2.13 ft) of sea level rise at the ocean boundary. Twelve of the resulting events were simulated for each of the year 50 FRM alternatives considered. Only the twelve events with peak residuals between 0.5 ft and 2.5 ft were used for the year 50 production simulations since those events covered the full range needed for the MCS analysis based on coincident sampling approach adopted for this study (Noble Consultants, 2012). The four events which included 3.5 ft of surge (Events 4, 8, 12, and 16) were not simulated under year 50 conditions.

8.1.2 River Inflows for Year 50 Production Simulations

The river inflows for the year 50 production simulations are identical to the river inflows for the year 0 production simulations, which are described in Section 6.1.2. For all inflows to the model with the exception of Coyote Creek and Guadalupe River, a constant inflow was used for all year 50 simulation events. For each model inflow and export, the average January flow was calculated using available daily flow data for all days during January from 1980 to 2011. The resulting average January flows represent elevated flows typical of winter conditions, but not extreme flood peaks, and were applied as constant inflow rates for all sixteen year 50 event simulations.

For Coyote Creek and the Guadalupe River, a relationship was developed between coastal surge and peak fluvial flow using historical flow data from the USGS and historic surge (residual) data

observed at San Francisco (9414290) as described in section 6.1.2. The inflow hydrographs used in the year 50 simulations for Coyote Creek and the Guadalupe River are identical to those shown in Figure 6.1-7.

8.1.3 Wind Boundary Conditions for Year 50 Production Simulations

The wind boundary conditions for the year 50 production simulations are identical to the wind boundary conditions for the year 0 production simulations, which are described in Section 6.1.3. To evaluate wind contribution for Year 50, six wind events (Table 6-3) were simulated for Event 1, Event 3, Event 13, and Event 15 (see Table 6-1). The wind setup for each of the six non-zero wind scenarios were simulated for each of these four events (see Table 6-3), and the wind setup for each wind scenario was calculated as the difference between the peak water surface elevation from the simulation with wind and the peak water surface elevation from the corresponding simulation without wind. In this context, the wind contribution includes both the wind setup at the evaluation locations, as well as any increase in water level that may have resulted due to overtopping of levees (see discussion in Section 6.3).

8.2 Description of Year 50 Flood Risk Management Alternatives

This section describes the Flood Risk Management (FRM) alternative evaluated under year 50 conditions. Because the NED alignment has not yet been finalized, only the Locally Preferred Alignment (LPA) was considered under year 50 conditions.

8.2.1 LPA FRM Alignments

The LPA alignment follows the existing levee alignment along the eastern side of Pond A12, the southern side of Pond A13 and Pond A16, and follows a new alignment through Pond A18 and across the existing waste water treatment plant settling ponds to connect to the existing Coyote bypass levee (Figure 8.2-1).

8.2.2 Ponds A9 through A15

The year 50 simulations assume that Ponds A9 through A15 have been restored between 2021 and 2031 following a phased Ecosystem Restoration (ER) plan as described by ESA PWA (2012). For the purposes of the Flood Risk Management analysis, the lower pond sedimentation rate based on the 100 mg/L sediment concentrations was assumed for all restored ponds. The restoration of Ponds A9 through A15 includes upland fill with a 1:30 slope along the FRM levee, a series of outboard levee breaches with both pilot channels which connect the breaches to the adjacent subtidal channel and starter channels within the ponds. The ecosystem restoration alternative also includes outboard and internal berm lowering, inboard levee breaches, ditch blocks, and sidecast berms, as shown in Figure 8.2-1.

8.2.3 Ponds A16 and A17

The year 50 simulations assume that Pond A17 has been opened to tidal action, and that A16 is maintained as a managed pond following the design plans by McMillen, LLC (2011) which

restores approximately 90 acres to full tidal action in Pond A17 and enhances management of nesting water birds in Pond A16. As part of this design, the A17 levee is lowered along Coyote Creek and Artesian Slough, the existing A17 intake structure is removed, and a new intake structure between pond A17 and Pond A16 is constructed in the southwest corner of Pond A17. The resulting configuration of Ponds A16 and A17 is shown in Figure 8.2-1.

8.2.4 Pond A18

The year 50 simulations assume that Pond A18 has been restored by 2026 following a phased Ecosystem Restoration (ER) plan as described by ESA PWA (2012). For the purposes of the Flood Risk Management analysis, the lower pond sedimentation rate based on the 100 mg/L sediment concentrations was assumed for Pond A18. The restoration of Pond A18 includes upland fill with a 1:30 slope along the FRM levee, four outboard levee breaches with both pilot channels which connect the breaches to the adjacent subtidal channel and starter channels within the ponds. The ecosystem restoration alternative for A18 also includes outboard berm lowering, ditch blocks, and sidecast berms, as shown in Figure 8.2-1.

8.2.5 New Chicago Marsh

The year 50 simulations assume that New Chicago Marsh continues to be operated as a managed marsh under the same operating assumptions used in year 0 conditions as described in Section 6.2.5.

8.2.6 Artesian Slough Tide Gate

The LPA FRM design assumes the installation of a tide gate on Artesian Slough at the location where the FRM levee alignment crosses Artesian Slough. The specific details of this tide gate have not yet been determined. Based on data collected by Santa Clara Valley Water District (SCVWD), it was assumed that there will be a side hinged restrained tide gate (96”x96”) with an aluminum and steel frame and door with a steel hinge assembly, and hydraulic controls (Sergio Jimenez, HDR, pers. comm.). It is expected that the structure will match the invert of the existing outflow from the San Jose Water Pollution Control Plant (WPCP). The size of the gate will be designed to accommodate San Jose WPCP plant discharge on maximum load, with some sort of automated closure. With the gate open, discharge would continue as it does under existing conditions. However, under flood conditions the gate would be closed and act as a continuation of the levee (Sergio Jimenez, HDR, pers. comm.). The screening alternative simulations assume that the Artesian Slough tide gate will be closed, and no discharge from the San Jose WPCP will be released into Artesian Slough.

8.2.7 Evaluation Locations

Predicted water levels for each of the year 50 event simulations were evaluated at twenty-three stations located along the project levees (Figure 8.2-2). The locations of each of the evaluation locations are provided in Table 6-5. The first ten evaluation stations are located along the outer levee of the existing salt ponds. Five stations are located along the inner levee along Pond A12, Pond A13, Pond A16, and Pond A18. One station (P14) is located in Artesian

Slough and one station is located in the connection to the Coyote Bypass (P17). Five stations are located inside NCM, and one station (P23) is located at the tide gate between Ponds A15 and A16 at the south end of Triangle Marsh.

8.2.8 Outer Levee Failure Conditions

Since all of the ponds within the project area, with the exception of Pond A16, are assumed to be opened to tidal action under year 50 conditions, no additional outer levee breaches in the project area were considered under year 50 conditions.

8.3 Year 50 Model Production Simulation Results

Twelve of the sixteen tidal events shown on Table 6-1 were simulated for the LPA FRM design (Figure 8.2-1) under year 50 conditions which include 0.649 m (2.13 ft) of sea level rise. The predicted peak water level for each event was evaluated at the twenty-three evaluation locations shown on Figure 8.2-2.

8.3.1 Peak Water levels for Year 50 Production Simulations without Wind

The predicted peak water surface elevation for the sixteen year 50 event simulations for the LPA FRM design without wind at the twenty-three evaluation locations are listed in Table 8-1.

Peak water surface elevations along the outer levees (Point 1 through Point 10) range from 9.00 ft under Scenario 1 to as high as 13.12 ft under Scenario 15. Along the inner levees, water surface elevations in Ponds A12 and A13 (Point 11 and Point 12) show similar elevations to the outer levee points for all events under year 50 conditions as a result of the breaching of the outer levees. Inside Pond A16 (Point 13) which remains as a managed pond in year 50, peak water levels for events 1, 2, and 5 are lower than in Ponds A12 and A13. However, for the remaining events significant overtopping of the levees around pond A16 occurs and the peak water levels in A16 are similar to peak water levels in Ponds A12 and A13 for the other nine events. Inside Pond A18 (Point 15 and Point 16), peak water levels range from 9.05 ft to 13.09 ft. As in Ponds A11 and A12, peak water levels along the inner levee in Pond A18 (Point 15 and Point 16) are similar to the outer levee elevations under year 50 conditions as a result of the breaching of the outer levees. In Artesian Slough (Point 14), peak water levels range from 9.07 ft to 13.09 ft. Point 17, which is located on the existing settling ponds is at a high elevation and is not wet for any of the scenarios. Inside New Chicago Marsh (Point 18 through Point 22), the water surface remains at the initial water surface of -0.3 ft in all scenarios, since local precipitation and runoff is not simulated, and no overtopping of the FRM levees surrounding New Chicago Marsh is predicted for the year 50 simulations with the LPA alignment.

Relative to the Year 0 LPA production simulations (Table 6-6), the predicted peak water levels at the outer levee locations (Point 1 through 10) for the year 50 simulations (Table 8-1) increase by less than the 0.649 m (2.13) ft of sea level rise applied at the open boundary. The average peak water level increase for Points 1 through 10 for the 12 events (120 points total) is 1.76 ft (0.54 m) relative to the year 0 LPA simulations without outer levee breaches. This result shows

that on average, opening large areas in the project area to tidal action reduces peak water levels during storm events (this is also seen by comparing Table 6-6 to 6-9 to assess the influence of the outer levee failures on peak water levels for year 0). However, relative to the Year 0 LPA production simulations which include outer levee breaches (Table 6-9), the predicted peak water levels at the outer levee locations (Point 1 through 10) for the year 50 simulations (Table 8-1) increase by slightly more than the 0.649 m (2.13) ft of sea level rise applied at the open boundary. The average peak water level increase for Points 1 through 10 for the 12 events (120 points total) is 2.29 ft (0.70 m) relative to the year 0 LPA simulations with outer levee breaches.

8.3.2 Effect of Wind on Peak Water levels for Year 50 Production Simulations

Six wind scenarios (Table 6-3) were simulated for Event 1, Event 3, Event 13, and Event 15 (Table 6-1) using the LPA FRM alignment, resulting in a total of twenty-four simulations with wind for year 50. The wind setup for each wind scenario was calculated as the difference between the peak water surface elevation from the simulation with wind and the peak water surface elevation from the corresponding simulation without wind. The contribution of wind to peak water surface elevation at twenty-three evaluation locations for the LPA FRM alignment are listed in Table 8-2.

Along the outer levees (Point 1 through Point 10), wind setup results in an increase in peak water level of between 0.21 and 1.55 ft. The largest increase in water surface elevation due to wind occurs at Point 1 and Point 10. In Artesian Slough (Point 14), wind setup results in an increase in peak water level of between 0.27 and 1.48 ft. The six wind simulations for Event 15 result in a smaller increase in peak water surface elevation due to wind than the wind simulations for Event 1, 3, and 13, particularly along the outer levees. Inside the restored ponds, (Point 11, Point 12, Point 15 and Point 16), wind results in an increase in peak water level of between 0.27 and 1.52 ft, which is similar to the wind setup along the outer levees at Points 1 through 10. Inside Pond A16 (Point 13), wind setup for Event 1 from the 30 mph and 40 mph wind events results in increased overtopping into Pond A16 (see Section 6.3.2). For Events 3, 13, and 15 peak water levels without wind are higher than the levees surrounding A16, so the wind setup for these events is similar to the wind setup predicted in the restored ponds. Inside New Chicago Marsh (Point 18 through Point 22), which is on the landward side of the LPA levee alignment, wind setup results in only very small changes in peak water surface elevation, with maximum increases in peak water surface elevation due to wind of between 0.00 and 0.05 ft.

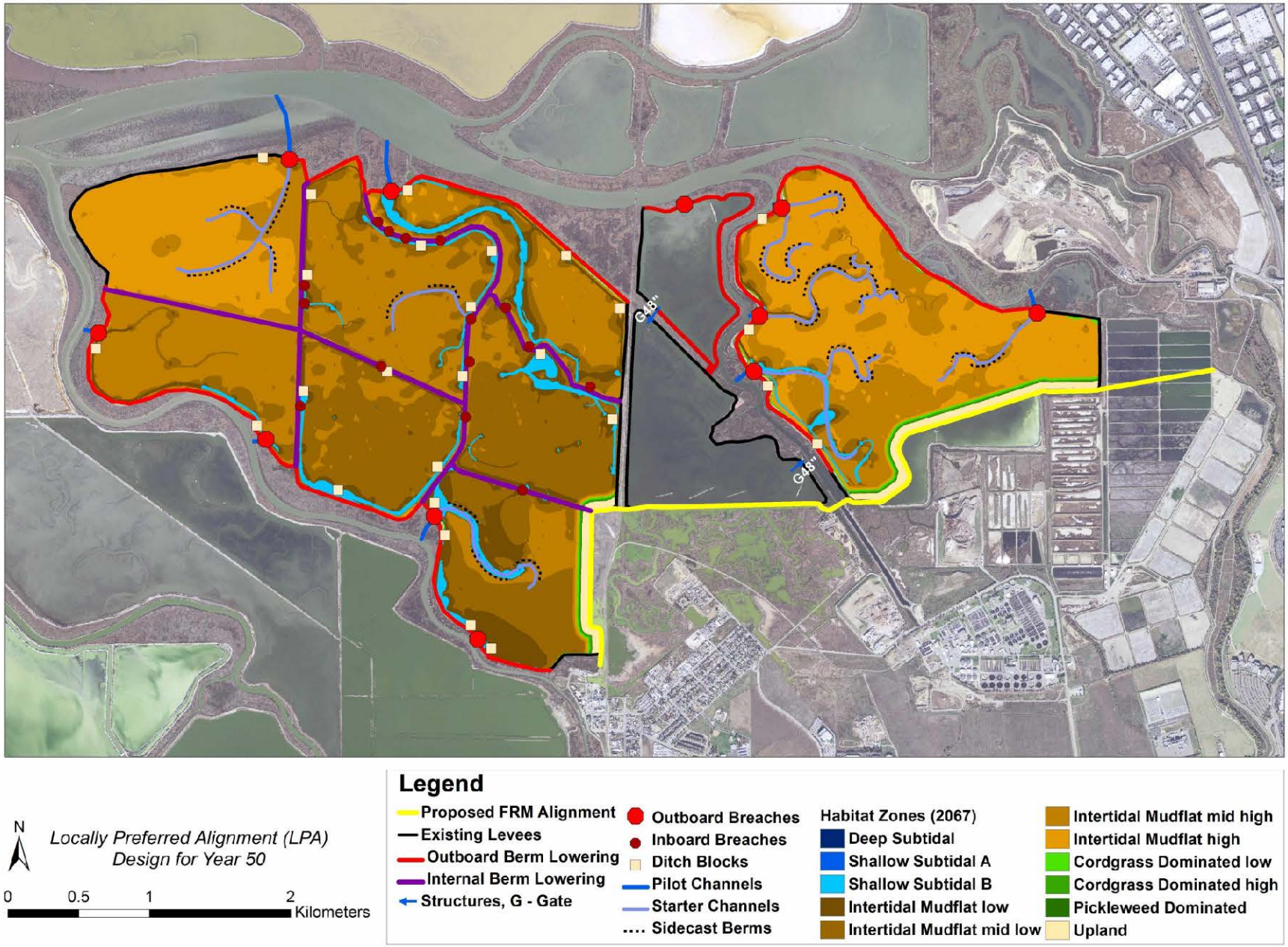

Figure 8.2-1 FRM levee alignment and ecosystem restoration elements for Locally Preferred Alignment (LPA) design for year 50.

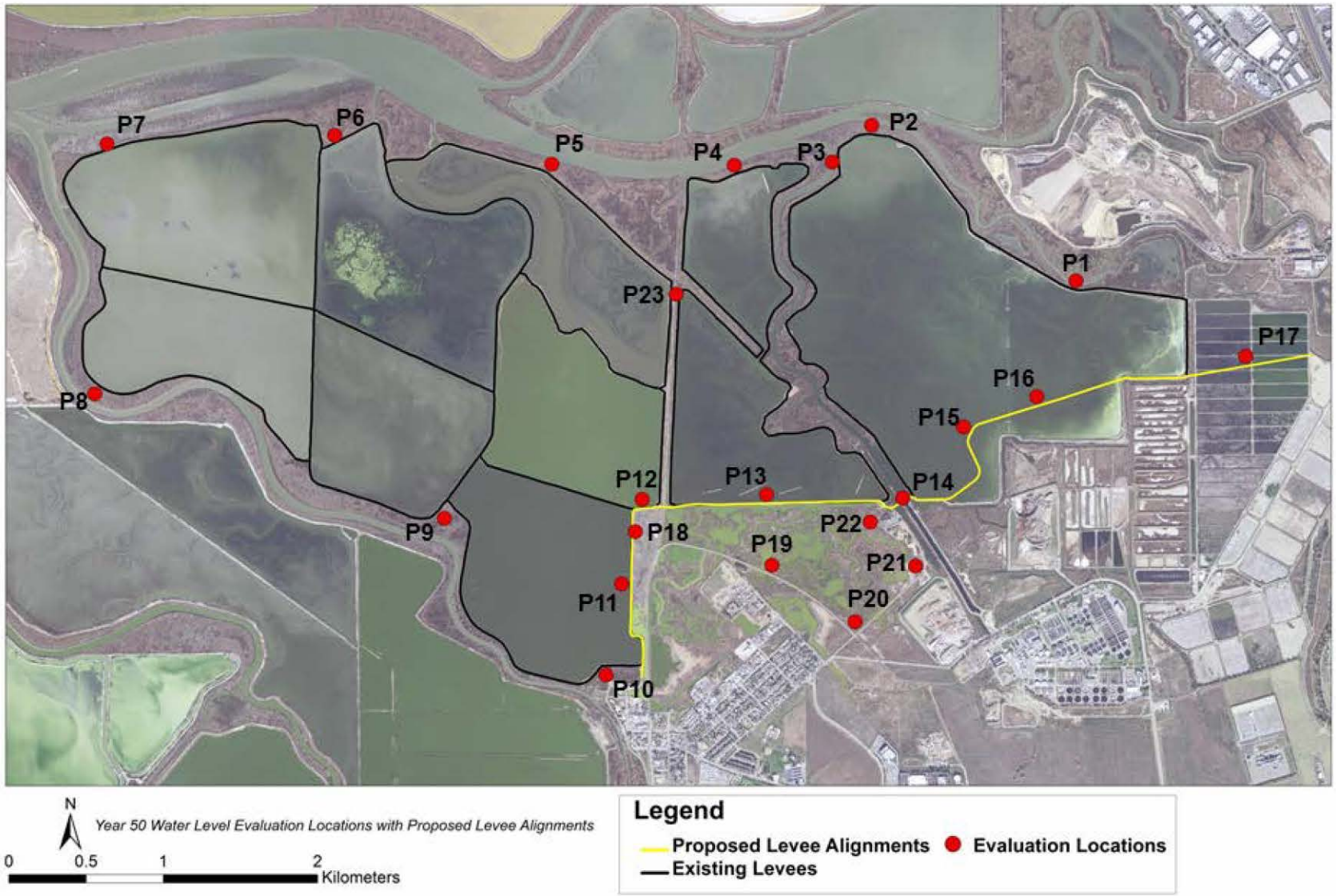

Figure 8.2-2 Locations used for evaluation of peak water levels for year 50 model simulations.

Table 8-1 Predicted peak water surface elevation [ft NAVD88] for year 50 LPA design scenarios at twenty-three evaluation locations.

Event	Tide		Evaluation Location																						
	Astronomical [ft MLLW]	Surge [ft]	1	2	3	4	5	6	7	8	9	10	11	12	13	14	15	16	17	18	19	20	21	22	23
1	5.15	0.5	9.03	9.16	9.00	9.13	9.18	9.18	9.13	9.16	9.22	9.30	9.23	9.22	6.63	9.07	9.05	9.05	dry	-0.30	-0.30	-0.30	-0.30	-0.30	8.52
2	5.15	1.5	10.18	10.11	10.10	10.02	10.09	10.09	10.16	10.12	10.13	10.27	10.16	10.16	9.71	10.17	10.17	10.17	dry	-0.30	-0.30	-0.30	-0.30	-0.30	10.03
3	5.15	2.5	11.31	11.25	11.24	11.14	11.18	11.17	11.15	11.16	11.22	11.31	11.23	11.22	11.22	11.30	11.30	11.31	dry	-0.30	-0.30	-0.30	-0.30	-0.30	11.20
4	5.15	3.5	-	-	-	-	-	-	-	-	-	-	-	-	-	-	-	-	-	-	-	-	-	-	-
5	5.85	0.5	9.91	9.84	9.82	9.78	9.91	9.91	9.90	9.90	9.94	9.99	9.95	9.95	6.92	9.91	9.90	9.90	dry	-0.30	-0.30	-0.30	-0.30	-0.30	9.70
6	5.85	1.5	11.00	10.94	10.93	10.83	10.88	10.86	10.85	10.83	10.92	11.00	10.93	10.92	10.93	10.99	10.99	10.99	dry	-0.30	-0.30	-0.30	-0.30	-0.30	10.89
7	5.85	2.5	12.03	11.98	11.97	11.89	11.90	11.88	11.87	11.87	11.92	11.98	11.93	11.93	11.93	12.02	12.02	12.03	dry	-0.30	-0.30	-0.30	-0.30	-0.30	11.92
8	5.85	3.5	-	-	-	-	-	-	-	-	-	-	-	-	-	-	-	-	-	-	-	-	-	-	-
9	6.55	0.5	10.76	10.68	10.67	10.56	10.68	10.67	10.72	10.66	10.72	10.75	10.74	10.74	10.76	10.74	10.74	10.74	dry	-0.30	-0.30	-0.30	-0.30	-0.30	10.65
10	6.55	1.5	11.80	11.74	11.73	11.61	11.72	11.71	11.72	11.70	11.76	11.79	11.77	11.76	11.77	11.79	11.79	11.79	dry	-0.30	-0.30	-0.30	-0.30	-0.30	11.74
11	6.55	2.5	12.65	12.62	12.61	12.54	12.58	12.57	12.58	12.56	12.60	12.62	12.61	12.60	12.60	12.64	12.64	12.65	dry	-0.30	-0.30	-0.30	-0.30	-0.30	12.57
12	6.55	3.5	-	-	-	-	-	-	-	-	-	-	-	-	-	-	-	-	-	-	-	-	-	-	-
13	7.25	0.5	11.47	11.40	11.39	11.28	11.36	11.35	11.34	11.35	11.39	11.42	11.40	11.40	11.40	11.45	11.45	11.46	dry	-0.30	-0.30	-0.30	-0.30	-0.30	11.38
14	7.25	1.5	12.39	12.35	12.34	12.26	12.29	12.27	12.27	12.26	12.30	12.33	12.31	12.31	12.31	12.38	12.38	12.39	dry	-0.30	-0.30	-0.30	-0.30	-0.30	12.29
15	7.25	2.5	13.09	13.08	13.08	13.07	13.08	13.07	13.07	13.06	13.09	13.12	13.10	13.09	13.09	13.09	13.09	13.09	dry	-0.30	-0.30	-0.30	-0.30	-0.30	13.09
16	7.25	3.5	-	-	-	-	-	-	-	-	-	-	-	-	-	-	-	-	-	-	-	-	-	-	-

Table 8-2 Contribution of wind to peak water surface elevation [ft] for year 50 LPA design scenarios at twenty-three evaluation locations.

Event	Wind		Evaluation Location																						
	Dir [deg]	Speed [mph]	1	2	3	4	5	6	7	8	9	10	11	12	13*	14	15	16	17	18	19	20	21	22	23
1	292.5	20	0.49	0.31	0.39	0.32	0.35	0.34	0.34	0.33	0.38	0.42	0.40	0.40	0.03	0.44	0.45	0.47	0.00	0.00	0.00	0.00	0.01	0.00	0.34
1	292.5	30	1.05	0.85	1.01	0.73	0.74	0.72	0.75	0.72	0.76	0.76	0.80	0.95	3.13	1.01	1.02	1.01	0.00	0.00	0.00	0.00	0.02	0.01	1.19
1	292.5	40	1.60	1.32	1.47	1.23	1.17	1.09	1.37	1.12	1.27	1.39	1.39	1.46	3.98	1.55	1.57	1.55	0.00	0.00	0.00	0.00	0.05	0.03	1.93
1	315.0	20	0.48	0.29	0.38	0.31	0.34	0.33	0.33	0.34	0.38	0.41	0.40	0.40	0.04	0.44	0.45	0.46	0.00	0.00	0.00	0.00	0.01	0.00	0.35
1	315.0	30	1.02	0.77	0.93	0.67	0.71	0.70	0.72	0.75	0.80	0.76	0.81	0.95	3.12	0.97	0.98	0.98	0.00	0.00	0.00	0.00	0.02	0.00	1.20
1	315.0	40	1.48	1.21	1.37	1.14	1.05	1.04	1.24	1.12	1.17	1.55	1.46	1.44	3.89	1.53	1.49	1.52	0.00	0.00	0.00	0.00	0.04	0.01	1.96
3	292.5	20	0.40	0.36	0.36	0.35	0.34	0.31	0.30	0.30	0.34	0.36	0.37	0.36	0.38	0.39	0.39	0.40	0.00	0.00	0.00	0.00	0.01	0.00	0.37
3	292.5	30	0.90	0.84	0.84	0.82	0.77	0.72	0.68	0.68	0.78	0.78	0.83	0.83	0.85	0.88	0.89	0.90	0.00	0.00	0.00	0.00	0.02	0.01	0.83
3	292.5	40	1.64	1.55	1.55	1.54	1.42	1.32	1.26	1.27	1.44	1.47	1.53	1.53	1.57	1.60	1.62	1.65	0.00	0.00	0.00	0.00	0.05	0.03	1.50
3	315.0	20	0.39	0.36	0.36	0.35	0.34	0.32	0.31	0.32	0.35	0.36	0.37	0.37	0.37	0.39	0.39	0.39	0.00	0.00	0.00	0.00	0.01	0.00	0.37
3	315.0	30	0.82	0.77	0.77	0.75	0.70	0.67	0.65	0.67	0.73	0.72	0.76	0.76	0.77	0.83	0.82	0.83	0.00	0.00	0.00	0.00	0.02	0.00	0.76
3	315.0	40	1.48	1.38	1.39	1.38	1.29	1.24	1.19	1.23	1.35	1.38	1.43	1.43	1.42	1.48	1.48	1.51	0.00	0.00	0.00	0.00	0.04	0.01	1.38
13	292.5	20	0.37	0.34	0.34	0.33	0.32	0.30	0.29	0.27	0.32	0.34	0.34	0.34	0.36	0.36	0.37	0.38	0.00	0.00	0.00	0.00	0.01	0.00	0.35
13	292.5	30	0.87	0.81	0.81	0.80	0.74	0.69	0.65	0.64	0.75	0.80	0.80	0.80	0.82	0.85	0.86	0.87	0.00	0.00	0.00	0.00	0.02	0.01	0.79
13	292.5	40	1.61	1.52	1.52	1.53	1.38	1.27	1.21	1.21	1.39	1.46	1.47	1.48	1.51	1.56	1.58	1.62	0.00	0.00	0.00	0.00	0.05	0.03	1.44
13	315.0	20	0.38	0.34	0.34	0.34	0.33	0.31	0.31	0.30	0.35	0.37	0.37	0.37	0.38	0.37	0.38	0.38	0.00	0.00	0.00	0.00	0.01	0.00	0.36
13	315.0	30	0.80	0.75	0.75	0.74	0.69	0.65	0.63	0.64	0.72	0.76	0.75	0.75	0.75	0.80	0.80	0.81	0.00	0.00	0.00	0.00	0.02	0.00	0.74
13	315.0	40	1.42	1.32	1.34	1.33	1.21	1.16	1.10	1.15	1.27	1.37	1.34	1.35	1.34	1.42	1.41	1.46	0.00	0.00	0.00	0.00	0.04	0.01	1.28
15	292.5	20	0.28	0.25	0.25	0.24	0.24	0.21	0.23	0.22	0.25	0.26	0.27	0.27	0.28	0.27	0.28	0.29	0.00	0.00	0.00	0.00	0.01	0.00	0.25
15	292.5	30	0.62	0.54	0.54	0.52	0.49	0.45	0.48	0.45	0.52	0.51	0.56	0.56	0.58	0.59	0.60	0.62	0.00	0.00	0.00	0.00	0.02	0.01	0.53
15	292.5	40	1.19	1.04	1.03	0.98	0.86	0.75	0.80	0.79	0.88	0.91	0.97	0.98	1.05	1.13	1.16	1.19	0.00	0.00	0.00	0.00	0.05	0.03	0.97
15	315.0	20	0.30	0.27	0.27	0.26	0.26	0.23	0.25	0.24	0.28	0.29	0.30	0.30	0.30	0.30	0.30	0.30	0.00	0.00	0.00	0.00	0.01	0.00	0.27
15	315.0	30	0.60	0.53	0.53	0.50	0.49	0.45	0.48	0.49	0.54	0.54	0.58	0.58	0.58	0.60	0.60	0.62	0.00	0.00	0.00	0.00	0.02	0.00	0.54
15	315.0	40	0.97	0.85	0.84	0.81	0.77	0.70	0.78	0.82	0.86	0.87	0.93	0.94	0.93	0.97	0.98	1.00	0.00	0.00	0.00	0.00	0.04	0.01	0.87

* Contribution of wind to peak water surface elevation inside the managed ponds includes the influence of wind setup on flow through pond control structures and wind induced overtopping as described in Section 6.3.2.

9. Summary and Conclusions

The South San Francisco Bay Shoreline Study (SSFBSS) is being conducted by the USACE San Francisco District (SPN) and is co-sponsored by the Santa Clara Valley Water District (SCVWD) and California Coastal Conservancy (CCC). The SSFBSS has the dual functions of providing shoreline protection and restoring salt ponds in Far South San Francisco Bay.

The UnTRIM San Francisco Bay-Delta model was refined to include a high resolution model grid and the most recent available high resolution bathymetric data in the project area (Section 3). The model was calibrated (Section 4) using observed water level data during periods with the most extensive spatial availability of water level observations in the project area in 2005 and 2011. The model was validated (Section 4) using peak water level data from five separate storm periods between 1983 and 2006. These simulation periods include ten of the 47 highest observed water levels during storm events based on a ranking of the maximum verified tide data value at the San Francisco NOAA tide station (9414290), including all of the top five ranked events. The resulting model was applied to predict peak water levels in the project area under with project conditions.

The calibrated and validated model was applied to a set of six preliminary alternatives (Section 5) to predict peak water levels in the project area for a single flood event. The six preliminary alternatives were developed by combining the two most likely Flood Risk Management (FRM) levee alignments, with a suite of ecosystem restoration (ER) options based on feedback from the Project Delivery Team (PDT) and the project sponsors. The results from these preliminary alternative simulations were used in the selection of the two alternatives to be used for detailed analysis of flood risks with project conditions.

Based on this suite of preliminary alternatives, two FRM alternatives were evaluated under year 0 (2017) conditions (Section 6). The two alternatives were the designated as the Locally Preferred Alignment (LPA) and a tentative National Economic Development (NED) alignment. A set of synthesized events that cover the ranges of all the controlling parameters, such as tide, residual surge, wind speed, and wind direction and levee failures was developed for year 0 conditions. Predicted peak water levels for each year 0 event were provided in lookup tables to allow for the interpretation of the responses of all the synthesized events randomly selected by the Monte Carlo Simulation (MCS) process during statistical analysis.

The year 50 project bathymetry was developed through a combination of historical analysis of bathymetric change in the project area, an analysis of predicted deposition in the project area through numerical simulation, and prediction of the potential for channel scour following the opening of the salt ponds to tidal action (Section 7). The year 50 simulations incorporate both the expected accretion within the project ponds, as well as estimated channel evolution in the vicinity of the project area.

The Locally Preferred Alignment (LPA) was combined with an Ecosystem Restoration (ER) scenario to develop project conditions for year 50 (2067), with 0.649 m (2.13 ft) of sea level rise (Section 8). The year 50 production simulations were also performed for a set of synthesized

events that cover the ranges of all the controlling parameters, such as tide, residual surge, wind speed, and wind direction. Predicted peak water levels for each year 50 event were provided in lookup tables to allow for the interpretation of the responses of all the synthesized events randomly selected by the Monte Carlo Simulation (MCS) process during statistical analysis. The results of MCS will be used to establish flood stage frequency and overtopping flow for mapping.

Acknowledgments

This project is being conducted for the USACE San Francisco District (SPN) as part of the San Francisco Bay Shoreline Study (SSFBSS) under the supervision of Frank Wu (USACE). The authors would also like to thank Frank Wu (SPN) and Lisa Andes (SPN) for guidance on technical aspects of the project. The authors would like to thank Amy Foxgrover (USGS), Greg Shellenbarger (USGS), Laura Valoppi (USGS), Ann Sturm (USACE), Al Gurevich (SCVWD), Jen Men Lo (SCVWD), Chia-Chi Lu (Noble Consultants, Inc.), Todd Ehret (NOAA), John Callaway (SFSU), John Bourgeois (South Bay Salt Pond Restoration Project), Eric Mruz (USFWS), Renée Spenst (Ducks Unlimited), Brenda Buxton (Coastal Conservancy), Meg Sedlak (SFEI), Mark Stacey (UC Berkeley), Rusty Holleman (UC Berkeley), Ed Gross, Frank Ludwig (Stanford University) Jeremy Lowe (ESA-PWA), Lindsey Sheehan (ESA-PWA), and Sergio Jimenez (HDR) for access to data and other information which was used for this project.

The high resolution DEM of Far South Francisco Bay was developed by James Zoulas (SPN). The authors would like to acknowledge the tremendous effort that went into the development of this DEM in order to meet the datum compliance standards for the project. The UnTRIM code was developed by Professor Vincenzo Casulli (University of Trento, Italy). The SediMorph model was originally developed at the German Federal Waterways Engineering and Research Institute in Hamburg (BAW-Hamburg) by Andreas Malcherek. The SediMorph model was provided for use on this project through a collaboration agreement with the German Federal Waterways Engineering and Research Institute (BAW). Lastly, the authors would like to thank Ralph Cheng (USGS, retired), for his comments and careful review of this report.

References

BAW, 2005. Mathematical Module SediMorph, Validation Document, Version 1.1, The Federal Waterways Engineering and Research Institute.

Bever, A.J., and M.L. MacWilliams, 2012 (in review). Simulating sediment transport processes in San Pablo Bay using coupled hydrodynamic, wave, and sediment transport models, submitted to Marine Geology special issue, "A multi-discipline approach for understanding sediment transport and geomorphic evolution in an estuarine-coastal system: San Francisco Bay."

Caffrey, J.M., 1995. Spatial and seasonal patterns in sediment nitrogen remineralization and ammonium concentrations in San Francisco Bay, California. Estuaries, 18(1B), 219-233

Casulli, V. 1990. Semi-implicit finite difference methods for the two-dimensional shallow water equations. Journal of Computational Physics. 86, 56-74.

Casulli, V. and R. T. Cheng, 1992, Semi-implicit finite difference methods for three-dimensional shallow water flow, Inter. J. for Numer. Methods in Fluids, Vol. 15, p. 629-648.

Casulli, V., and Cattani, E. 1994. Stability, accuracy and efficiency of a semi-implicit method for three-dimensional shallow water flow. Computers and Mathematics with Applications, 27(4), 99-112.

Casulli, V., 1999. A semi-implicit numerical method for non-hydrostatic free-surface flows on unstructured grid, in Numerical Modelling of Hydrodynamic Systems, ESF Workshop, pp. 175-193, Zaragoza, Spain.

Casulli, V. and R.A. Walters, 2000. An unstructured, three-dimensional model based on the shallow water equations, International Journal for Numerical Methods in Fluids 2000, 32: 331 - 348.

Casulli, V. and Zanolli, P., 2002. Semi-Implicit Numerical Modelling of Non-Hydrostatic Free-Surface Flows for Environmental Problems, Mathematical and Computer Modelling, 36: 1131 - 1149.

Casulli, V. and Zanolli, P., 2005. High Resolution Methods for Multidimensional Advection-Diffusion Problems in Free-Surface Hydrodynamics, Ocean Modelling, 2005, v. 10, 1-2, p. 137-151.

[CDWR] California Department of Water Resources, 1986. DAYFLOW program documentation and data summary user's guide. California Department of Water Resources, Sacramento.

Cheng, J., and Wu, F. 2008. South San Francisco Bay Shoreline Study, Documentation of Data Analysis, Memorandum for Record, CESPN-ET-EW, 14 January 2008.

Cheng, R.T., Casulli, V., and Gartner, J.W., 1993. Tidal residual intertidal mudflat (TRIM) model and its applications to San Francisco Bay, California. Estuarine, Coastal and Shelf Science, 369, 235-280.

Cheng, R. T. and V. Casulli, 1996. Modeling the Periodic Stratification and Gravitational Circulation in San Francisco Bay, in Proceedings of 4th Inter. Conf. on Estuarine and Coastal Modeling, Spaulding and Cheng (Eds.), ASCE, San Diego, CA, October 1995, p.240-254.

Cheng, R. T., and V. Casulli, 2002. Evaluation of the UnTRIM model for 3-D Tidal Circulation, Proceedings of the 7th International Conference on Estuarine and Coastal Modeling, St. Petersburg, FL, November 2001, 628-642.

Cheng, R T. and R. E. Smith, 1998, A Nowcast Model for Tides and Tidal Currents in San Francisco Bay, California, Ocean Community Conf. '98, Marine Technology Society, Baltimore, Nov. 15-19, p. 537-543.

City of San Jose, 2011. Self-Monitoring Program 2010 Annual Report, Pond A18 in Santa Clara County, Prepared for California Regional Water Quality Control Board, Prepared by: City of San Jose Environmental Services Department, January 31, 2011.

Deleersnijder, E., Beckers, J.M., Campin, J.M., El Mohajir, M., Fichefet, T., and Luyten, P., 1997. Some mathematical problems associated with the development and use of marine models." The Mathematics of Models for Climatology and Environment, Vol. 148., J.I. Diaz, ed., Springer Verlag, Berlin, Heidelberg.

DHI, 2010. Regional Coastal Hazard Modeling Study for North and Central San Francisco Bay, Final Draft Report, September 2010.

ESA PWA, 2012. Shoreline Study Preliminary Alternatives and Landscape Evolution, Memorandum to Brenda Buxton (California State Coastal Conservancy), February 10, 2012.

Foxgrover, A.C., Jaffee, B.E., Hovis, G.T., Martin, C.A., Hubbard, J.R., Samant, M.R., and S.M. Sullivan, 2007. 2005 Hydrographic Survey of South San Francisco Bay, California, U.S. Geological Survey, Open File Report 2007-1169.

Foxgrover A.C., Finlayson, D.P., Jaffe, B.E., Takekawa, J.Y., Thorne, K.M., and K.A Spragens, 2011a. 2010 Bathymetric Survey and Digital Elevation Model of Corte Madera Bay, California, U.S. Geological Survey, Open File Report 2011-1217.

Foxgrover, A.C., Finlayson, D.P., and B.E. Jaffe, 2011b. 2010 Bathymetry and Digital Elevation Model of Coyote Creek and Alviso Slough, South San Francisco Bay, California, U.S. Geological Survey, Open File Report 2011-1315.

Gross, E.S., Koseff, J.R., and Monismith, S.G., 1999. Three-dimensional salinity simulations of South San Francisco Bay. Journal of Hydraulic Engineering 125 (11), 1199-1209.

Gross, E.S., and Schaaf & Wheeler, 2003. South Bay Salt Ponds Initial Stewardship Plan: South San Francisco Bay Hydrodynamic Model Results Report. Prepared for Cargill Salt.

Gross, E.S., M. L. MacWilliams and W. Kimmerer, 2006. Simulating Periodic Stratification in San Francisco Bay, Proceedings of the Estuarine and Coastal Modeling Conference, ASCE.

Hubel, B., 2012. Technical Memo, San Francisco South Bay Shoreline Study, Levee Breach Dimensions, 18 April, 2012.

Huzzey, L.M., Cloern, J.E., and Powell, T.M., 1990. Episodic changes in lateral transport and phytoplankton distribution in South San Francisco Bay: Limnology and Oceanography, 35: 472-478.

Kantha, L.H., Clayson, C.A., 1994. An improved mixed layer model for geophysical applications, Journal of Geophysical Research, 99, 25235–25266.

Large, W., and Pond, S., 1981. Open ocean momentum flux measurements in moderate to strong winds, Journal of Physical Oceanography, 11, 324-336.

Letter, J. V., and A.K., Sturm, 2010. Long wave modeling for South San Francisco Bay Shoreline Study: without Project Conditions, ERDC/CHL Draft Final Report, 21 May 2010.

Lippert, C. and Sellerhoff, F., 2007. Efficient Generation of Unstructured Orthogonal Grids, The 7th Int. Conf. on Hydroscience and Engineering (ICHE-2006), Sep. 10 – Sep. 13, Philadelphia, USA.

MacWilliams, M.L., and Cheng, R.T., 2007. Three-dimensional hydrodynamic modeling of San Pablo Bay on an unstructured grid, The 7th Int. Conf. on Hydroscience and Engineering (ICHE-2006), Sep. 10 – Sep. 13, Philadelphia, USA.

MacWilliams, M.L., and E.S. Gross, 2007. UnTRIM San Francisco Bay-Delta Model Calibration Report, Delta Risk Management Study, prepared for CA Department of Water Resources, March 2007.

MacWilliams, M.L., E.S. Gross, J.F. DeGeorge, and R.R. Rachiele, 2007. Three-dimensional hydrodynamic modeling of the San Francisco Estuary on an unstructured grid, IAHR, 32nd Congress, Venice Italy, July 1-6, 2007.

MacWilliams, M.L., Salcedo, F.G., and E.S. Gross, 2008. San Francisco Bay-Delta UnTRIM Model Calibration Report, POD 3-D Particle Tracking Modeling Study, Prepared for California Department of Water Resources, December 19, 2008, 344 p.

MacWilliams, M.L., Salcedo, F.G., and E.S. Gross, 2009. San Francisco Bay-Delta UnTRIM Model Calibration Report, Sacramento and Stockton Deep Water Ship Channel 3-D Hydrodynamic and Salinity Modeling Study, Prepared for US. Army Corps of Engineers, San Francisco District, July 14, 2009, 574 p.

MacWilliams, M.L., Bever, A.J., and E.S. Gross, 2012. Three-dimensional Sediment Transport Modeling for San Francisco Bay RDMMP, Draft Final Report, San Francisco Bay Regional Dredged Material Management Plan, Prepared for US. Army Corps of Engineers, San Francisco District, June 2012.

Malcherek, A., 2001. Hydromechanik der Fließgewässer, Bericht Nr. 61, Institut für Strömungsmechanik and Elektron, Rechen im Bauwesen der Universität Hannover, Universität Hannover, Hannover.

McMillen, LLC. 2011. Alviso Pond A16-A17 Restoration Design Modification Implications to Existing Environmental Permits. Submitted to USFWS. Prepared August 18, 2011.

Mruz and Albertson, 2008. New Chicago Marsh Water Management Plan, Prepared for Don Edwards San Francisco Bay National Wildlife Refuge, Updated September 2008.

Nagy, L., 2006. Estimating Dike Breach Length from Historical Data, Periodica Polytechnica, Serial Civil Engineering, Vol. 50, No. 2, pp 125-139.

NOAA, 1990. Published Benchmark Sheet for 9414575 Coyote Creek, Alviso Slough, California, Superseded Bench Mark, Publication Date 02/22/1990, http://tidesandcurrents.noaa.gov/benchmarks/benchmarks_old/9414575.html

NOAA, 1993. Solar and Meterological Surface Observations Network, Western Region (Volume 3), Version 1.0, September 1993.

NOAA, 2012. NOAA Center for Operational Oceanographic Products and Services, NOAA Tides and Currents, http://tidesandcurrents.noaa.gov/

Noble Consultants, 2012. Monte Carlo Simulation Under With Project Conditions For South San Francisco Nay Shoreline Study, Draft Summary Report, prepared for U.S. Army Corps of Engineers San Francisco District, June 2012.

[NRC] National Research Council, 1987. Responding to Changes in Sea Level: Engineering Implications, National Academy Press: Washington, D.C.

Partheniades, 1965. Erosion and Deposition of Cohesive Soils, Journal of the Hydraulics

Division, ASCE, 91(HY1):105-138.

PWA, 2006. Flood Analyses Report, submitted to California State Coastal Conservancy, U.S. Fish & Wildlife Service, California Department of Fish and Game, Revised, July 2006.

PWA, 2007. South Bay Salt Pond Restoration Project, Final Environmental Impact Statement/Report, December 2007.

[RMA] Resource Management Associates, 2005. Flooded Islands Pre-Feasibility Study: RMA Delta Model Calibration Report, prepared for CA Department of Water Resources for submittal to California Bay-Delta Authority, June 30.

Stacey, M.T., 1996. Turbulent mixing and residual circulation in a partially stratified estuary. Ph.D. thesis, Dept of Civil Engineering, Stanford University, 209 pp.

Stacey, M., Holleman, R., and E. Gross, 2011. Test Application of a High Resolution 3-dimensional Hydrodynamic Model (SUNTANS) to San Francisco Bay, prepared for San Francisco Estuary Institute (SFEI), Oakland, CA.

Swanson, R.L., 1974, Variability of Tidal Datums and Accuracy in Determining Datums from Short Series of Observations, NOAA Technical Report NOS 64, 41p.

USACE, 1984. San Francisco Bay Tidal Stage vs. Frequency Study, US Army Corps of Engineers San Francisco District, October 1984.

USACE, 2011. Sea Level Change Considerations for Civil Works Programs, Circular No. 1165-2-212, Department of the Army, U.S. Army Corps of Engineers, Washington DC, 1 October 2011.

Warner J.C., Sherwood C.S., Arango H.G., Signell R.P., 2005a. Performance of four turbulence closure models implemented using a generic length scale method. Ocean Modeling 8:81-113.

Warner, J. C., Geyer, W.R. and J.A. Lerczak, 2005b. Numerical modeling of an estuary: A comprehensive skill assessment, J. Geophys. Res., 110, C05001, doi:10.1029/2004JC002691.

Warner J.C., Sherwood, C.R., Signell, R.P., Harris, C.K., and H.G. Arango, 2008. Development of a three-dimensional, regional, coupled wave, current, and sediment-transport model. Computers and Geosciences 34:1284-1306.

Willmott, C., 1981. On the validation of models, Physical Geography, 2, 184–194.